UNCLASSIFIED

AD 268 209

Reproduced
by the

ARMED SERVICES TECHNICAL INFORMATION AGENCY
ARLINGTON HALL STATION
ARLINGTON 12, VIRGINIA

ASD TECHNICAL NOTE 61-66

AN INVESTIGATION OF THE MATERIALS
AND CONSTRUCTIONS OF TENSION MEMBERS
FOR USE IN AIRCRAFT ARRESTMENT EQUIPMENT

DONALD F. HAUSKNECHT
RICHARD KESSLER
MICHAEL F. DARIENZO

AMERICAN MACHINE & FOUNDRY COMPANY
MECHANICS RESEARCH DIVISION

JUNE 1961

XEROX

AERONAUTICAL SYSTEMS DIVISION

NOTICES

When Government drawings, specifications, or other data are used for any purpose other than in connection with a definitely related Government procurement operation, the United States Government thereby incurs no responsibility nor any obligation whatsoever; and the fact that the Government may have formulated, furnished, or in any way supplied the said drawings, specifications, or other data, is not to be regarded by implication or otherwise as in any manner licensing the holder or any other person or corporation, or conveying any rights or permission to manufacture, use, or sell any patented invention that may in any way be related thereto.

AN INVESTIGATION OF THE MATERIALS
AND CONSTRUCTIONS OF TENSION MEMBERS
FOR USE IN AIRCRAFT ARRESTMENT EQUIPMENT

DONALD F. HAUSKNECHT
RICHARD KESSLER
MICHAEL F. DARIENZO

AMERICAN MACHINE & FOUNDRY COMPANY
MECHANICS RESEARCH DIVISION

JUNE 1961

AERONAUTICAL SYSTEMS DIVISION
AIR FORCE SYSTEMS COMMAND
UNITED STATES AIR FORCE
WRIGHT-PATTERSON AIR FORCE BASE, OHIO

FOREWORD

This Technical Note is submitted in accordance with Item VIII, Project No. MR 1135 of Air Force Contract No. AF 33(616)-7152, under which the work was performed by the American Machine & Foundry Company, Mechanics Research Division, Niles, Illinois.

The investigation was conducted and the Technical Note prepared under the supervision of Norman F. Eslinger, project engineer and acknowledgment is made to Dr. G. L. Neidhardt and Mr. F. T. Sasaki of the Mechanics Research Division of American Machine & Foundry Company, and to Mr. V.V. Vary, the Wright Air Development Division project engineer on this program for their contributions to this effort. In addition, appreciation is due to the Celanese Corporation of America, the National-Standard Company of Niles, Michigan, and the Bethlehem Steel Company for their cooperation in furnishing materials, time and information during the course of the program.

PREPARED BY:

Donald F. Hausknecht

Richard Kessler

Michael F. Darienzo

REVIEWED BY:

G. L. Neidhardt
Group Leader
Engineering Mathematics Group

APPROVED BY:

D. E. Arenson
Assistant General Manager
Mechanics Research Division

ASD TN 61-66

ii

ABSTRACT

This Technical Note was prepared in order to present the results of an analytical investigation and experimental verification of the dependency of the impact tolerance of tension members on their geometrical and material characteristics. In addition, tests were also conducted to determine the impact tolerance of those tension members which promised superior performance. The work presented herein is part of a program dealing with the problems of aircraft arrestment at high landing velocities.

In general all tests showed good correlation with predicted values. These correlations verify the use of the developed analytical methods in establishing an expected impact tolerance for materials whose mechanical properties are known.

The tests indicated that the highest transverse impact tolerances were exhibited by nylon and Fortisan specimens in that order, with Fiberglass a probable choice for third position.

It was not considered necessary for the purposes of this report to test the longitudinal impact tolerance of nylon. However, the strong correlation encountered between the predicted and the test data values for the longitudinal impact tolerance properties of the specimens tested indicate that again the highest longitudinal impact tolerance belongs to nylon as predicted. Of the two textile materials tested, Fortisan exhibits the highest value at 234-281 knots. All of the materials tested show superior impact tolerances, both longitudinal and transverse, over that of the improved plow steel rope as presently employed in tension members for the arrestment of aircraft when landing.

PUBLICATION REVIEW

This report has been reviewed and is approved.

FOR THE COMMANDER:

VERYL V. VARY
Asst Chief, Base Equipment Branch
Aerospace Ground Eqp Engr Div
Deputy for Systems Engineering

NOTATION

A Element area, normal to the longitudinal axis, inches^2

AE Tension member elastic modulus. Equivalent to the slope of the member's tension-strain relationship, pounds

c Strain-wave velocity (convex-up stress-strain curve), feet/second

c_o Strain-wave velocity at point of zero strain, feet/second

$c*$ Velocity of kink, feet/second

$c\bullet$ Velocity of kink at point where $c = c*$ feet/second

c_s Strain-wave velocity in direction of loading (concave-up stress-strain curve), feet/second

D Diameter of the helix between the centerlines of the coiled element, inches

d Element diameter, inches

E, G Moduli of elasticity (linear), pounds/inch^2

I Moment of inertia of element area about bending axis, in^4

J Polar moment of inertia of element, in^4

K_ℓ, K_t Material parameters for longitudinal or transverse excitation respectively, feet/second

L Length of the tension member, inches

m Ratio of helix diameter to element diameter, dimensionless

n Number of turns of an element in a helix

s Length of helix element, inches

T Tensile force, pounds

$T\bullet$ Tensile force, pounds at point where $c = c*$

u Longitudinal impact velocity, feet/second

$u\bullet$ Longitudinal impact velocity of cable at point where $c = c*$, feet/second

u_1 Component of u under lower convex-up section of stress-strain curve, feet/second

u_2 Component of u under secant across concave-up section of stress-strain curve, feet/second

u_3 Component of u under upper convex-up section of stress-strain curve, feet/second

v_ℓ, v_t Longitudinal or transverse excitation velocity, respectively, feet/second

$v_\ell^\bullet, v_t^\bullet$ Longitudinal or transverse excitation velocity, respectively, at point where $c = c^*$, feet/second

$\propto$ Lay angle of an element in a strand, angular degrees

γ Helix angle (complement of the lay angle), angular degrees

δ Elongation of a helical spring along the spring axis, inches

ϵ Strain, inches/inch or percent (%)

ϵ_1 Maximum strain produced by the impact, inches/inch or percent (%)

$\epsilon^\bullet$ Strain at point where $c = c^*$, inches/inch or percent (%)

ϵ_{eff} Effective strain of rope, inches/inch

μ Mass density per lineal inch of coil axis, slugs/inch

μ_ϵ Mass density per lineal inch of elongated specimen

ν Poisson's ratio

ρ Mass density per unit volume of a material, $lb.sec^2/in^4$

σ_B Normal stress due to bending, pounds/inch^2

$\sigma_{c\ell}, \sigma_{ct}$ Maximum normal combined stress, longitudinal & transverse respectively, psi

σ_D Normal stress due to direct tension, pounds/inch^2

τ Shearing stress due to torsion, pounds/inch^2

β Acute angle between aircraft path and cable

ϕ Kink angle

$\phi^\bullet$ Kink angle at point where $c = c^*$

TABLE OF CONTENTS

TABLE OF CONTENTS (Continued)

TABLE OF CONTENTS (Continued)

LIST OF ILLUSTRATIONS

LIST OF ILLUSTRATIONS (Continued)

LIST OF ILLUSTRATIONS (Continued)

LIST OF ILLUSTRATIONS (Continued)

LIST OF ILLUSTRATIONS (Continued)

LIST OF ILLUSTRATIONS (Continued)

LIST OF ILLUSTRATIONS (Continued)

LIST OF TABLES

LIST OF CHARTS

SECTION 1

INTRODUCTION

1.0 <u>Purpose and Scope</u>

Conventional aircraft-arresting gear employ wire rope to exert the desired decelerating force on the aircraft during landing, in order to r duce the length of runway below that which would be required for an unassisted landing. Present practical limitations on the impact tolerance of wire rope to less than 200 knots restrict the maximum stalling velocity to a relatively low value and as a consequence impose a compromise of aircraft performance at altitude.

The purpose of the study of the geometrical and material parameters which determine the impact tolerance of tension members is to define the areas of possible improvement and to develop new tension members capable of resisting impacts of 400 knots. Initial effort along these lines was presented in WADC Technical Report 59-495 which described studies of aircraft-arresting gear cables (Reference 1). This present work continues that theoretical analysis, and it includes experimental verification of the results of the investigation presented herein. Methods are developed for selecting materials possessing outstanding impact properties and the impact performances predicted are presented in this technical note.

The test phase of the program was conducted for the purpose of testing those materials which were indicated by the methods of analysis presented herein to possess superior impact tolerance and to verify the predicted values of impact tolerance for various linear and non-linear

materials. To accomplish this purpose static tests were conducted to establish impact tolerance predictions, followed by a series of dynamic tests to demonstrate experimentally the correlation between the predicted and the actual impact tolerances. The dynamic tests consist of both longitudinal and transverse impact tests and are included in this technical note presentation.

1.1 The Analytical Approach

In the following sections the dependency of the impact behavior of tension members on their geometric and material parameters is discussed and independently developed. This presumption that no mutual influences exist between variations in the material and geometrical parameters was later found to be justified except for negligible effects displayed by ranges of Poisson's ratio.

In the beginning of the program, the degree of improvement in impact tolerance that could be achieved by geometrical variation alone was un- known. The determination of the upper bound of possible improvement in the impact tolerance was initially intended since, if it could be shown that even in a configuration most sensitive to geometrical changes little improvement is possible as a result of these changes, then further effort on this phase of the program could be concluded. On the other hand, if the theoretical improvement possible was demonstrated to be large, then the effort would be continued in order to determine the specific geometri- cal characteristics which could be incorporated in the design of new tension members.

2

In order to evaluate the upper bounds of possible improvement as a result of geometrical variation, a tension member was developed possessing the practical advantages of a wire rope, of a configuration which would permit mathematical analysis, yet would still retain a sensitivity to changes of geometry similar to that of the wire rope. Since the problem involves several geometrical parameters, a simple physical representation was desired which would include these parameters in such a way that an appropriate combination of changes in these parameters would lead to the greatest theoretical increase possible in the impact tolerance of the tension member.

The studies treating with the influence of material characteristics on the impact tolerance of tension members include linear and nonlinear materials. WADC Technical Report 58-217, (Reference 2), which is concerned with an analytical approach to the problem of alleviating dynamic tensions in aircraft arresting gear cables, develops analytical techniques for dealing with linear materials. Procedures for analyzing nonlinear materials are developed in this present work.

In Reference 2, no restriction was placed on the tension-strain characteristics of the material in developing the expressions dealing with longitudinal and transverse impacts. However, in Reference 1 only specific cases were analyzed on the basis of linear characteristics. This present work extends the analysis to nonlinear materials as well.

1.2 Test Technique

The static test requirements for the testing phase of the program required no special equipment and the necessary data was procured through the use of an Instron Tensile Testing Instrument as reported herein in Section 4.0.2.

3

For the dynamic testing phase, the critical test conditions and the high velocities anticipated at the outset of the program to be required for establishing longitudinal and transverse impact tolerances necessitated an economical and dependable method for producing suitable impact conditions.

The longitudinal impact test required the design and use of a testing facility consisting of a track mounted missile propelled by an explosive charge whose composition determined the resulting velocity of the missile. In addition, techniques were developed to insure pure longitudinal impact of the specimen and provisions had to be made to stop the missile within a reasonable distance after impacting the specimen.

The transverse impact test was found to be amenable to the use of velocity controlled, solid, 12-gauge shot gun slugs. The velocity control and adequate impact accuracy of this method was established by a pre-liminary test series which are part of the data presented in this technical note. The success of this early test series justified the development of the technique around which the transverse tests were planned. This method could not be used for the longitudinal impact tests because it would not produce pure longitudinal impact under the available conditions.

4

SECTION 2

STUDY OF GEOMETRICAL PARAMETERS

2.0 The Analytical Model

In order to perform an analysis of the effects of geometrical modifi-
cations on the impact tolerance of a tension member, a mathematical model
must be established which preserves the basic parameters throughout the
range of their variation. In addition, the model selected had to have the
practical advantages of wire rope, principally flexibility, and since the
method of approach should establish the upper bound of possible theoretical
improvement, the model configuration selected was that which would permit
the maximum increase in impact tolerance. The selection was made from
several suitable geometrical configurations including the cylindrical and
conical helix, the chain, and the braid.

The model chosen consists of a single circular solid element, wound
into a cylindrical helical coil. This simplified configuration has its
usefulness in that its analysis provides knowledge of the behavior of an
elastic tension member having a geometry of basic interest and, to a large
extent, having the general configuration of a conventional wire rope.
Also, as the helix angle is allowed to vary from 0° to 90°, configura-
tions ranging from a solid bar to a tight spring are available for analysis
as well as any ratio of coil diameter to wire diameter.

It is to be noted that the model described above does not incorporate
radial support. The effect of radial support can be qualitatively evaluated

5

from the outset; radial support tends to make the member less elastic and to behave more as a solid bar. Analytically, radial support can be introduced to represent a more realistic situation such as that existing in a conventional wire rope. The helical model will be analyzed first without, and then with, the radial support.

The generalized model configuration to be analyzed in the following sections embraces all practical geometries and variations of interest. However, any deviation from the selected helical model being analyzed would not lead to a superior impact tolerance. While no rigorous analysis is presented, it can be intuitively demonstrated that the radially supported helix configuration previously described is superior to other geometries to which the model generally applies. Some of these geometries are as follows:

1. Multiple circular elements wound into a cylindrical helical strand

2. Multiple strands of Case 1 wound into a cylindrical helical coil

3. Multiple annular layers of strands would into a cylindrical helical coil

4. Plaited or braided tension member

5. Non-circular elements wound into a cylindrical helical strand

Cases 1, 2 and 3 above can be dismissed immediately from further consideration as possible methods of improvement because they have, in essence, the same geometry as the radially supported model analyzed,

except that their multiplicity of elements introduces contact stresses which tend to decrease their impact tolerance.

It would appear that the inter-element contact stresses would preclude any advantage of Case 4 as well, because in plaited or braided geometry the element cross-over angle is extreme and contact stresses high.

If non-circular elements wound into a cylindrical helical strand are considered as a possible geometrical modification, it does not appear that any advantage will be acquired because the stresses induced under impact are derived from direct tension, torsion and bending. If element bending is prevented by radial support, the element is subject to the same tensile load regardless of element cross-sectional shape. However, torsional stresses are dependent upon the element's cross-sectional geometry. Any cross-section other than circular would lead to higher torsional stresses for equal cross-sectional area.

While contact stresses might be minimized by an element cross-sectional geometry providing large contact areas, its usefulness is significant only where fatigue life or gross bending is of greater significance than maximum impact tolerance.

From the foregoing considerations, the analysis of geometrical influences in tension members is believed comprehensive and to be applicable to all practical geometries.

2.1 Mathematical Analysis

2.1.1 Helical Spring Model

Figure 1 shows the helical spring model with the significant geometric parameters necessary to define the mathematical model.

In Timoshenko's Strength of Materials (Reference 3), the elongation of a helical spring due to a longitudinally tensile force is given as,[1]

$$\delta = T \frac{D^2}{4} \ s \ \left(\frac{\cos^2 \gamma}{G\,J} + \frac{\sin^2 \gamma}{E\,I} \right), \tag{2.1}$$

where the two terms on the right are due to torsion and bending of the wire respectively. In order that this equation apply for any γ between zero and $\frac{\pi}{2}$, (i.e. ranging from the tightest coil to a straight wire), a term must be added which takes into account the elongation due to the strain caused by the component of the tension along the axis of the wire. From the free-body diagram of Figure 2a, this component is seen to be $T \sin \gamma$. Adding the corresponding term to Equation (2.1),

$$\delta = T \frac{D^2}{4} \ s \ \left(\frac{\cos^2 \gamma}{G\,J} + \frac{\sin^2 \gamma}{E\,I} \right) + \frac{T \ S \ \sin^2 \gamma}{E\,A} \tag{2.2}$$

---

[1] If the diameter of the wire is not small in comparison with the coil diameter, the torsional rigidity (GJ) should be modified by the correction factor, as indicated in Reference 3,

$$K = 1 + \frac{3\,\left(\frac{d}{D}\right)^2}{16\,\left[1 + \left(\frac{d}{D}\right)^2\right]}\ .$$

However, it will be seen that this correction factor can only decrease the impact capabilities of the model and hence lessen the improvement which would otherwise be found.

8

$$S = \int_B^C ds$$
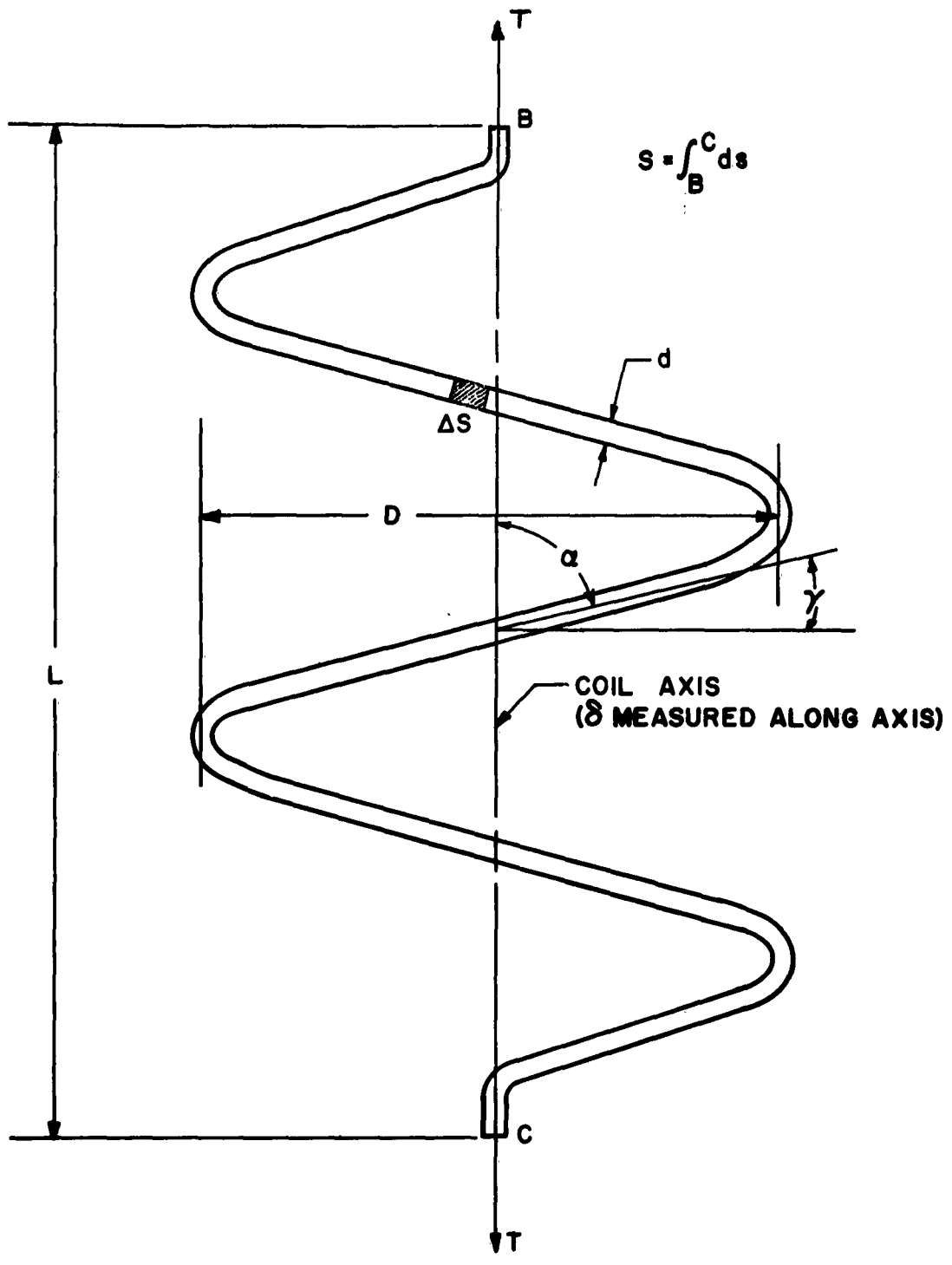
Figure 1
Helical Element Model

9
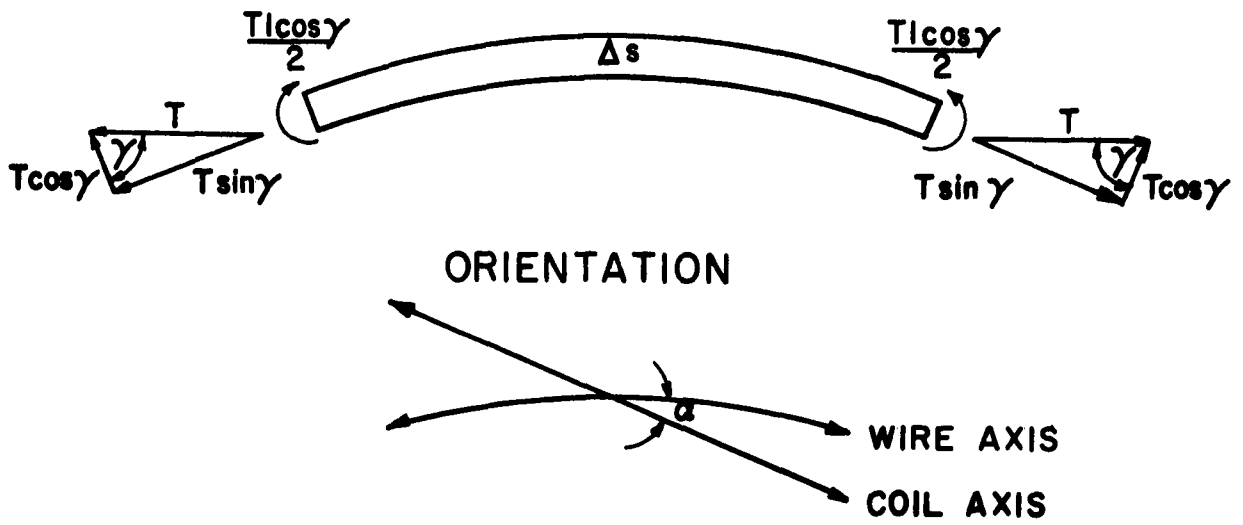
Figure 2a
Free-Body Diagram of a Section of the Helical Model
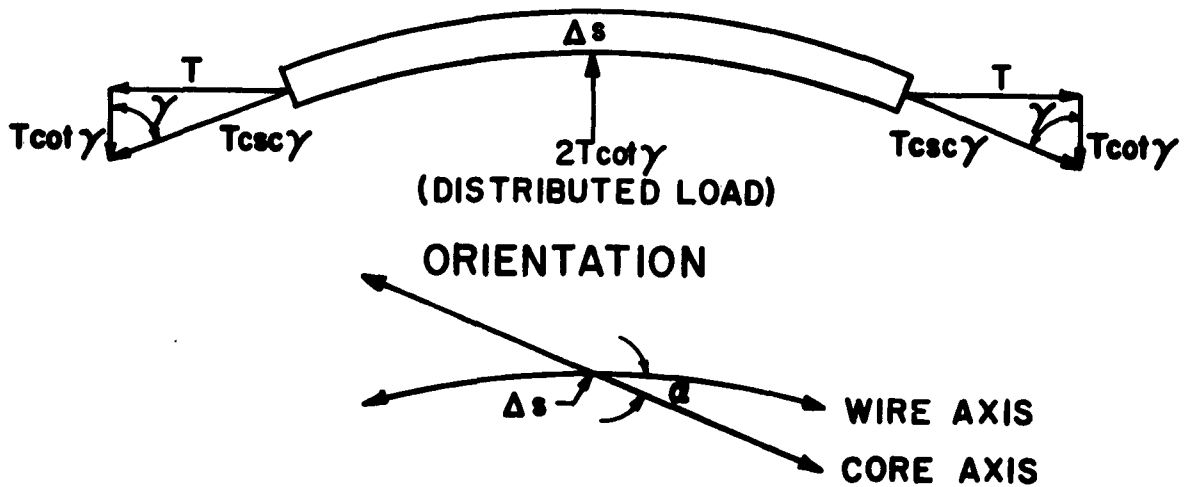
Figure 2b
Free-Body Diagram of a Section of the Radially Supported Helical Model

If Equation (2.2) is divided by L (the axial length of the helix segment being considered), then that equation gives an effective "strain" for the coil spring, reducing to the usual strain, $\epsilon = \frac{\sigma}{E}$, for a straight wire in tension. Geometrically, $\frac{s}{L}$ can now be seen to be equal to csc γ (Figure 3).

$$csc\ \gamma = \frac{s}{L}$$
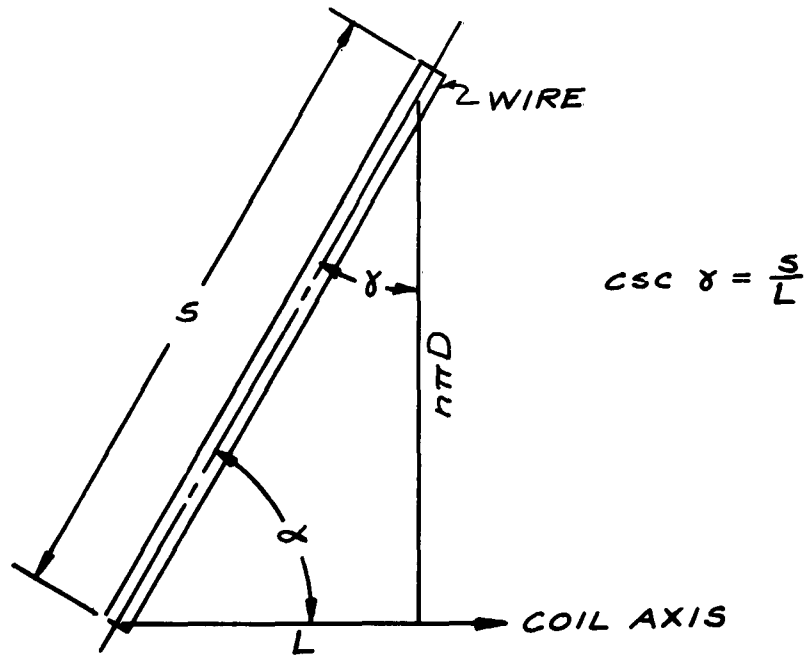
Figure 3

LENGTH OF WIRE UNWRAPPED FROM THE HELIX

Rewriting Equation (2.2) after division by L, and grouping the common factors, it becomes,

$$\epsilon_{eff} = T\ csc\ \gamma\ (\frac{D^2\ cos^2\ \gamma}{4\ G\ J} + \frac{D^2\ sin^2\ \gamma}{4\ E\ I} + \frac{sin^2\ \gamma}{E\ A}) \qquad (2.3)$$

11

It is now possible to write an analytical relationship for $Æ$, which, in Reference 1 was indicated to be an important parameter.

$$Æ = \frac{T}{\epsilon_{eff}} = \frac{\sin \gamma}{\frac{D^2 \cos^2 \gamma}{4 \, G \, J} + \frac{D^2 \sin^2 \gamma}{4 \, E \, I} + \frac{\sin^2 \gamma}{E \, A}} \qquad (2.4)$$

Taking a wire of a circular cross-section, as was already implied in footnote 1, page 5, and defining $m = \frac{D}{d}$, Equation (2.4) after simplification becomes,

$$Æ = \frac{A \, E \, \sin \gamma}{\sin^2 \gamma + 4m^2 \, (1 + \nu \cos^2 \gamma)} \qquad (2.5)$$

where G has been replaced by $\frac{E}{2(1 + \nu)}$, and I and J have been written in terms of the wire diameter, d, and the cross-sectional area, A.

Also, having an expression for the length of wire per unit length of coil, $\frac{s}{L}$, the following relationship for the linear mass density of the coil, μ , can be written

$$\mu = \rho \, \frac{\text{Volume of Wire}}{\text{unit length}} = \rho \frac{s}{L} \, A = \rho \, A \, \csc \gamma \qquad (2.6)$$

The basic equations developed by F. O. Ringleb in an investigation of cable dynamics (Reference 5) can be written in a form convenient to the present analysis:

$$T_\ell = v_\ell \; Æ \qquad (2.7)$$

$$T_t = \left(\frac{v_t}{\sqrt{1 + \frac{\sigma}{E}} - \frac{1}{2} \sqrt{\frac{\sigma}{E}}} \right)^{4/3} \sqrt[3]{\frac{Æ \, \mu^2}{4}}$$

However, the equation for T_t can be further simplified when $\frac{\sigma}{E}$ is negligibly small compared with unity ($\frac{\sigma}{E} < 10\%$) as is the case for the materials presented in Table I, page 31, of this Technical Note. The resulting approximation is as follows:

$$T_t = v_t^{4/3} \sqrt[3]{\frac{Æ \, \mu^2}{4}} \qquad (2.8)$$

12

Substituting Equations (2.5) and (2.6) into (2.7) and (2.8), it is found that

$$T_\ell = v_\ell \quad A \left[\frac{E \rho}{\sin^2 \gamma + 4m^2 (1 + \cos^2 \gamma)} \right]^{1/2} \tag{2.9}$$

$$T_t = (v_t)^{4/3} A \left\{ \frac{E \rho^2 \csc \gamma}{4 \left[\sin^2 \gamma + 4m^2 (1 + \nu \cos^2 \gamma) \right]} \right\}^{1/3} \tag{2.10}$$

Equations (2.9) and (2.10), however, can not be used to calculate the stresses, and in particular the combined stress which is produced in the wire by the tension T_ℓ or T_t . Therefore, unless the ultimate tension for a particular geometrical configuration is known, it is not possible to predict the velocity at which the member will break.

The maximum allowable combined normal stress induced at the most critical point in the wire cross-section will define the maximum impact velocity.

As a matter of completeness of the analysis performed on the basis of the combined maximum normal stress, it is necessary to demonstrate the needlessness of a maximum combined shearing stress criterion for determining the optimum geometry. Clearly, the shear criterion would be the index necessary to evaluate the impact tolerance at large lay angles where torsion and possible bending predominate.

The curves of Figures 5, 6, 9 and 10 show the velocities at which a failure will occur due to the combined normal stress. The maximum impact tolerance shown on these curves is the straight tension element case ($\alpha = 0$) during transverse impact. Torsion and bending are completely absent in this case and are negligible also at small lay angles. Since the shear criterion will therefore not apply at or near $\alpha = 0$ for the optimum case, its applicability at other

13

points along the curves has little significance because, irrespective of the

impact velocity determined by the normal stress criterion, the element will be

limited to lower velocities on the basis of the shear stress criterion. Hence,

the normal stress criterion leads to a relative conservatism at $\alpha = 0$ in

comparison with $\alpha = \pi/2$.
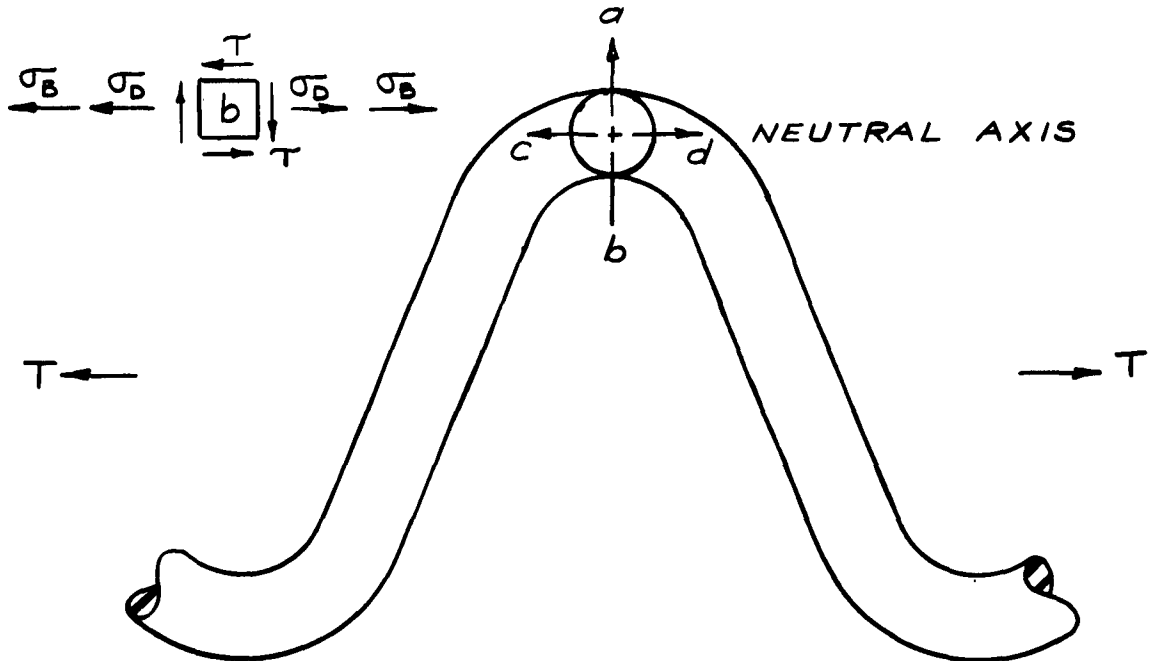
Figure 4

LOCATION AND STATE OF STRESS AT THE CRITICAL POINT
IN THE CROSS-SECTION OF A HELICAL SPRING

In Figure 4, the critical point b as determined on inspection is

subject to direct tension, bending, and torsional stresses as defined by,

$$\sigma_D = \frac{T}{A} \sin \gamma \qquad (2.11)$$

$$\sigma_B = \frac{4 \, m \, T}{A} \sin \gamma \qquad (2.12)$$

$$\tau = \frac{2 \, m \, T}{A} \cos \gamma \qquad (2.13)$$

Adding Equations (2.11), (2.12) and (2.13) by means of the classical

equation for the maximum normal combined stress yields,

$$\sigma_c = \frac{T}{2A} \left[(1 + 4m) \sin \gamma + \sqrt{(1 + 8m) \sin^2 \gamma + 16m^2} \right] \tag{2.14}$$

By substituting T_ℓ , Equation (2.7), and T_t, Equation (2.8), for the tensile

force, T, in Equation (2.14) and solving for v_ℓ and v_t respectively,

$$v_\ell = \frac{2 \sigma_{c\ell} \left[\sin^2 \gamma + 4m^2 (1 + \nu \cos^2 \gamma) \right]^{1/2}}{\left[E \rho \right]^{1/2} \left\{ \sin \gamma (1 + 4m) + \left[(1 + 8m) \sin^2 \gamma + 16m^2 \right]^{1/2} \right\}} \tag{2.15}$$

$$v_t = \frac{\left[2 \sigma_{ct} \right]^{3/4} \left\{ 4 \sin \gamma \left[\sin^2 \gamma + 4m^2 (1 + \nu \cos^2 \gamma) \right] \right\}^{1/4}}{\left[E \rho^2 \right]^{1/4} \left\{ (1 + 4m) \sin \gamma + \left[(1 + 8m) \sin^2 \gamma + 16m^2 \right]^{1/2} \right\}^{3/4}} \tag{2.16}$$

Equations (2.15) and (2.16) are the expressions of the mathematical model

by which the impact tolerances of a helical configuration may be determined

depending upon the two shape parameters γ and m, and the four material

parameters E, ρ, σ and ν . These equations are restricted to materials

having linear stress-strain relationships.

In order to give the model a more explicit meaning, the graphs of

limiting longitudinal and transverse impact velocities are shown in Figures

5 and 6 respectively. These curves were arbitrarily plotted for σ = 200,000 psi,

$E = 30 \times 10^6$ psi, $\rho = 7.32 \times 10^{-4}$ slugs/in^3, $\nu = 0.3$ and varying γ for

four representative values of m.

It can be seen from Figures 5 and 6 that the transverse impact

tolerances for the same helix are everywhere better than the longitudinal

15

impact capabilities, except for lay angles over approximately 80°. However, as m increases, the longitudinal impact levels will increase while the transverse levels will decrease. Further, it appears from Figure 5 that for large values of m, the longitudinal impact velocity is increased very little by increasing m. For this reason, and since the transverse case is considerably superior, there is no purpose in exploiting the slight improvement in the longitudinal tolerance by using large values of m because the coil diameter will rapidly become impractical for reasonable values of the wire diameter.

In Equations (2.15) and (2.16) the impact tolerances v_ℓ and v_t are determined by both material characteristics and geometrical characteristics. It is possible to isolate these influences as follows, where K_ℓ and K_t are the longitudinal and transverse impact tolerance parameters, respectively, and are functions of material characteristics alone:

$$K_\ell = \frac{\sigma}{\sqrt{E\rho}} \tag{2.17}$$

$$K_t = \frac{2^{1/2}\,\sigma^{3/4}}{(E\rho^2)^{1/4}} \tag{2.18}$$

Equation (2.18) is an approximation obtained by neglecting the strain $(\frac{\sigma}{E})$ produced by impact and is to be used only for relatively small strains $(\frac{\sigma}{E} < 10\%)$. The exact solution is

$$K_t = \frac{2^{1/2}\,\sigma^{3/4}}{(E\rho^2)^{1/4}} \left[\sqrt{1 + \frac{\sigma}{E}} - 1/2\sqrt{\frac{\sigma}{E}}\right]^{1/2}$$

16
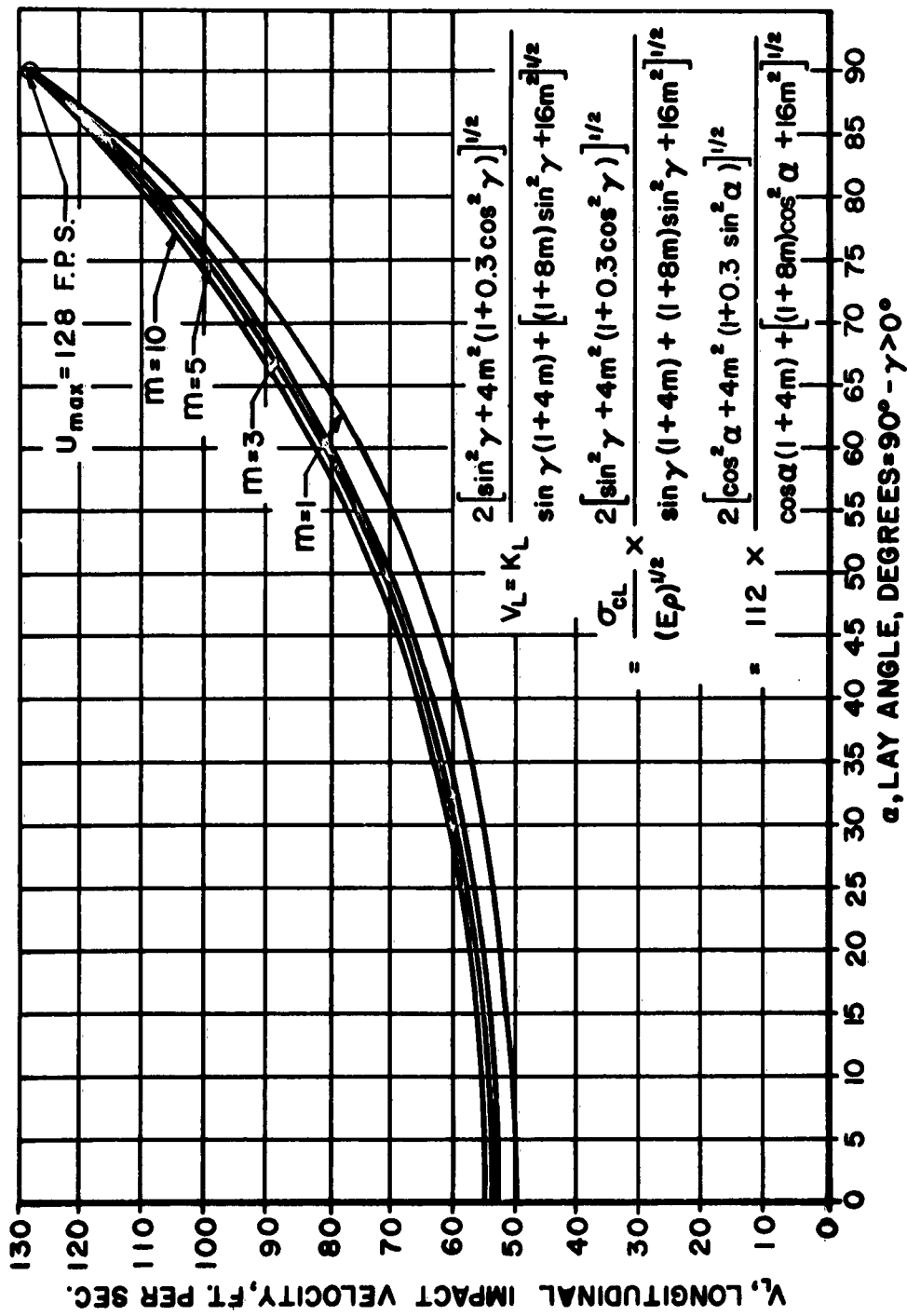
HELICAL SPRING OF 200,000 P.S.I. STEEL (K_L = 112 F.P.S.)
LONGITUDINAL IMPACT VELOCITY vs. LAY ANGLE

Figure 5

$$V_L = K_L \frac{2\left[\sin^2\gamma + 4m^2(1+0.3\cos^2\gamma)\right]^{1/2}}{\sin\gamma(1+4m) + \left[(1+8m)\sin^2\gamma + 16m^2\right]^{1/2}}$$

$$= \frac{\sigma_{cL}}{(E\rho)^{1/2}} \times \frac{2\left[\sin^2\gamma + 4m^2(1+0.3\cos^2\gamma)\right]^{1/2}}{\sin\gamma(1+4m) + (1+8m)\sin^2\gamma + 16m^2\right]^{1/2}}$$

$$= 112 \times \frac{2\left[\cos^2\alpha + 4m^2(1+0.3\sin^2\alpha)\right]^{1/2}}{\cos\alpha(1+4m) + \left[(1+8m)\cos^2\alpha + 16m^2\right]^{1/2}}$$

17
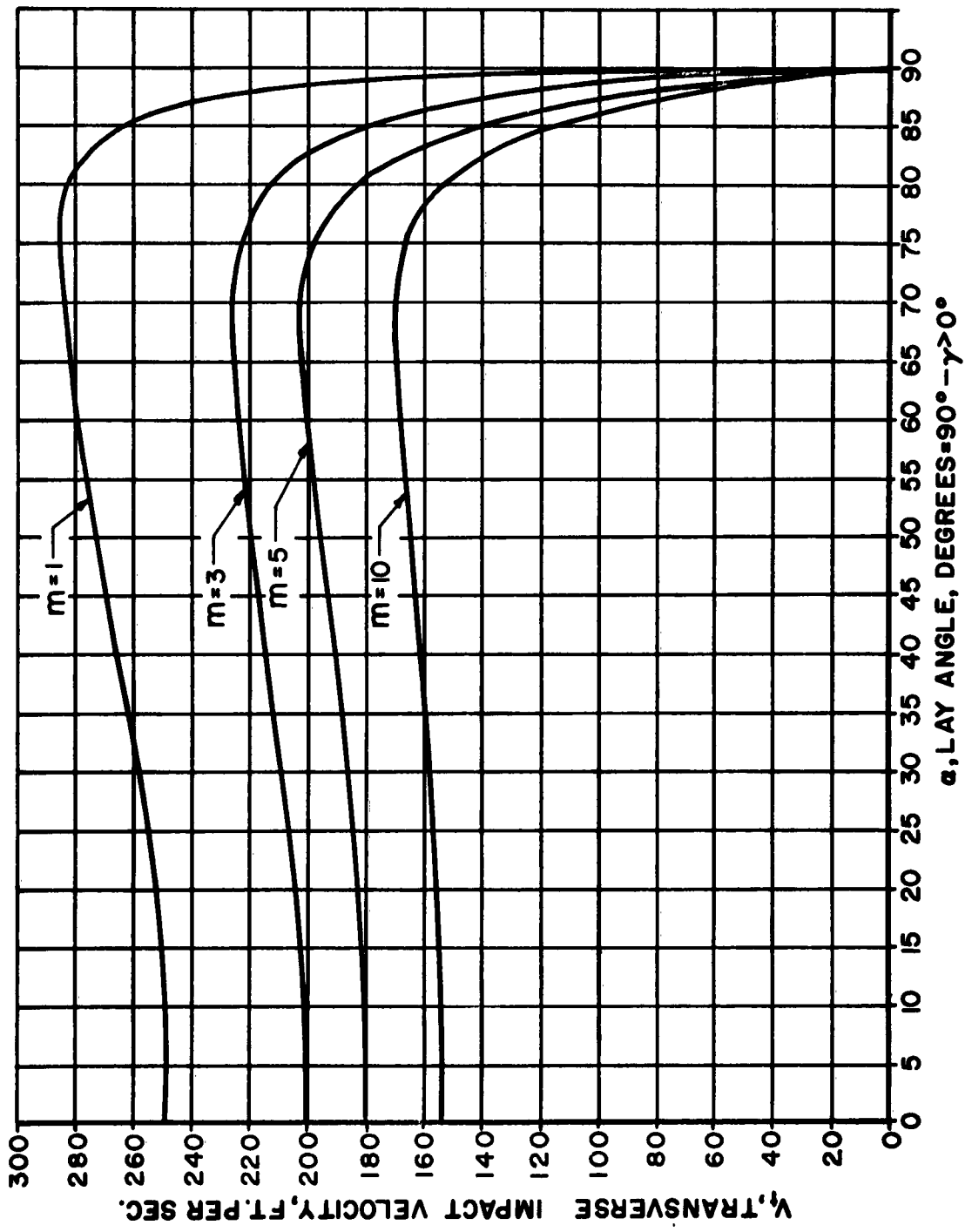
HELICAL SPRING OF 200,000 P.S.I. STEEL (K₁ = 557 F.P.S.)
TRANSVERSE IMPACT VELOCITY vs. LAY ANGLE
Figure 6

Equations (2.17) and (2.18) will be recognized later to be the limiting impact velocities for a straight wire and therefore can serve as selective criteria for materials.

Dividing Equations (2.15) and (2.16) by K_ℓ and K_t, the geometrical parameters are isolated as follows:

$$\frac{v_\ell}{K_\ell} = \frac{2\left[\sin^2 \gamma + 4m^2 (1 + \nu \cos^2 \gamma)\right]^{1/2}}{(1 + 4m) \sin \gamma + \sqrt{(1 + 8m) \sin^2 \gamma + 16m^2}} \qquad (2.19)$$

$$\frac{v_t}{K_t} = \frac{\left\{8 \sin \gamma \left[\sin^2 \gamma + 4m^2 (1 + \nu \cos^2 \gamma)\right]\right\}^{1/4}}{(1 + 4m) \sin + (1 - 8m) \sin^2 + 16m^2)^{1/2 \ 3/4}} \qquad (2.20)$$

While ν can vary from 0 to 0.5 in its theoretical limitations and for most materials is about 0.3, it has restricted influence in Equations (2.19) and (2.20). Therefore, the curves of Figures 7 and 8 are plotted for a constant value of 0.3 for ν and represent essentially geometrical effects.

The normalized ordinates of Figures (7) and (8), together with the material parameters defined in Equations (2.17) and (2.18), will yield the impact tolerances of any helical configuration.

It is to be further noted in Figures 5, 6, 7 and 8, that while the curves terminate at discrete points on the ordinate, they are actually discontinuous at $\alpha = 0$ and instead have a common point of intersection. This point can be immediately found from Equations (2.17) and (2.18), to

which Equations (2.15) and (2.16) are reduced when $\alpha = 0$. Therefore, at $\alpha = 0$,

$$v_\ell = K_\ell, \text{ and} \qquad (2.21)$$

$$v_t = K_t \qquad (2.22)$$

It is emphasized, then, that the curves of Figures 5, 6, 7 and 8 are un-defined by Equations (2.15) and (2.16) for $\alpha = 0$; it is further noted that, geometrically, α can be zero only when m is zero, which is the case of a straight wire. (The case $\alpha = 0$ with $m \neq 0$ would present an eccentrically loaded straight wire.)

2.1.2 Radially-Supported Helical Model

A study of the impact tolerances theoretically obtainable from the curves of Figures 5, 6, 7 and 8 reveals that the simple coil model has, under the most favorable selection of variables, impact tolerances much less than those of conventional wire ropes, except when the helix de-generates to a straight wire $(\alpha = 0)$ or, under longitudinal impact only, a helix angle greater than 80°. (Even then, combined shear stresses may preclude the higher longitudinal impacts.) Consequently, modifications were incorporated into the model to represent radial support such as that manifested in a conventional rope.

Presuming a massless core providing only radial support to the helix, but making no contribution to relieving the tensile load, it is clear that the equations of the previous section must be altered in order to account for the difference in loading. Bending will no longer occur since the

$$\frac{V_L}{K_L} = \frac{V_L}{\frac{\sigma_{cL}}{(E\rho)^{1/2}}} = \frac{2\left[\sin^2\gamma + 4m^2(1+0.3\cos^2\gamma)\right]^{1/2}}{\sin\gamma(1+4m)+\left[(1+8m)\sin^2\gamma+16m^2\right]^{1/2}}$$

$$= \frac{2\left[\cos^2\alpha + 4m^2(1+0.3\sin^2\alpha)\right]^{1/2}}{\cos\alpha(1+4m)+\left[(1+8m)\cos^2\alpha+16m^2\right]^{1/2}}$$

HELICAL SPRING

$\frac{V_L}{K_L}$ vs. LAY ANGLE

Figure 7

21

$$\frac{V_t}{K_t} = \frac{V_t}{\dfrac{2^{1/2}\sigma^{3/4}}{E^{1/4}\rho^{1/2}}}$$

$$= \frac{\left\{8\sin\gamma\left[\sin^2\gamma + 4m^2(1+0.3\cos^2\gamma)\right]\right\}^{1/4}}{\left\{(1+4m)\sin\gamma + \left[(1+8m)\sin^2\gamma + 16m^2\right]^{1/2}\right\}^{3/4}}$$

$$= \frac{\left\{8\cos\alpha\left[\cos^2\alpha + 4m^2(1+0.3\sin^2\alpha)\right]\right\}^{1/4}}{\left\{(1+4m)\sin\alpha + \left[(1+8m)\cos^2\alpha + 16m^2\right]^{1/2}\right\}^{3/4}}$$

α, LAY ANGLE, DEGREES $= 90° - \gamma > 0°$

HELICAL SPRING

$\dfrac{V_t}{K_t}$ vs. LAY ANGLE

Figure 8

22
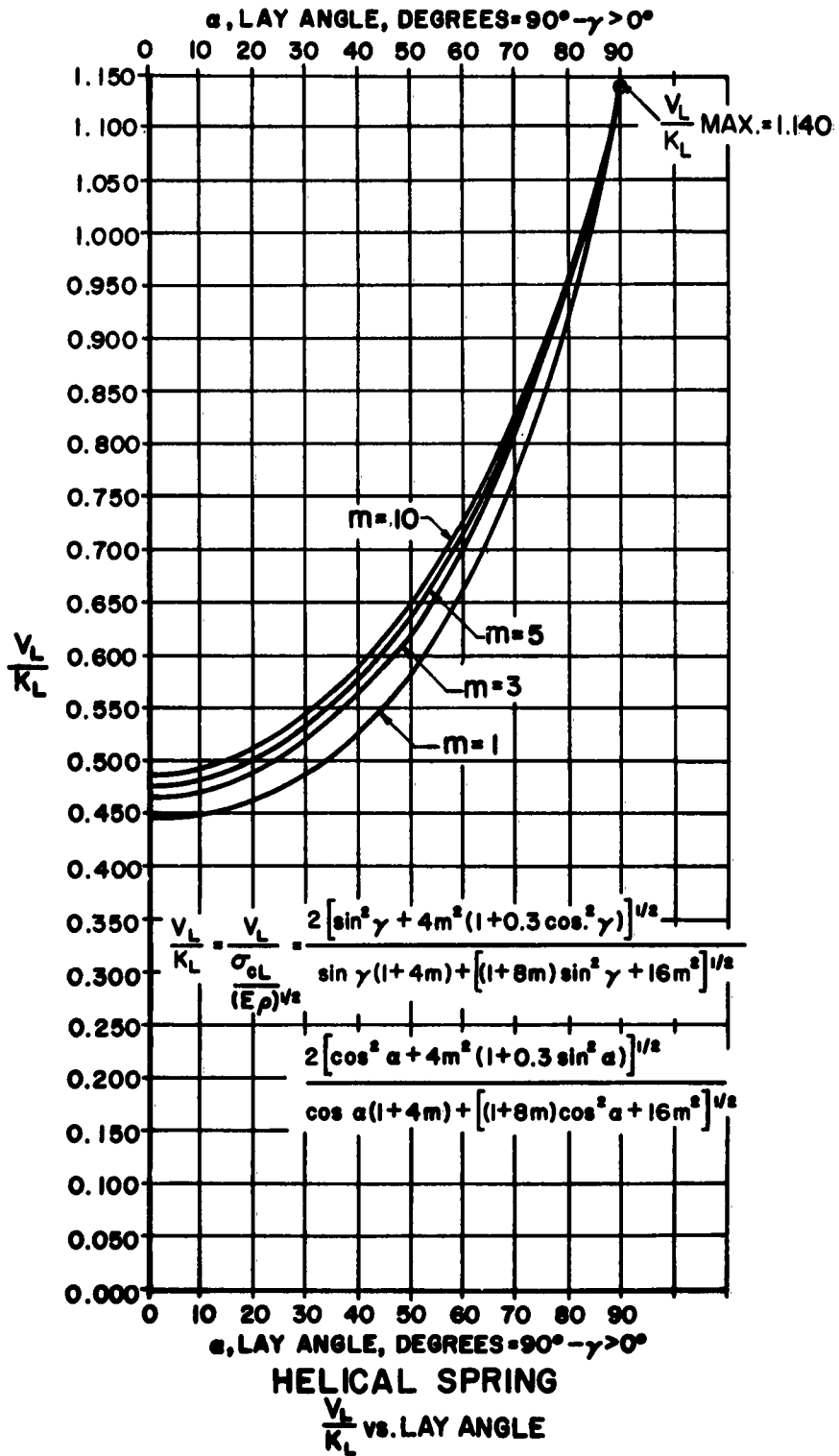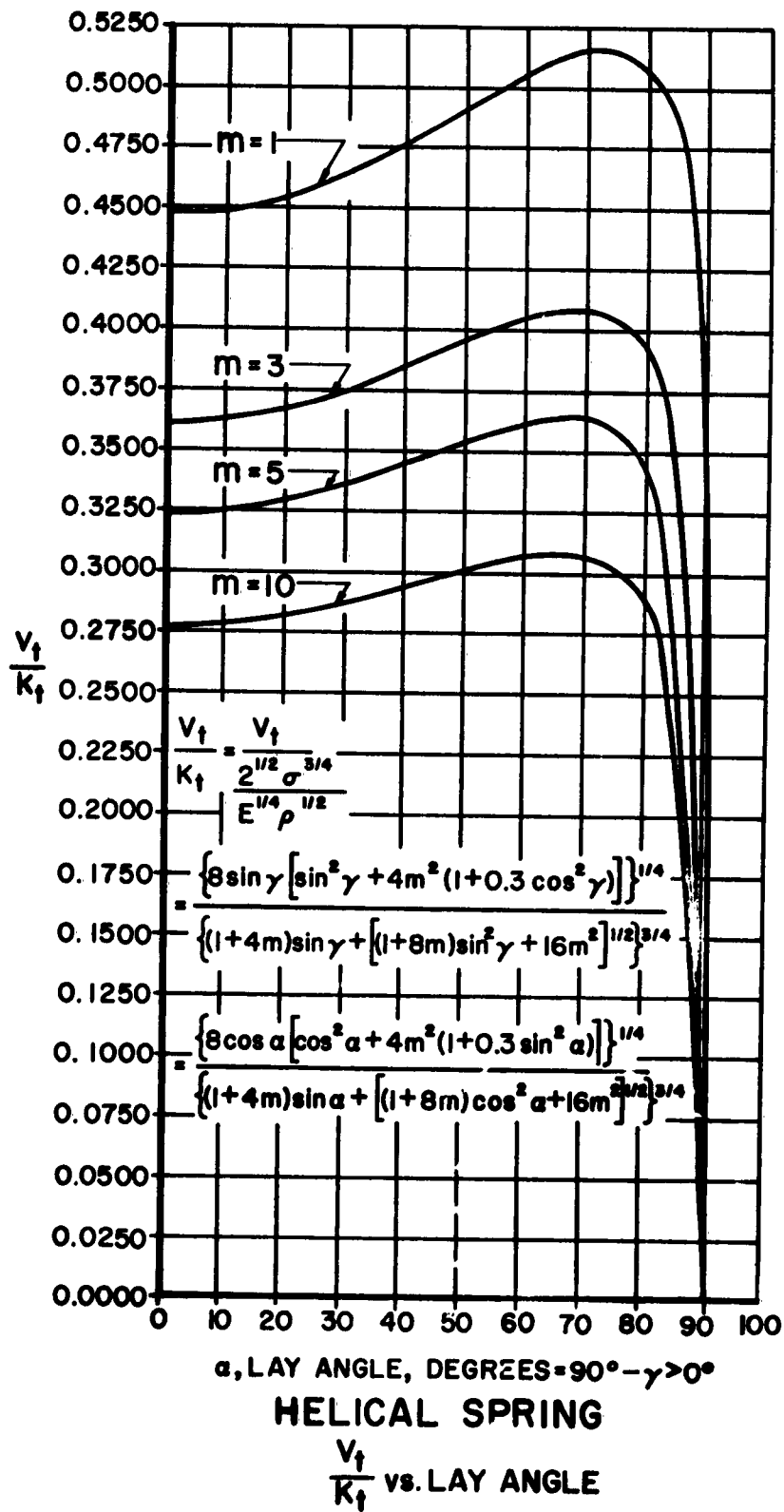
helical wire is now restrained radially. Upon drawing a free body diagram, Figure 2b, page 10, of an element Δs of the wire, the component of direct tension is found to be considerably different than in Figure 2a.

Rewriting the equation for the effective strain, ϵ_{eff}, by dropping the term due to bending and changing the component of direct tension from $(T \sin \gamma)$ to $(T \csc \gamma)$, Equation (2.3) is then[3]

$$\epsilon_{eff} = T \csc \gamma \; (\frac{D^2 \cos^2 \gamma}{4 \, G \, J} + \frac{1}{E \, A})$$ (2.23)

and $\mathbb{E}$ is therefore

$$\mathbb{E} = \frac{T}{\epsilon_{eff}} = \frac{A \, E \, \sin \gamma}{4m^2 \cos^2 \gamma + 4m^2 \, \nu \, \cos^2 \gamma + 1}$$ (2.24)

T_ℓ and T_t are then

$$T_\ell = v_\ell \quad A \left[\frac{E \rho}{1 + 4m^2 \cos^2 \gamma \, (1 + \nu)} \right]^{1/2}$$ (2.25)

$$T_t = (v_t)^{4/3} \; A \left\{ \frac{E \rho^2 \quad \csc \gamma}{4 \quad \left[1 + 4m^2 \cos^2 \gamma \, (1 + \nu) \right]} \right\}^{1/3}$$ (2.26)

Because there is no bending, the maximum combined normal stress will now be located at any point on the circumference of the cross-section of the wire. The shearing stress due to torsion remains unchanged and is given by Equation (2.13), but the stress due to direct tension on the wire will now be

---

[3] The radial forces on wire ropes are discussed in a paper by F. H. Hruska (Reference 4). This resolution of the forces merely approximates the effect of radial deformation due to contact stresses.

23

$$\sigma_D = \frac{T}{A} \csc \gamma \qquad (2.27)$$

and the equation for the maximum combined normal stress is then

$$\sigma_c = \frac{T}{2A} \left[\csc \gamma + (\csc^2 \gamma + 16m^2 \cos^2 \gamma)^{1/2} \right] \qquad (2.28)$$

Replacing T in Equation (2.28) by Equation (2.25) for T_ℓ and Equation (2.26) for T_t and solving the same for v_ℓ and v_t respectively, it is found that

$$v_\ell = \frac{\sigma_{c\ell}}{(E\rho)^{1/2}} \; \frac{2 \left[1 + 4m^2(1 + \nu) \cos^2 \gamma \right]^{1/2}}{\csc \gamma + (\csc^2 \gamma + 16m^2 \cos^2 \gamma)^{1/2}} \qquad (2.29)$$

$$v_t = \frac{2^{1/2}(\sigma_{ct})^{3/4}}{(E\rho^2)^{1/4}} \; \frac{\left\{ 8 \sin \gamma \left[1 + 4m^2 \cos^2 \gamma (1 + \nu) \right] \right\}^{1/4}}{\left[\csc \gamma + (\csc^2 \gamma + 16m^2 \cos^2 \gamma)^{1/2} \right]^{3/4}} \qquad (2.30)$$

Plotting Equations (2.29) and (2.30), using the same material parameters as the previous section, produces considerably different curves, as shown by Figures 9 and 10, than the corresponding ones for the unsupported helical spring. Both the ordinate and abcissa intercepts are the same for any value of m in the transverse or in the longitudinal cases. As opposed to the previous curves for the unsupported helical spring, the ordinate intercepts are not points of discontinuity. The continuity of the curves of Figures 9 and 10 follows from the occurrence of the $\cos^2 \gamma$ in each term in which m occurs. Hence, when γ equals 90° (α equals 0°) the terms containing $\cos^2 \gamma$ become zero irrespective of the value of m.
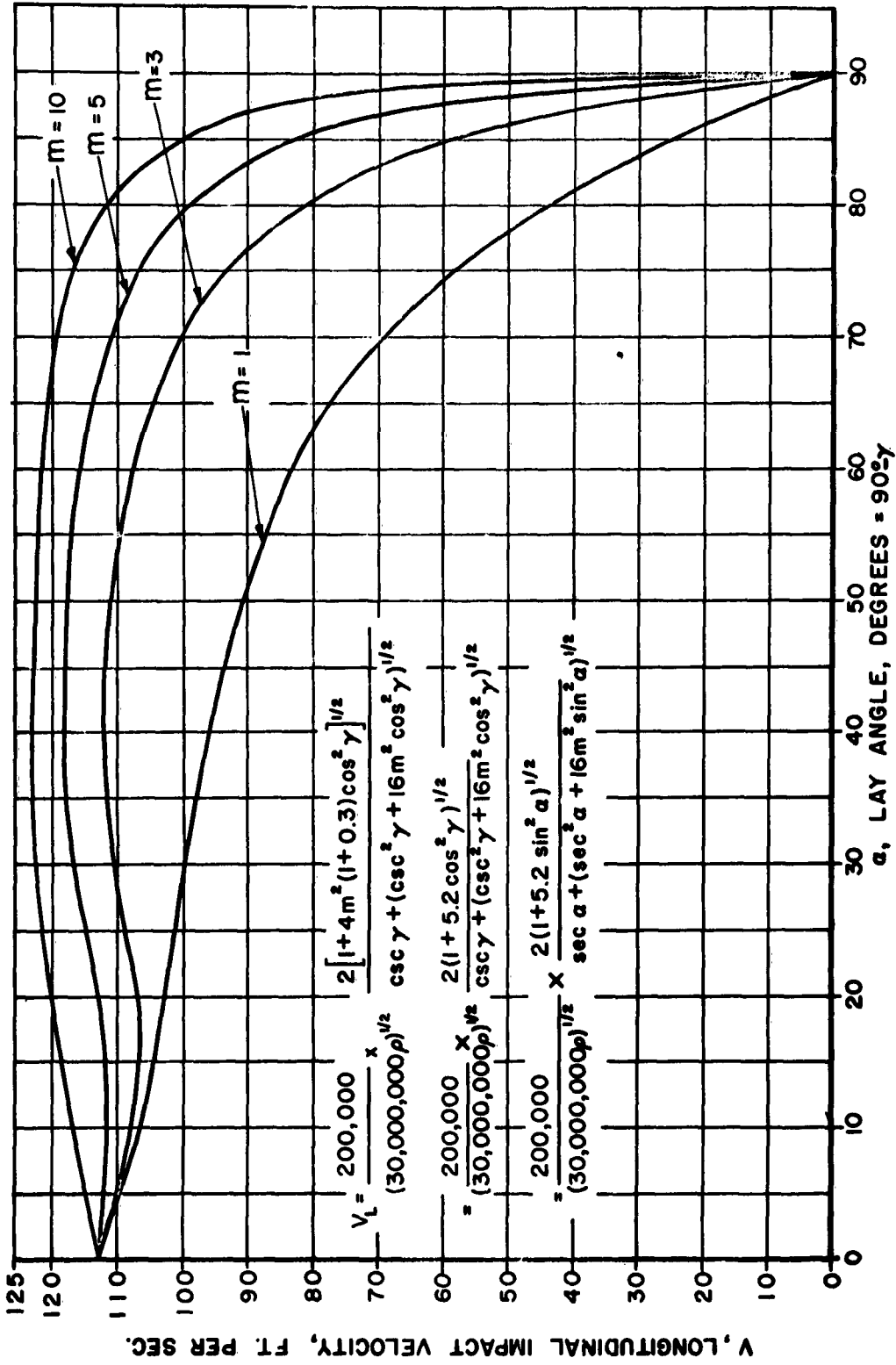
PLOW STEEL RADIALLY SUPPORTED HELIX
LONGITUDINAL IMPACT VELOCITY vs. LAY ANGLE

Figure 9

$$V_L = \frac{200,000}{(30,000,000\rho)^{1/2}} \times \frac{2\left[1+4m^2(1+0.3)\cos^2\gamma\right]^{1/2}}{\csc\gamma+(\csc^2\gamma+16m^2\cos^2\gamma)^{1/2}}$$

$$= \frac{200,000}{(30,000,000\rho)^{1/2}} \times \frac{2(1+5.2\cos^2\gamma)^{1/2}}{\csc\gamma+(\csc^2\gamma+16m^2\cos^2\gamma)^{1/2}}$$

$$= \frac{200,000}{(30,000,000\rho)^{1/2}} \times \frac{2(1+5.2\sin^2\alpha)^{1/2}}{\sec\alpha+(\sec^2\alpha+16m^2\sin^2\alpha)^{1/2}}$$

α, LAY ANGLE, DEGREES = $90^\circ - \gamma$

V, LONGITUDINAL IMPACT VELOCITY, FT. PER SEC.
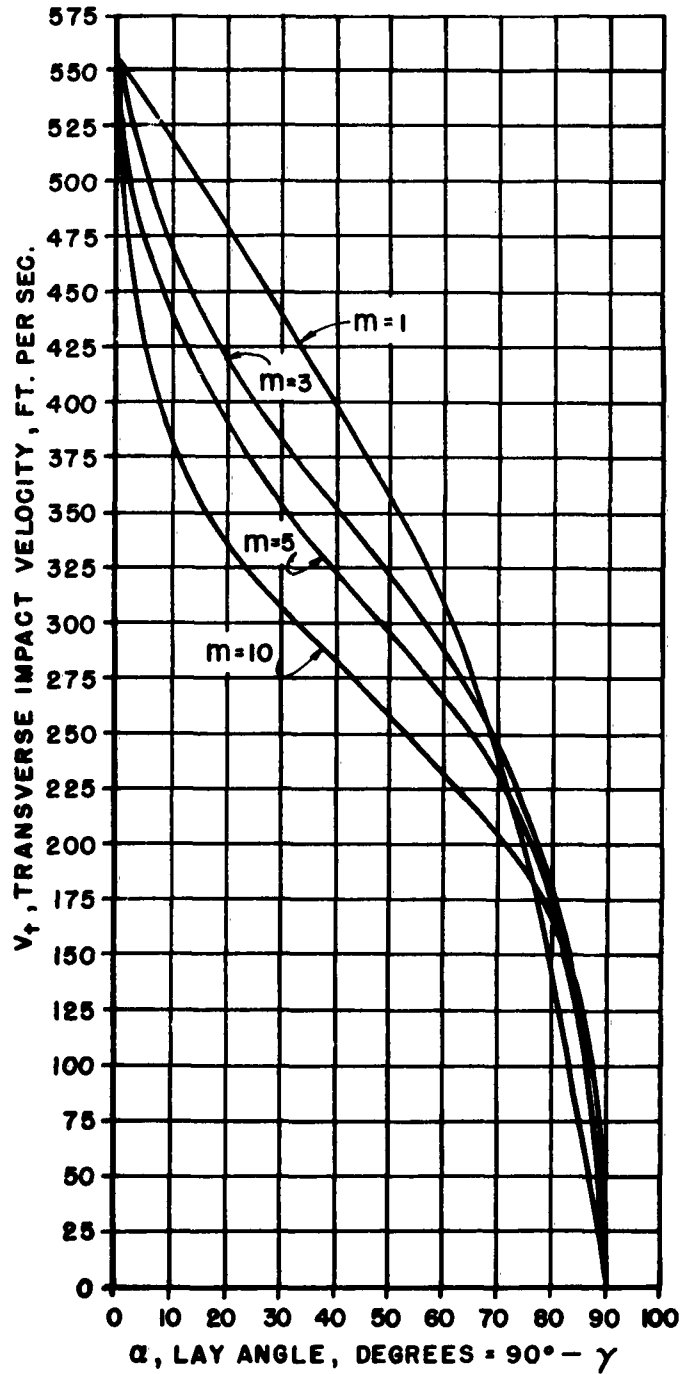
RADIALLY SUPPORTED HELIX
200,000 PSI STEEL

TRANSVERSE IMPACT
VELOCITY vs. LAY ANGLE

Figure 10

26

For convenience the ratios of the velocities to the material factors are once more plotted as a function of α as was done for the unsupported helical spring model. Figures 11 and 12 show these curves which are, as in the previous case, based on the presumption that because the material parameter, ν, does not possess a wide enough range of possible variations, it will not significantly affect the ratio figures plotted for $\nu = 0.3$.

RADIALLY SUPPORTED HELIX

$\dfrac{V_L}{K_L}$ vs. LAY ANGLE

Figure 11

$$\frac{V_t}{K_t} = \frac{\left[8\sin\gamma(1+5.2\,m^2\cos^2\gamma)\right]^{1/4}}{\left[\csc\gamma+(\csc^2\gamma+16m^2\cos^2\gamma)^{1/2}\right]^{3/4}}$$

$$= \frac{\left[8\cos\alpha(1+5.2\,m^2\sin^2\alpha)\right]^{1/4}}{\left[\sec\alpha+(\sec^2\alpha+16m^2\sin^2\alpha)^{1/2}\right]^{3/4}}$$

m=1

m=3

m=5

m=10

a, LAY ANGLE, DEGREES $= 90° - \gamma > 0°$
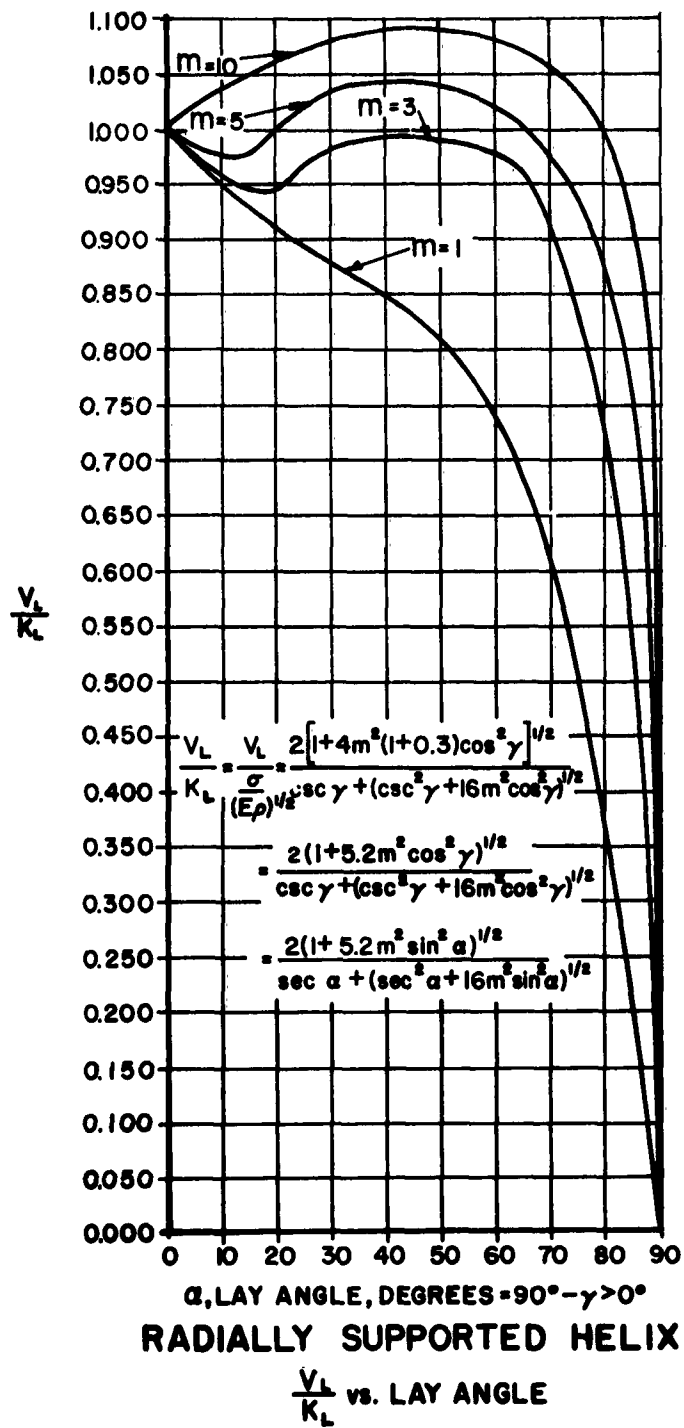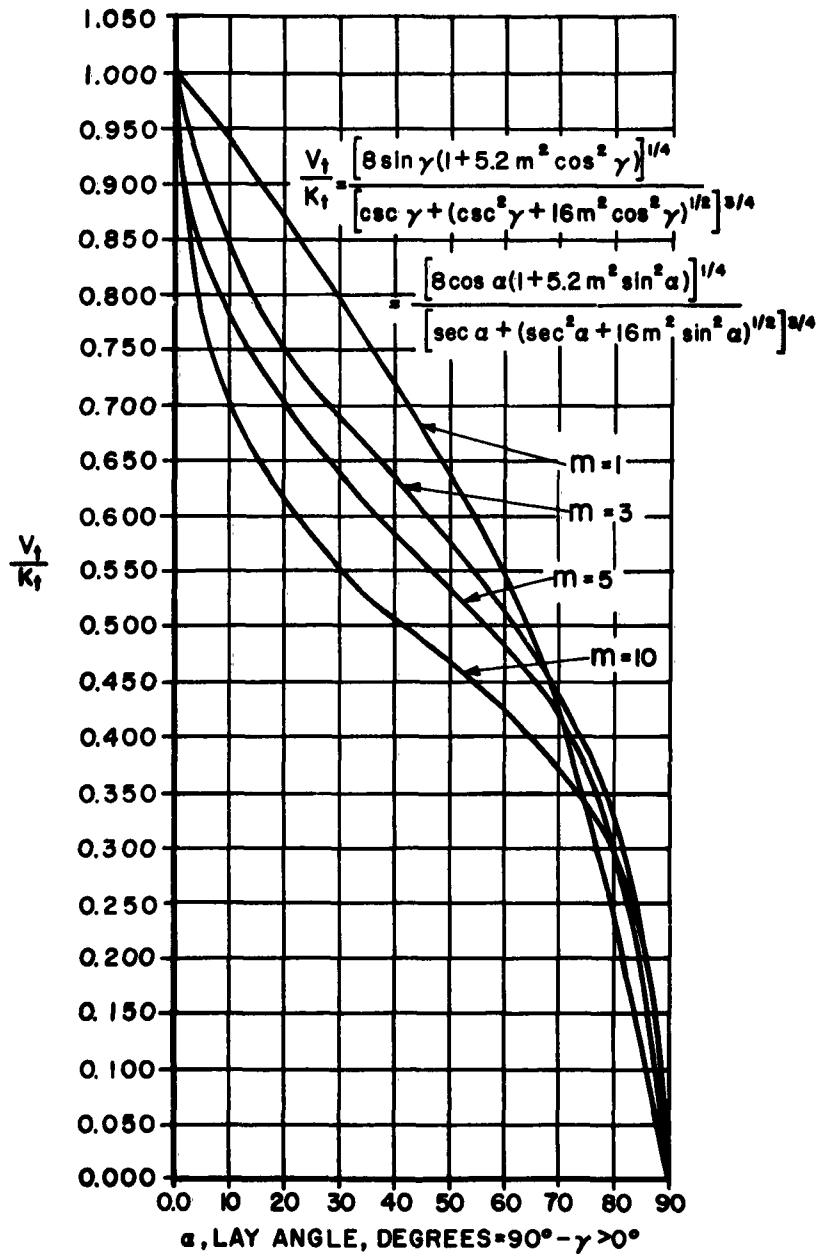
RADIALLY SUPPORTED HELIX

$\dfrac{V_t}{K_t}$ vs. LAY ANGLE

Figure 12

29

SECTION 3

STUDY OF MATERIAL PARAMETERS

3.0 General Considerations

Methods of analysis for linear materials were presented in Reference 1 and specific cases were analyzed for transverse and longitudinal impacts. For linear materials, the longitudinal impact is given by,

$$v_{\ell} = c \, \epsilon_{max}$$

and for transverse impacts is, from Equation 2.2.1 in Reference 2.

$$v_t = c \left\{ \epsilon_{max}(1 + \epsilon_{max}) - \left[\sqrt{\epsilon_{max}(1 + \epsilon_{max})} - (\epsilon_{max} - \epsilon_o) \right]^2 \right\}^{1/2}$$

where ϵ_{max} is the strain of the material at maximum tension.

The following sections develop similar analytical procedures for determining the impact tolerance for nonlinear materials. The general procedure is presented and the results of several materials are given; sample calculations are included in Appendix B.

The maximum longitudinal and transverse impact tolerances for several linear materials are presented in Table I. These values were calculated using manufactuer's data and other information of a general nature for the particular material being investigated. These predicted impact tolerances were evaluated for the purpose of comparison so as to select the materials indicating outstanding impact tolerance properties. It will be noticed

30

TABLE I

SOME PROPERTIES OF TYPICAL LINEAR MATERIALS

Material	σ (psi)	$\sigma^{3/4}$	E (psi)	$E^{1/2}$	$E^{1/4}$	w (lbs/cu in)	$\rho = \dfrac{w}{386}$ (lb-sec²/in⁴)	$\rho^{1/2}$	$E^{1/2}\rho^{1/4}$	$E^{1/4}\rho^{1/4}$	$\dfrac{\sigma}{E^{1/2}\rho^{1/2}}$ in./sec.	$\dfrac{\sigma^{3/4}}{E^{1/4}\rho^{1/2}}$ in./sec.	$\dfrac{\sigma^{3/4}}{E^{1/4}\rho^{1/2}}$ ft./sec.	v_ℓ(fps) $\dfrac{\sigma}{E^{1/2}\rho^{1/2}}$	v_c(fps) $\dfrac{\sqrt{2}(\sigma)^{3/4}}{E^{1/4}\rho^{1/2}}$
Steel Alloy 98B7140	190,000	7,610	29,000,000	5390	73.4	0.283	0.000733	0.0271	146	1.999	1,026	3,823	319	85	451
Stainless Steel PH 15-7 MoRh 950	225,000	10,330	29,000,000	5390	73.4	0.277	0.000717	0.0268	144	1.966	1,562	5,252	438	130	619
Beryllium Copper	200,000	9,450	18,400,000	4290	65.5	0.297	0.000773	0.0278	119	1.82	1,680	5,190	433	140	612
Aluminum	24,000	1,930	10,000,000	3160	56.2	0.098	0.000254	0.0159	50.2	0.894	478	2,158	180	40	254
Inconel	105,000	5,840	31,000,000	5570	74.6	0.307	0.000795	0.0282	157	2.103	668	2,786	232	56	328
High Tension Fortisan (Saponified Acetate Rayon)	138,000	7,160	3,553,000	1885	43.42	0.0556	0.000144	0.012	22.6	0.4263	6,110	16,790	1,399	508	1,979
Magnesium	51,000	3,390	6,500,000	2550	50.5	0.0648	0.0001625	0.01275	32.5	0.644	1,570	5,263	439	131	620
Monel	170,000	8,370	26,000,000	5100	71.4	0.319	0.000826	0.0287	146	2.048	1,165	4,099	341	97	482
Fiberglas	250,000	11,180	10,730,000	3280	55.8	0.0917	0.0002377	0.01542	50.6	0.861	4,940	12,990	1,082	411	1,530
Titanium Alloy 13V-11Cr-3Al	200,000	9,450	15,500,000	3940	62.7	0.163	0.000422	0.0205	80.8	1.285	2,475	7,360	614	206	868
Titanium Alloy 4Al-4Mn	140,000	7,240	15,500,000	3940	62.7	0.163	0.000422	0.0205	80.8	1.285	1,730	5,138	428	144	605
Improved Plow Steel	240,000	10,850	29,000,000	5390	73.4	0.283	0.000733	0.0271	146	1.999	1,643	5,460	455	137	643
Plow Steel	180,000	8,795	29,000,000	5390	73.4	0.283	0.000733	0.0271	146	1.999	1,232	4,400	369	103	521
High Tensile Steel	500,000	19,000	29,000,000	5390	73.4	0.283	0.000733	0.0271	146	1.999	3,425	9,570	797	285	1,129

that Fiberglas and Fortisan showed properties superior to the metallic materials for both longitudinal and transverse impacts.

3.1 Analysis of Nonlinear Materials

As pointed out in Reference 2, Appendix A, Page 101, the velocity of propagation of a singularity in a cable depends on the slope of a line joining two points on its ension-strain curve. If this curve is nonlinear, then a second singularity might either overtake the first or fall further behind it, depending on their relative velocities. In general, a longitudinal wave would not propagate undistorted if the tension-strain relation is nonlinear. It is the purpose of the present investigation to study the effects of this nonlinearity on the ability of a cable to tolerate impact velocities.

The fundamental relationships to be employed in the treatment of non-linear materials were developed in Reference 2 which, except for specific cases, were not restricted to linear materials. The present analysis requires that a technique for treating the variation in the propagation velocity of a longitudinal singularity, which characterizes a nonlinear material, be formulated. This technique is then applied to a study of several materials exhibiting nonlinear properties. The materials involved in this presentation are as follows:

1. Stainless Steel (7 x 19 E.A. Cable)   5. Cotton 12/1

2. Nylon 300   6. Polyethylene

3. Silk   7. Wool

4. Cotton 50/1   8. Fortisan 36

3.1.1 Longitudinal Impact Velocity

This phase of the present study is concerned with the longitudinal impact velocity tolerance of a tension member constructed from material exhibiting nonlinear stress-strain properties. Because the preliminary studies of Section 2 relate the geometrical configurations with corresponding impact tolerances, the tension members now considered are treated without regard to configuration. Starting with an available tension-strain or stress-strain diagram, or a tenacity (strength per unit weight or T/μ) versus strain diagram for fibrous materials, the procedure begins with a tabulation of the data presented by the curve, using suitable strain increments. The equations for evaluating the velocity of propagation of a longitudinal singularity, as derived in Reference 2, are presented to illustrate their application.

$$c^2 = \frac{1}{\mu} \frac{T_2 - T_1}{\epsilon_2 - \epsilon_1} = \frac{1}{\mu} \frac{dT}{d\epsilon} = \frac{1}{\rho} \frac{d\sigma}{d\epsilon} \qquad (3.1)$$

$$u = \int_{\epsilon_0}^{\epsilon} c_\epsilon \, d\epsilon = \int_{\epsilon_0}^{\epsilon} \left(\frac{\frac{dT}{d\epsilon}}{\mu} \right)^{1/2} d\epsilon = \int_{\epsilon_0}^{\epsilon} \left(\frac{\frac{d\sigma}{d\epsilon}}{\rho} \right)^{1/2} d\epsilon \qquad (3.2)$$

Since u is equal to the longitudinal velocity of impact, the **maximum** velocity u is the longitudinal impact tolerance of the member.

As is indicated by the expression for determining c in Equation (3.1), the slope along the tension-strain curve between two points must be measured or calculated. In order to facilitate this operation, the curves are approximated, where practical, by analytic expressions with the aid of a log-log or semi-log plot. This process is illustrated in Figures 14, 20,

33

and 61. The equations obtained are then differentiated to obtain their slopes. Where this method is not practical to apply, methods of graphical differentiation can be used to determine the slopes. The value of c at each desired value of strain is then calculated with Equation (3.1) and the data tabulated for each strain value, using convenient intervals of strain.

The value of u (cable velocity) as indicated in Equation (3.2), is equal to the summation of the products of c and $\Delta \epsilon$, which is the area under the c versus ϵ curve. In the case where the stress-strain curve is an explicit equation, the value of u is obtained by integrating the equation resulting from the solution for c of the explicit stress-strain equation. In the case where graphical methods of differentiation are used to determine c at each increment point, the value of u is obtained by an accumulative summation of the individual areas, as measured or approximated for each increment of strain. The maximum value of u for a tension member as found and tabulated above will represent the longitudinal impact tolerance of the particular material.

There is, however, a special condition which arises whenever the stress-strain curve is, or becomes, concave upwards (see Figure 21, page 48, for example of curves which are concave upwards). If the slope at each increment of such a curve is used in Equation (3.1), the procedure leads to the anomalous condition that during the loading process the points of higher strain are moving faster than those of lower strain; a point would have both high and low strains simultaneously since the higher velocity wave would overtake the slower. The physical impossiblity of two strain levels existing

34

at the same point at the same time precludes the use of the slope at each point along the original curve. The effective slope at any point along the curve cannot exceed the value of the slope of the secant which is drawn so as to linearize the concave section of the curve up to the point in question as shown in Figure 21, page 48. The values of the slope of these secant lines are then used in Equation (3.1) for finding the values of c at each of the points.

It is tacit in the above analysis that the stress-strain curve of the material is predicated upon dynamic conditions if high-order accuracy of the results is required. However, if static moduli are used, as was always the case in this report, then lower impact tolerance predictions are likely to result because static test conditions usually indicate a lower ultimate stress than dynamic tests, which, from the standpoint of material selection, is conservative.

3.1.2 Transverse Impact Velocity

This section of the investigation is concerned with the determination of the transverse impact tolerance in a nonlinear tension member. Since the transverse impact conditions generate an additional transverse wave disturbance or kink, both the longitudinal impact velocity (u) and the velocity (c*) of the kink must be determined in order to evaluate the transverse impact velocity. Equation (3.2) of Section 3.1.1 and Equation (A.20) of Reference 2 are used in this investigation and are listed now for convenience.

$$u = \int_{\epsilon_o}^{\epsilon} c_\epsilon \, d\epsilon$$

$$(c^*)^2 = \frac{T}{\mu} (1 + \epsilon) = \frac{\sigma}{\rho} (1 + \epsilon) \tag{3.3}$$

where ϵ can assume any value within the limitations of a particular material.

When the strain ϵ in equation 3.3 is the maximum strain (ϵ_i) produced by the impact, two cases can occur in the evaluation of the kink velocity $c^*(\epsilon_i)$. One case is that when $c^* \leq c$ and the other case is where $c^* > c$. The value of the strain ϵ which satisfies the relationship $c^* = c$ is defined as $\epsilon^{\circledast}$. The value of c^* and c at strain $\epsilon^{\circledast}$ is defined as $c^{\circledast}$ and the value of u at strain $\epsilon^{\circledast}$ is defined as $u^{\circledast}$.

Under the initial impact conditions the kink velocity $c^*(\epsilon_i)$ for any strain ϵ_i (even $\epsilon_i > \epsilon^{\circledast}$) cannot exceed $c^{\circledast}$, so that the value of c^* in terms of ϵ_i is given by the following bounded relationship:

$$(c^*)^2 = \begin{cases} \dfrac{T}{\mu}(1+\epsilon_i) = \dfrac{\sigma}{\rho}(1+\epsilon_i) & \text{when } \epsilon_i \leq \epsilon^{\circledast} \\ (c^{\circledast})^2 & \text{when } \epsilon_i > \epsilon^{\circledast} \end{cases} \qquad (3.4)$$

From Equation $(2.2.1)$ in Reference 2, the following equation for the transverse impact velocity v_t was developed for the case $c^* \leq c$:

$$v_t^2 = (c^*)^2 - \left\{ c^* \cos\left[\beta - \frac{\pi}{2} + \arccos \frac{(c^* - u)\sin\beta}{c^*} \right] \right\}^2 \qquad (3.5)$$

When $c^* > c$, in which case $c^*(\epsilon_i) = c^{\circledast}$ (see Equation 3.4), the value of v_t is given by the equation

$$v_t^2 = (c^{\circledast} + u - u^{\circledast})^2 - \left\{ (c^{\circledast} + u - u^{\circledast}) \cos\left[\beta - \frac{\pi}{2} + \arccos \frac{(c^{\circledast} - u^{\circledast})\sin\beta}{c^{\circledast} + u - u^{\circledast}} \right] \right\}^2 \qquad (3.6)$$

For $\beta = \pi/2$, Equation (3.5) and Equation (3.6) become
$$v_t^2 = (c^*)^2 - (c^* - u)^2 \text{ and}$$
$$v_t^2 = (c^{\circledast} + u - u^{\circledast})^2 - (c^{\circledast} - u^{\circledast})^2 \text{ respectively.}$$

The procedure outlined under Section 3.1.1 will be used to evaluate u and $u^\oplus$, which are needed to arrive at an evaluation of v_t, the transverse impact velocity, as indicated in the equations listed above. Having found u and $u^\oplus$ it remains only to find c^* and $c^\oplus$ from Equation (3.4). This value of c^* or $c^\oplus$ is then used to determine the value of $c^* - u$ or $c^\oplus - u^\oplus$ and $c^\oplus + u - u^\oplus$ and these calculated items are substituted in Equation (3.5) or Equation (3.6) to give values for v_t for corresponding values of ϵ_i. Similar to the determination of u, the longitudinal impact velocity, the v_t at the maximum ϵ_i which the material can sustain is the transverse impact tolerance of the member. Again, the qualification regarding the dynamic stress-strain curve, as pointed out in Section 3.1.1, applies to this present analysis as well.

The choice of Equation (3.5) or Equation (3.6) is predicated on the determination of the value of the strain $\epsilon^\oplus$. Since the kink velocity c^* equals the longitudinal wave velocity c at this particular strain $\epsilon^\oplus$, then the kink will precede the part of the longitudinal wave front corresponding to strains higher than $\epsilon^\oplus$ and this part accordingly will be on the oblique segment of the cable immediately behind the kink. To determine the value of $c^\oplus$ the relationship $c^*(\epsilon^\oplus) = c(\epsilon^\oplus)$ where c^* and c are given by Equations (3.3) and (3.1), must be solved for $\epsilon^\oplus$, either by setting Equation (3.1) equal to Equation (3.3) or graphically by the intersection of the c and c^* curves, depending on the initial method of evaluating the slopes of the stress-strain curve. It might be also noted here that the value of $u^\oplus$ is found by substituting $\epsilon^\oplus$ in Equation (3.2) or by a graphical method, whichever applies.

37

In order to illustrate the procedure and to compare the impact toler-
ance of several materials, a series of graphs are drawn of the following
relationships in Figures 13 through 66, for $\beta = \pi/2$ (perpendicular impact):

1. T/μ (tenacity or strength per unit weight), T, or σ versus ϵ,
    Natural Scale (Also Logarithmic Scale if usable)

2. c and c^* versus ϵ 5. v_t versus T/μ, T, or σ

3. u versus ϵ 6. ϕ versus ϵ

4. v_t versus ϵ

The curves presented in Figures 67 and 68, pages 94 and 95 respectively,
provide further useful comparative information. Impact tolerances are listed
in Table II, page 96.

3.2 Criteria for Selecting Superior Materials

Criteria can be established for determining the impact tolerance of
linear and nonlinear materials for both longitudinal and transverse impacts.
These criteria are now presented.

3.2.1 Linear Materials

For transverse impacts, the relationships developed in Section 2 demon-
strate that for optimum configuration of a straight bar, the maximum trans-
verse impact tolerance reduces to a combination of Equation (2.18) and
Equation (2.22) which, it will be observed, includes only material properties,
as follows:

$$v_t = \frac{2^{1/2}\sigma^{3/4}}{(E\rho^2)^{1/4}} \tag{3.7}$$

38

Equation (3.7) can be used as the criterion for determining the transverse impact tolerance for a linear material when max. $\epsilon < 10\%$.

For longitudinal impacts a combination of Equation (2.17) and Equation (2.21), each developed in Section 2, was used for comparative purposes. It also involves only material properties as follows:

$$v_\ell = \frac{\sigma}{\sqrt{E\rho}} \tag{3.8}$$

The above equation does not produce the maximum longitudinal impact tolerance because the straight bar configuration which it represents is not the optimum configuration for longitudinal impact conditions. However, it can be used for purposes of comparison because geometrical parameters are independent of material and affect all materials equally. Consequently, the optimum configuration would be the same for all materials, and a comparison between different materials of the same configuration other than optimum would reflect exactly the corresponding comparison between the same materials in their optimum configuration, i.e., a comparison between their maximum longitudinal impact tolerances.

3.2.2 Nonlinear Materials

For both longitudinal and transverse impacts with nonlinear materials, relative superiority can be found by comparing v_t or u by means of the analytical methods discussed in Section 3.1.2. Unfortunately, no simple analytical criterion is available for determining the relative impact tolerances for nonlinear materials, and the numerical procedures described in Section 3.1 must be employed.

7 x 19 STAINLESS STEEL WIRE ROPE
TENSION vs. STRAIN
Figure 13

7 x 19 STAINLESS STEEL WIRE ROPE
TENSION vs. STRAIN

$T_s = 2380$

$T_2 = 2,800\ \epsilon^{0.18}$

$T_1 = 200,000\ \epsilon$

T (TENSION) LBS.

10,000
9
8
7
6
5
4
3
2
1,000
9
8
7
6
5
4
3
2
100
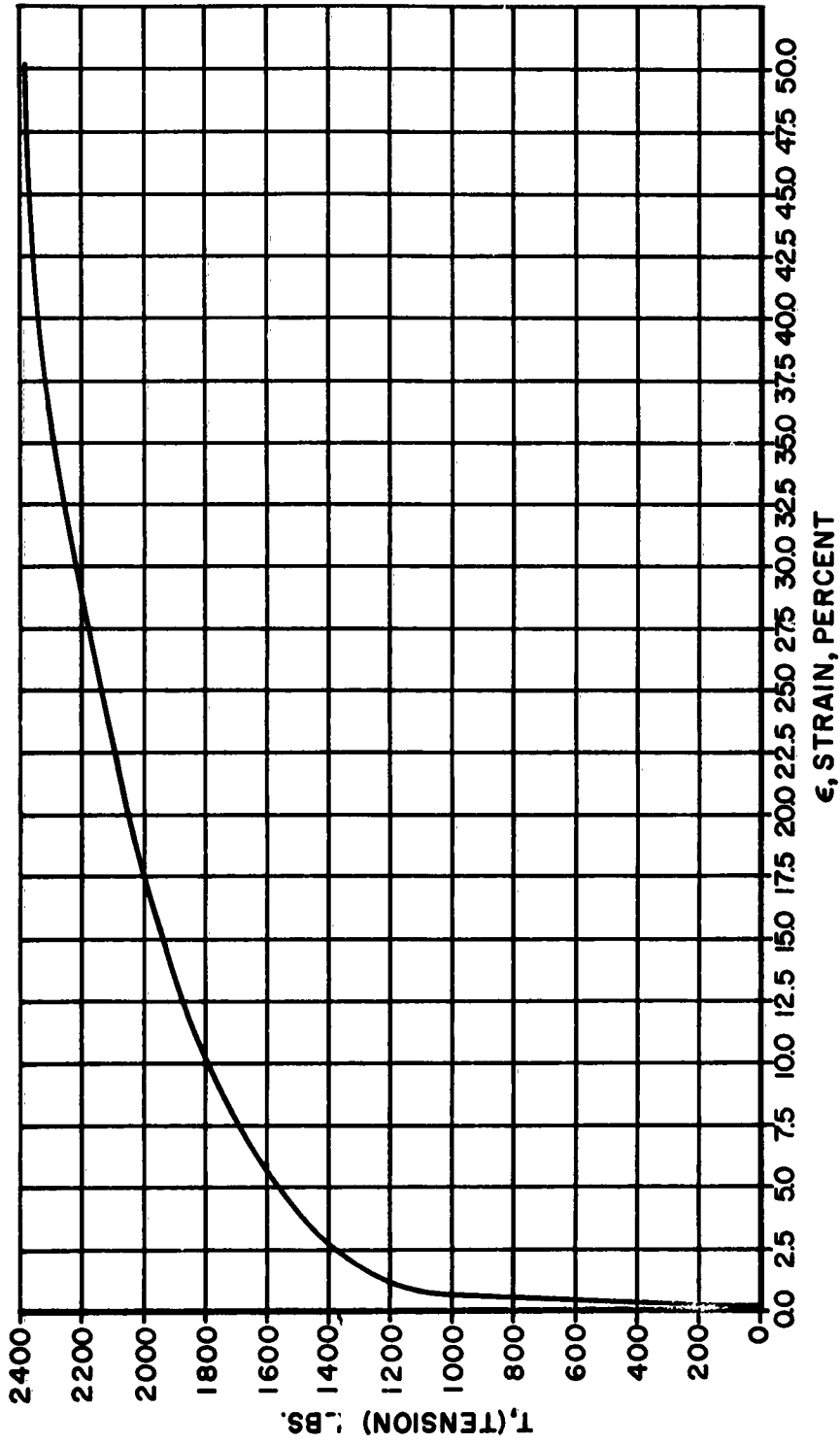
ϵ (STRAIN)

Figure 14

7x19 STAINLESS STEEL WIRE ROPE
SONIC & KINK VELOCITIES vs. STRAIN
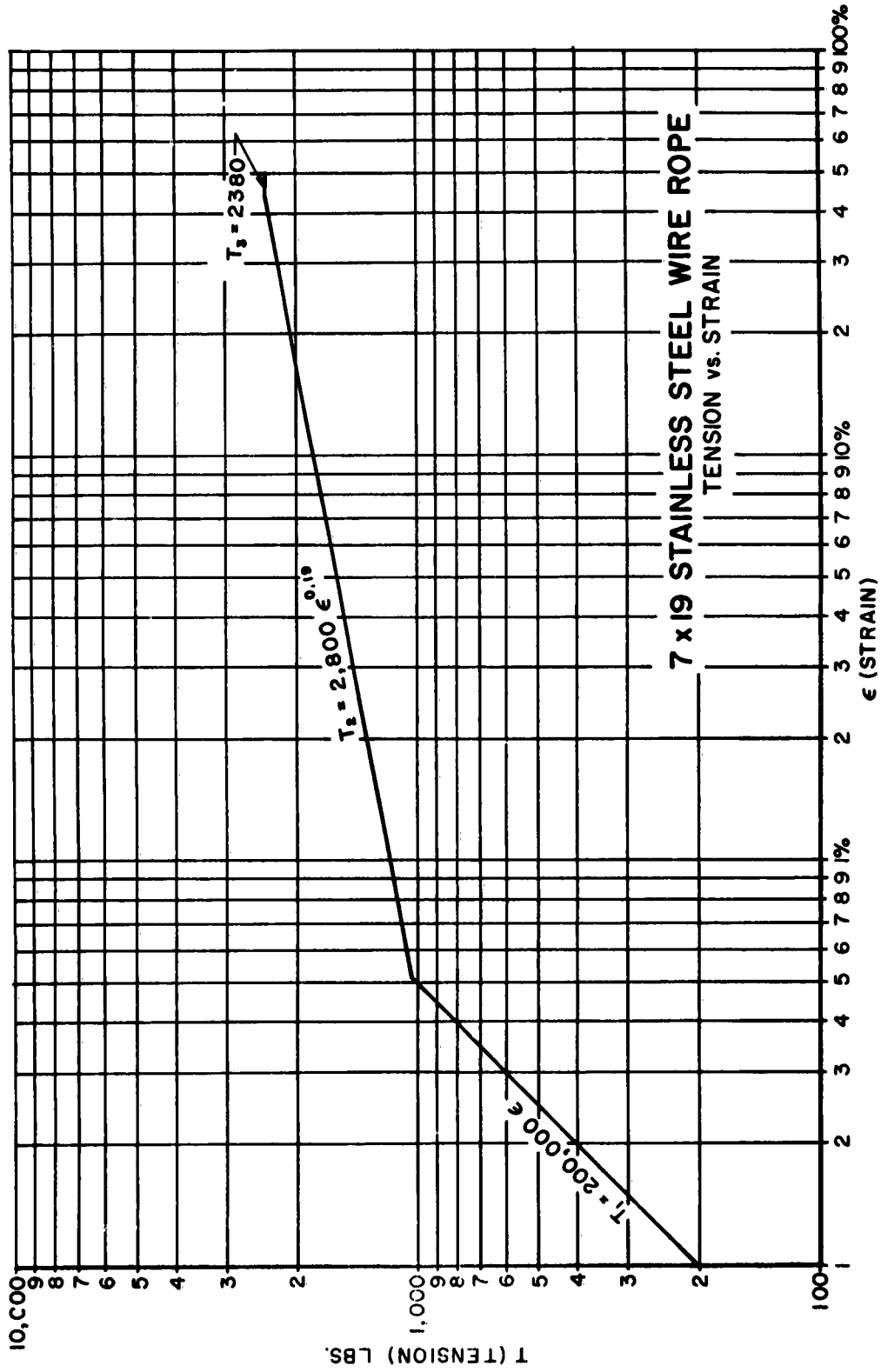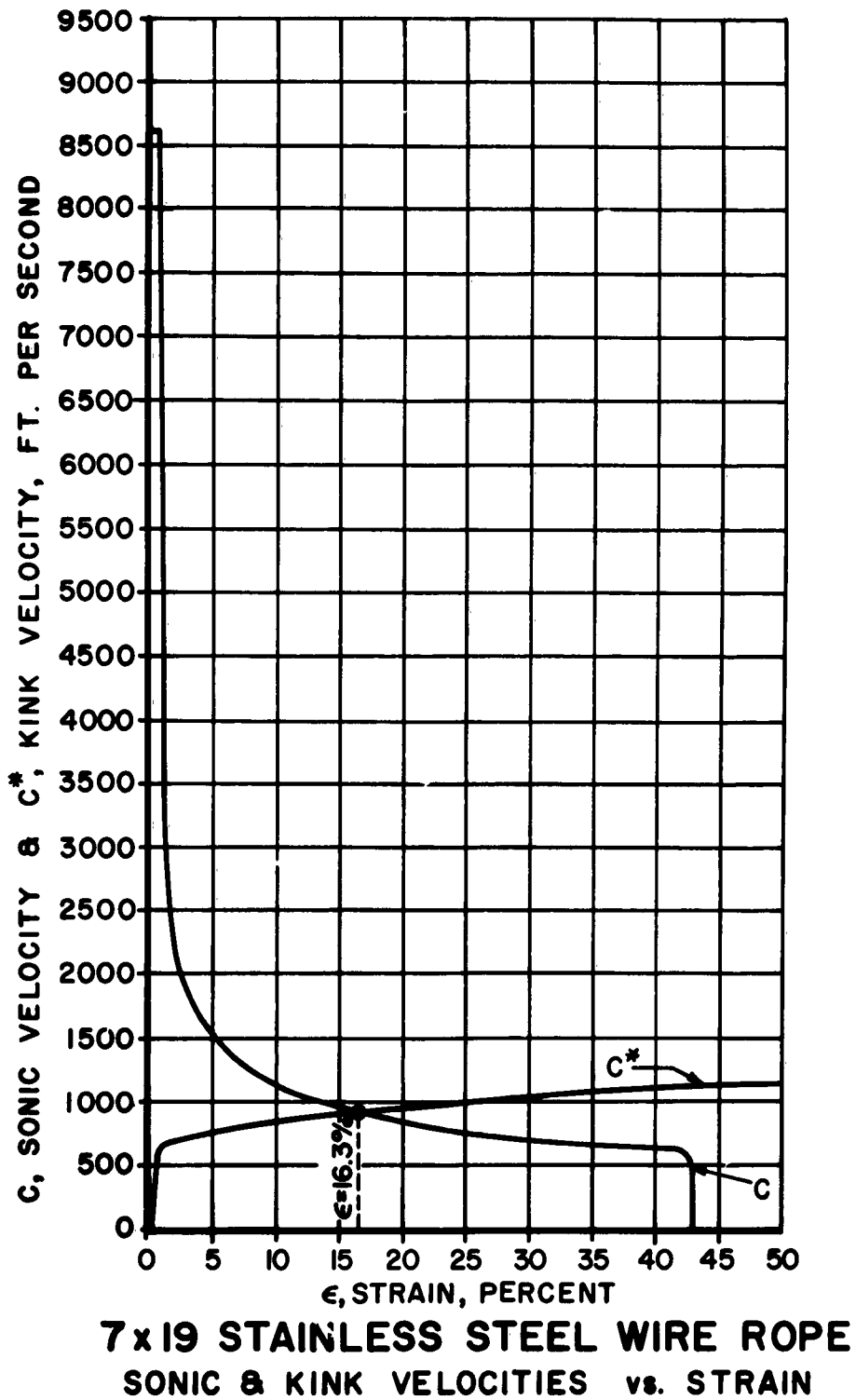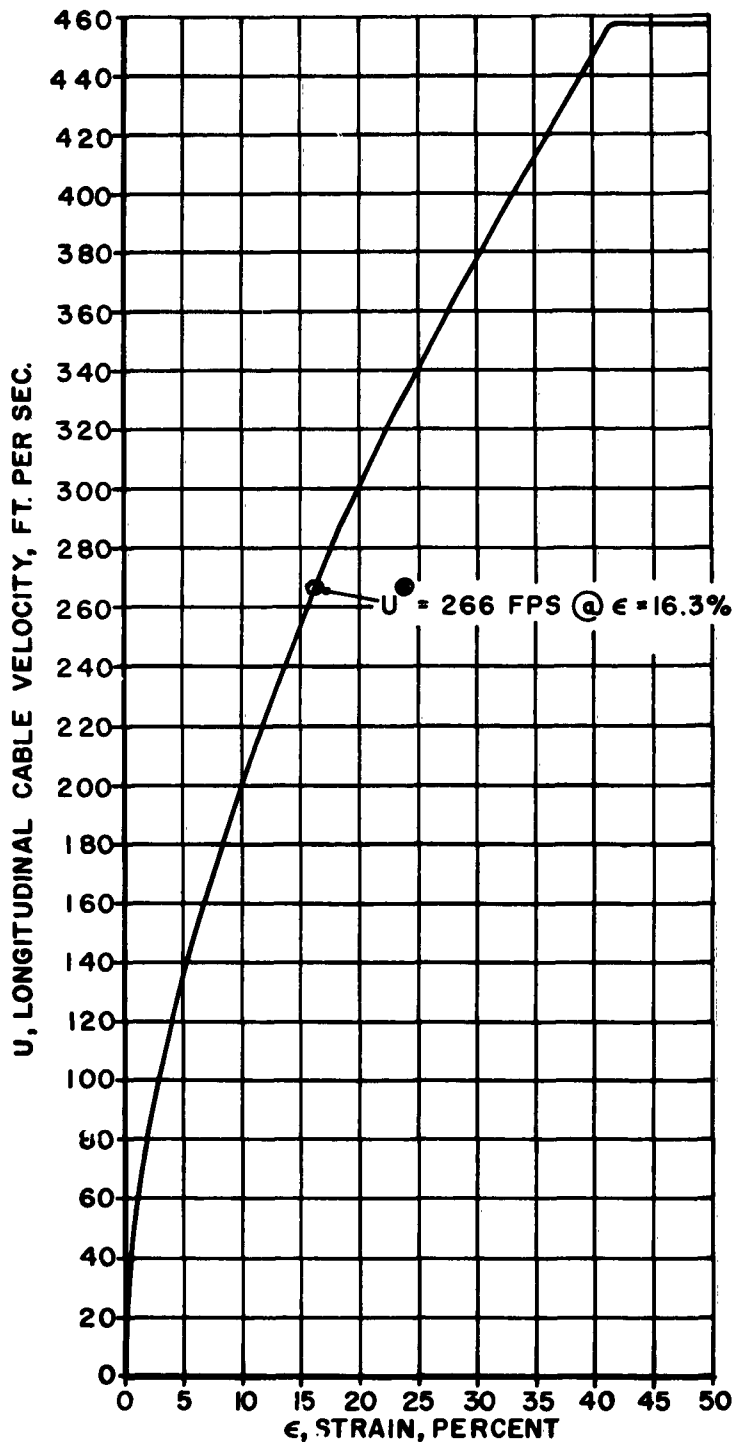
Figure 15

7 x 19 STAINLESS STEEL WIRE ROPE
LONGITUDINAL CABLE VELOCITY vs. STRAIN

Figure 16
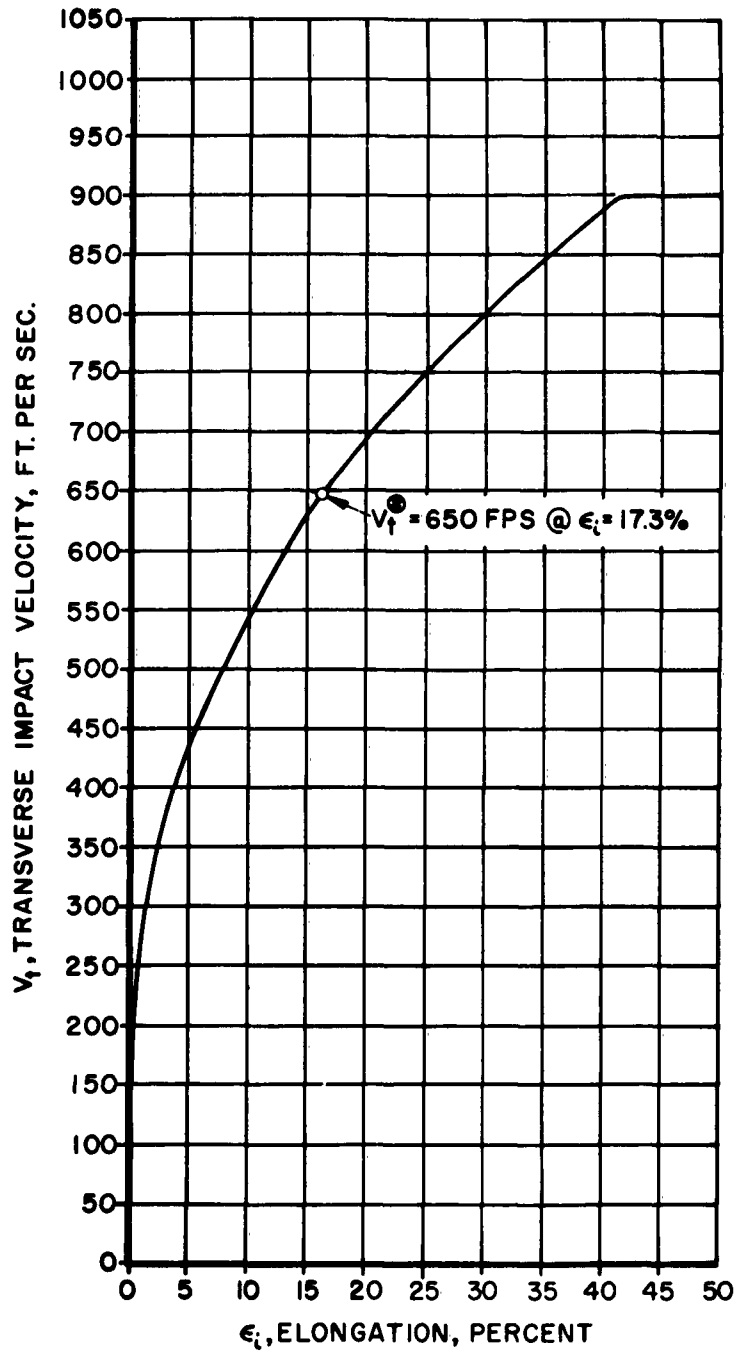
7 x 19 STAINLESS STEEL WIRE ROPE
TRANSVERSE IMPACT VELOCITY vs. STRAIN

Figure 17

7 x 19 STAINLESS STEEL WIRE ROPE
TRANSVERSE IMPACT VELOCITY vs. TENSION

Figure 18

$\phi^{\circledR} = 44\frac{1}{2}° @ \epsilon_i = 0.163$
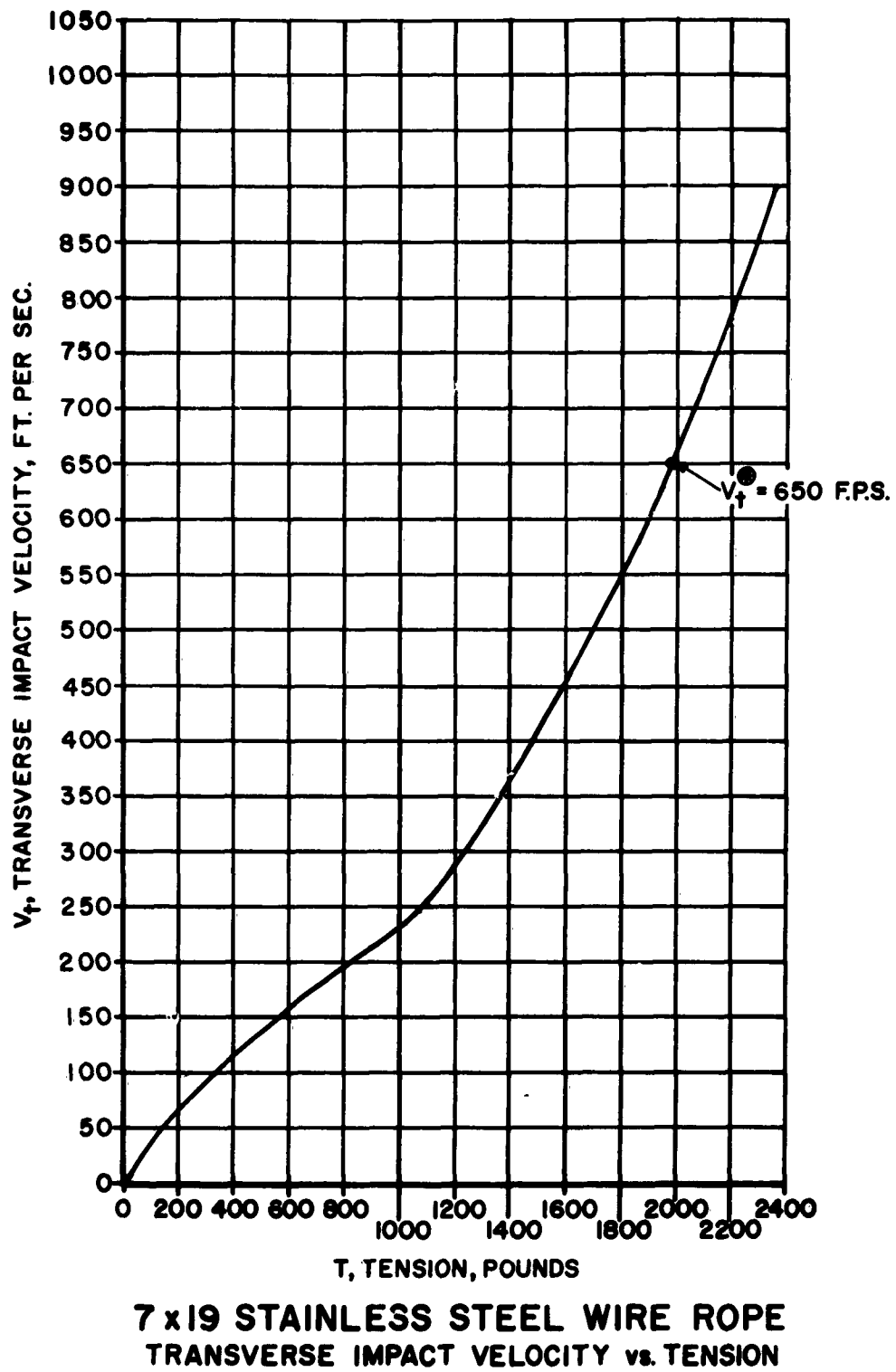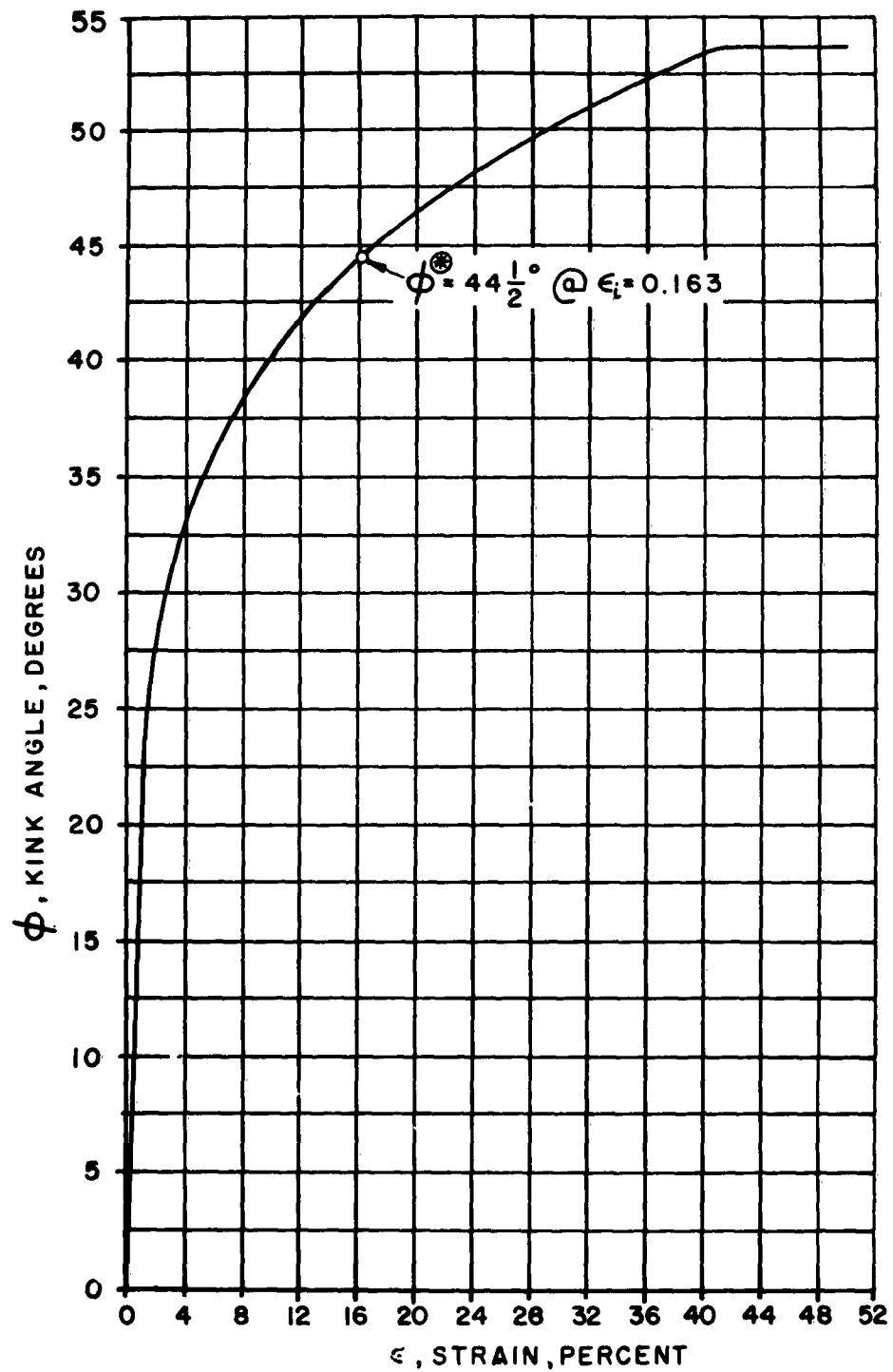
7/32"- 7 x 19 E.A. STAINLESS STEEL WIRE ROPE
KINK ANGLE VS. STRAIN

Figure 19
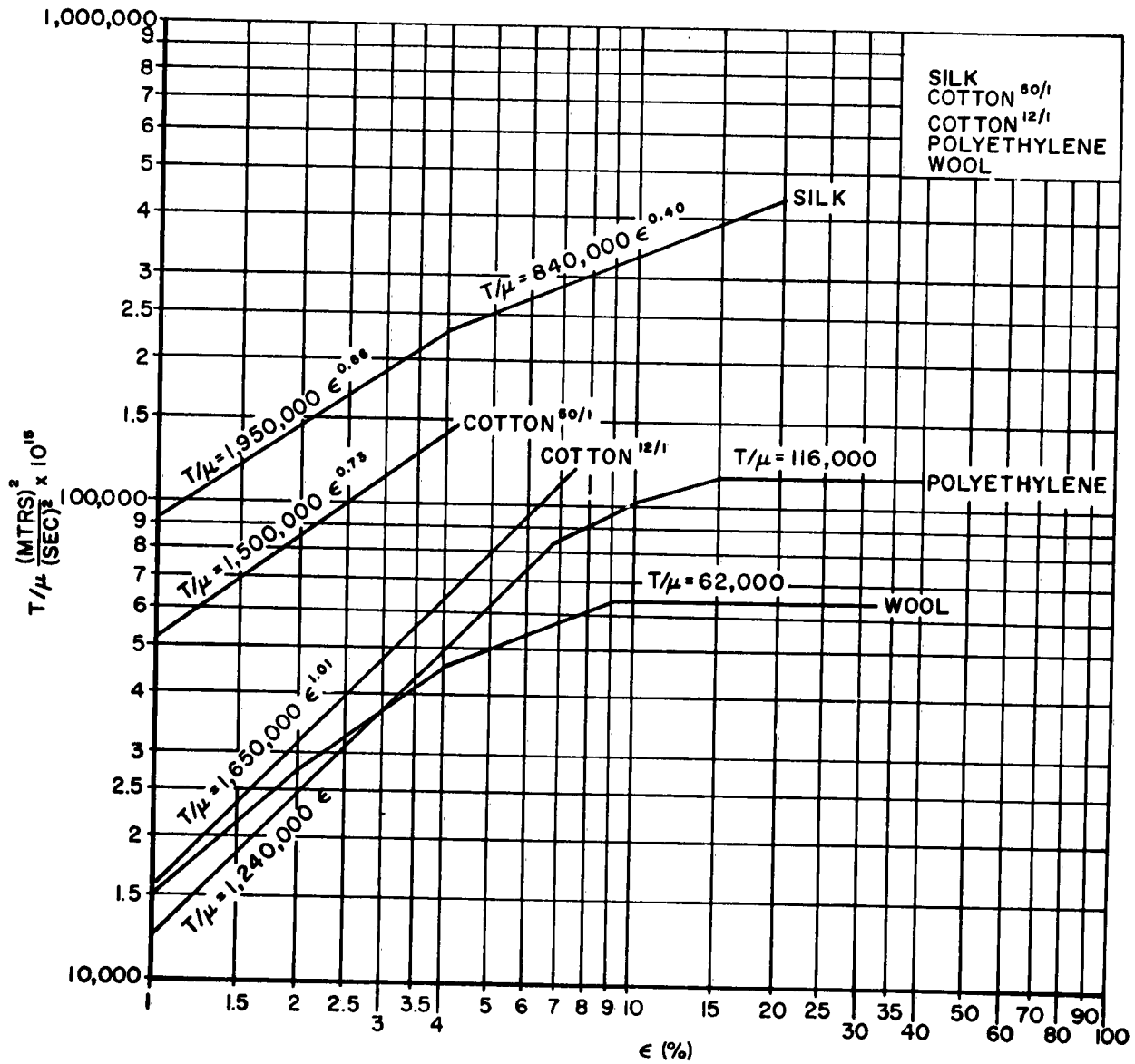
STRESS – STRAIN CURVES (LOG-LOG)
@ 21°C. (70°F.) & 65% R.H.

Figure 20

47
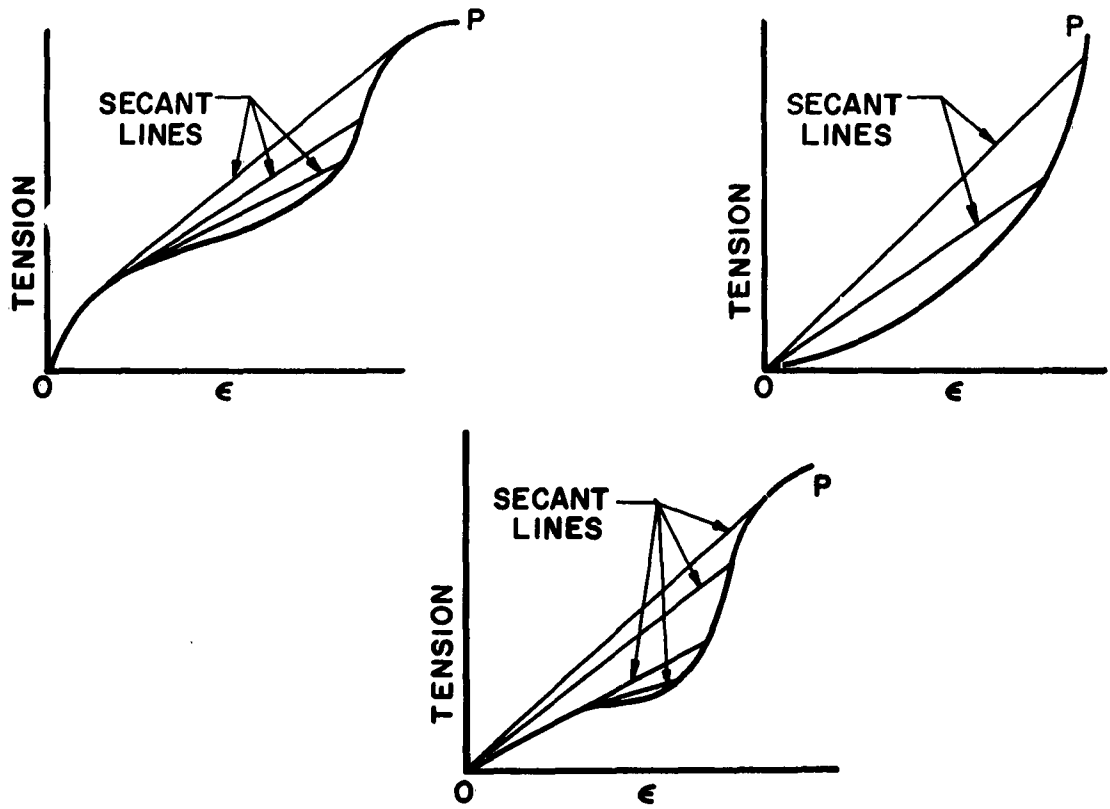
Figure 21

Secant Slope Lines for Typical Concave-Up Stress-Strain Diagrams

NYLON 300
TENACITY vs. STRAIN
@ 21°C. & 65% R.H.

Figure 22

NYLON 300
TENACITY vs. STRAIN
@ 21°C. & 65% R.H.

Figure 23

NYLON 300
SONIC & KINK VELOCITIES vs. STRAIN
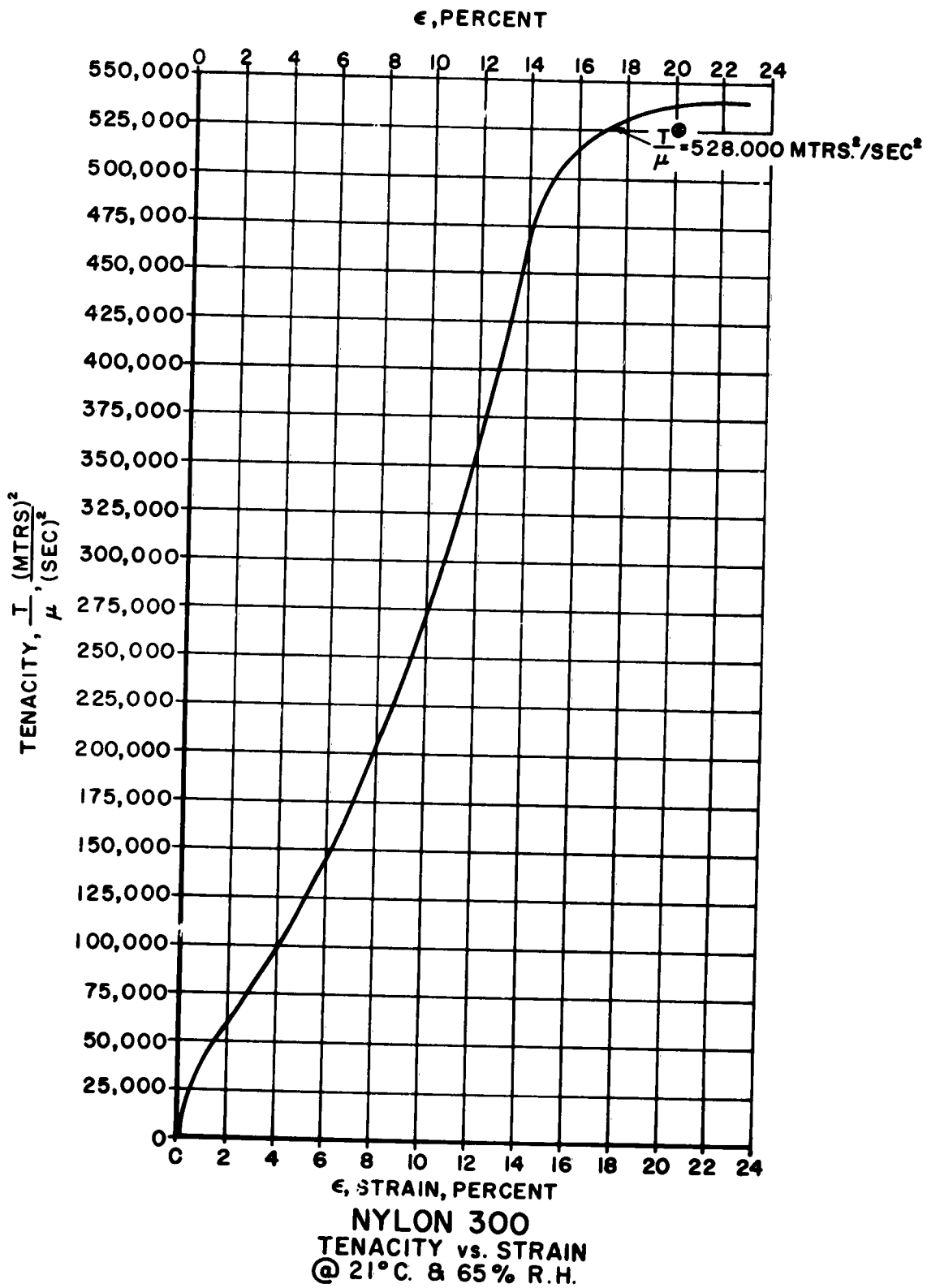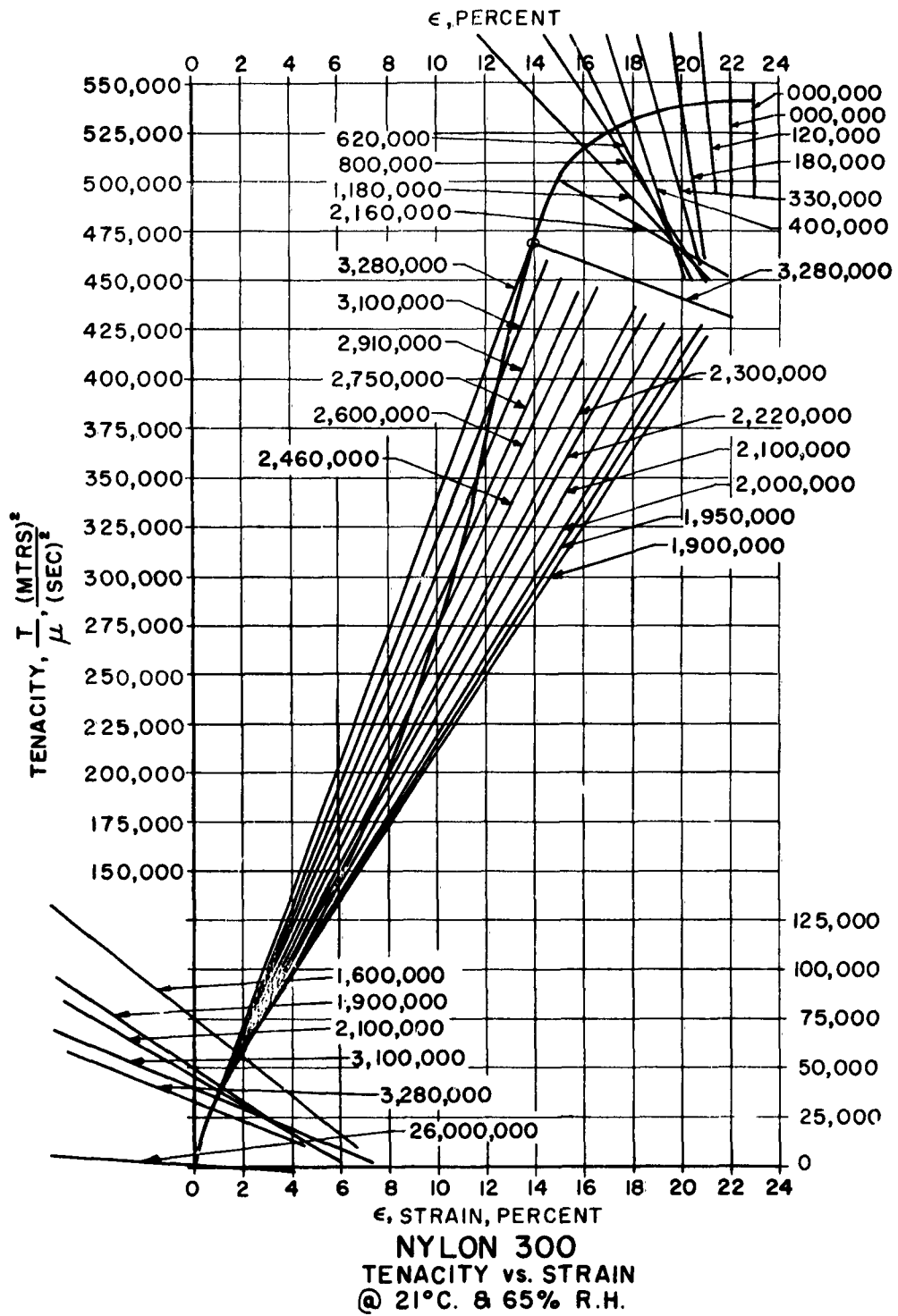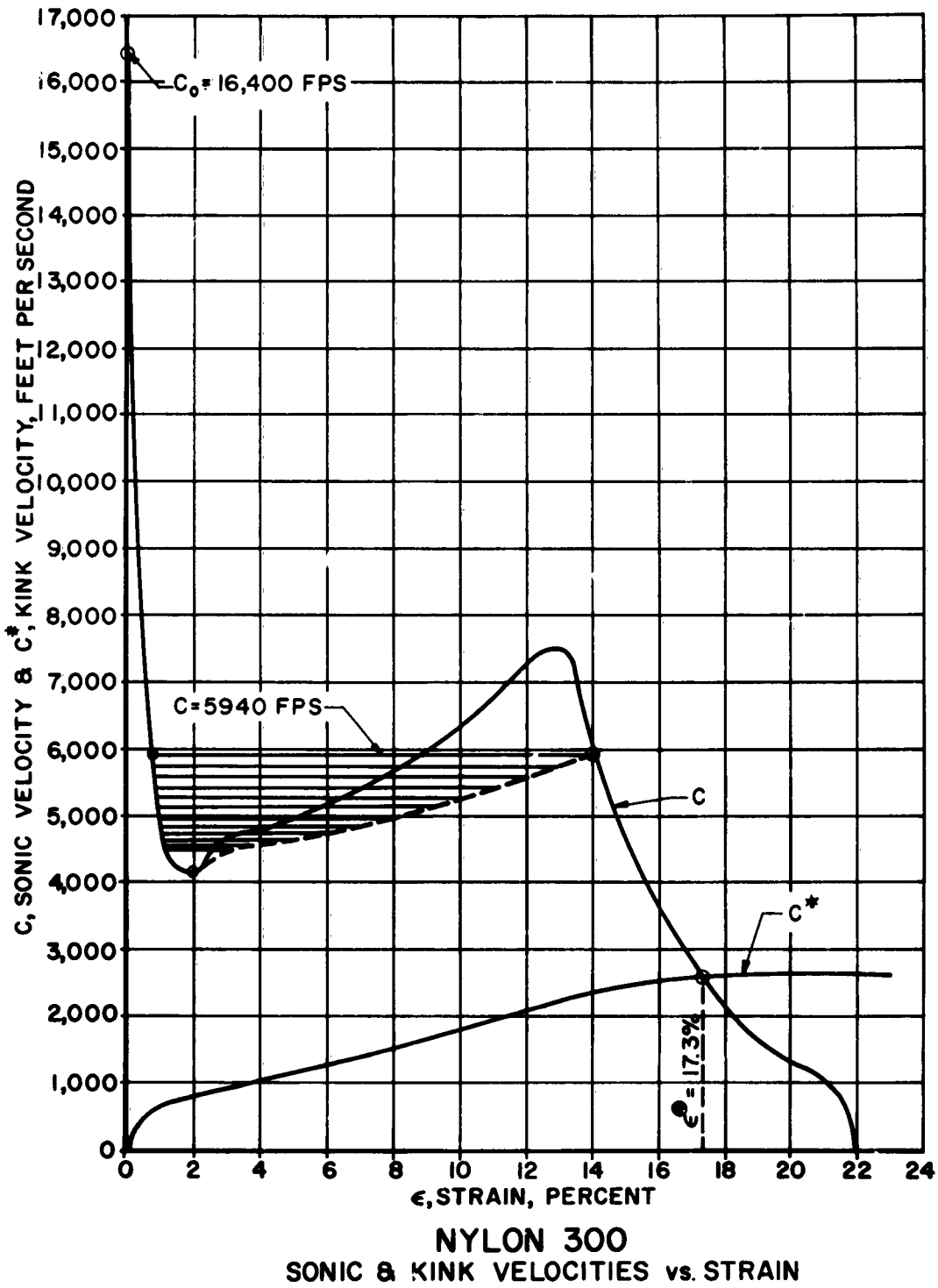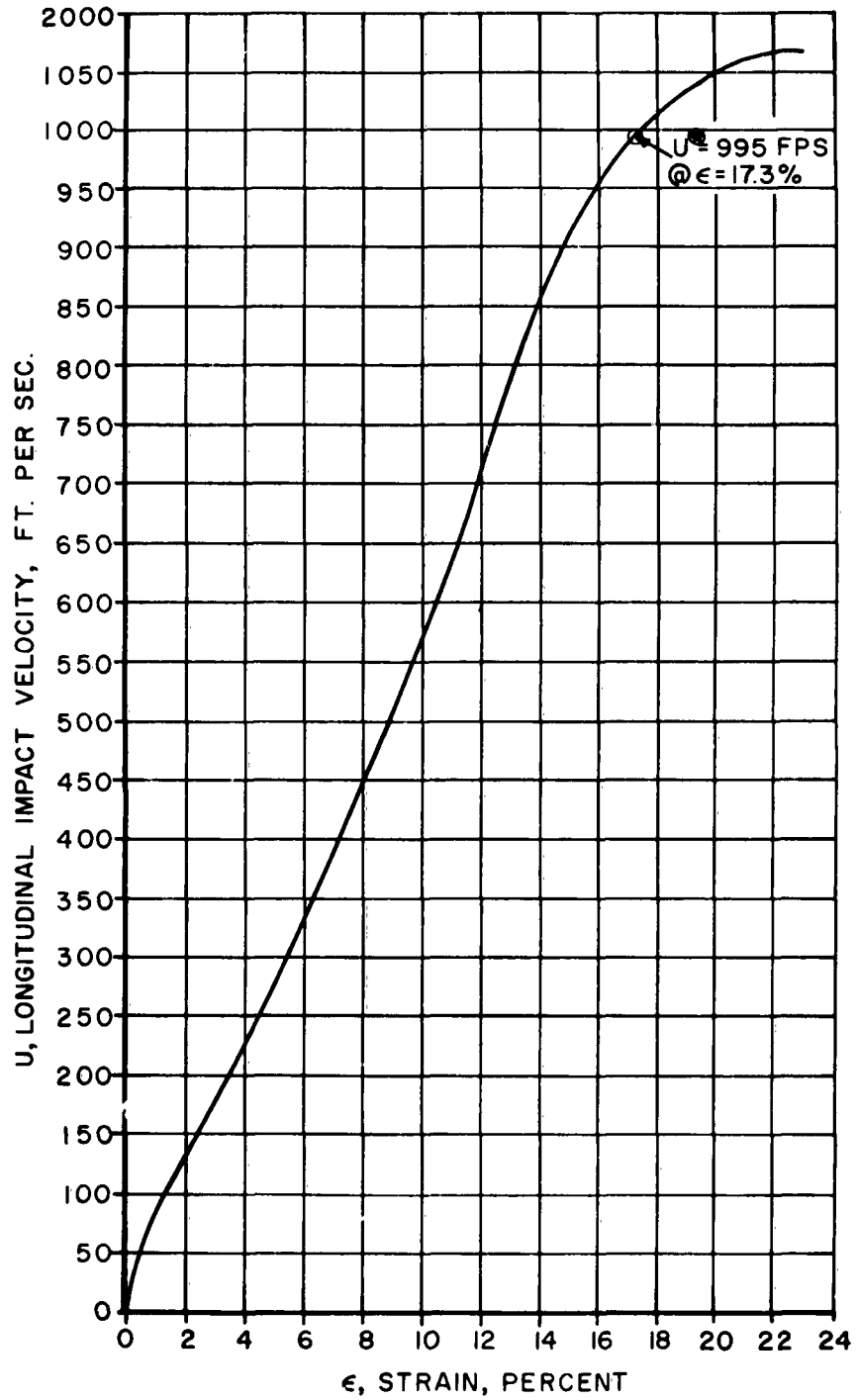
Figure 24

NYLON 300
LONGITUDINAL IMPACT VELOCITY vs. STRAIN

Figure 25
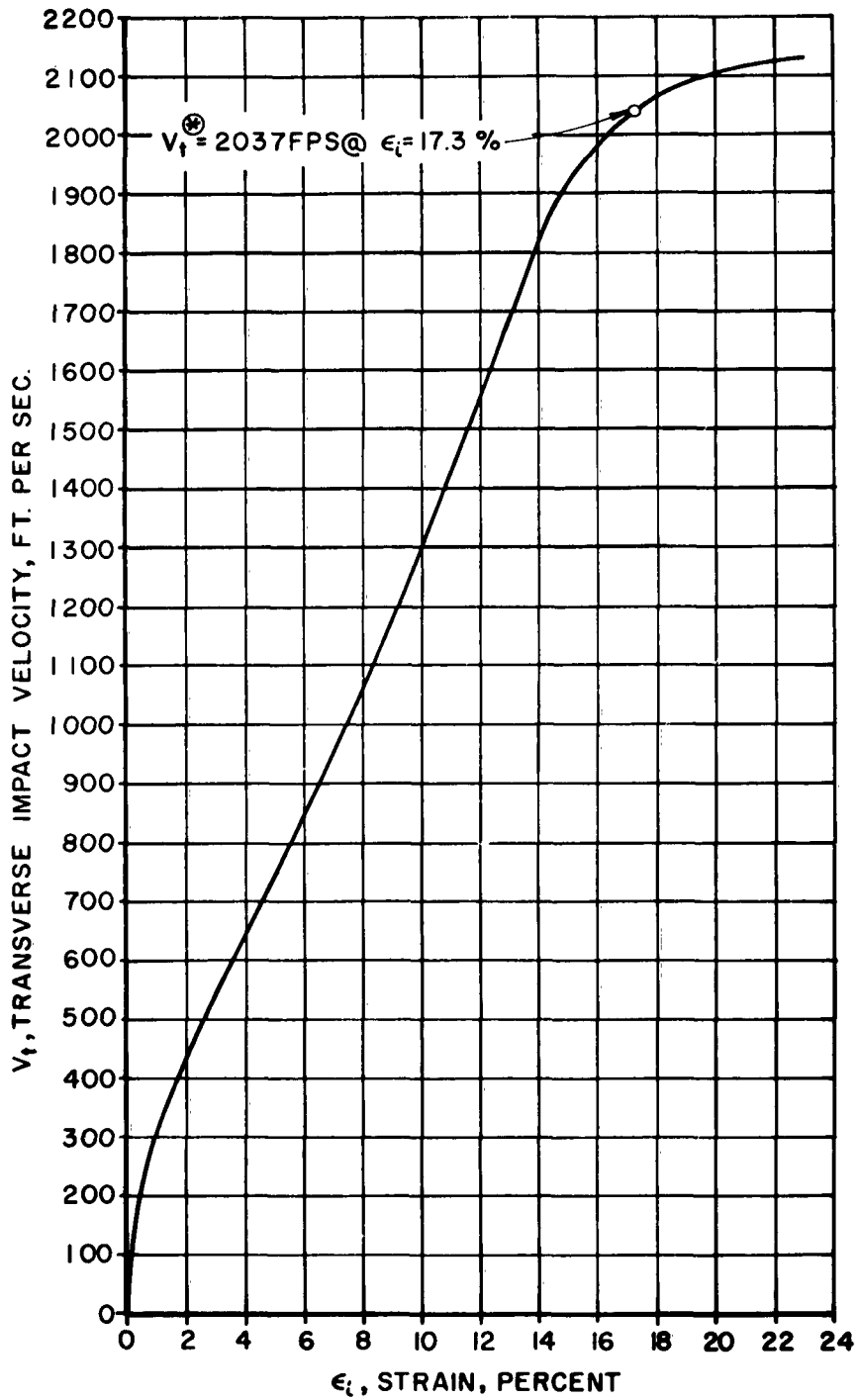
NYLON 300

TRANSVERSE IMPACT VELOCITY vs.
STRAIN

Figure 26

NYLON 300
TENACITY vs.TRANSVERSE IMPACT VELOCITY

Figure 27

NYLON 300
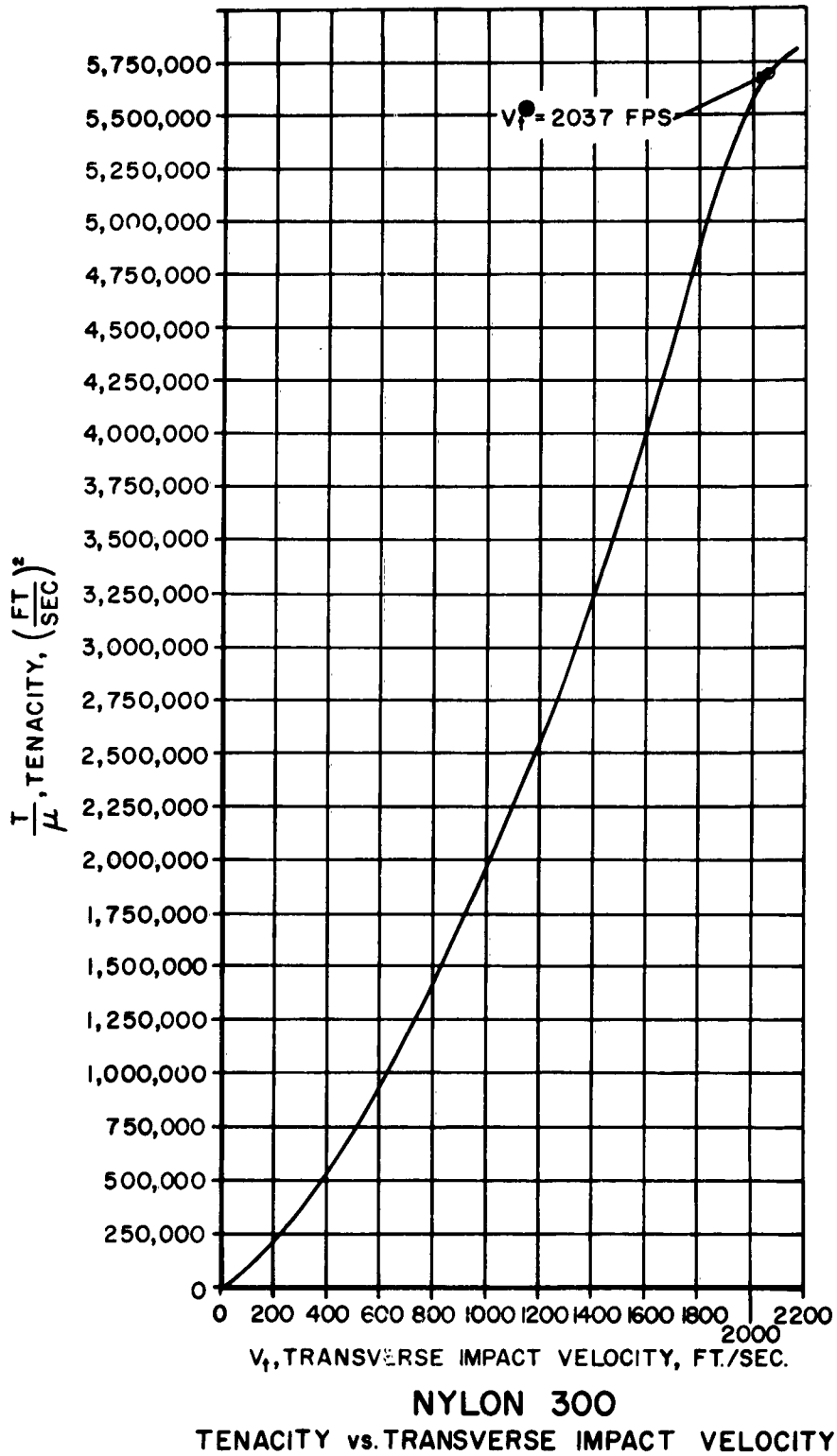
@ 21° C. & 65% R.H.
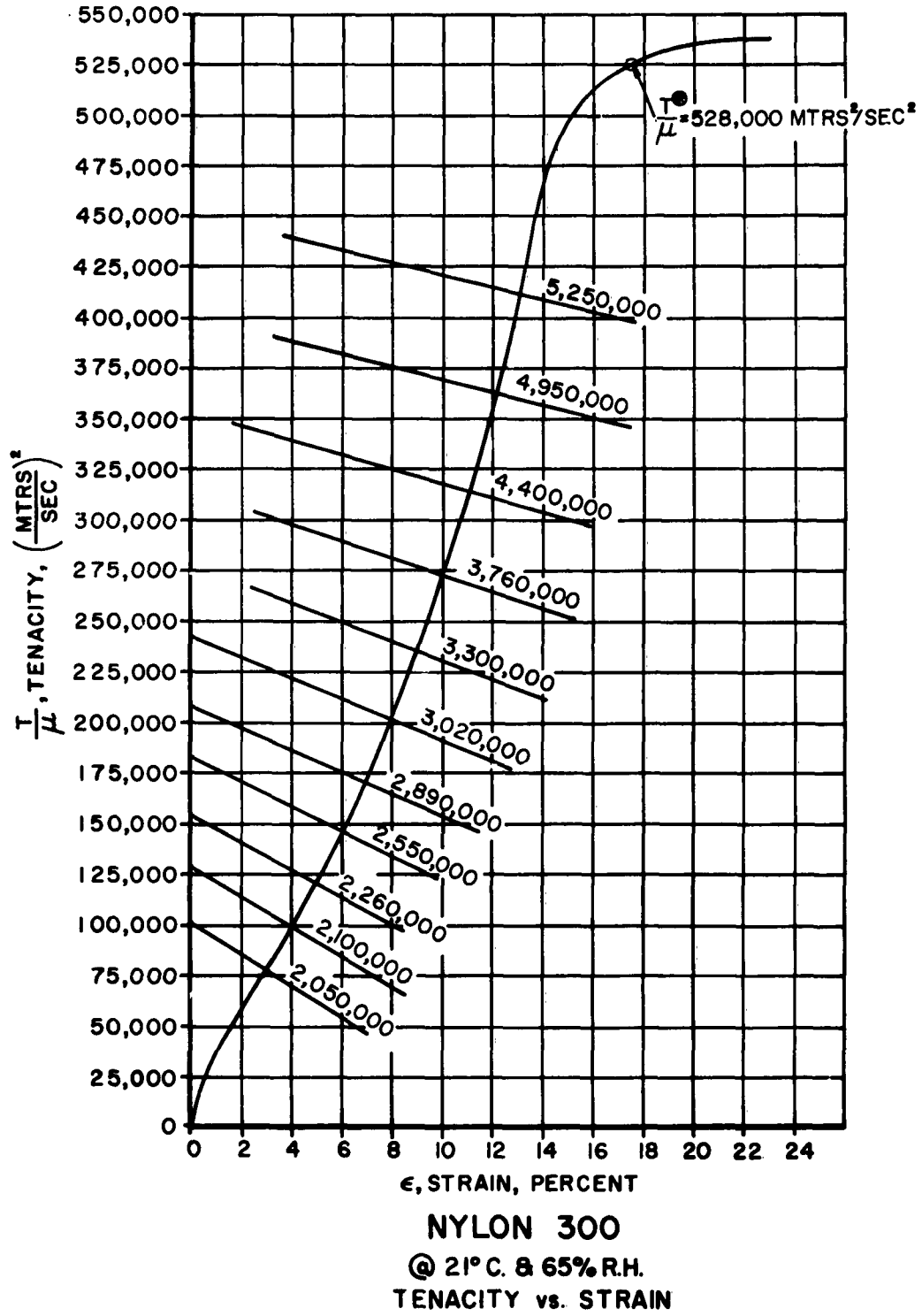
TENACITY vs. STRAIN
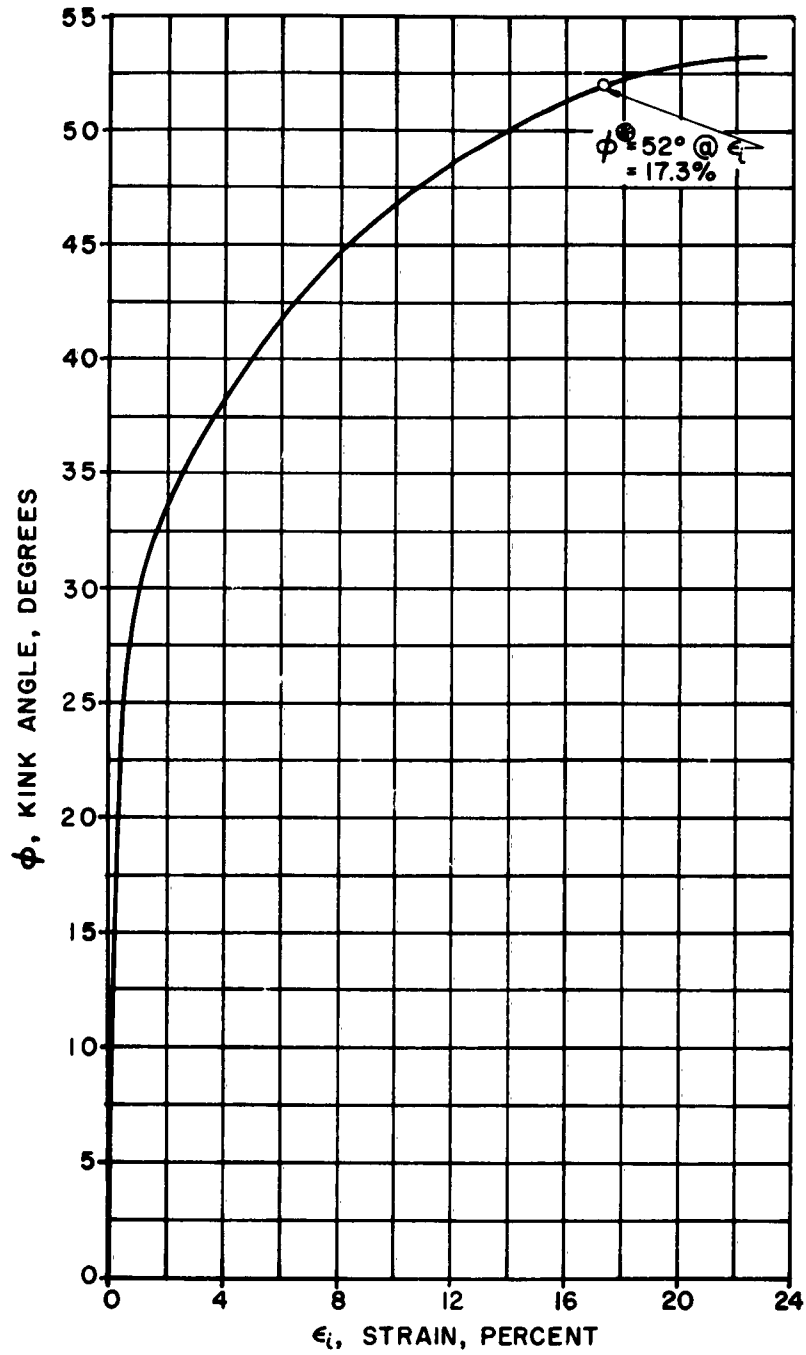
Figure 28

NYLON 300
KINK ANGLE vs. STRAIN

Figure 29
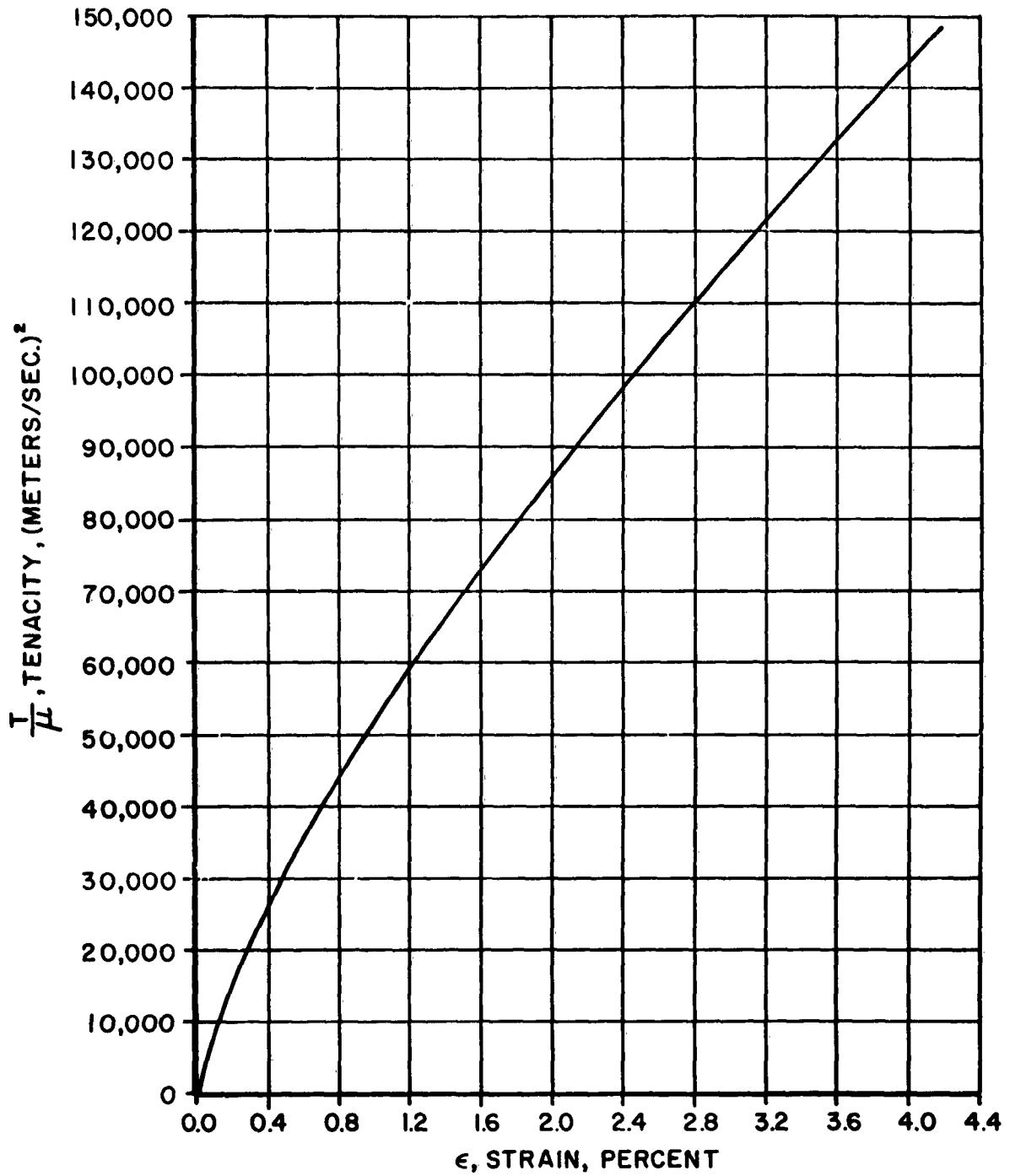
COTTON 50/1

TENACITY vs. STRAIN

$$\frac{T}{\mu} = 1,500,000\ \epsilon^{0.7 \circ}$$

@ 21°C. & 65% R.H.

Figure 30

$C_o = 9000$ FPS

$C = 1046 \, \epsilon^{-0.156}$

C^*

C, SONIC VELOCITY & C^*, KINK VELOCITY, FT. PER SECOND

ϵ, STRAIN, PERCENT
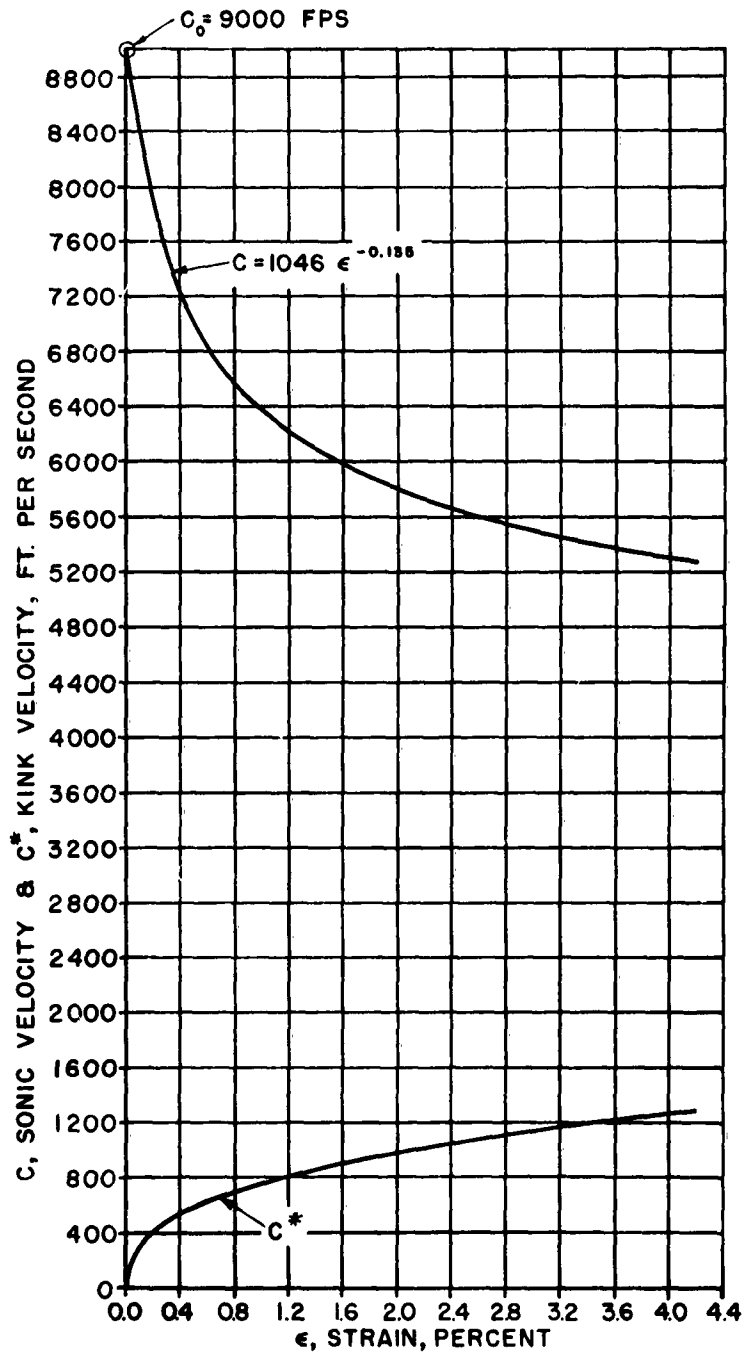
COTTON 50/I
SONIC & KINK VELOCITIES
vs. STRAIN
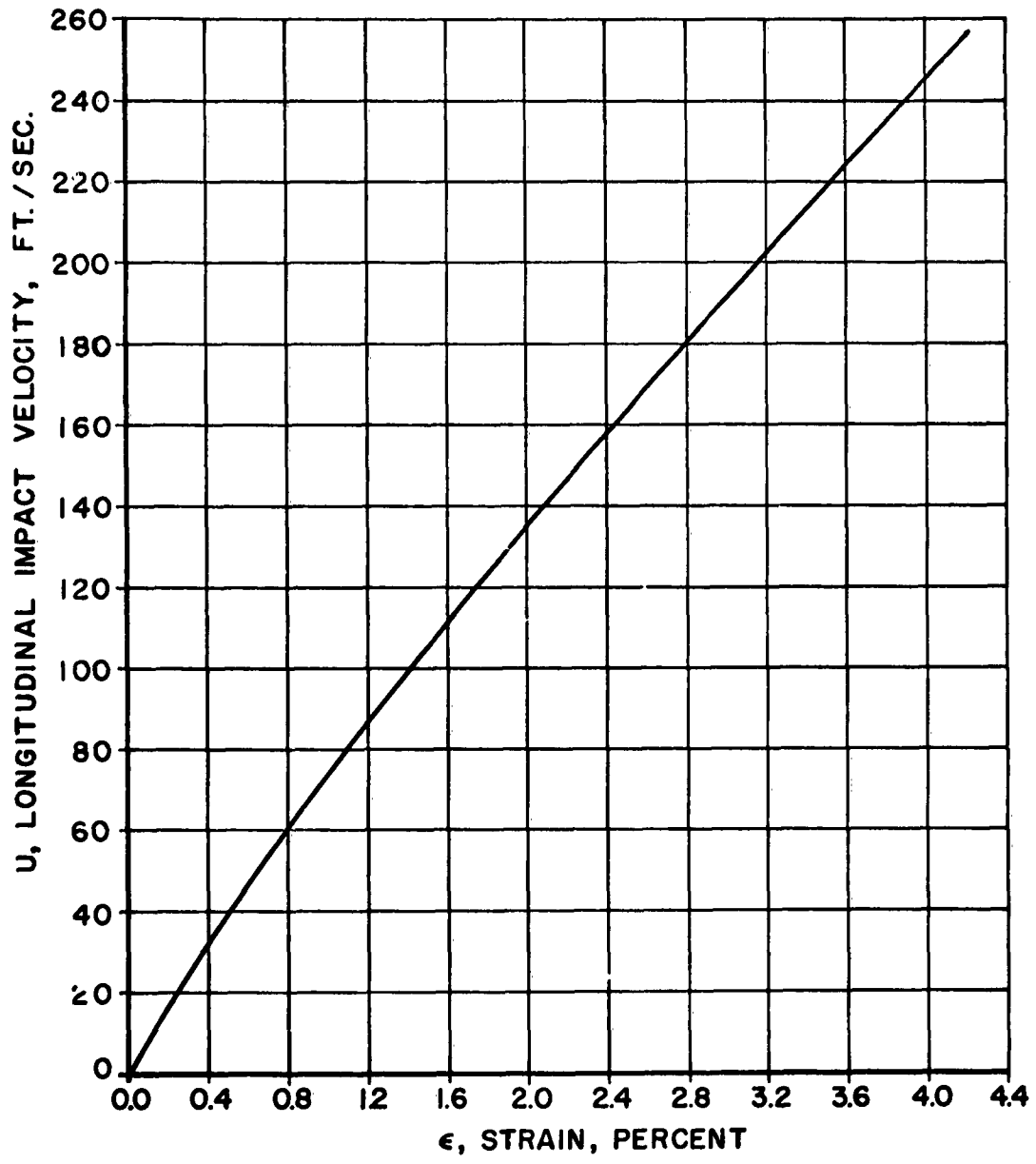
Figure 31

COTTON 50/I

LONGITUDINAL IMPACT
VELOCITY vs. STRAIN
$U = 1209 \; \epsilon^{0.865}$

Figure 32
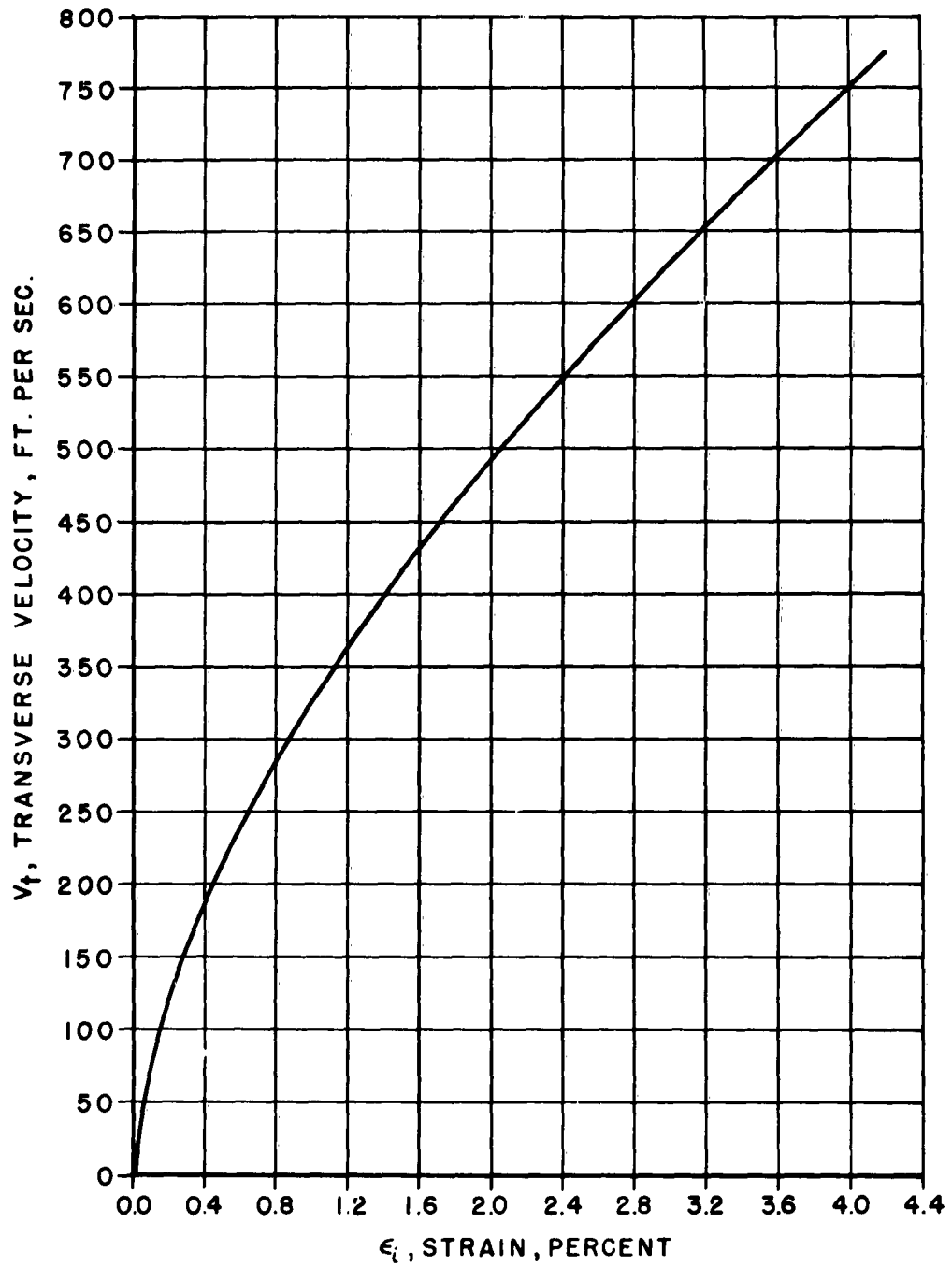
COTTON 50 / 1
TRANSVERSE IMPACT VELOCITY vs. STRAIN

Figure 33
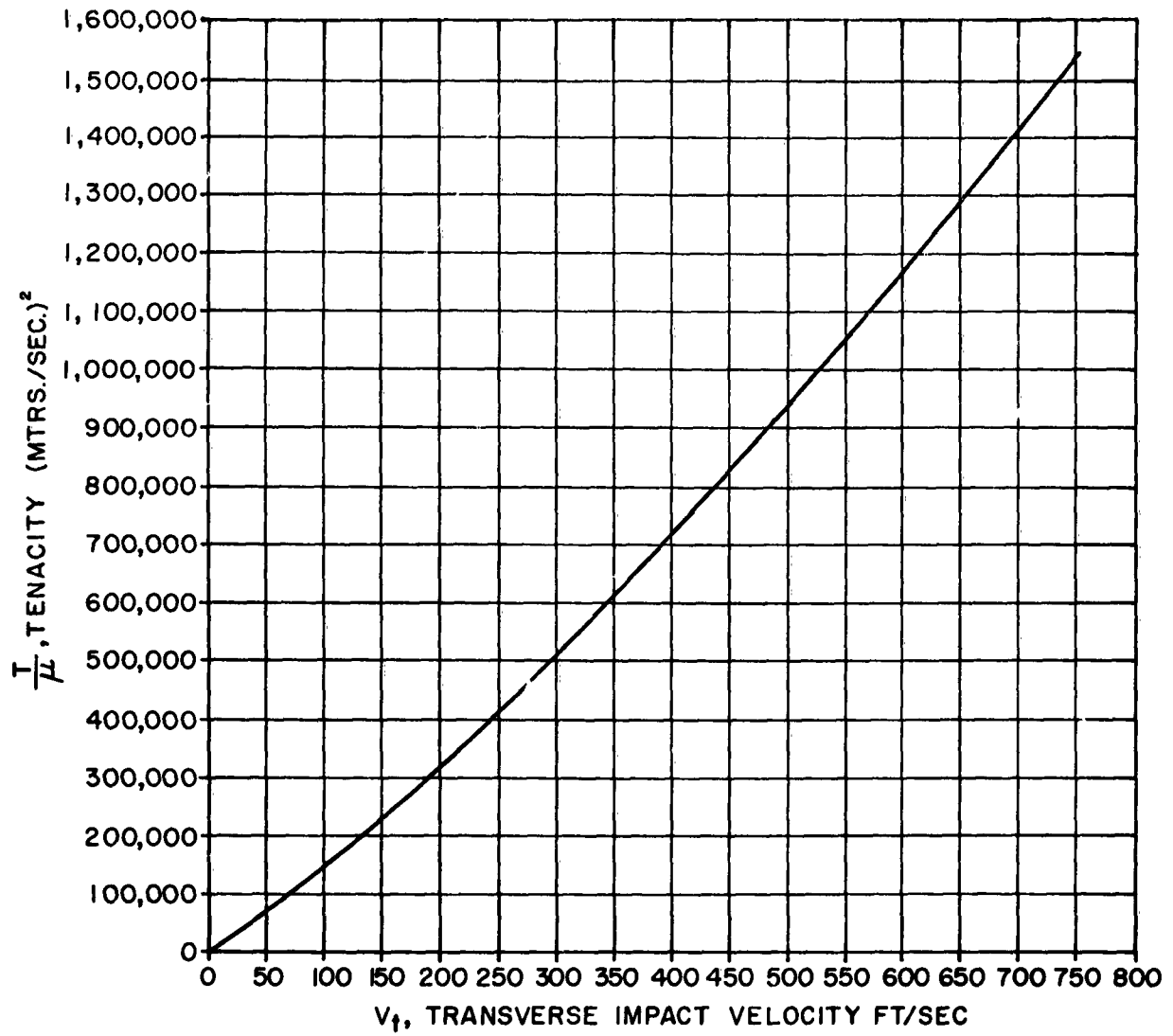
COTTON 50/1
TENACITY vs. TRANSVERSE
IMPACT VELOCITY

Figure 34
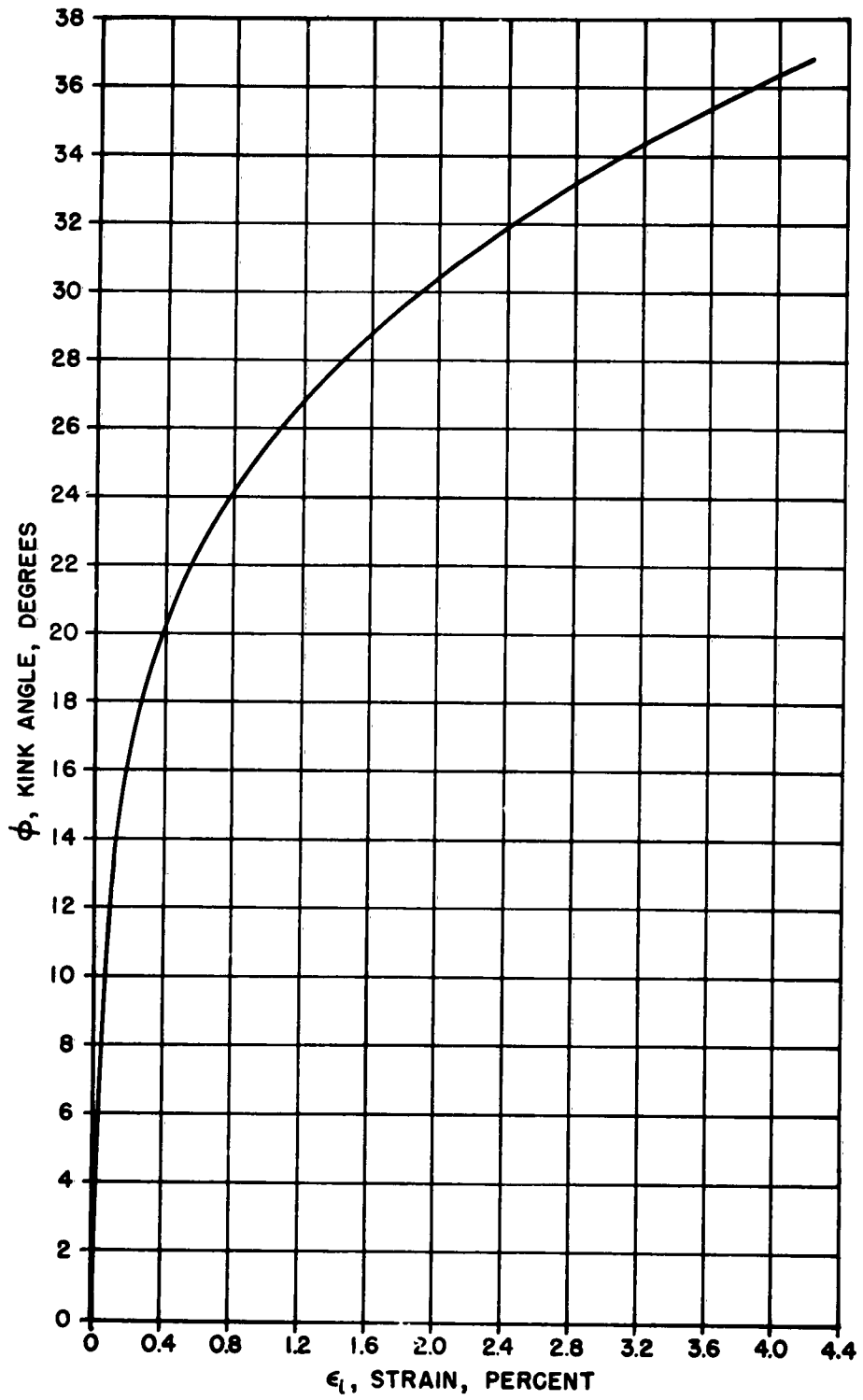
COTTON 50/1
KINK ANGLE vs. STRAIN

Figure 35
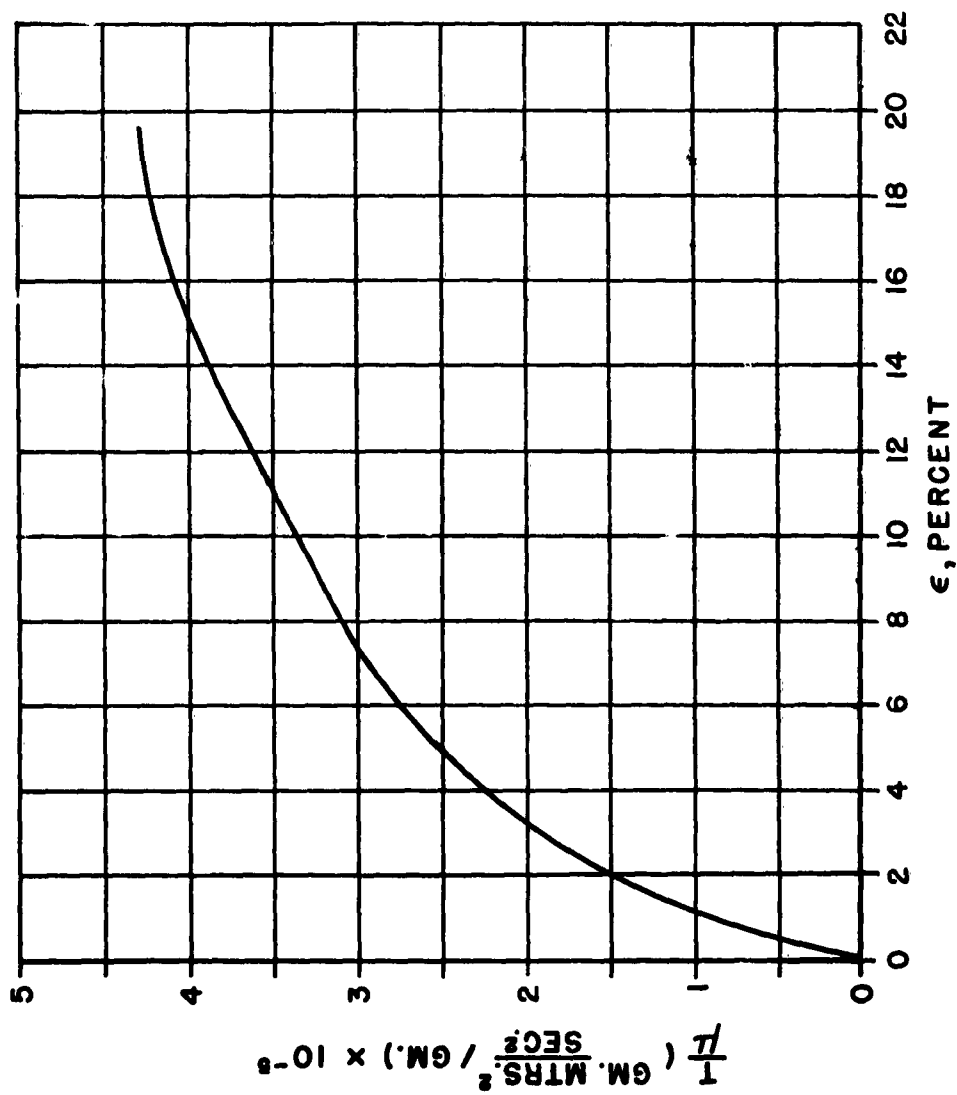
SILK

TENACITY vs. STRAIN CURVE (FROM SUSICH & BACKER, T.R.J., 21,482 1951)
@ 21°C. (70°F.) & 65% RELATIVE HUMIDITY

Figure 36

63
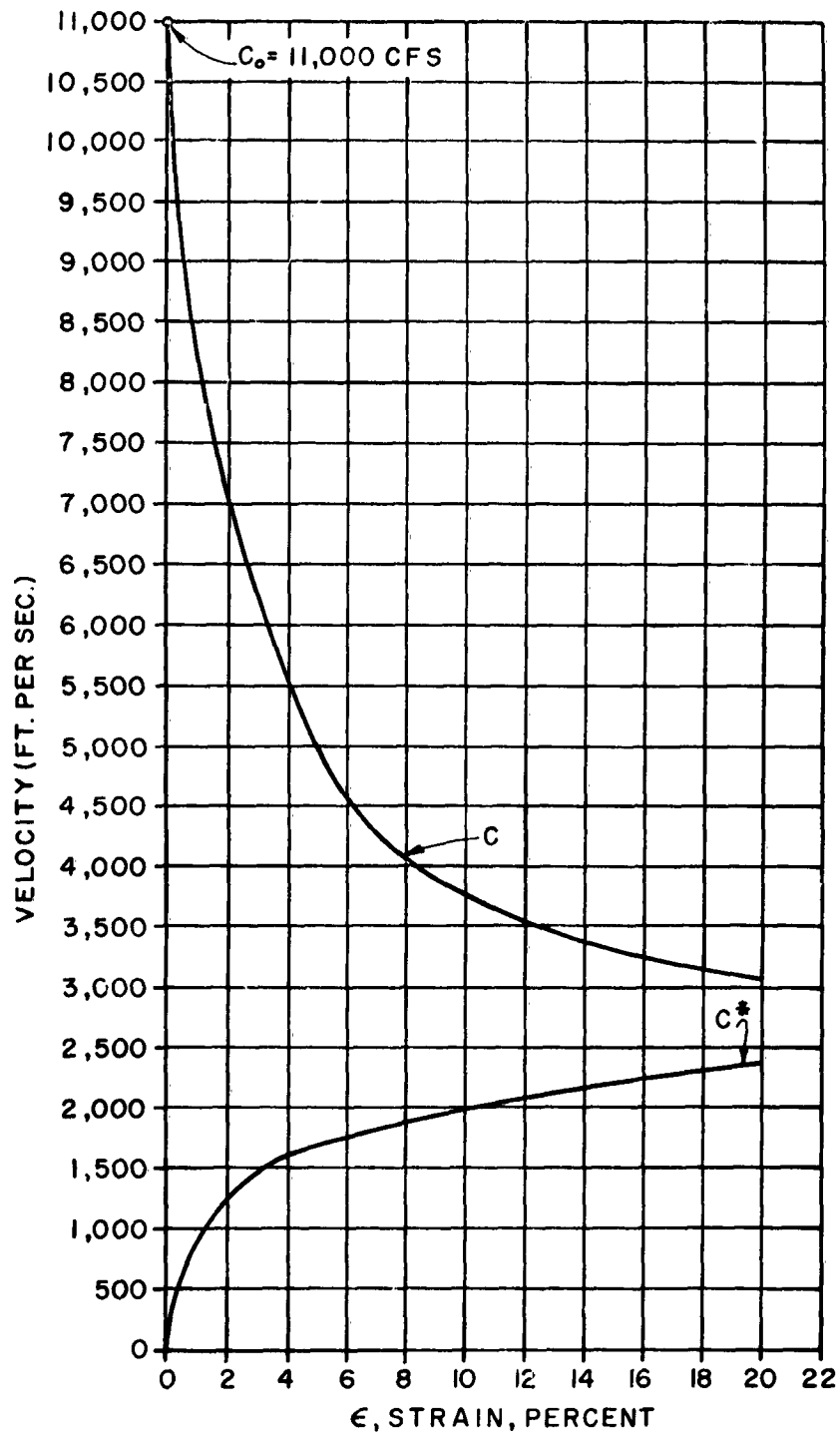
SILK
SONIC & KINK VELOCITIES
vs. STRAIN

Figure 37
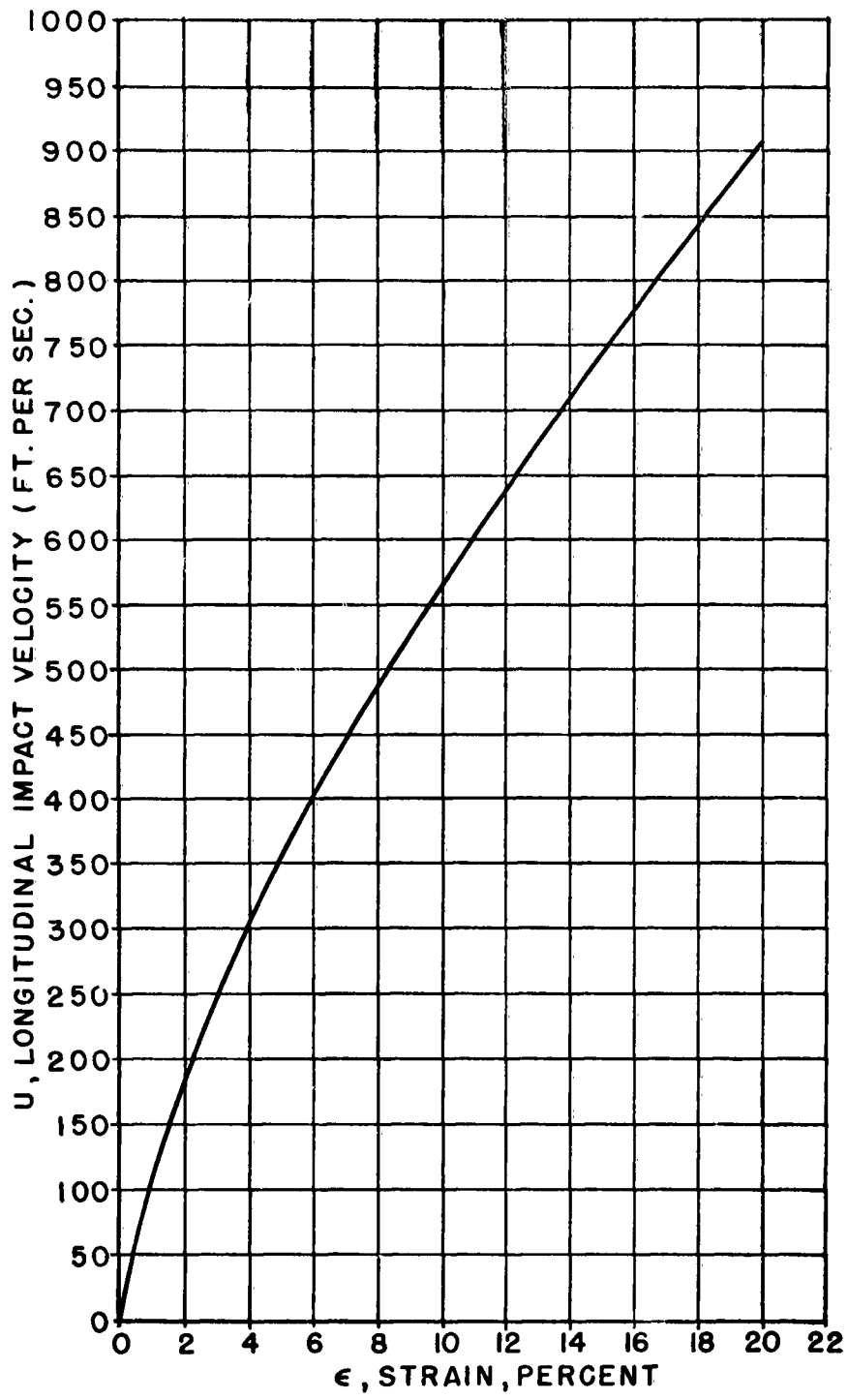
SILK
LONGITUDINAL IMPACT
VELOCITY vs. STRAIN

Figure 38
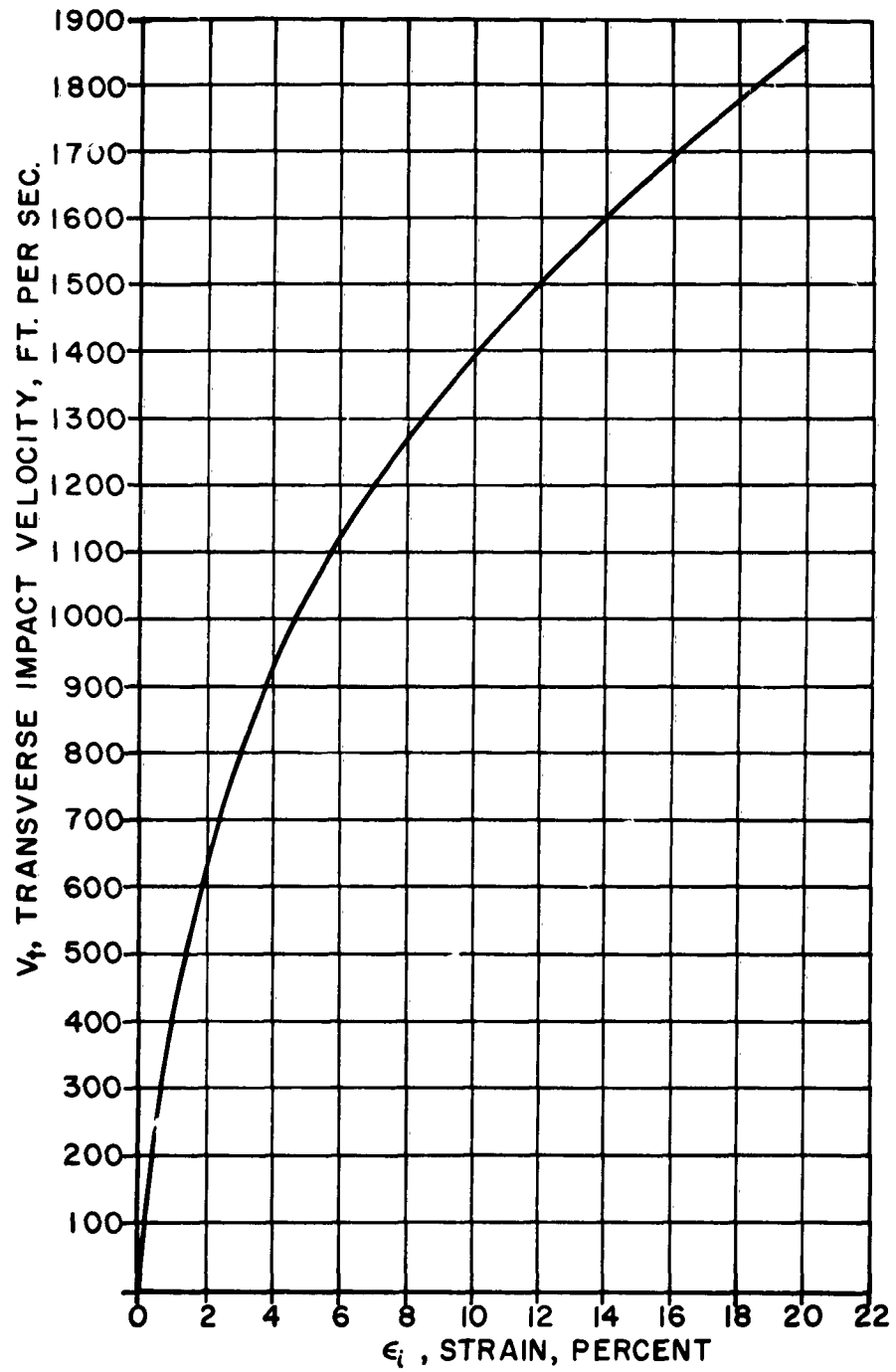
65

SILK
TRANSVERSE IMPACT
VELOCITY vs. STRAIN

Figure 39
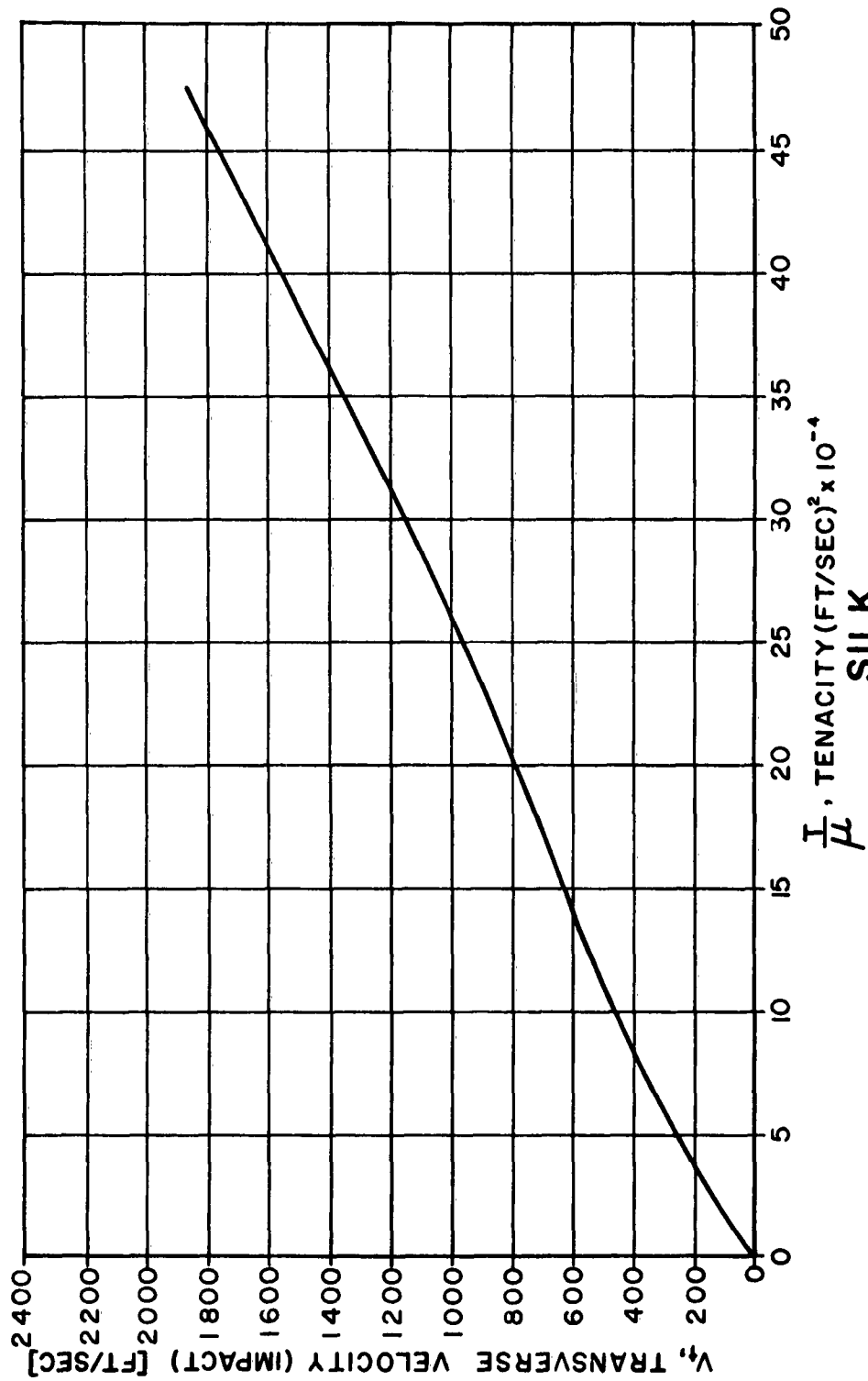
TRANSVERSE IMPACT VELOCITY vs. TENACITY

SILK

Figure 40

$\frac{T}{\mu}$, TENACITY $(FT/SEC)^2 \times 10^{-4}$

V_t, TRANSVERSE VELOCITY (IMPACT) [FT/SEC]

SILK
KINK ANGLE ϕ - % STRAIN
Figure 41

COTTON 12/1

TENACITY vs. STRAIN

$\dfrac{T}{\mu} = 1,650,000 \; \epsilon^{1.01}$

@ 21°C. & 65% R.H.

ϵ, STRAIN, PERCENT

$\dfrac{T}{\mu}$, TENACITY, (MTRS/SEC)^2

Figure 42

69

COTTON 12/1

SONIC & KINK VELOCITIES vs. STRAIN

Figure 43

ε, STRAIN, PERCENT

c, SONIC VELOCITY & c*, KINK VELOCITY, FT/SEC
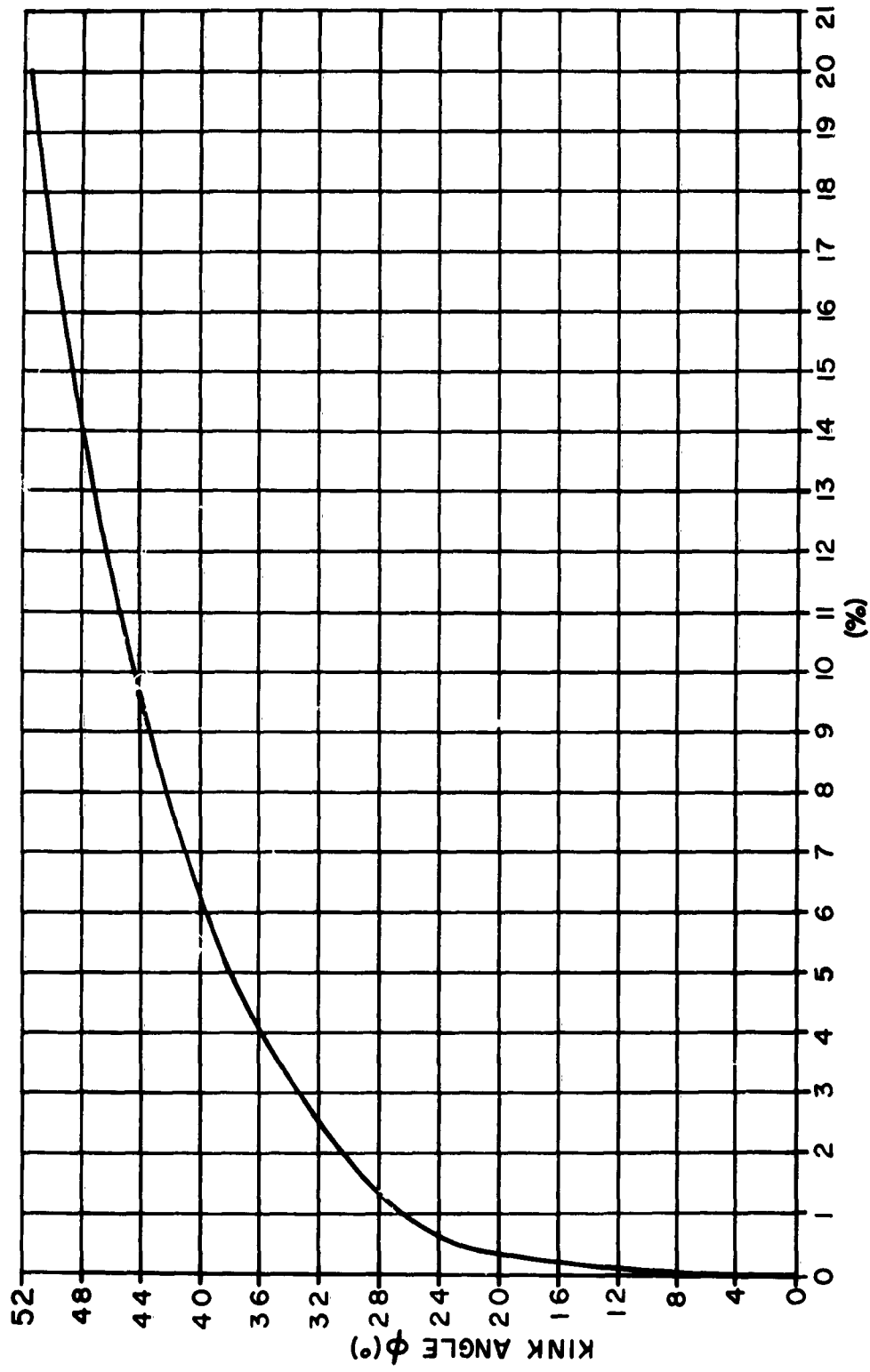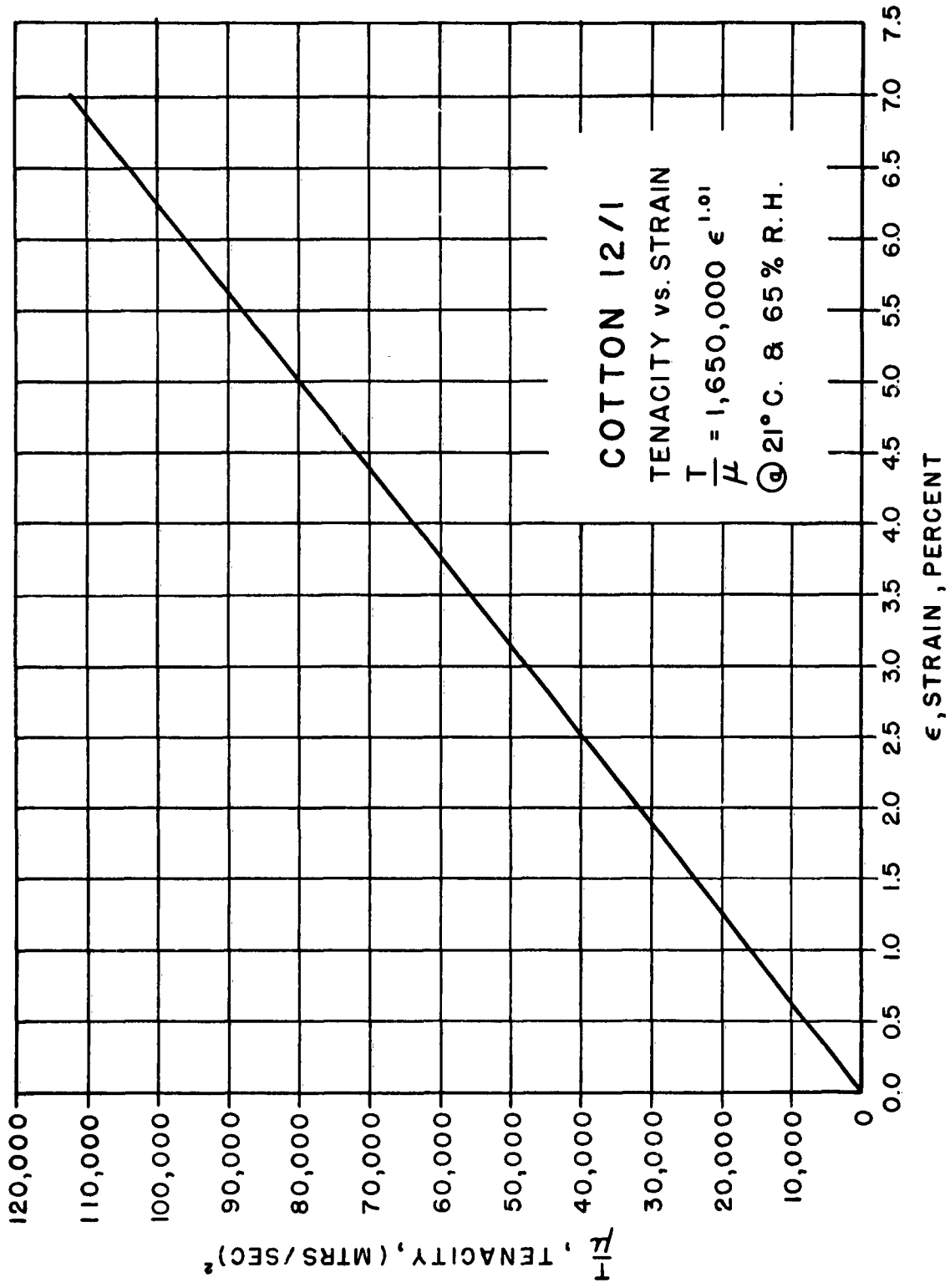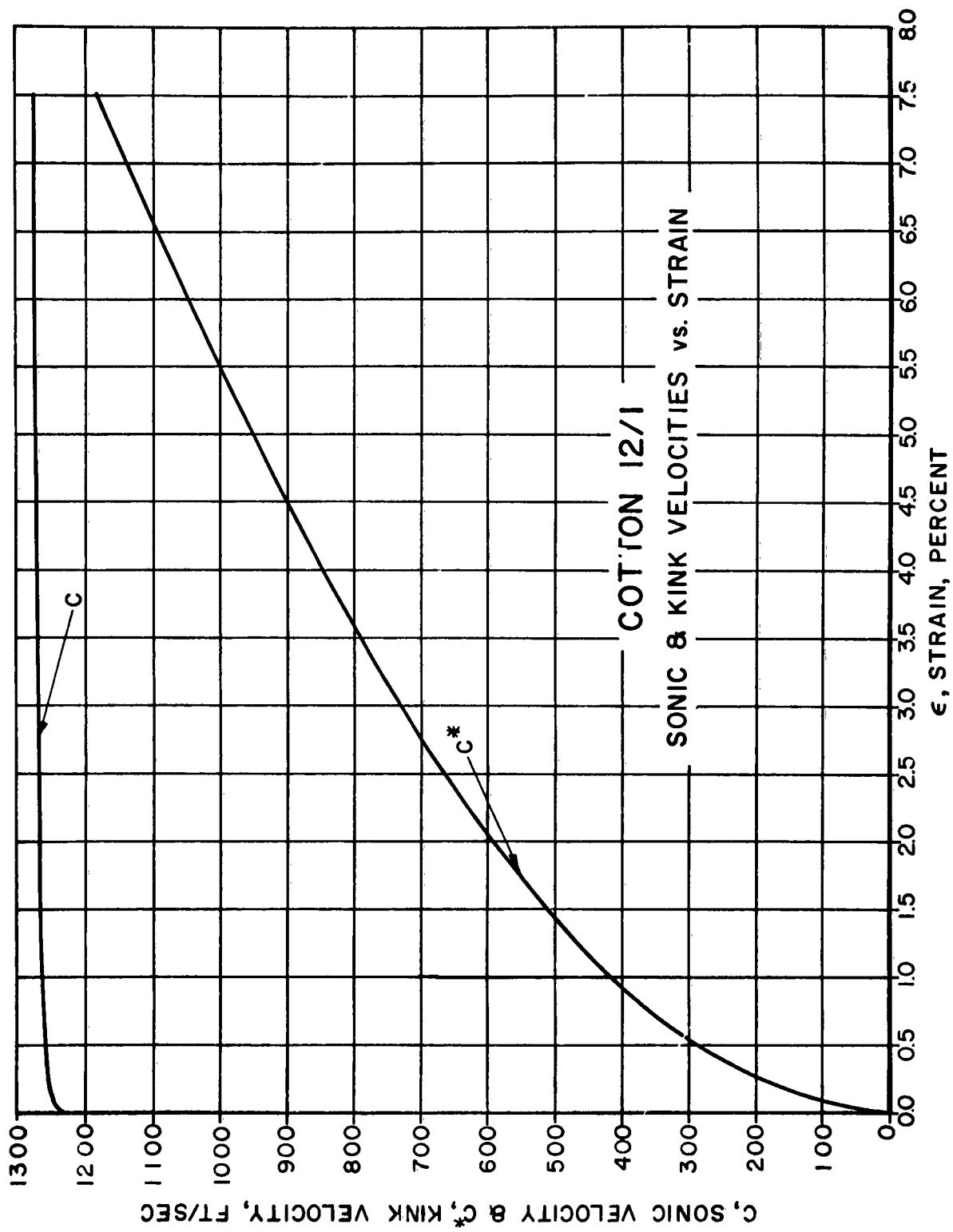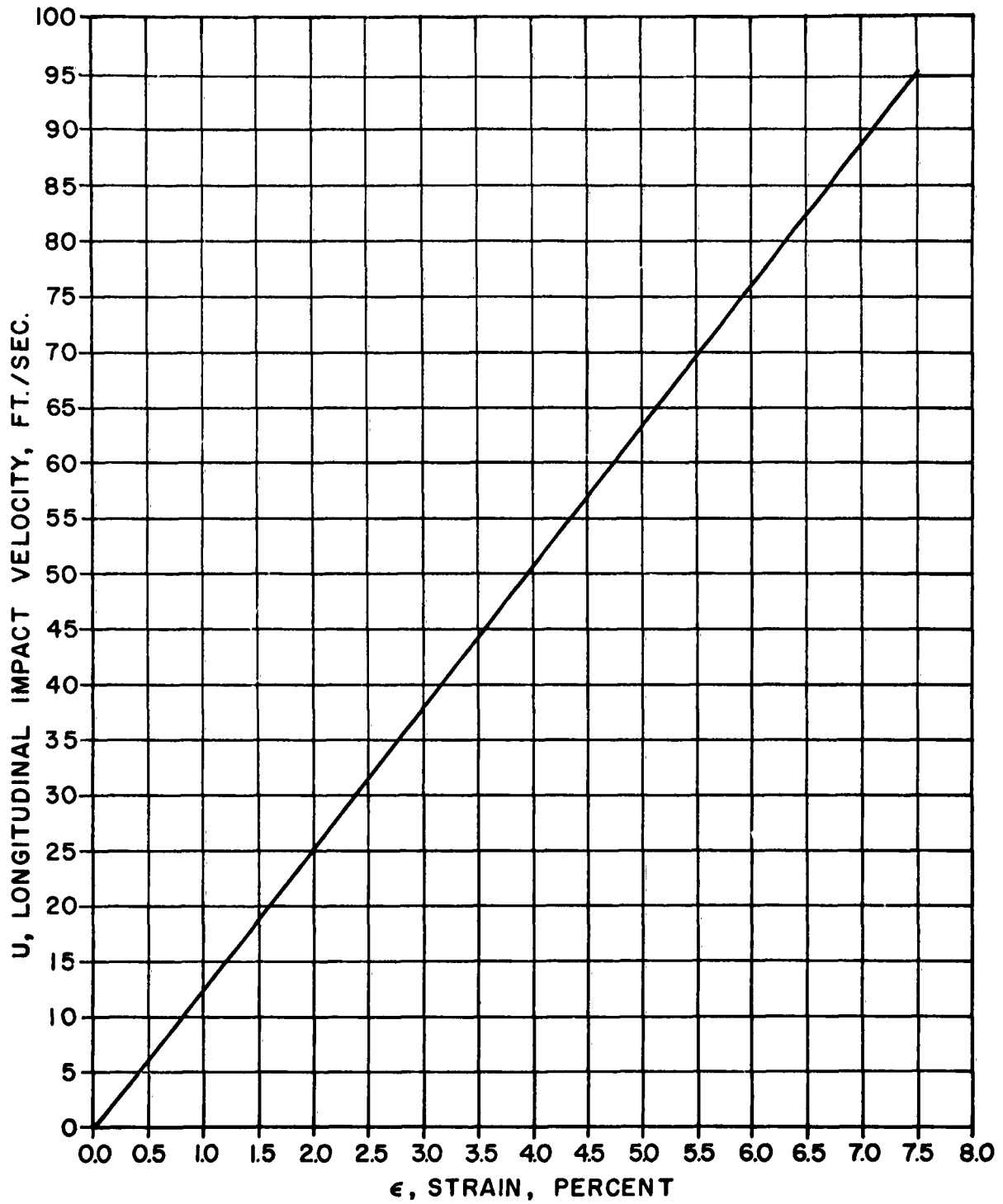
COTTON 12/1

LONGITUDINAL IMPACT
VELOCITY vs. STRAIN

Figure 44

71

COTTON 12/1
TRANSVERSE IMPACT
VELOCITY vs. STRAIN
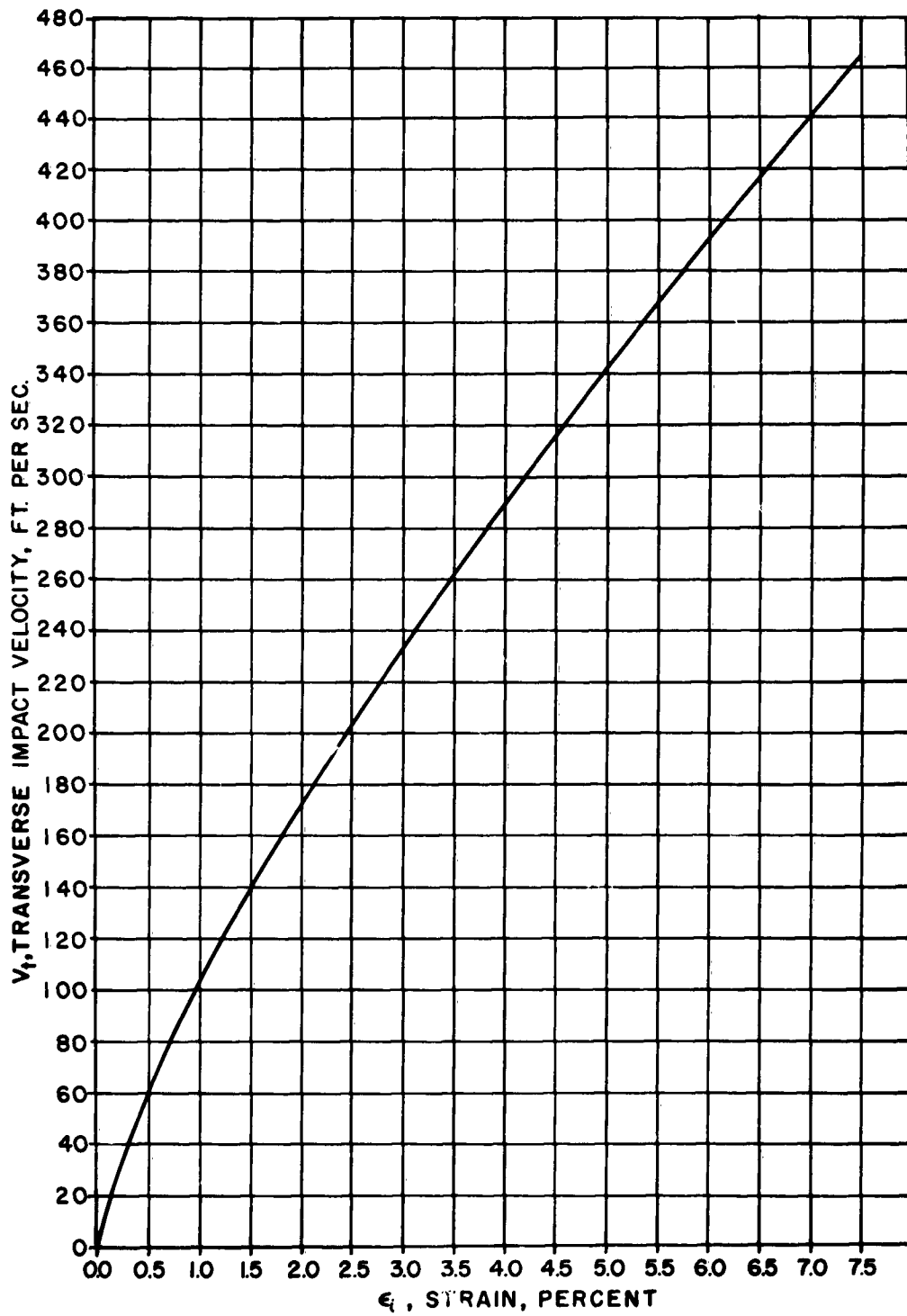
Figure 45

COTTON 12/1
TRANSVERSE IMPACT VELOCITY vs.
TENACITY
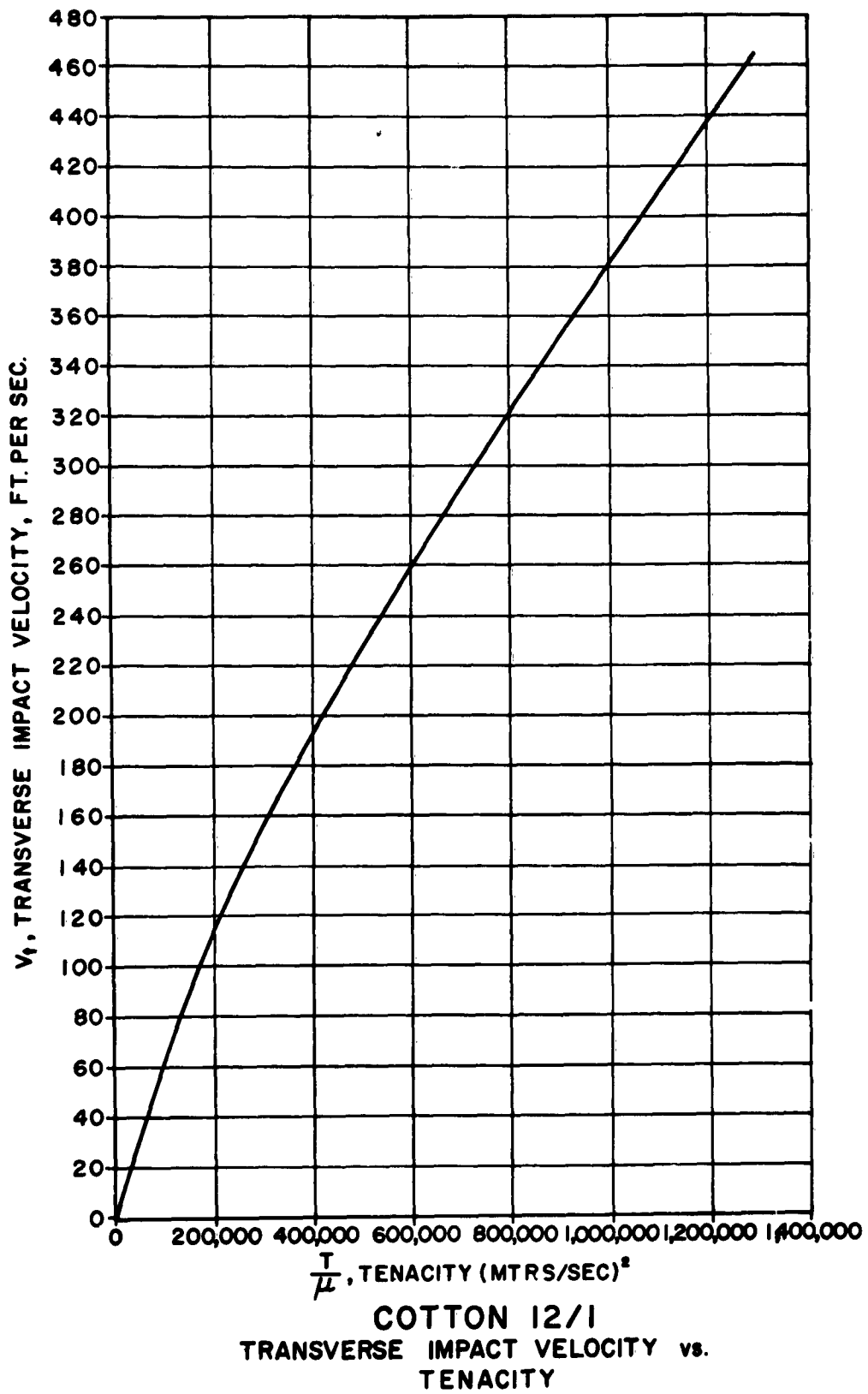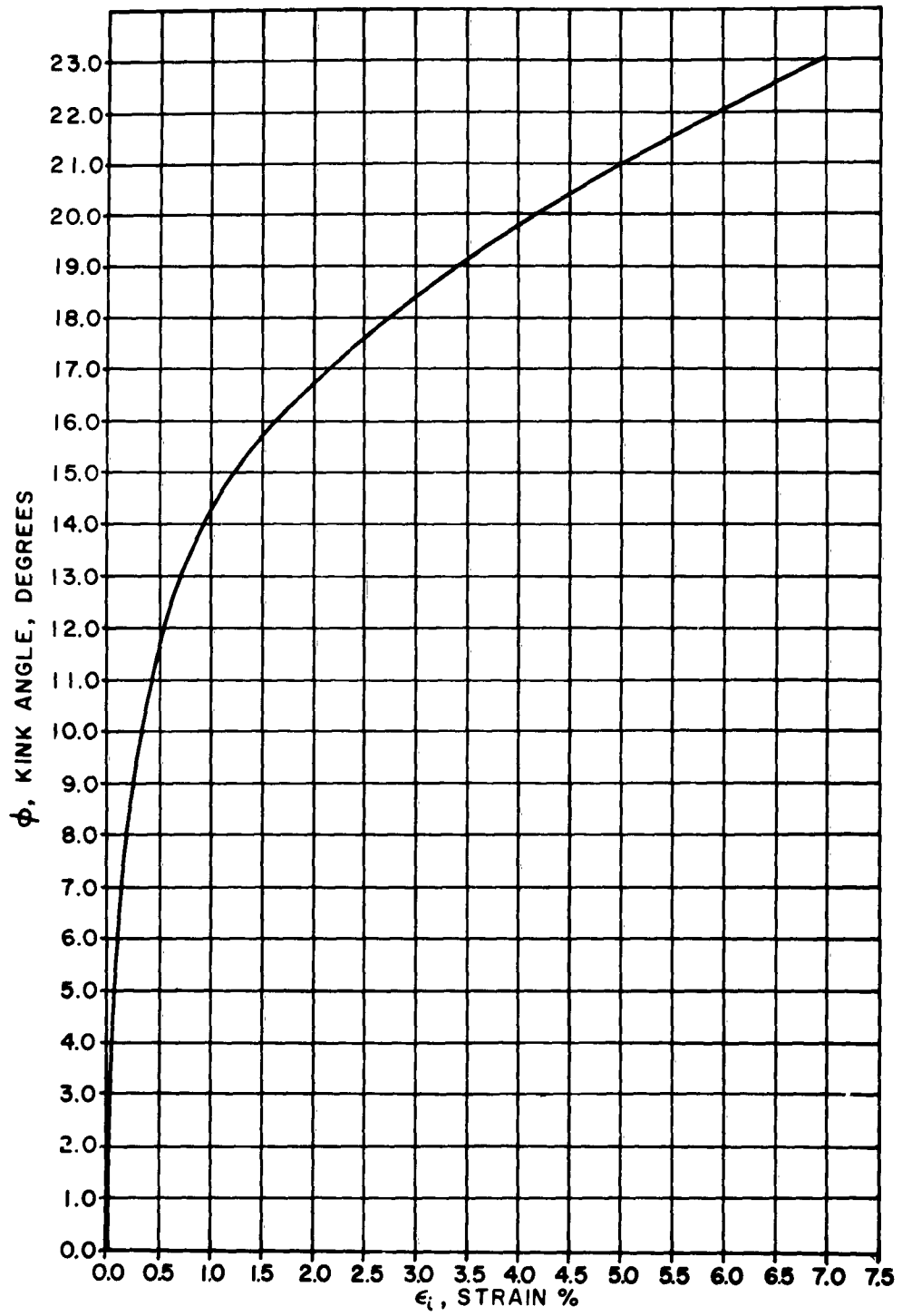
Figure 46

COTTON 12/1
KINK ANGLE vs. STRAIN

Figure 47

COTTON 12/1
TRANSVERSE IMPACT VELOCITY vs.
TENACITY
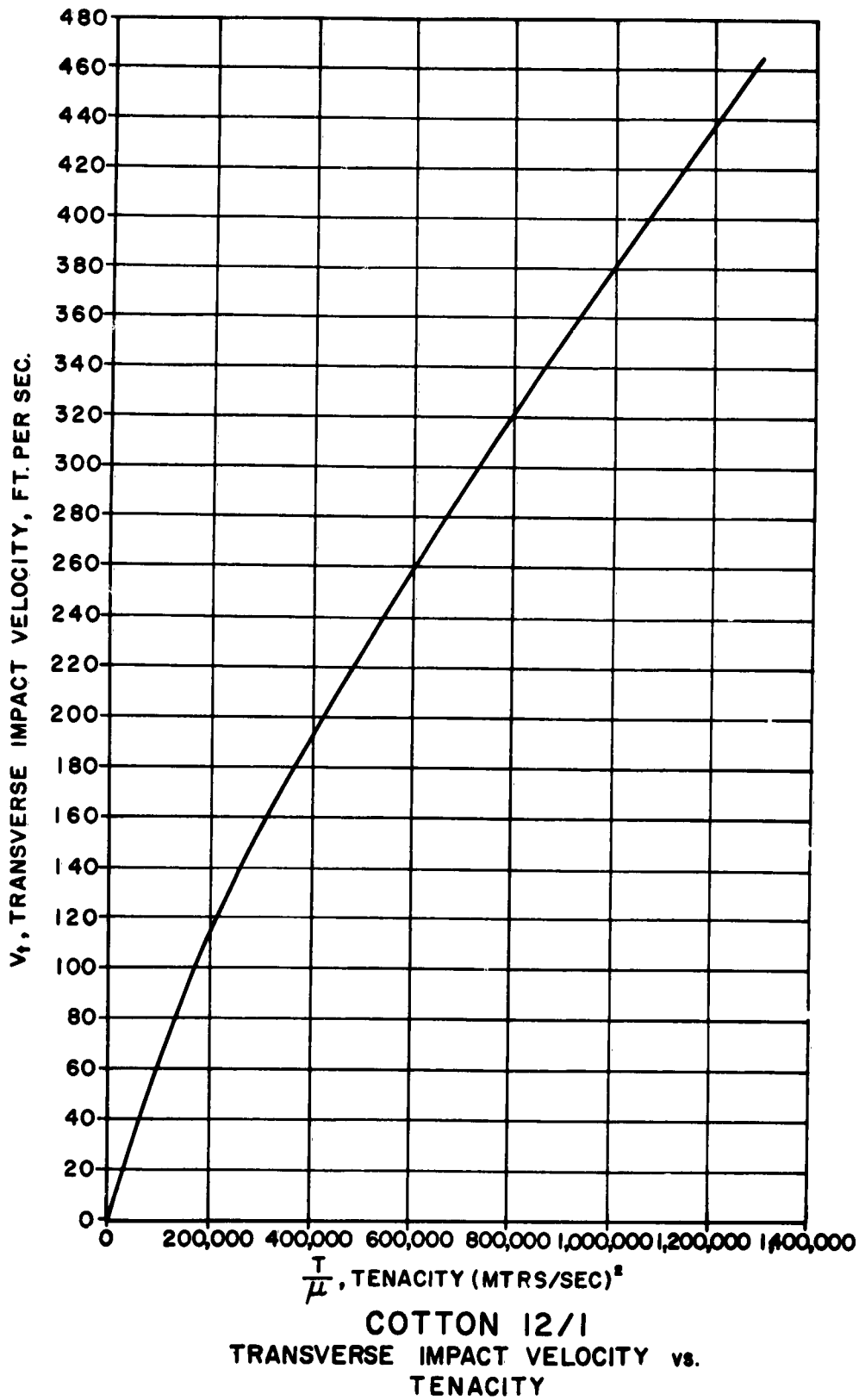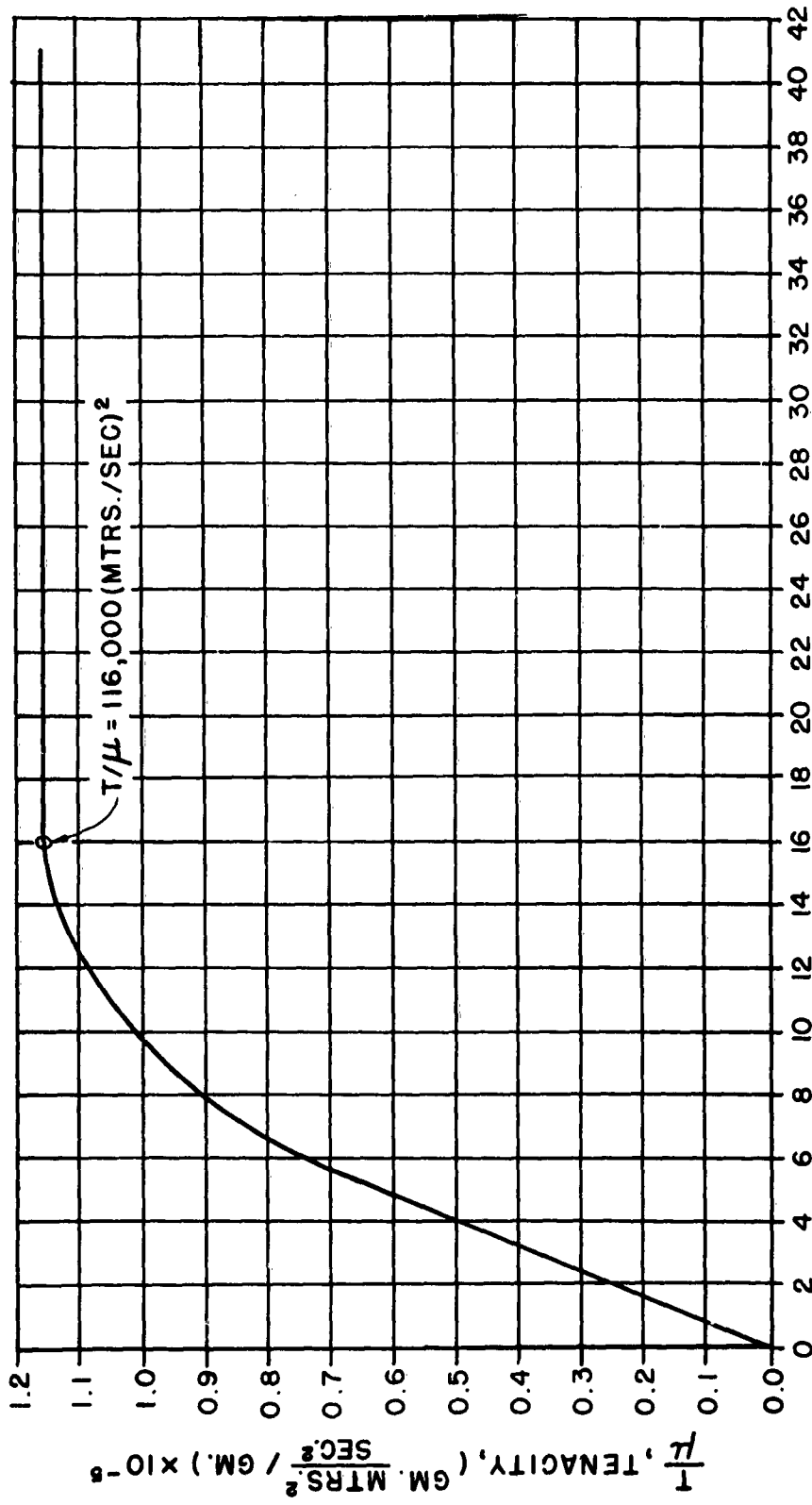
Figure 46

POLYETHYLENE

TENACITY vs. STRAIN CURVE (FROM SUSICH & BACKER, T.R.J., 21,482 1951) @ 21°C. (70°F.) & 65% RELATIVE HUMIDITY

Figure 48

$T/\mu = 116,000 \, (MTRS./SEC)^2$

ϵ, STRAIN, PERCENT

$\frac{T}{\mu}$, TENACITY, $(GM. \frac{MTRS.^2}{SEC.^2} / GM.) \times 10^{-6}$
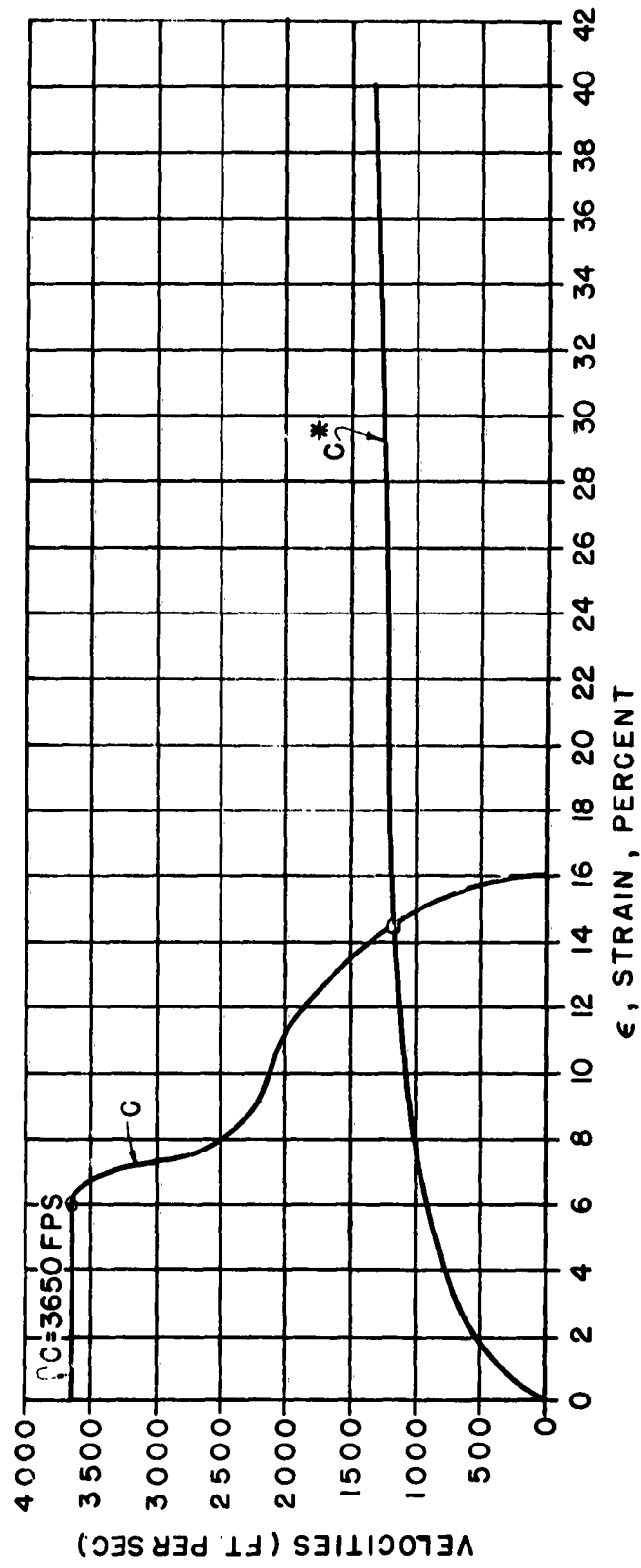
POLYETHYLENE

SONIC & KINK VELOCITIES VS. STRAIN

Figure 49
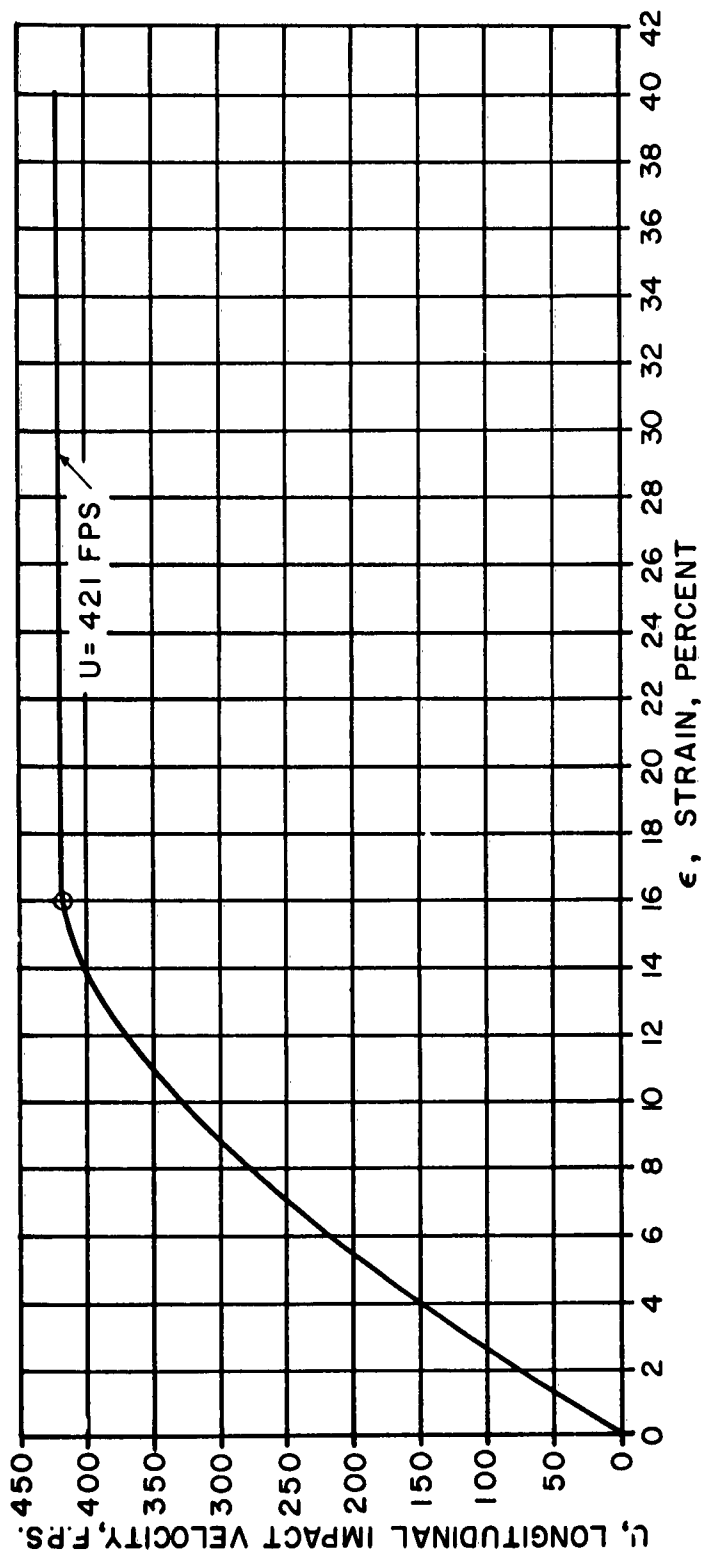
POLYETHYLENE
LONGITUDINAL IMPACT
VELOCITY vs. STRAIN

Figure 50

$V_t = 913$ FPS

$V_t = 898$ FPS at $\epsilon_i = 14.5\%$

ϵ_i, STRAIN , PERCENT

V_t, TRANSVERSE IMPACT VELOCITY (FT./SEC.)
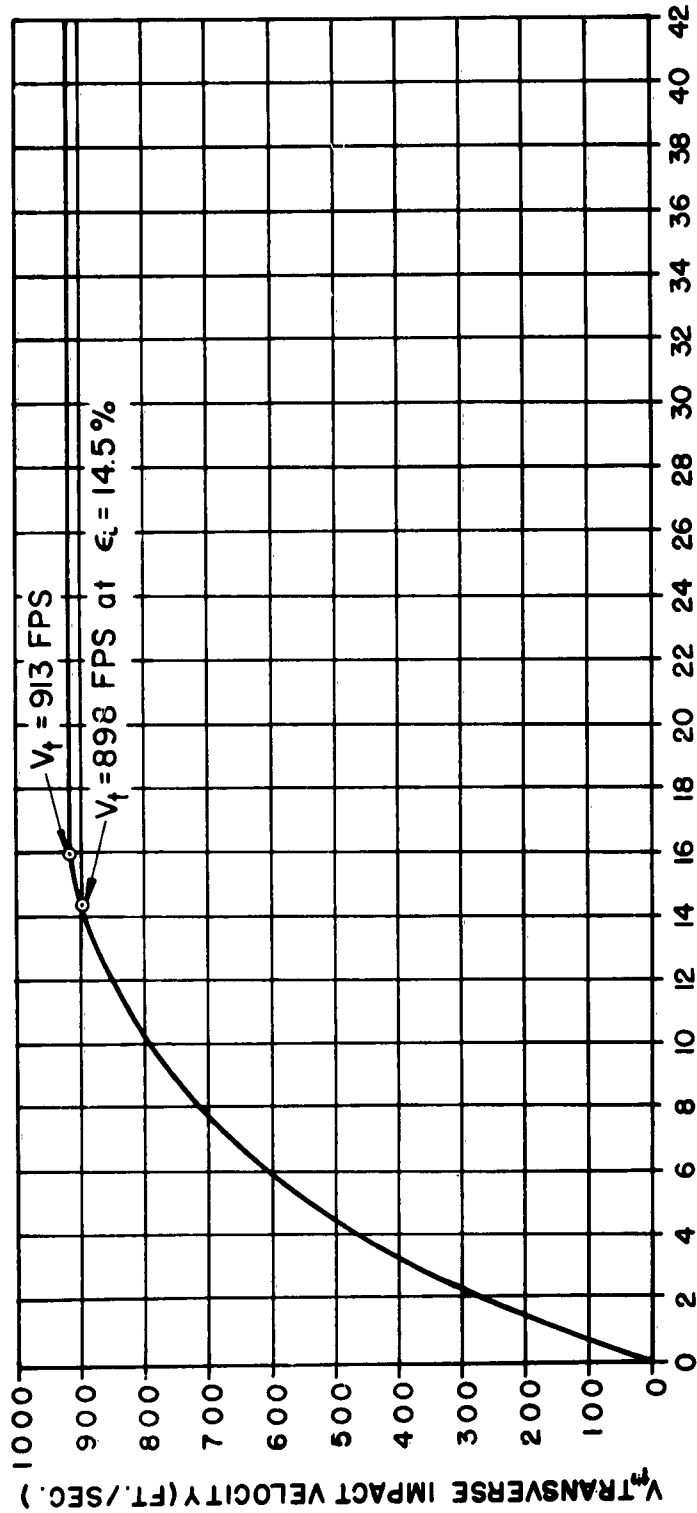
POLYETHYLENE
TRANSVERSE IMPACT
VELOCITY vs. STRAIN

Figure 51

78
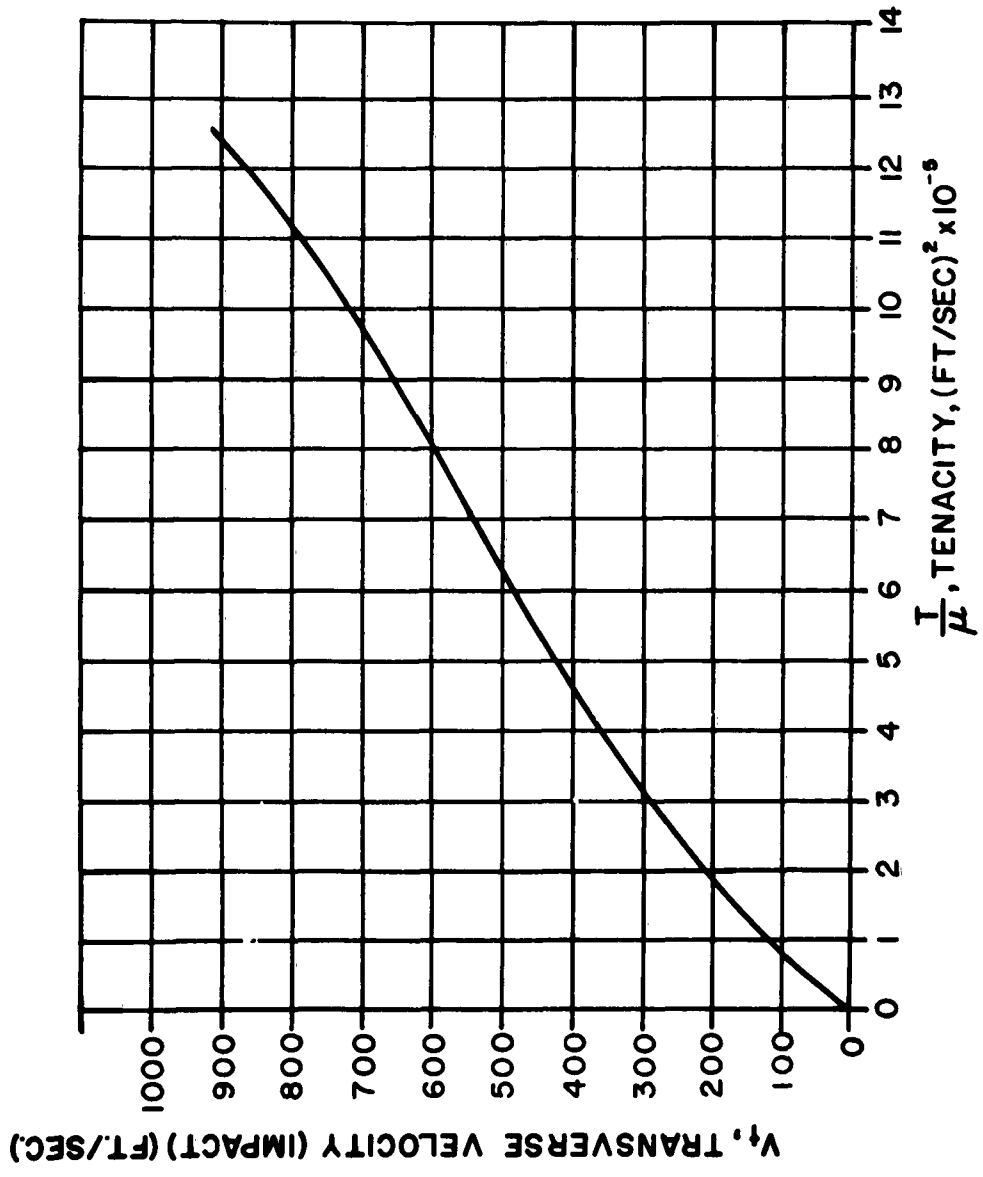
POLYETHYLENE
TRANSVERSE IMPACT
VELOCITY vs. TENACITY

Figure 52

79
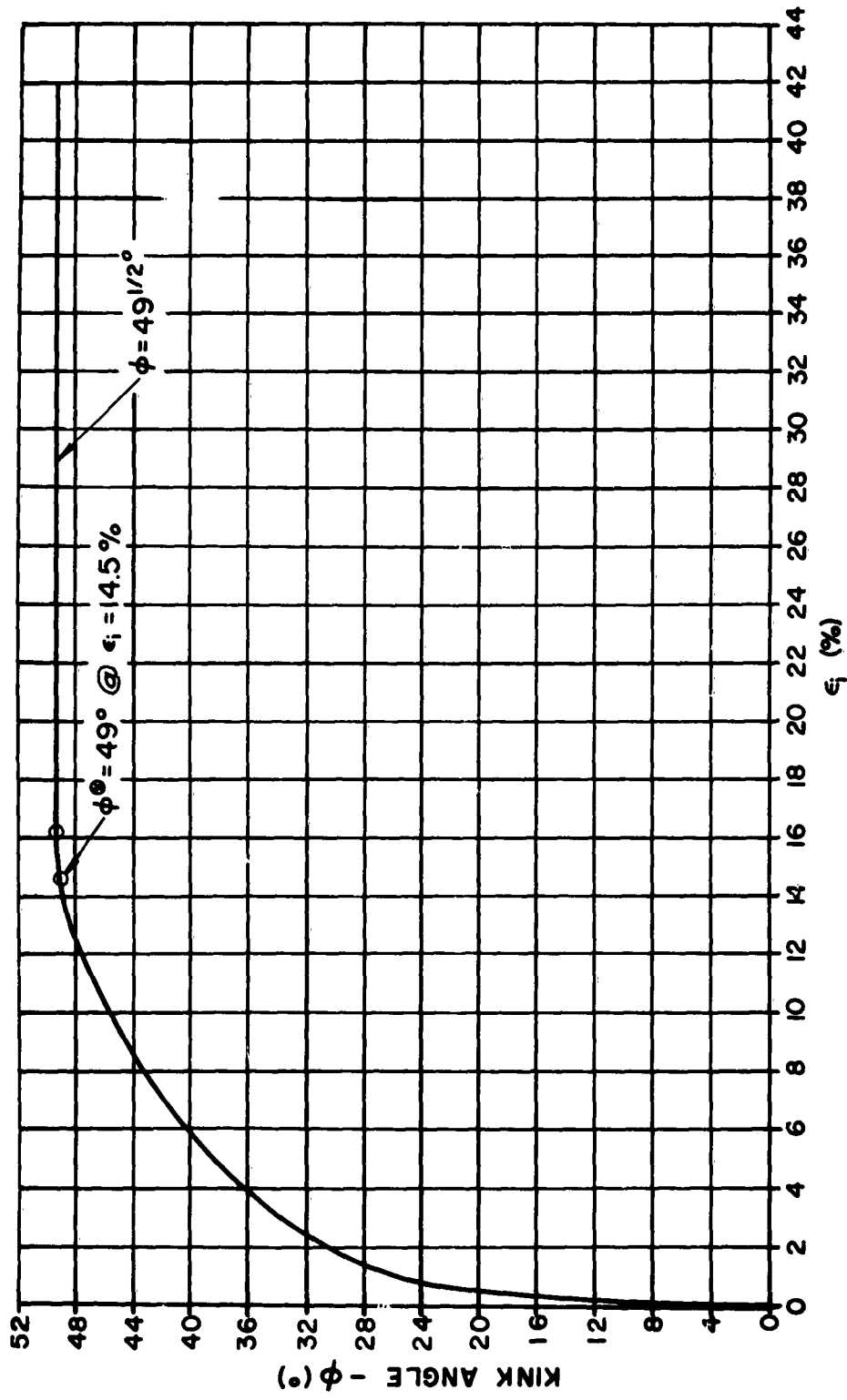
POLYETHYLENE
KINK ANGLE ϕ vs. STRAIN
Figure 53

$\phi = 49 \, 1/2°$

$\phi = 49° @ \, \epsilon_i = 14.5\%$

$\phi° = 49° @ \, \epsilon_i = 14.5\%$

ϵ_i (%)

KINK ANGLE $- \phi$ (°)

ϵ, STRAIN, PERCENT
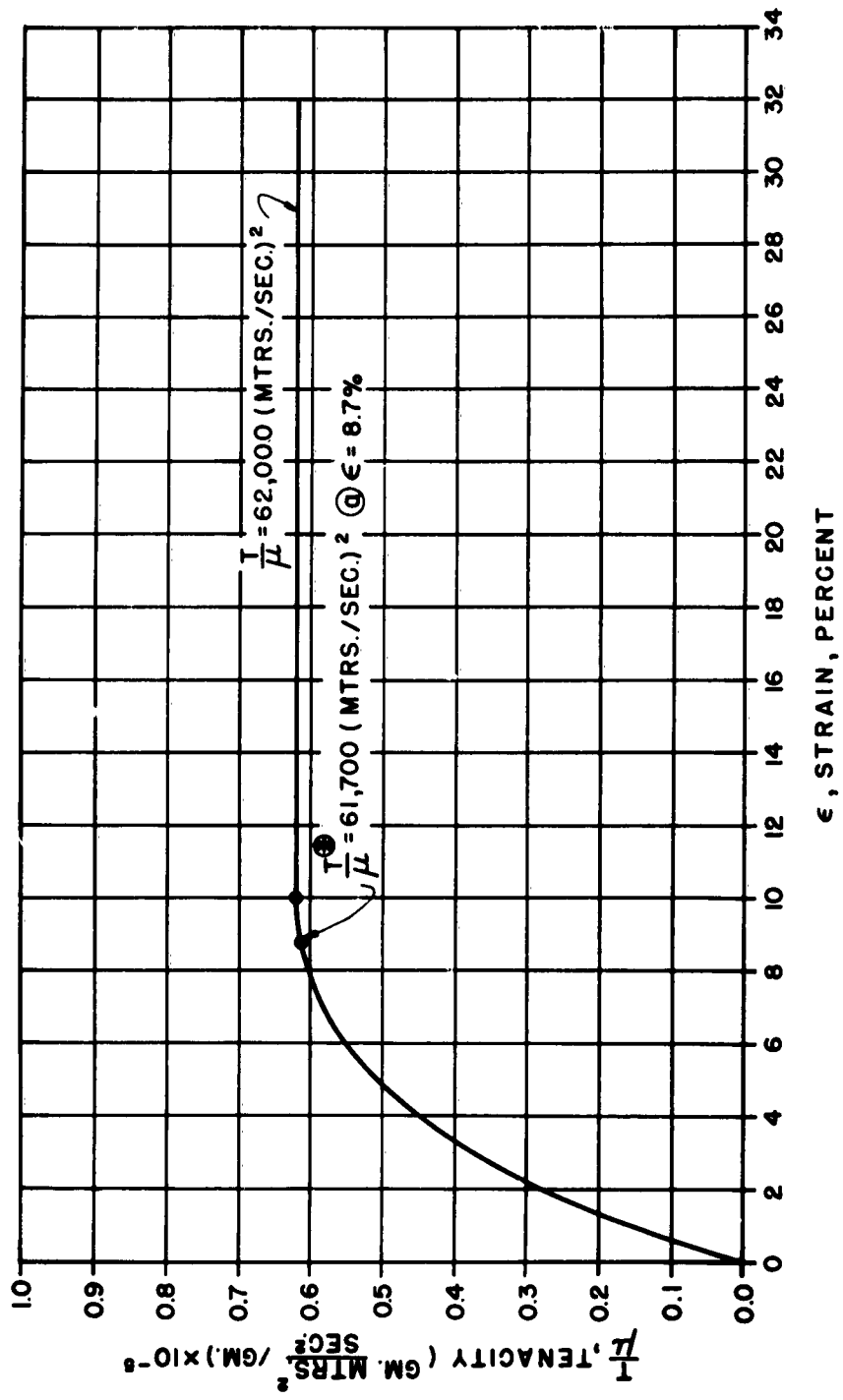
WOOL

TENACITY vs. STRAIN CURVE (FROM SUSICH & BACKER, T.R.J., 21,482[1951])
@ 21°C. (70°F.) & 65% RELATIVE HUMIDITY

Figure 54
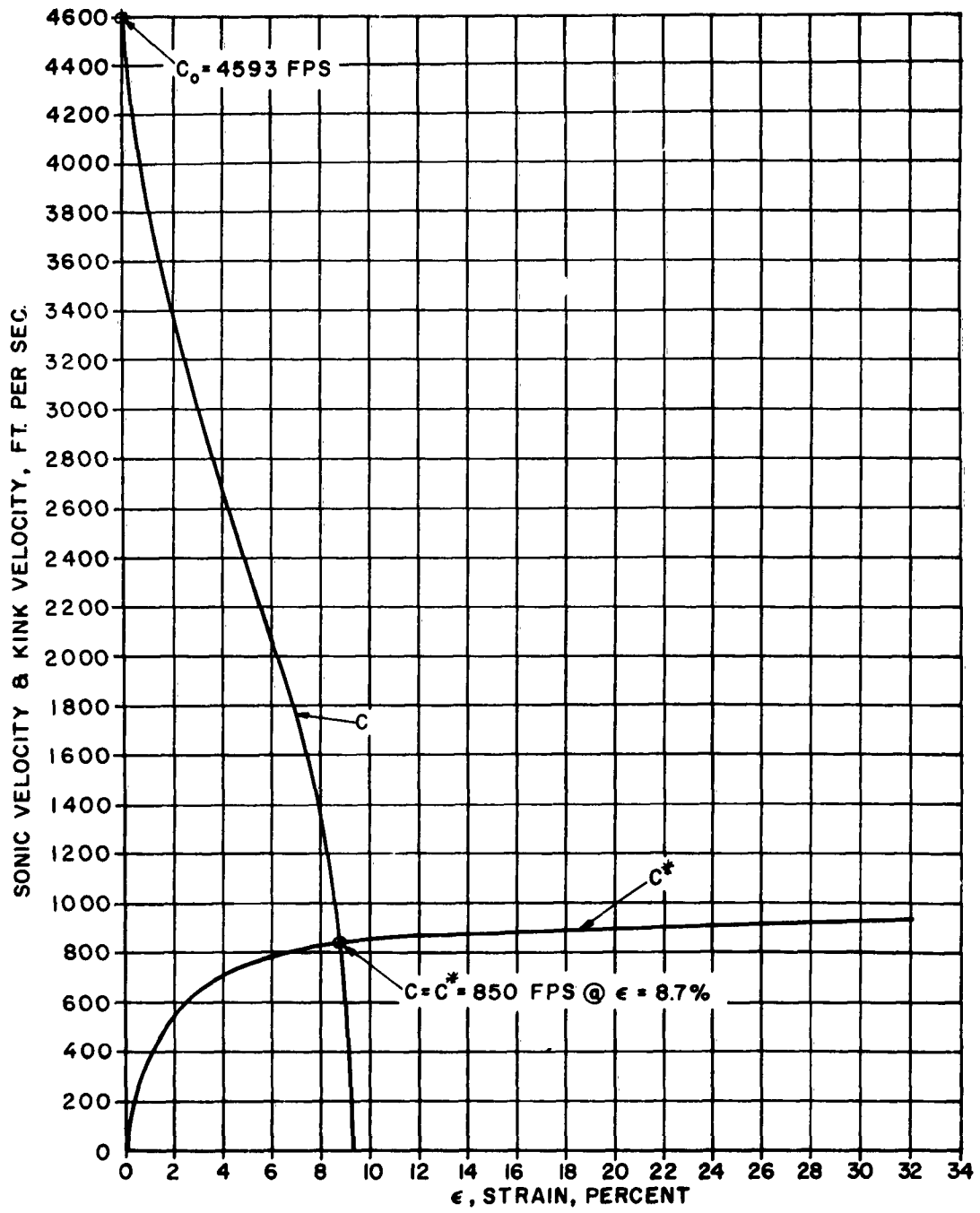
WOOL

SONIC & KINK
VELOCITIES vs. STRAIN

Figure 55

82

WOOL

LONGITUDINAL IMPACT VELOCITY vs STRAIN
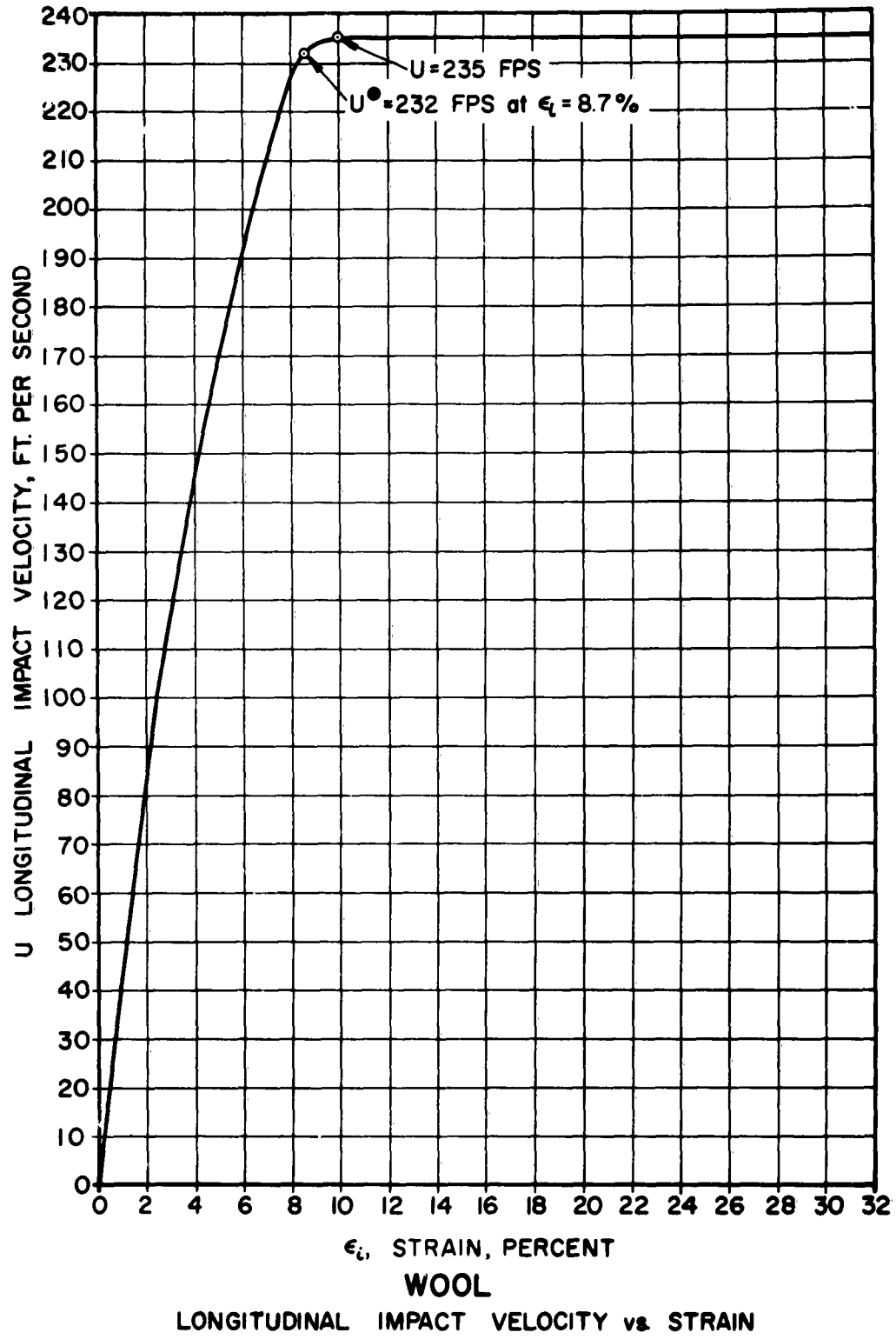
Figure 56

WOOL

TRANSVERSE IMPACT
VELOCITY vs. STRAIN

$V_f = 588$ FPS

$V_f^\bullet = 583$ FPS @ $\epsilon = 8.7\%$

$V_f^\bullet = 583$ FPS

V_t, TRANSVERSE IMPACT VELOCITY, FT. PER SEC.

ϵ_t, STRAIN, PERCENT
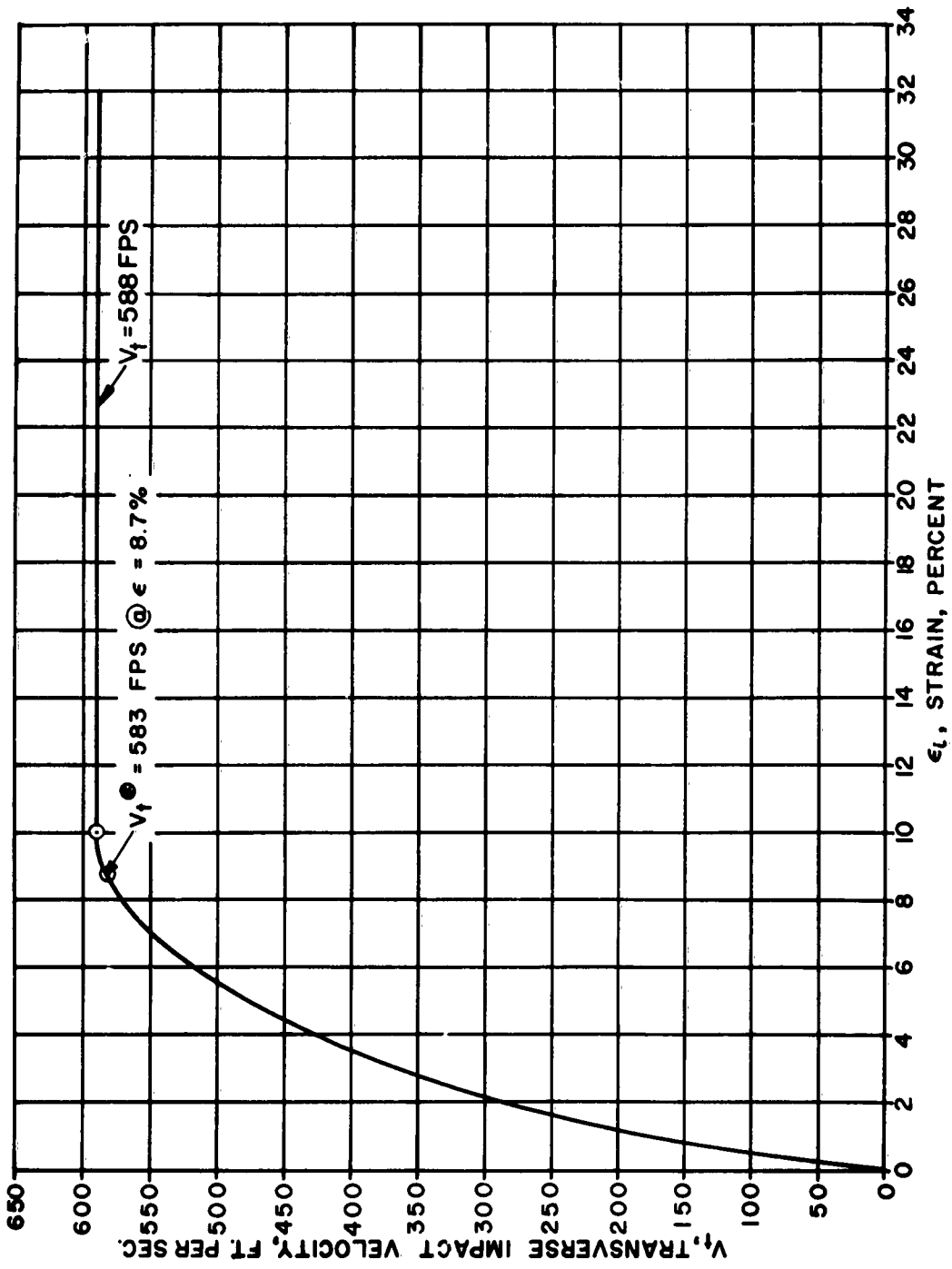
Figure 57

WOOL
TRANSVERSE IMPACT
VELOCITY vs. TENACITY
Figure 58

$V_f = 583$ FPS

$\frac{T}{\mu}$, TENACITY (FT./SEC.)^2

V_f, TRANSVERSE IMPACT VELOCITY, FT. PER SEC.

85

$\phi = 43\text{-}3/5°$

$\phi = 43\text{-}2/5°$ at $\epsilon_i = 8.7\%$
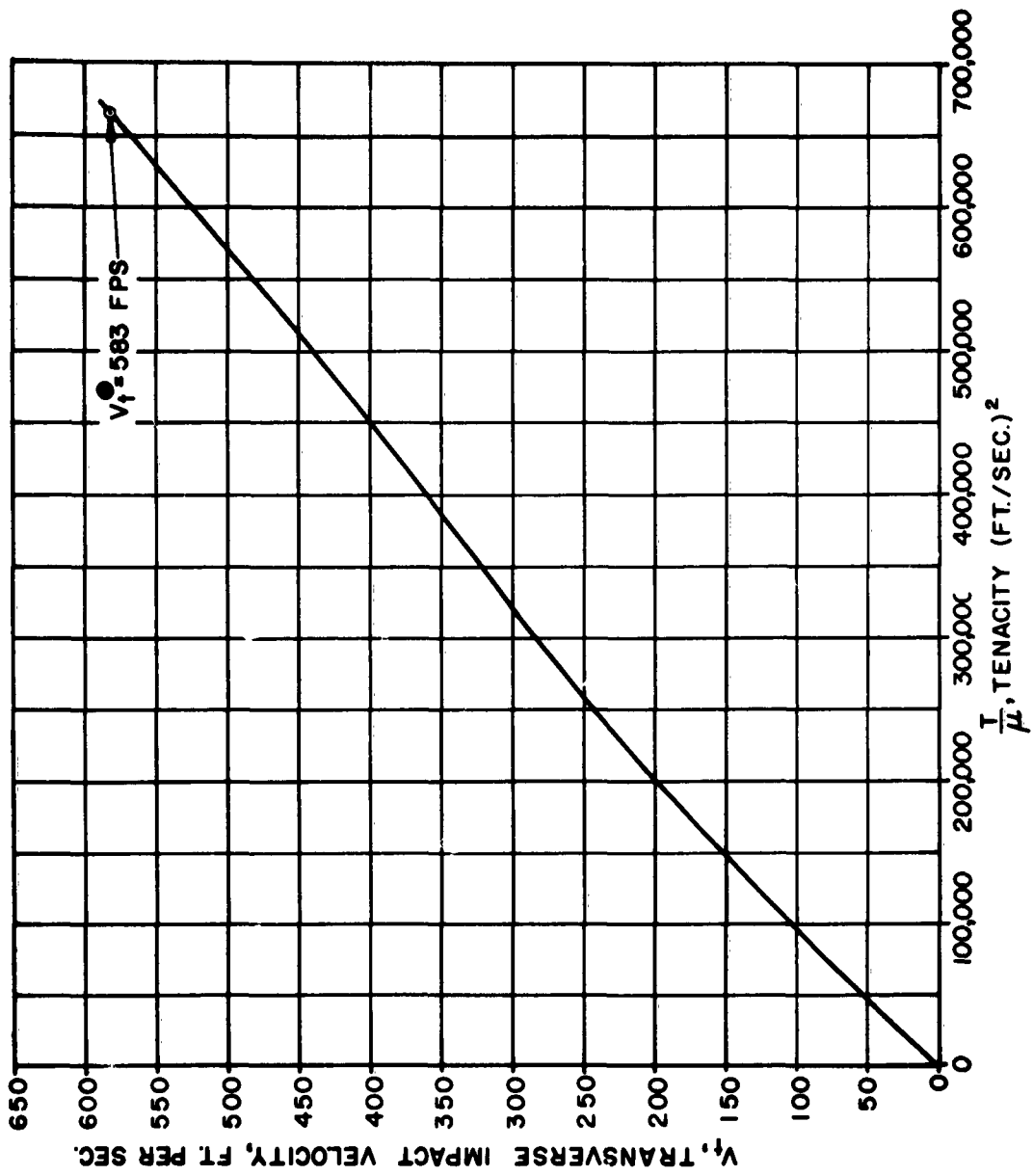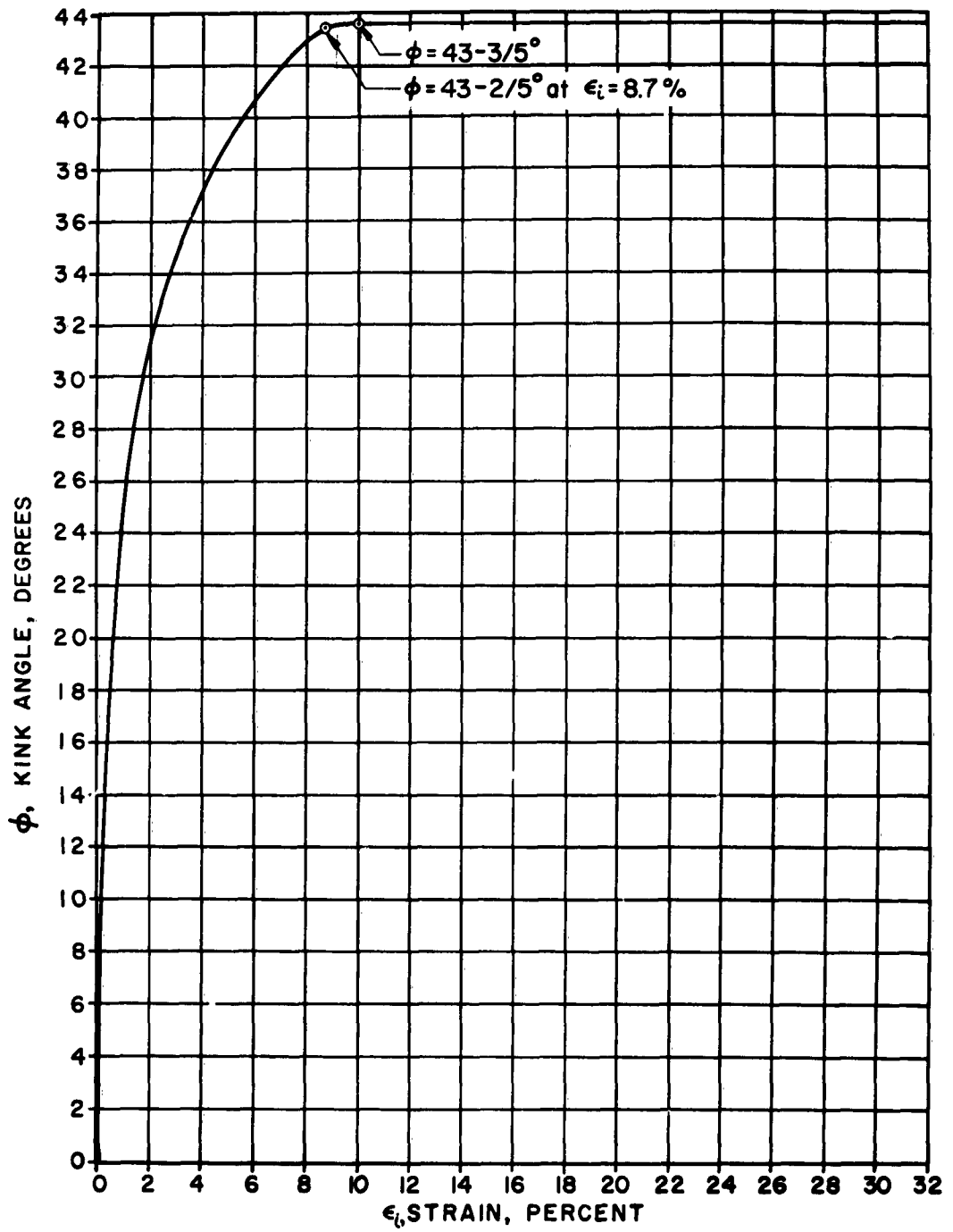
WOOL

KINK ANGLE vs. STRAIN

Figure 59
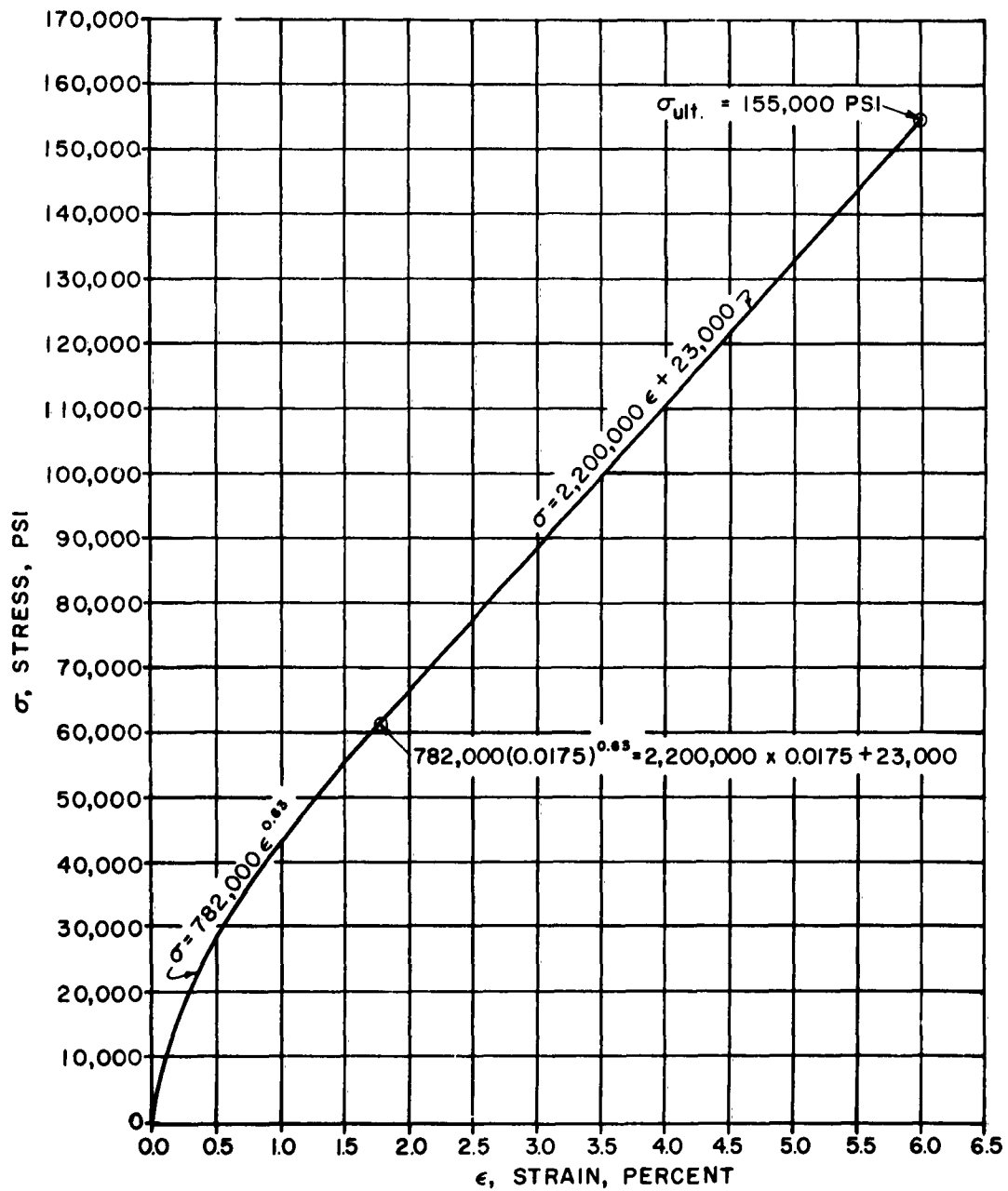
FORTISAN - 36
(CELANESE CORP. OF AMERICA)
STRESS-STRAIN DIAGRAM

Figure 60
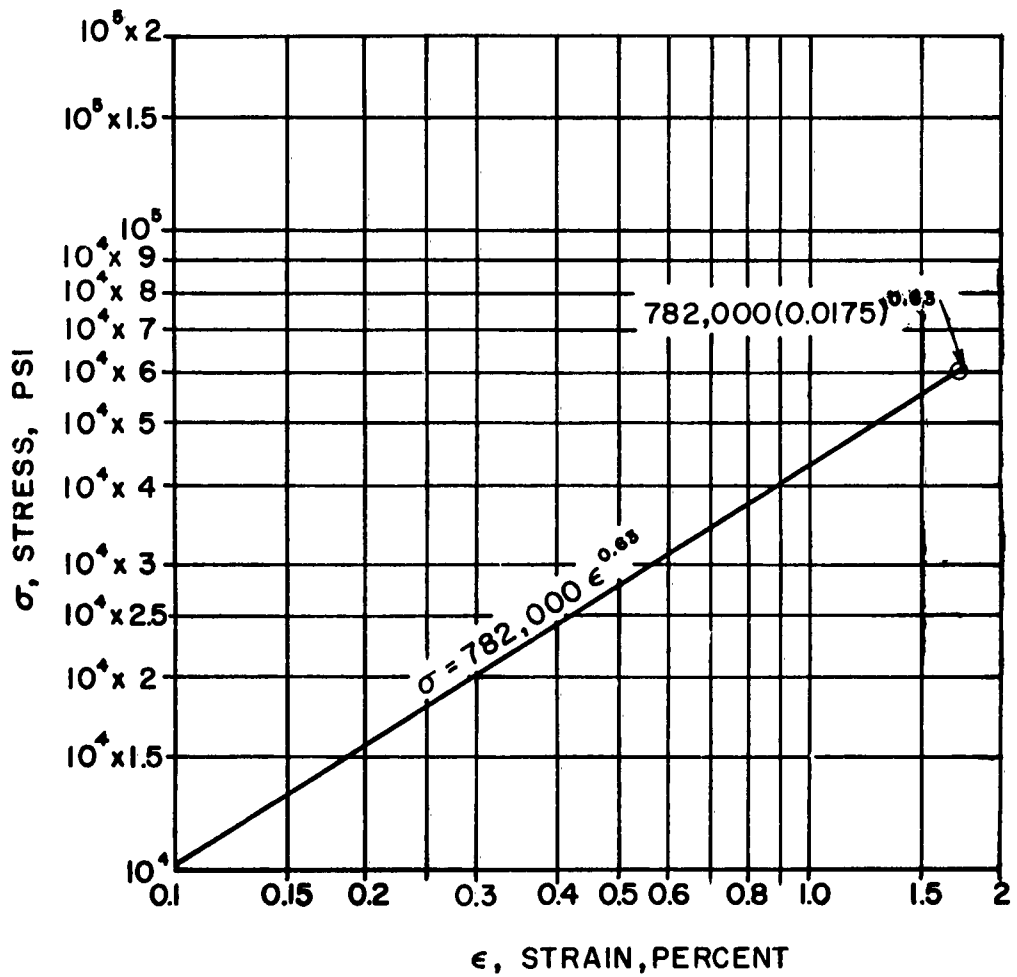
FORTISAN — 36
(CELANESE CORP. OF AMERICA)
STRESS-STRAIN DIAGRAM

Figure 61
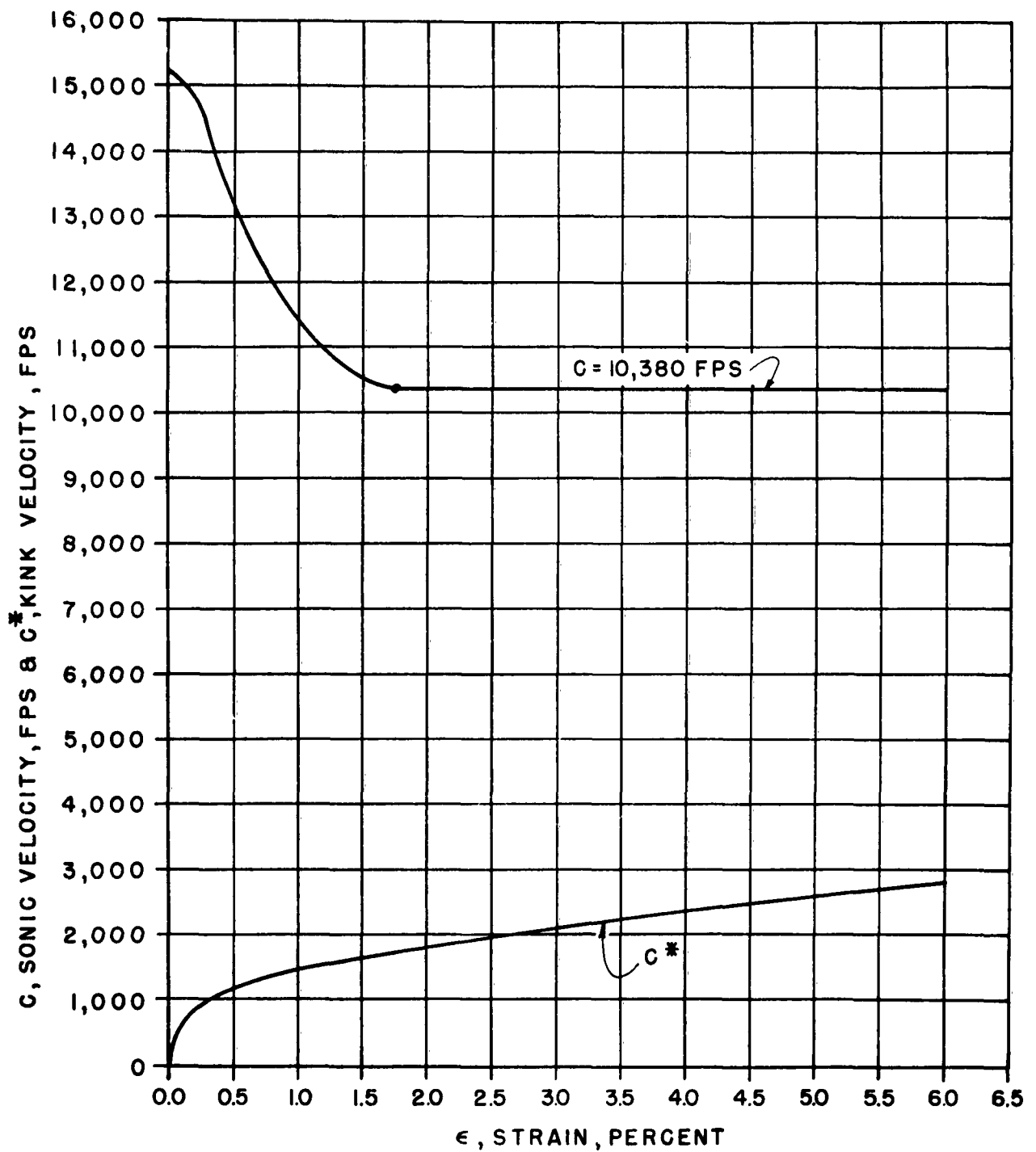
FORTISAN – 36
(CELANESE CORP. OF AMERICA)
SONIC VELOCITY & KINK
VELOCITY vs. STRAIN

Figure 62
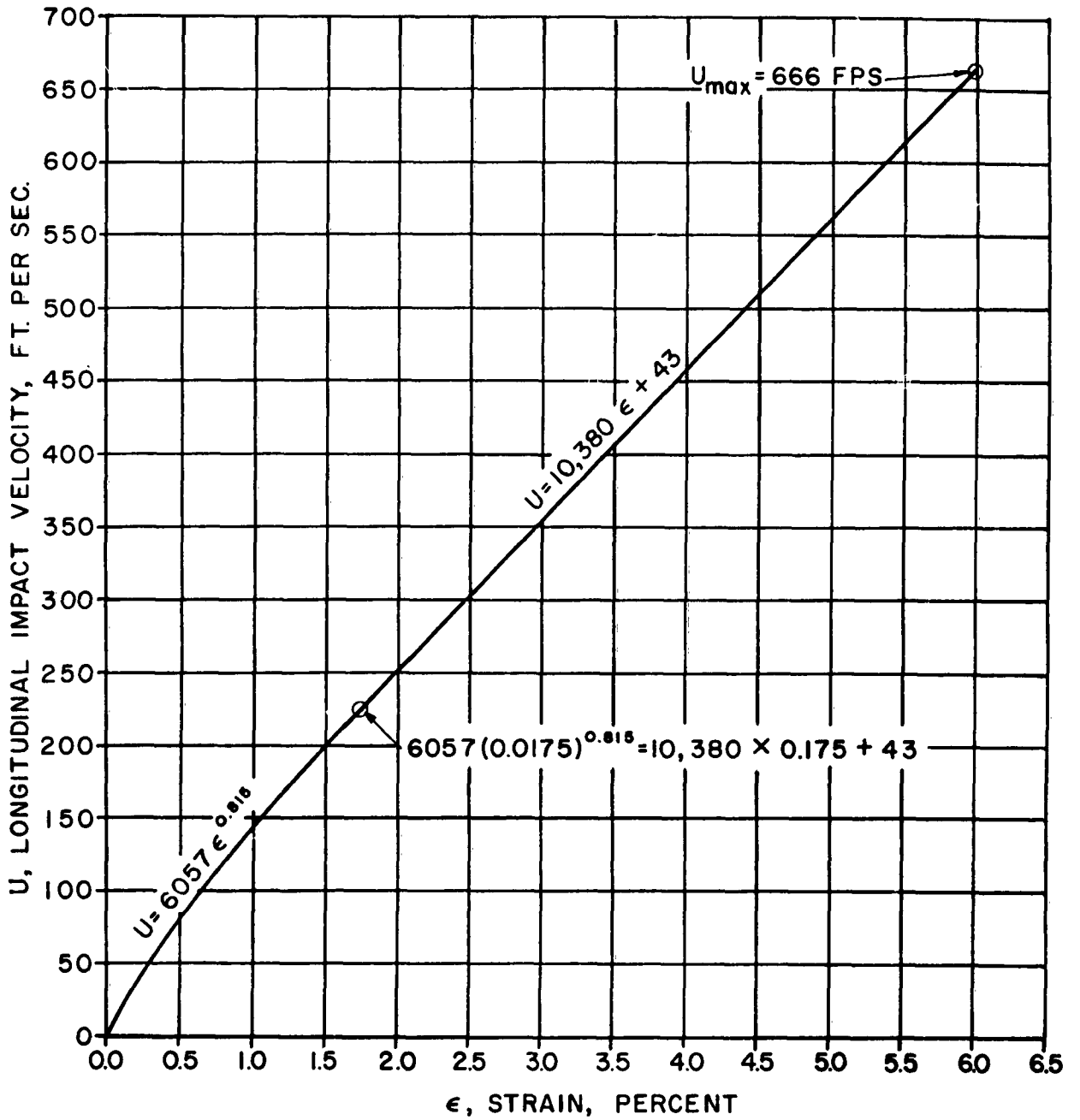
FORTISAN - 36

(CELANESE CORP. OF AMERICA)

LONGITUDINAL IMPACT
VELOCITY vs. STRAIN

Figure 63

FORTISAN-36
(CELANESE CORP. OF AMERICA)

TRANSVERSE IMPACT
VELOCITY vs. STRAIN
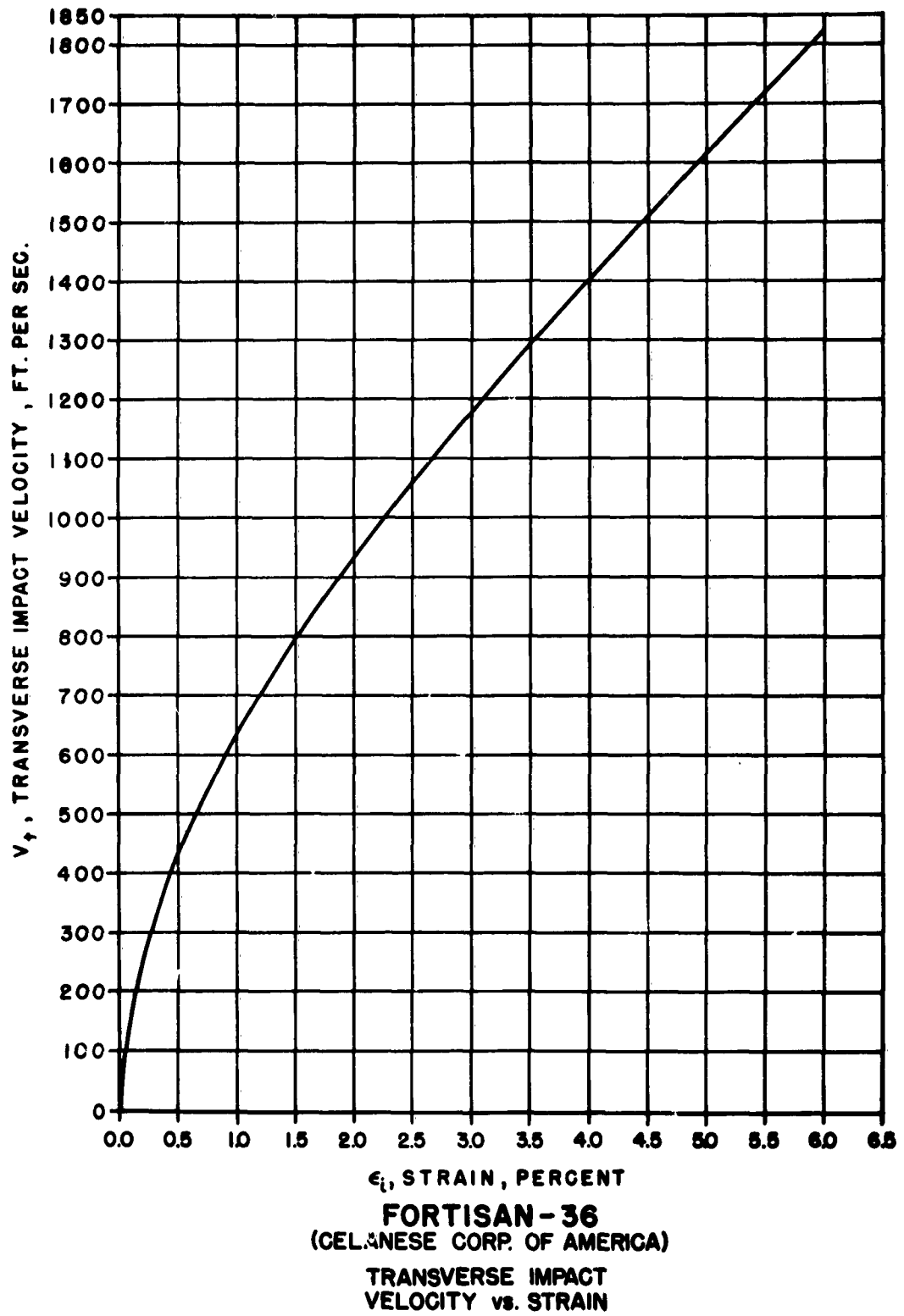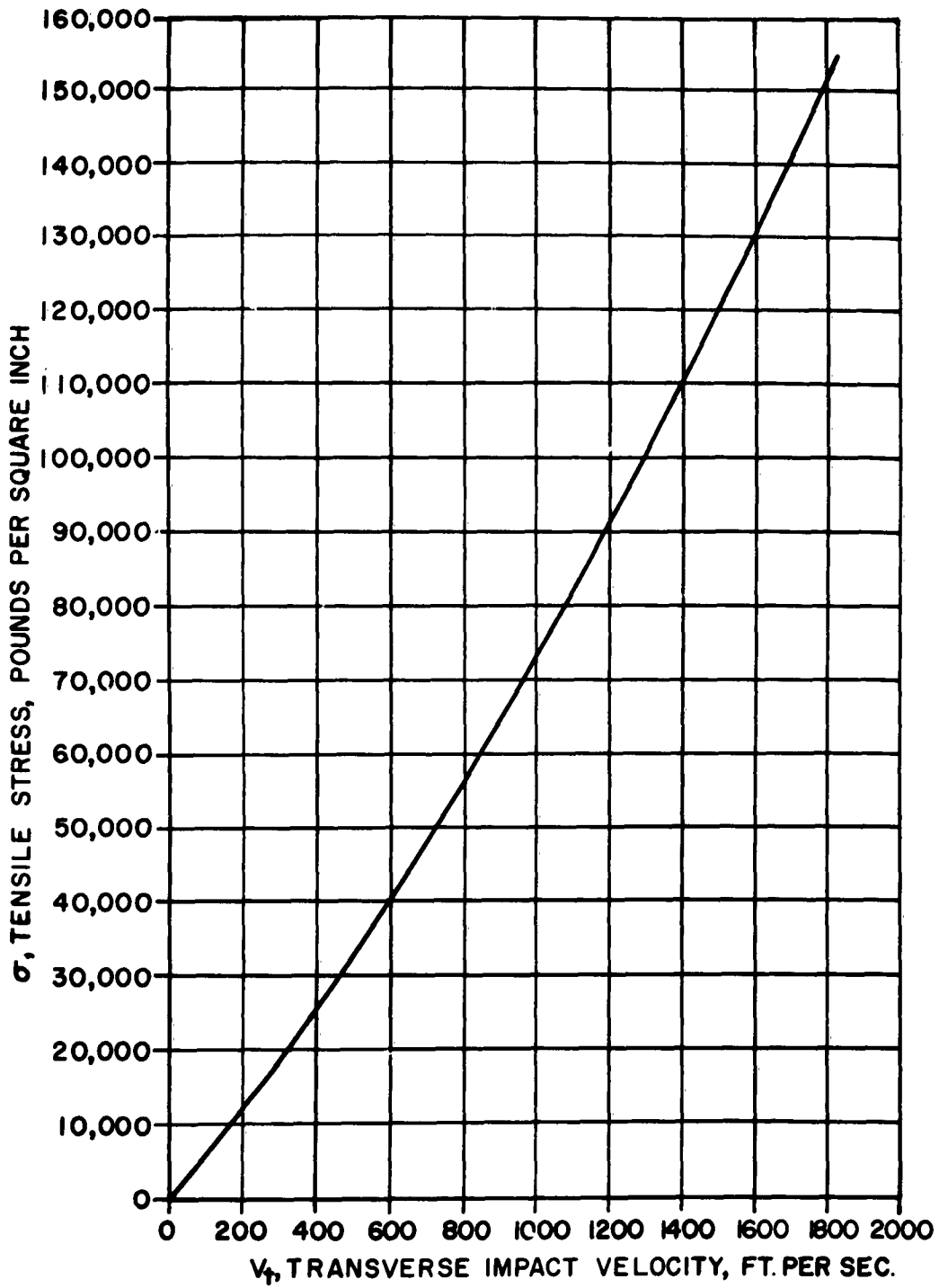
Figure 64

FORTISAN - 36

(CELANESE CORP. OF AMERICA)

TENSILE STRESS vs.
TRANSVERSE IMPACT VELOCITY
Figure 65
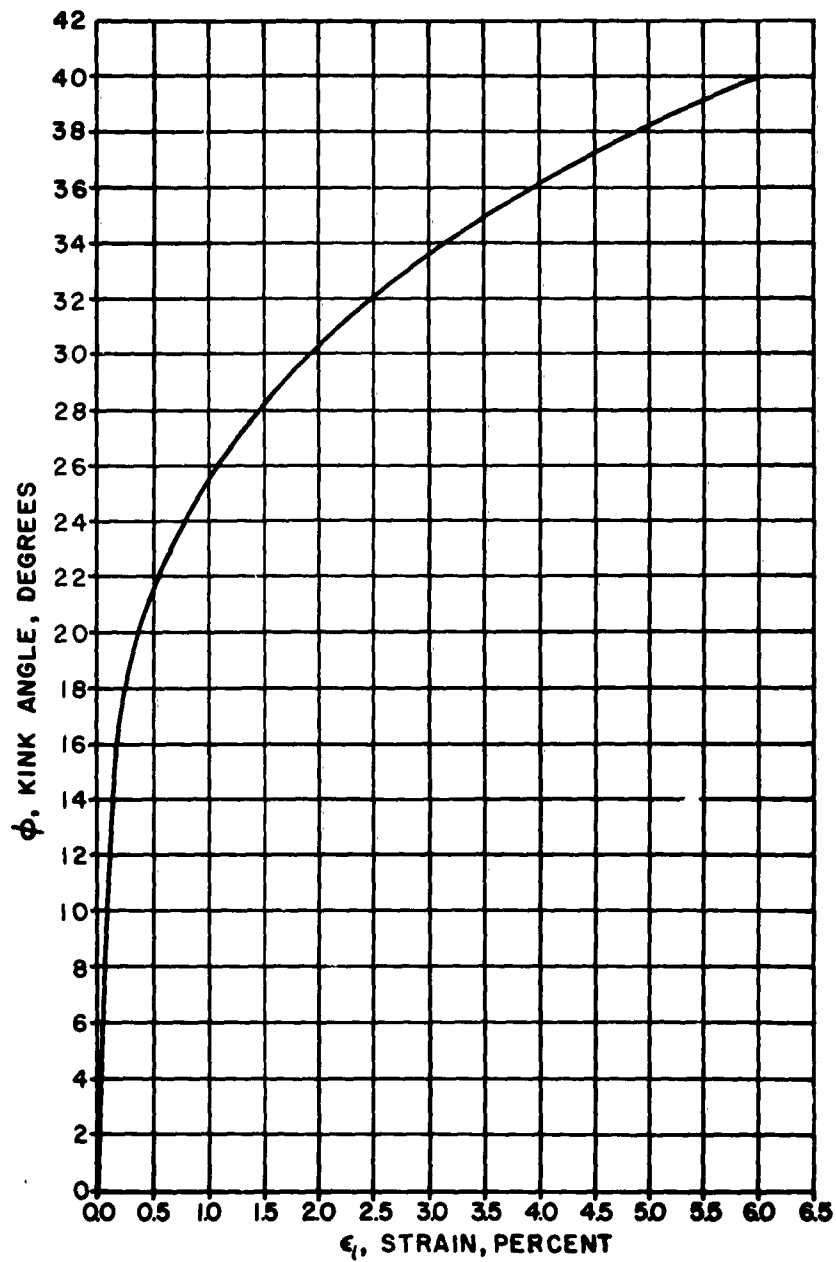
FORTISAN - 36
(SAPONIFIED ACETATE RAYON)
CELANESE CORP. OF AMERICA
KINK ANGLE vs. STRAIN

Figure 66

93
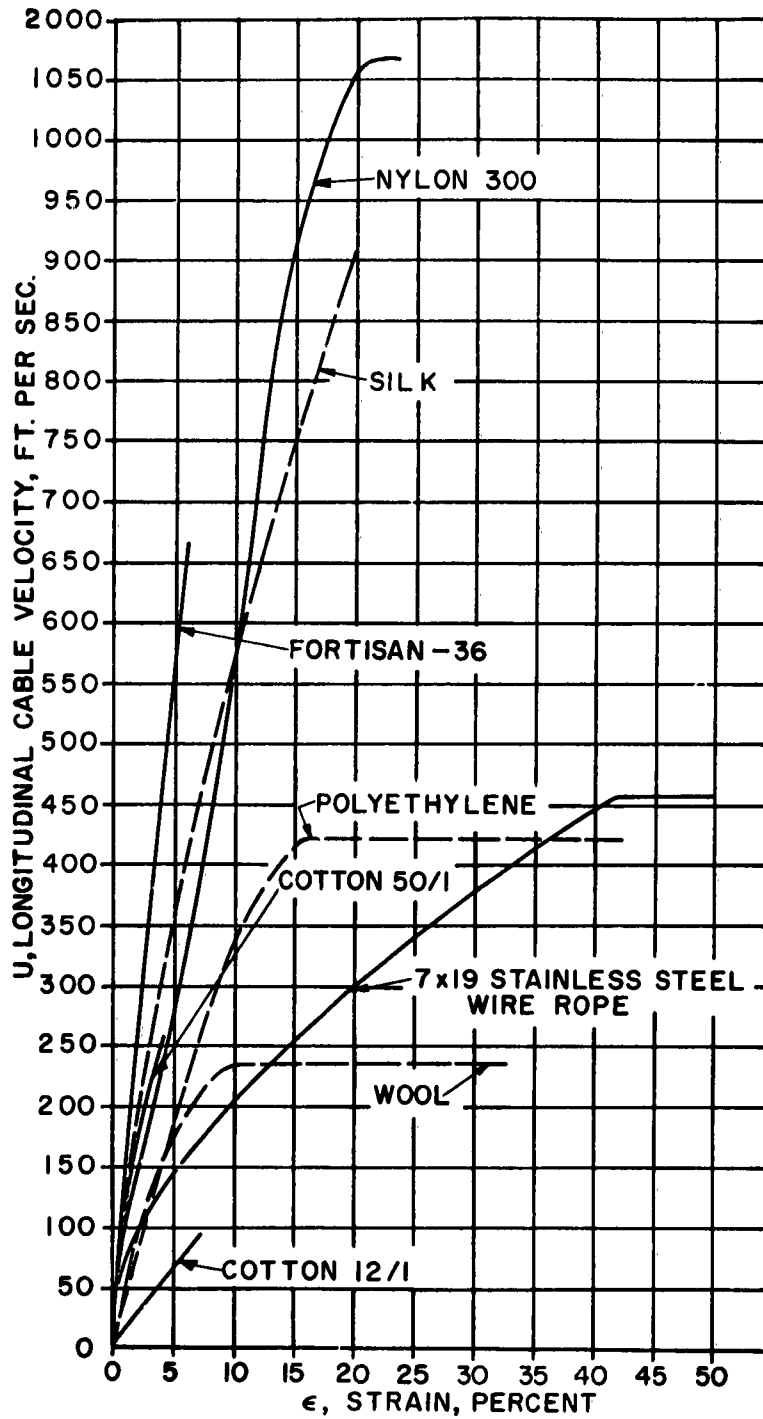
VARIOUS MATERIALS
LONGITUDINAL CABLE
VELOCITY vs. STRAIN

Figure 67

94

VARIOUS MATERIALS

TRANSVERSE IMPACT VELOCITY VS. STRAIN
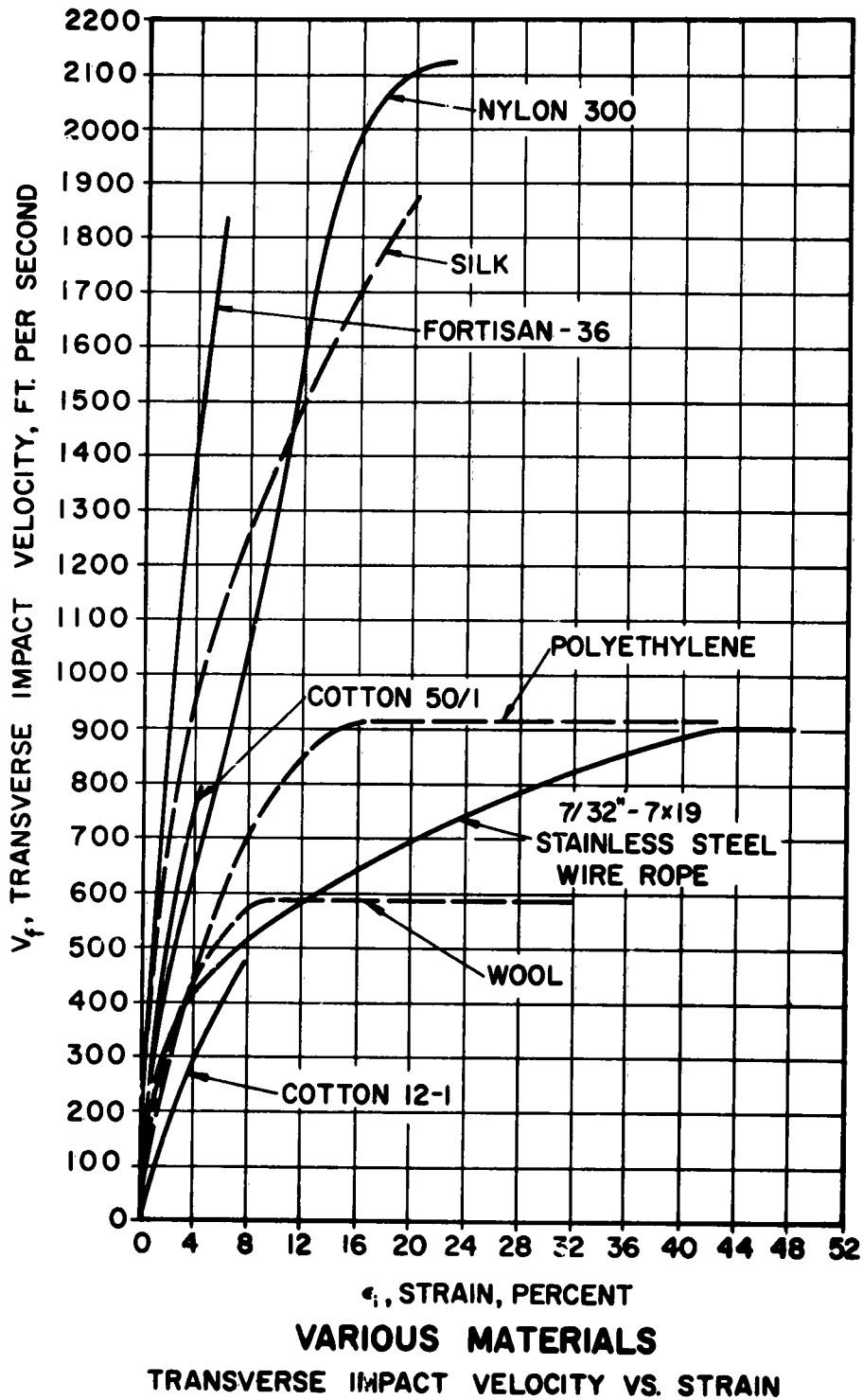
Figure 68

TABLE II - IMPACT TOLERANCES OF TYPICAL NON-LINEAR MATERIALS

Material	7 x 19 E.A. Stainless Steel Cable	Textiles at 21°C (70°F) and 65% Relative Humidity						
		Nylon 300	Silk	Cotton 50/1	Cotton 12/1	Poly-ethylene	Wool	Fortisan 36
Max. ϵ	0.5	0.23	0.2	0.042	0.075	0.42	0.32	0.06
$\dot{\epsilon}$	0.163	0.173	-	-	-	0.145	0.087	-
Max. u (fps)	457	1066	907	258	95	421	235	666
Max. $1 + \epsilon$	-	-	1.2	1.042	1.075	-	-	1.06
Max. $(c^*)^2$	-	-	5,700,000	1,664,000	1,392,000	-	-	8,030,000
Max. c^* (fps)	-	-	2387	1290	1180	-	-	2834
$\dot{c}$	926	2580	-	-	-	1189	850	-
$\dot{u}$ (fps)	266	995	-	-	-	410	232	-
Max. c^* - Max. u	-	-	1480	1032	1085	-	-	2168
$(\text{Max. } c^* - \text{Max. } u)^2$	-	-	2,190,000	1,065,000	1,177,000	-	-	4,700,000
Max. $\left[(c^*)^2 - (c^* - \dot{u})^2\right]$	-	-	3,510,000	599,000	215,000	-	-	3,330,000
Max. $u - \dot{u}$	191	71	-	-	-	11	3	-
$(\dot{c} + u - \dot{u})$	1117	2651	-	-	-	1200	853	-
$\dot{c} - \dot{u}$	660	1585	-	-	-	779	618	-
Max. $(\dot{c}+u-\dot{u})^2$	1,248,000	7,030,000	-	-	-	1,440,000	728,000	-
$(\dot{c} - \dot{u})^2$	436,000	2,510,000	-	-	-	607,000	382,000	-
Max. $\left[(\dot{c}+u-\dot{u})^2-(\dot{c}-\dot{u})^2\right]$	812,000	4,520,000	-	-	-	833,000	346,000	-
Max. $(v_r)^2$	812,000	4,520,000	3,510,000	599,000	215,000	833,000	346,000	3,330,000
Max. v_t (fps)	901	2126	1873	774	464	913	588	1825
$\dfrac{\text{Max. } c^* - \text{Max. } u}{\text{Max. } c^*}$	-	-	0.622	0.8000	0.91949	-	-	0.765
$\dfrac{\dot{c} - \dot{u}}{\dot{c} + u - \dot{u}}$	0.5909	0.5979	-	-	-	0.649	0.7245	-
Arccos $\dfrac{\text{Max. } c^* - \text{Max. } u}{\text{Max. } c^*}$	-	-	$51\frac{1}{2}°$	$36\frac{4}{5}°$	23.1°	-	-	40°
Arccos $\dfrac{\dot{c} - \dot{u}}{\dot{c} + u - \dot{u}}$	$53\frac{3}{4}°$	$53\frac{1}{4}°$	-	-	-	$49\frac{3}{5}°$	$43\frac{3}{5}°$	-
Max. ϕ	$53\frac{3}{4}°$	$53\frac{1}{4}°$	$51\frac{1}{2}°$	$36\frac{4}{5}°$	23.1°	$49\frac{3}{5}°$	$43\frac{3}{5}°$	40°

SECTION 4

STATIC TESTS

4.0 Tensile Tests

The testing phase of the program was initiated with a series of tensile tests on selected specimens because the mechanical properties of a specimen are necessary to predict its impact tolerance from which the dynamic testing velocity can be programmed. The mechanical properties required are as follows:

1. Modulus of Elasticity (Æ) or (E)

2. Ultimate Tensio⌐ (T) or Stress (σ_u^-)

3. Maximum Strain (ϵ_{max})

The values of these parameters listed above were determined by performing a static tension-strain test on prepared sections of the selected specimens that were to be used in the dynamic tests. The results of these static tests were represented by tension-strain curves which were then used to predict the impact velocities as outlined in Section 3 of this note.

4.0.1 Test Specimens

In preparation for the static tension tests, specimens of tension members representing various geometrical configurations and materials were selected. These selections were based on the analytical predictions derived from the methods of Section 3.2, which are listed in Tables I and II. The most promising of the materials analyzed were selected for the test program.

97

In addition, materials in present use on arresting gear systems were also analytically investigated and included in the test program for purposes of comparison and for verification of their known present performance in actual full scale use.

The following is a list of the materials which were selected to be tested:

1. 1/8-inch diameter, 6 x 19, improved plow steel wire rope

2. 1/16-inch diameter, improved plow steel, single wire

3. 1/16-inch diameter, plow steel, single wire

4. 0.010-inch diameter, (0.85-0.90 carbon) steel, single wire (500,000 psi)

5. 7/32-inch diameter, 7 x 19, E.A. stainless steel wire rope

6. 1/16-inch diameter, E.A. stainless steel, single wire

7. 1/16-inch diameter, titanium alloy (13V-11Cr-3Al), single wire

8. 1/8-inch diameter, 3-strand Fiberglas cord, untreated, approximately 45° lay angle

9. 1/8-inch diameter, 3-strand Fiberglas cord, neoprene treated, approximately 45° lay angle

10. 0.052-inch diameter, 3-strand Fiberglas cord, untreated, approximately 45° lay angle

11. 0.062-inch diamter, 3-strand Fiberglas cord, neoprene treated, approximately 45° lay angle

12. 1/8-inch diameter, 3-strand nylon cord, approximately 45° lay angle

13. 1/8-inch diameter, 3-strand Fortisan 36 cord, approximately 8° lay angle

14. 0.0152-inch diameter, multiple filament, Fortisan 36 single strand, 0.8Z twist

4.0.2 Test Fixture

The tensile tests were performed using an Instron Tensile Testing Instrument, Model TTC-ML (See Figure D.1-1, page 186). The specimens listed in Section 4.0.1, page 98, were placed in the holding jaws of the Instron as is illustrated in Figure D.1-2, page 187. The Instron Instrument is capable of extending the length of a specimen at controlled rates of strain. This phenomenon produces a tensile force in the specimen depending on its resistance which is a function of the material properties of the specimen. The tensile force produced is recorded on the instrument chart, which is calibrated to a predetermined load scale and revolves at predetermined constant speed. This load versus time relationship represents a load versus strain record of the tensile test.

4.0.3 Test Procedure

The specimens tested were placed in the Instron Instrument and subjected to the tensile tests using the following procedures:

1. The gage length of the specimen was governed by the extensibility range of the Instron Instrument and the percent elongation properties of the material being tested, said elongation being predetermined approximately from the manufacturer's data.

2. The rate of extension of the specimen during the test was preset on the Instron Instrument prior to beginning the test and was based on a time period of approximately ten to fifteen minutes to complete each test. The chart speed was conveniently preset prior to testing so as to produce a chart curve of reasonable dimensions.

3. The extension of each specimen was initiated and continued until failure occurred. All additional data, needed to properly identify each specimen and to evaluate the chart curve produced, were tabulated after each test. (See Appendix C1, page 139).

SECTION 5

DYNAMIC TESTS

5.0 Longitudinal Impact Tests

This part of the test program was conducted to determine the longitu-dinal impact tolerances of representative samples of the specimens listed in Section 4.0.1. Due to time and weather limitations, no attempt was made to cover the entire test specimen group but only to produce sufficient data to verify the validity of the analytic method used to predict the longitu-dinal impact properties of materials. While transverse impact tolerances are more critical and useful for the purposes of the present research program it is in the interests of the overall theoretical development to verify the longitudinal impact phase of the analytical method since the value of this particular property is a component calculation in the method used to determine the transverse impact velocity. Moreover, it may be that under different conditions of practical usage, the longitudinal impact tolerance of a tension member will be the important property to be evaluated. It does not follow that a verification of the method for the transverse impact predictions necessarily verifies the method for use in the prediction of longitudinal impact velocities. Each phase must be tested experimentally and the following is intended to describe the testing program for longitu-dinal impact tests.

5.0.1 Test Specimens

The following specimens were selected for the longitudinal impact tests and were prepared in lengths of 20 ft.

1. 1/8-inch diameter, 6 x 19, improved plow steel wire rope

2. 1/16-inch diameter, E. A. stainless steel, single wire

3. 1/16-inch diameter, titanium, single wire

4. 1/8-inch diameter, 3-strand Fiberglas cord, neoprene treated, approximately 45° lay angle

5. 1/8-inch diameter, 3-strand Fortisan 36 cord, approximately 8° lay angle.

It was intended to determine the impact properties of the 0.010 inch diameter high tensile steel wire and the 1/8-inch diameter, 3-strand Fiberglas cord, untreated specimen but time and weather did not permit the completion of these two test series.

5.0.2 Test Fixtures

In order to produce longitudinal impact velocities up to 675 ft. per second a sled type missile was used, propelled along a 100 ft. 30 lb. rail track by an explosive charge detonated in a gun chamber at one end of the track (See Figure D2.1-2, page 190). The front end of the sled was provided with a hook configuration for impacting the test specimen without introducing kinking effects upon impact. The sled was also equipped with a scoop-like attachment to provide a means of stopping the sled after impact with the specimen within the 100 ft. length of track provided. The braking force was obtained by deflection over a 170° angle of a column of water entering the scoop from a water filled trough located along the center of the track and starting about 5 feet from the specimen impacting area. The water was contained in the trough by means of two water filled plastic bags placed in the trough at each end until the sled scoop made

contact with and ruptured the bag at the specimen end of the trough. This particular bag was then replaced with a new one and the trough refilled after each test. (See Figures D2.1-3, D2.1-5, D2.1-6, pages 190 and 191.)

The muzzle velocities of the sled were determined from the impulse-momentum relationship obtained during the firing of the sled,through enlarged photographic images of the pressure-time curve as recorded on an oscilloscope instrument. A chronometer (Figure D2.1-4, page 190) was used to verify the validity of the results of the impulse-momentum data in a sample series of tests conducted without specimens by measuring the time elapsed between fractures upon impact with the sled of two conducting break-wires placed 36" apart along the track. (See Tests a to f, page 156). Contact of the sled with the first wire was made just after the entire sled tube left the end of the gun muzzle, so that the sled had attained its maximum velocity before contact with the measuring instrumentation. Because of time limitations due to the uncertainty of weather conditions suitable for testing it was impractical to use the chronometer-breakwire system throughout the testing.

5.0.3 Test Procedure

The following procedure was used in conducting the longitudinal impact tests:

1. The six velocity tests without specimen outlined in Section 5.0.2 were conducted first using progressively higher velocities controlled by the composition and quantity of the explosive charge. Data was collected and recorded for each test. Correlation was then established to justify the use of the impulse-momentum method for determining the velocities throughout the rest of the longitudinal test program.

103

2. The two ends of the specimen were attached to fixed points with a low tension strength thread to simulate a free ended condition. The same thread was tied to points along the center of the specimen and attached to fixed points so as to support the specimen in the shape of a triangle with a curved vertex at the same height as the impacting hook of the sled. (See Figure D2.1-1, page 190).

3. Prior to firing the sled the water trough was filled after damming the ends with the water filled plastic bags. The gun chamber was then loaded with an explosive charge designed to provide the velocity equivalent to the longitudinal impact velocity as predicted from the static tests.

4. The gun was then fired with the sled piston inserted in the firing chamber and braked to a stop after impacting the specimen by means of the water brake scoop described in Section 5.0.2. The trough lost some water after this braking action and the water bag at the specimen end, which was ruptured during the test run, was replaced and the water trough refilled. The sled was returned to its position in the gun barrel by removing the plastic bag for a short interval to allow the sled to slide past it.

5. The test specimen was then examined for evidences of failure due to impact. All data was collected and recorded for each test (Appendix C2.1, page 155). If the specimen was found undamaged, testing of the same type specimen was continued using progressively higher velocities until failure occurred. If on the other hand, the specimen was found damaged, the testing of the same type specimen was continued using progressively lower velocities until no damage was observed. If the difference between the lowest velocity

causing damage and the highest velocity resisted without damage was too great, the difference was reduced by additional tests at velocities intermediate between the two values.

5.1 Transverse Impact Tests

The transverse impact tests were conducted to determine the transverse impact tolerances of selected materials and establish a correlation with the analytical method used to predict the transverse impact tolerance of these materials. Because the present methods of arresting high speed aircraft in landing makes use of the transverse impact in a tension member, this transverse impact investigation of the present program is expected to be of greatest value. Therefore tests were conducted using the complete list of materials as outlined in Section 4.0.1.

The impacting sled employed in conducting the longitudinal impact velocity tests was incapable of providing the high transverse impact velocities which analytical predictions indicated as necessary to produce failure in a test specimen. In order to provide the required controllable transverse impact velocities, use was made of impacting slugs fired from a shot-gun. It was found by a preliminary test series, that adequate impact accuracy and velocity control of solid, 12-gauge shot-gun slugs could be obtained. The success of this early test series justified the development of the technique around which the transverse test program was planned.

5.1.1 Test Specimens

The following specimens of tension members representing various geometrical configurations and materials were tested for transverse impact tolerance:

105

1. 1/8-inch diameter, 6 x 19, improved plow steel wire rope

2. 1/16-inch diameter, improved plow steel, single wire

3. 1/16-inch diameter, plow steel, single wire

4. 0.010-inch diameter, (0.85-0.90 carbon) steel, single wire (500,000 psi)

5. 7/32-inch diameter, 7 x 19, E.A. stainless steel wire rope

6. 1/16-inch diameter, E.A. Stainless steel, single wire

7. 1/16-inch diameter, titanium alloy (13V-11Cr-3Al), single wire

8. 1/8-inch diameter, 3-strand Fiberglas cord, untreated, approximately 45° lay angle

9. 1/8-inch diameter, 3-strand Fiberglas cord, neoprene treated, approximately 45° lay angle

10. 0.052-inch diameter, 3-strand Fiberglas cord, untreated, approximately 45° lay angle

11. 0.062-inch diameter, 3-strand Fiberglas cord, neoprene treated, approximately 45° lay angle

12. 1/8-inch diameter, 3-strand nylon cord, approximately 45° lay angle

13. 1/8-inch diameter, 3-strand Fortisan 36 cord, approximately 8° lay angle

14. 0.0152-inch diameter, multiple filament, Fortisan 36 single strand, 0.8Z twist

5.1.2 Test Fixture

As mentioned in section 5.1, use was made of a 12 gauge shot-gun firing a solid slug. Initial tests were conducted while firing off-hand with a 12-gauge model 50 Winchester shotgun having a 30-inch full choke barrel. These initial tests were performed merely to demonstrate the feasibility of the technique; the weapon was mounted later on a rigid gun mount and instrumentation was added to measure the velocity of each shot. The velocity

measurements were made by using two breakwires placed at 8 inches and 44 inches from the end of the gun barrel. These wires were severed upon impact with the shotgun slug during each firing and the time interval between wire breaks was recorded by means of electric chronographs connected to the breakwires.

5.1.3 Test Procedure

The test specimens, approximately 20-feet long, were suspended in a nearly horizontal position between two fixed points at a distance approximately 8 feet from the end of the gun barrel. The two ends of the tension members were connected to each of these fixed points with a low tension strength thread to simulate a free ended condition. The slug was fired at the velocity in the neighborhood of the predicted impact velocity of the specimen and aimed to strike the center of the specimen at a 90° angle.

After impact the specimen was examined for failure and if such failure occured, additional shots were fired at the same type specimen at progressively lower velocities until impact was resisted without failure. If failure did not occur initially the additional shots were fired at progressively higher velocities until failure did occur. If the difference between the lowest velocity causing failure and the highest velocity resisted without failure was too great, the difference was reduced by additional tests at velocities intermediate between the two values. Any visible damage to the specimen was considered a failure.

Photographs presented in Figures D2.2-2 to D2.2-5, page 196, illustrate the test set-up. Figure D2.2-2 shows the test set-up used in the preliminary evaluation of the methods to be used for conducting the tests (Tests No. 1 to 62). Figures D2.2-3 and D2.2-4 are two views of the test set-up used to conduct the tests under the established program (Test No. 63 to 337). Figure D2.2-5 illustrates the end tieups to simulate a free ended condition of the test specimen.

SECTION 6

ANALYSIS OF DYNAMIC TEST DATA

6.0 Test Data Reduction

The test data for the dynamic tests conducted as outlined in Section 5 are presented in Appendix C2, page 154, of this report. The longitudinal impact velocities as presented in Appendix C2.1, page 155, were calculated using the impulse momentum method from the enlarged photographic image of the pressure time curves. The area under each of these curves was computed using a planimeter. From the area and the known grid scale of the curve, the impulse is determi .ed and combined with known mass of the sled to obtain the velocity of the sled.

From the data obtained in the dynamic tests, Charts I & II were constructed to determine the distribution pattern for each series of impact tests on a particular specimen. These outlines were helpful in defining the area of critical impact velocity. At velocities below the lower limit of the range, the specimen can be expected to resist failure, while at velocities above the upper limit of the range, failure of the specimen can be expected. At velocities within the range the impact tolerance is uncertain. However, the closer the velocity within the unpredictable range is to the lower limit, the higher the probability that the specimen will resist failure and the opposite probability exists when the velocity is closer to the upper limit. The greater the number of tests conducted over a range of velocities, the more positive can the identification be made of the critical area of failure. Because of this last consideration, it is noteworthy that although the tests as presented in this report are not large

Round No.	1/8" Improved Plow Steel Wire Rope	1/16" Titanium Wire 13V-11Cr-3Al	1/8" Treated Fiberglas Cord	1/16" Stainless Steel Wire	1/8" Fortisan 36 Cord	0.010" High Tensile Steel Wire
1	60 NF					
2	72 NF					
3	88 NF					
4	107 NF					
7	154 NF					
11		187 NF				
6	229 NF					
8	229 F					
9		234 NF				
12		240 NF				
25			276 NF			
13		284 F				
5						
10		308 NF				
26			308 NF			
27					352 NF	
32			359 NF			
14						
24			368 F			
31						392 F
28					396 NF	
15						411 F
18			414 F			
23			414 F			
16			429 F			
17				445 NF		
20				457 NF		
22				474 F		
30					475 F	
29					516 F	
19				520 F		
21				548 F		
Range FPS	229	240-284	359-368	457-474	396-475	<392
Predict Mfr. FPS	129	208	382	484	643	286
Predict Test FPS	204	282	260	570	504	343

DATA REDUCTION CHART I

F = Failure   NF = No Failure

Distribution of Longitudinal Impact Test Data
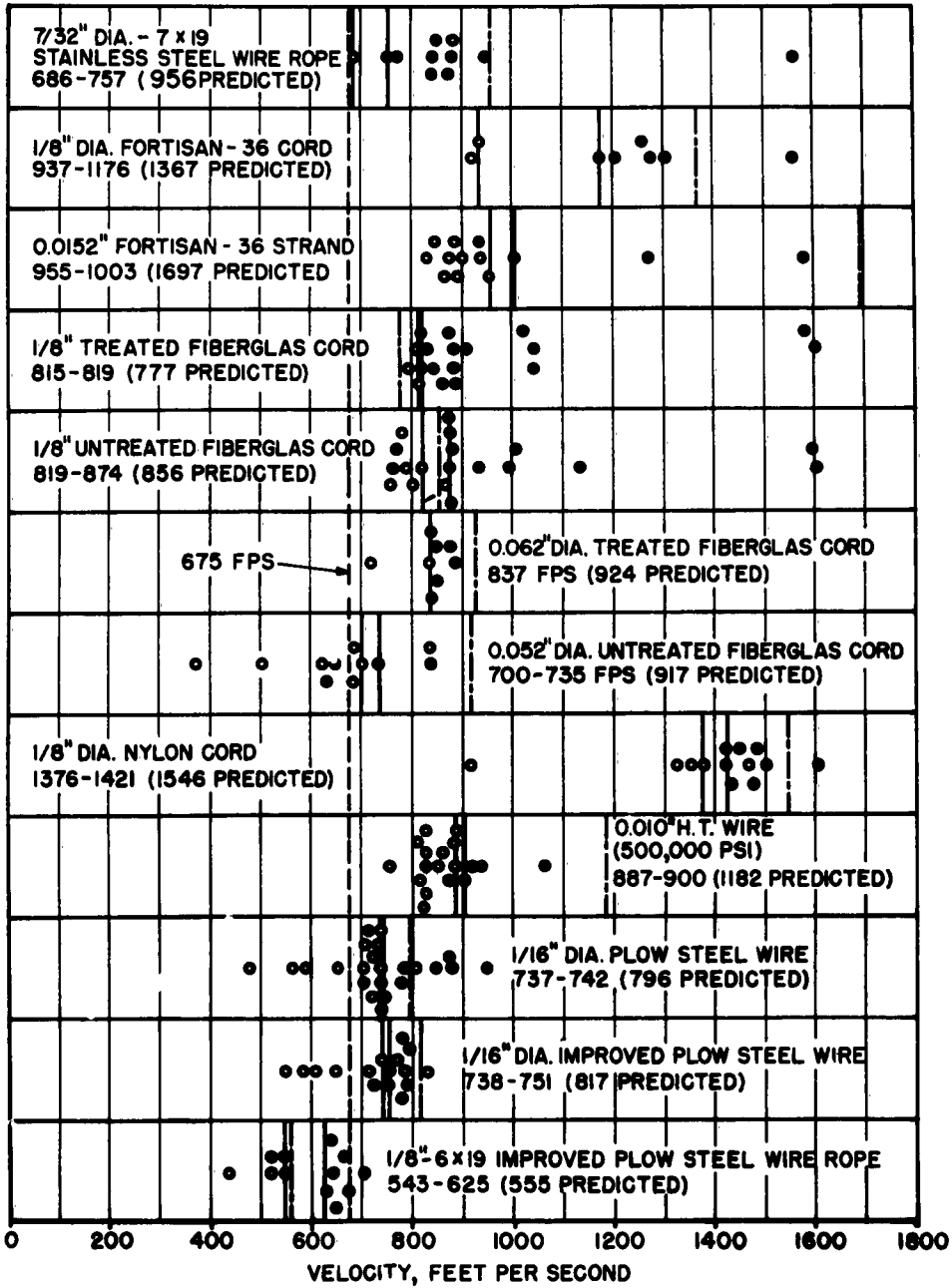
DATA REDUCTION CHART II

PICTORIAL REPRESENTATION OF
TRANSVERSE IMPACT TEST DATA

FAILURE
NO FAILURE

LIMITS (TEST)
CALCULATED

RANGE: 898–930 FPS
PREDICTION: 1026 FPS

675 FPS

VELOCITY, FEET PER SECOND

1/16" DIA. STAINLESS STEEL WIRE

RANGE: 761–795 FPS
PREDICTION: 972 FPS

675 FPS

VELOCITY, FEET PER SECOND

1/16" DIA. TITANIUM WIRE
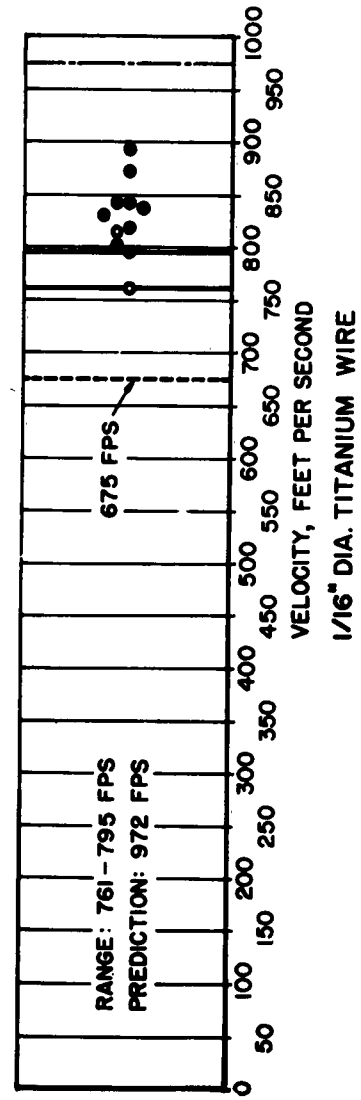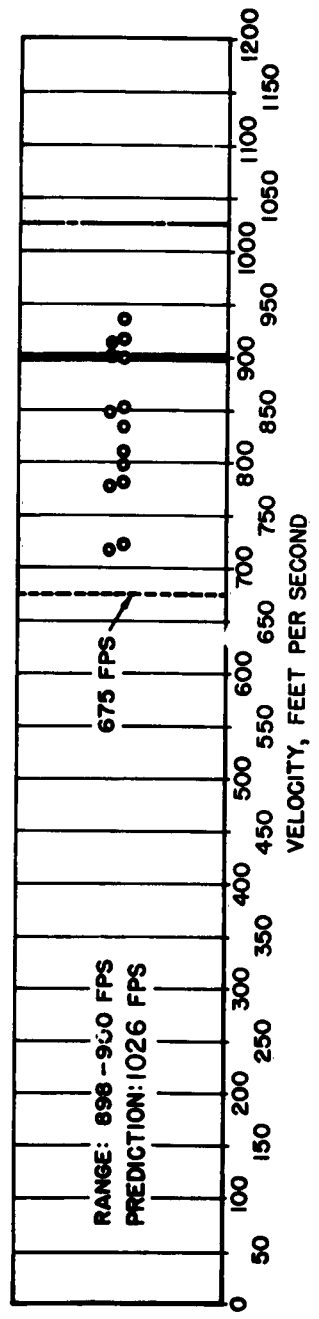
DATA REDUCTION CHART II (CONTINUED)

PICTORIAL REPRESENTATION OF
TRANSVERSE IMPACT TEST DATA

112

in number, they nevertheless resulted in a fairly narrow domain of critical velocities. While some change in the domains could occur with greater statistical data, it is felt that the results as given here are valid enough to justify confidence in their use for comparative purposes when attempting to find a material of superior longitudinal or transverse impact tolerance.

As an example of the method used to interpret the results presented by the data, the evaluation of the upper and lower limits of the transverse impact velocity range for 1/8-inch diameter, untreated Fiberglas cord is presented. The velocities listed in the test for this specimen were plotted and resulted in a distribution as shown in Data Reduction Chart II. This chart shows that every transverse impact above 874 fps causes complete failure of the specimen while impacts below 819 fps show non-failures or incomplete failures. There are two instances out of eight impacts (759 fps and 769 fps) that show incomplete failures (1 strand broken). These latter points were discarded in establishing limits because they occur in an area surrounded by no-break impacts, and further, since the failures are incomplete, it is possible that the impact was not a clean hit; that it struck only one strand and cut it with the sharp edged ridges of the slug. Moreover, the single strand, composed of individual twisted fibers, when subjected to an impact by itself, would lack the support of the rest of the cord (2 strands) and would exhibit less resistance to impact velocity than the cord. With this questionable data eliminated, the failure domain was established. The single non-failure at 864 fps can not be reliably established

113

as the lower limit of impact tolerance because the separation between 819 and 864 is too broad and without any intermediate data. Further, the non-failure point at 864 fps is too close to the definite evidence of failure at 874 fps to justify, without additional data, that it represents the lower limit. The limit points are then established as 819 fps for a lower limit below which no failures will occur and 874 fps as an upper limit above which failures will always occur. As stated previously, although the choice of these limits is based on a comparatively small number of tests, the number of tests are sufficient to point out a definite range of velocities which define the transverse impact tolerance of a tension member. It may be that a greater number of tests will define this range more sharply and may even change the limit points somewhat but the present results are consistent enough to justify confidence in the methods used.

The reasoning used in the above interpretation is typical of that employed to establish upper and lower limits for those cases of question-able test data both in longitudinal and transverse impact tests. However, in most instances, the test data was readily reduced to reliable domains of impact tolerances. The consistent data very much favors confidence in the results of the tests.

6.1 Test Model Similitude

Prior to evaluating the results of the data presented in Appendix A, page 123, it is pointed out that the present test study involves the use of model configurations instead of prototype tension members. For the present purposes of this investigation, modeling is most convenient and economical because of the numerous test specimens involved.

114

For the proper interpretation of the test data from dynamic models, it is essential that the model type system have dynamic, geometric, and kinematic similitude to the prototype system. To provide this in the present testing program, the model laws, as presented in Reference 1, were used, since they were developed for similitude to a full-scale arresting gear mechanism. The model laws developed in Reference 1 established a direct relationship between model and prototype velocity parameters. Therefore, the impact velocity data obtained for the test model-specimens will be the same for the prototype tension members they represent.

6.2 Correlation of Test and Predicted Results

For the purpose of correlating the results of the tests outlined in this report with predicted expectations, predicted impact tolerance values were calculated from static test results (Appendix C1, page 139) for each tested tension member using the methods developed in Section 3. These calculated values are presented in Chart I and in Chart III with the upper and lower limits of velocity values as interpreted from the test data using the method outlined in section 6.0 above. It is observable that reasonably good correlation between test and predicted values was achieved in a majority of the cases. It is therefore plausible that the analytical methods of Section 3 are accurate and useful in preliminary evaluation of new tension members.

CHART III

TRANSVERSE IMPACT TOLERANCES

Test Specimen	Velocity Impact Tol.(fps)		
	Test Results		Calculated
	Lower lim.	Upper lim.	Predictions
1/8" diameter - 6 x 19 Improved Plow Steel Rope	543	625	555
1/16" diameter - Improved Plow Steel, Single Wire	738	751	817
1/16" diameter - Plow Steel, Single Wire	737	742	796
7/32" diameter - 7 x 19, E. A. Stainless Steel Rope	686	757	1956
0.010" diameter - (.85-.95 carbon) Steel, Single Wire (500,000 psi)	887	900	1182
1/8" dia. - 3 Strand Fiberglas Cord, Untreated, Approximately 45° Lay Angle	819	874	856
1/8" dia. - 3 Strand Fiberglas Cord, Neoprene Treated, Approximately 45° Lay Angle	815	819	777
0.052" dia. - 3 Strand Fiberglas Cord, Untreated, Approximately 45° Lay Angle	700	735	917
0.068" dia. - 3 Strand Fiberglas Cord, Neoprene Treated Approximately 45° Lay Angle	837	837	924
1/8" dia. - 3 Strand Nylon Cord, Approximately 45° Lay Angle	1376	1421	1546
1/8" dia. - 3 Strand Fortisan 36 Cord, Approximately 8° Lay Angle	937	1176	1367
0.0152" dia. - Multiple Filament, Fortisan 36, Single Strand 0.8 Z Twist	955	1003	1697
1/16" dia. - Stainless Steel, Single Wire	898	900	1026
1/16" dia. - Titanium, Single Wire	761	795	972

SECTION 7

SUMMARY AND CONCLUSIONS

7.0 Summary

This technical note presents the results of analytical studies and related tests to determine the influence of geometrical and material characteristics on the impact tolerance of tension members. The effects of constuctional configuration on combined stresses in the elements of a tension member were analyzed. Methods and procedures for evaluating the impact tolerance of linear and nonlinear materials were presented and criteria for selecting materials of superior impact tolerances were given. Tests were conducted to establish the validity of these criteria.

In summary the analytical studies indicated the existence and magnitude of the influence of certain geometrical and material properties of a tension member on the expected impact tolerance of the member. The dynamic test results appear to confirm the presence of this influence in the degree indicated analytically. The analytical studies also provided a method of selecting superior materials and the dynamic tests substantially supported the analytical methods as well.

The longitudinal impact test results (Chart I) indicate reasonably close correlation with the predicted values (based on static tests) and establishes confidence in the predicted values for longitudinal impact tolerance of any material. No attempt was made to determine the influence of geometry on the longitudinal impact tolerance of a material.

117

The transverse impact test results (Chart III) also indicate reasonably close correlation with the predicted values (based on static tests) and in addition verify the analytically predicted influence of the geometrical properties of a material on the transverse impact tolerance. In the two cases tested to confirm geometric influence predictions, i.e. improved plow steel rope and single wire and stainless steel rope and single wire, the single wire specimens showed superior transverse impact performance over their stranded (rope) counterparts, as expected from the predicted transverse impact tolerance.

All three textile materials tested, i.e. nylon, Fortisan and Fiberglas, showed transverse impact tolerances above the minimum requirements for the proposed arresting system (400 knots). Of the metal specimens tested, all except the presently employed improved plow steel rope exceeded the minimum transverse impact tolerances required.

7.1 Conclusions

In certain instances, some definite conclusions can be made regarding the dependency of the impact tolerance of a tension member on its geometry and material. In other cases, the trend of certain characteristics can be simply deduced when their effects are readily discernible. Based on the investigations set forth in this technical note, the following conclusions and deductions are presented:

1. The fundamental parameters that determine impact tolerance, as was first indicated in Reference 2, are the tension-strain curve, lineal mass density of the tension member, and the ultimate strength of the material.

118

2. Non-linear materials having elastic moduli decreasing with strain give higher impact tolerances than would be expected from materials of the same ultimate strength and strain whose elastic moduli remain constant or increase with strain. This characteristic was analytically established in Section 3 of this technical note.

3. Present wire rope geometries approach the optimum impact tolerance of a straight bar. Solid straps or wires, therefore, would provide some increase in performance over wire ropes but their flexibility may not be adequate. Increased flexibility can be achieved by employing several thin straps or wires, the total sectional area of which would be sufficient to develop the required arresting tension. However, a wire rope presents no problems of orientation while achieving practically the same impact tolerance.

4. Conventional arresting gear wire rope as represented in the improved plow and plow steel specimens proved to have the lowest impact tolerance of all the materials tested and is therefore the least acceptable for high speed arresting gear applications.

5. While nylon appears to be a superior material from the standpoint of high impact tolerance, it is approached in performance by high tension Fortisan. However, textile materials are highly sensitive to deterioration of strength under heating due to impact. Fiberglas, with a proven transverse impact tolerance in the neighborhood of 800 feet per second, is highly elastic and, it is expected, would not display a destructive rise in temperature because plastic deformation and the attendant conversion into heat of the strain energy are precluded.

119

6. While all of the metallic specimens tested, except improved plow steel rope, exceeded the 400 knot (675 fps) minimum requirement in their transverse impact tolerance capacities, the highest transverse impact tolerance (approximately 900 fps) was exhibited by a newly developed high tensile, high carbon content (.85-.95) steel wire. Its tolerance value is higher than the Fiberglas material tested but lower than the Fortisan. Reports from the steel wire manufacturer indicate that there are good possibilities of weaving the wire into a wire rope suitable for use in an arresting gear mechanism. It must be considered however, that the wire rope constructed with this high tensile steel would show a transverse impact tolerance lower than that of the single steel wire. As a matter of fact, the transverse impact tolerance of such a wire rope might even be lower than the transverse impact tolerance of the Fiberglas specimen tested, since this latter specimen was tested in the rope configuration. In addition, it is worth noting that the specific gravity of the steel is three times that of Fiberglas.

7. The stainless steel wire rope, identified as American Chain & Cable Company, Inc., 7 x 19 E.A. Cable, shows considerable promise in that it displays a transverse impact tolerance of approximately 700 feet per second. Its energy absorbing capacity may make it suitable for direct arrestment of aircraft without another accompanying energy absorber.

8. In general, on the basis of transverse impact tolerance alone, the most promising of the materials tested appear to be the three textiles, i.e., nylon, Fortisan and Fiberglas, in that order. While nylon and Fortisan

are undoubtedly superior to any of the metallic materials tested, the superiority of Fiberglas over the high tensile wire is questionable. In as much as there may be other factors to consider in the final selection of a particular material for an arresting device, such as thermal properties, cost, weight, availability, etc., it is recommended that further investigation of the influence of these factors be conducted before the final selection is made.

REFERENCES

1. WADC TR 59-495, Model Tests and Studies of the Problems of Dynamic Tensions in Aircraft-Arresting Gear Cables, American Machine & Foundry Company, Mechanics Research Division, October 1959.

2. WADC TR 58-217, ASTIA Document No. AD155542, An Analytical Approach to the Alleviation of Dynamic Tensions in Aircraft Arresting Gear Cables, American Machine & Foundry Company, May 1958, Neidhardt, Eslinger and Sasaki.

3. Strength of Materials, Part II by S. Timoshenko, D. Van Nostrand Company, Inc., 3rd Edition, June 1957, New York, New York.

4. Radial Forces on Wire Ropes, Wire and Wire Products, May 1952, pp. 459-463, F. H. Hruska.

5. NAMC Report NAEF-ENG 6169, Cable Dynamics, F. O. Ringleb, 27 December 1956.

APPENDIX A

CLARIFICATION OF THE USE OF THE PRINCIPLE OF COINCIDIZATION

FOR NONLINEAR MATERIALS

A.1 Introduction

In Reference 2, the principle of coincidization was enunciated and in
several cable-dynamics problems its usefulness was demonstrated in deter-
mining the total effect of several events having interdependent effects.
Its application to nonlinear materials deserves some clarification.

Upon impact of a nonlinear material whose stress-strain curve is
concave-up, the resulting increase in strain must propagate as a sudden
jump because the higher strains tend to propagate faster than the lower
strains. Conversely, if the stress-strain curve of the material is
convex-up, the lower strains will propagate faster than the higher strains,
and the strain wave will not propagate as a sudden jump but will spread
out into an ever-lengthening wave as it propagates.

The question arises as to whether the strain wave produced in a
convex-up material can be regarded, for purposes of calculation, as a
single sudden jump. This consolidation of the strain wave may at first
appear to be justified on the basis of the principle of coincidization.

It should be observed from the outset that consolidation of such a
strain wave does not meet the conditions of applicability (page 67 of
Reference 2) of the principle of coincidization, because the continuous
growth of the wave length precludes the reaching of a steady state in

which the wave length eventually becomes negligible. The principle can be applied only when a steady state is approached, and then to calculate only the steady state but no preceding states.

Furthermore, the argument by which the principle was established could have been stated equivalently from the viewpoint of an observer who backs away from the cable at constant velocity. Thus, consider two successive longitudinal impacts on the end of a cable of nonlinear (convex-up) material. Shortly after the two impacts, when the observer has backed away 50 feet from the cable, suppose he sees that the two resulting waves are respectively 15 feet and 20 feet long and are separated by a distance of 3 feet (there must be a distance separating the waves because there was a time interval between the occurrence of the two impacts). Much later, when the observer has backed away 50 miles, he will see that the two waves now are respectively 15 miles and 20 miles long but are still separated by a distance of only 3 feet. Clearly, the 3-foot separation distance is now negligible, which indicates that essentially the same final result would have been reached had the two impacts been coincident. Equally clearly, the wave lengths have not become negligible. Therefore, there is no reason to suppose that the strain waves can be consolidated into a single jump in strain.

In order to confirm the fact that expanding strain waves cannot be consolidated for calculation purposes, it will now be temporarily assumed that they can be consolidated in the hope that a contradiction will result.

A.2 Analysis

Suppose that an expanding strain wave can be regarded as a single jump in strain. Then the formulas for the propagation of jump-type singularities in strain apply, and the strain ϵ produced by a longitudinal impact of velocity v_ℓ is given by

$$\epsilon = \frac{v_\ell}{c} \qquad (A.1)$$

where c is the propagation velocity of a longitudinal wave. For a tension member having a nonlinear tension-strain relationship as shown in Figure A.1, the value of c depends upon the strain increment associated with the impact. From Equation (A.11) in Appendix A, Reference 2,

$$c = \sqrt{\frac{1}{\mu} \frac{T_2 - T_1}{\epsilon_2 - \epsilon_1}} \qquad (A.2)$$

where μ is mass per unit length of the cable, and the subscripts refer to the points along the tension-strain curve associated with the impact as shown in Figure A.1. The quantity $\dfrac{T_2 - T_1}{\epsilon_2 - \epsilon_1}$ in Equation (A.2) represents the slope of the secant modulus between the typical points 1 and 2.

Let it be desired to find the longitudinal impact velocity by means of consolidation of strain waves required to produce a strain ϵ_2 and tension T_2 in the material of Figure A.1 having an initial strain $\epsilon_o = 0$ and initial tension $T_o = 0$. If consolidation of strain waves is to apply, the actual velocity required to bring the strain from ϵ_1 to ϵ_2 along the curve would be the same as the sum of the velocities to go from ϵ_o to

125
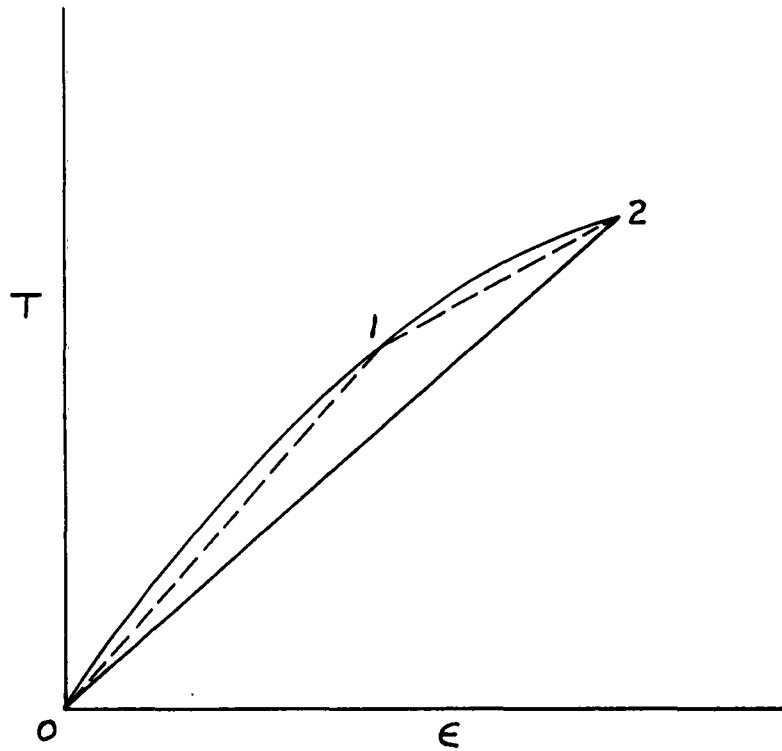
Figure A.1   Tension-Strain Curve

ϵ_1 and ϵ_1 to ϵ_2, using the secant moduli. Thus for any increment along the curve, from Equations (A.1) and (A.2),

$$\Delta v_\ell = \frac{\Delta \epsilon}{\sqrt{\mu}} \left(\frac{\Delta T_\ell}{\Delta \epsilon}\right)^{1/2} \tag{A.3}$$

and,

$$\Delta v_{0-1} = \frac{\epsilon_1 - \epsilon_0}{\sqrt{\mu}} \left(\frac{T_1 - T_0}{\epsilon_1 - \epsilon_0}\right)^{1/2}$$

$$\Delta v_{1-2} = \frac{\epsilon_2 - \epsilon_1}{\sqrt{\mu}} \left(\frac{T_2 - T_1}{\epsilon_2 - \epsilon_1}\right)^{1/2} \left.\vphantom{\begin{array}{c}1\\1\\1\end{array}}\right\} \tag{A.4}$$

$$\Delta v_{0-2} = \frac{\epsilon_2 - \epsilon_0}{\sqrt{\mu}} \left(\frac{T_2 - T_0}{\epsilon_2 - \epsilon_0}\right)^{1/2}$$

It is now postulated that if the impact velocity is found on the basis of the secant modulus in a single calculation, the result would be a velocity greater than that obtained on the basis of two or more increments. Thus,

$$\Delta v_{0-1} + \Delta v_{1-2} \overset{?}{\leqq} \Delta v_{0-2} \quad \text{or, from Equation (A.4),}$$

$$\left[(\epsilon_1 - \epsilon_0)(T_1 - T_0)\right]^{1/2} + \left[(\epsilon_2 - \epsilon_1)(T_2 - T_1)\right]^{1/2}$$
$$\overset{?}{\leqq} \left[(\epsilon_2 - \epsilon_0)(T_2 - T_0)\right]^{1/2} \tag{A.5}$$

Squaring both sides of the inequality gives the following:

$$\left[(\epsilon_1 - \epsilon_0)(T_1 - T_0)\right] + 2 \left[(\epsilon_1 - \epsilon_0)(T_1 - T_0)\right]^{1/2} \left[(\epsilon_2 - \epsilon_1)(T_2 - T_1)\right]^{1/2}$$
$$+ \left[(\epsilon_2 - \epsilon_1)(T_2 - T_1)\right] \overset{?}{\leqq} \left[(\epsilon_2 - \epsilon_0)(T_2 - T_0)\right];$$

$$\left[(\epsilon_1 - \epsilon_0)(T_1 - T_0)\right] + 2 \left[(\epsilon_1 - \epsilon_0)(T_1 - T_0)\right]^{1/2} \left[(\epsilon_2 - \epsilon_1)(T_2 - T_1)\right]^{1/2}$$
$$+ \left[(\epsilon_2 - \epsilon_1)(T_2 - T_1)\right] \overset{?}{\leqq} \left[(\epsilon_1 - \epsilon_0 + \epsilon_2 - \epsilon_1)(T_1 - T_0 + T_2 - T_1)\right].$$

Transposing terms gives:

$$2\left[(\epsilon_1-\epsilon_0)(T_1-T_0)\right]^{1/2}\left[(\epsilon_2-\epsilon_1)(T_2-T_1)\right]^{1/2}\overset{?}{\leq}\left[(\epsilon_1-\epsilon_0+\epsilon_2-\epsilon_1)(T_1-T_0+T_2-T_1)\right]$$
$$-\left[(\epsilon_1-\epsilon_0)(T_1-T_0)\right]-\left[(\epsilon_2-\epsilon_1)(T_2-T_1)\right];$$

$$2\left[(\epsilon_1-\epsilon_0)(T_1-T_0)\right]^{1/2}\left[(\epsilon_2-\epsilon_1)(T_2-T_1)\right]^{1/2}\overset{?}{\leq}(\epsilon_1-\epsilon_0)(T_1-T_0)+(\epsilon_1-\epsilon_0)(T_2-T_1)$$

$$+(\epsilon_2-\epsilon_1)(T_1-T_0)+(\epsilon_2-\epsilon_1)(T_2-T_1)-(\epsilon_1-\epsilon_0)(T_1-T_0)-(\epsilon_2-\epsilon_1)(T_2-T_1);$$

$$2(\epsilon_1-\epsilon_0)^{1/2}(T_1-T_0)^{1/2}(\epsilon_2-\epsilon_1)^{1/2}(T_2-T_1)^{1/2}\overset{?}{\leq}(\epsilon_1-\epsilon_0)(T_2-T_1)+(\epsilon_2-\epsilon_1)(T_1-T_0);$$

$$0\overset{?}{\leq}(\epsilon_1-\epsilon_0)(T_2-T_1)-2(\epsilon_1-\epsilon_0)^{1/2}(\epsilon_2-\epsilon_1)^{1/2}(T_1-T_0)^{1/2}(T_2-T_1)^{1/2}+(\epsilon_2-\epsilon_1)(T_1-T_0);$$

$$0\overset{?}{\leq}\left[\sqrt{(T_2-T_1)(\epsilon_1-\epsilon_0)}-\sqrt{(T_1-T_0)(\epsilon_2-\epsilon_1)}\right]^2 \tag{A.6}$$

It is clear from Equation (A.6) that since the right member appears as a second power, it is always positive or zero. Therefore, Equation (A.5) is written as,

$$\left[(\epsilon_1-\epsilon_0)(T_1-T_0)\right]^{1/2}+\left[(\epsilon_2-\epsilon_1)(T_2-T_1)\right]^{1/2}\leq\left[(\epsilon_2-\epsilon_0)(T_2-T_0)\right]^{1/2} \tag{A.7}$$

and therefore from Equation (A.4),

$$\Delta v_{0-1}+\Delta v_{1-2}\leq\Delta v_{0-2} \tag{A.8}$$

The conclusion is, then, that the principle of coincidization does not justify the calculation of the longitudinal impact tolerance in a single computation on the basis of the secant modulus. The degree of the non-linearity of the tension-strain curve governs the amount of error. Note that the equality in Equation (A.6) implies

$$(T_2 - T_1)(\epsilon_1 - \epsilon_0) = (T_1 - T_0)(\epsilon_2 - \epsilon_1) \qquad (A.9)$$

which can be rewritten as

$$\frac{T_2 - T_1}{\epsilon_2 - \epsilon_1} = \frac{T_1 - T_0}{\epsilon_1 - \epsilon_0} \qquad (A.10)$$

Therefore, the equality in Equation (A.8) holds only for linear materials, and the strong inequality must hold for nonlinear materials.

It is also deducible that, if a linear material can be found whose modulus is equal to the ultimate secant modulus of a nonlinear (convex-up) material having the same ultimate strength, then the linear material would have a higher impact tolerance than the nonlinear material.

A similar investigation for transverse impact has shown that consolidation of expanding strain waves leads to impact velocities which are sometimes greater and sometimes smaller than the true value. No relation for predicting the result was found for this case.

A.3 Conclusion

The foregoing analysis does not preclude the coincidization of several events in a nonlinear material into one coincidized problem. However, it does show conclusively that, in the application of the principle of coincidization to a nonlinear material, the gradient of sonic velocity with strain cannot be ignored in solving the coincidized problem.

129

APPENDIX B

SAMPLE CALCULATIONS FOR NONLINEAR MATERIALS

B.1 General Remarks

In order to clearly illustrate the method for evaluating the impact
tolerance of a nonlinear material, the following calculations are given in
detail, to demonstrate the procedures and to show the results for the case
of Nylon 300. The calculations for Nylon were chosen because they illustrate
the use of the secant method and also include a situation in which $c < c^*$.
See Section 3.1.2, page 36. This latter condition requires a modification
of the initial velocity vector diagram and a consequent change in the
mathematical relations used to evaluate the transverse velocity.

B.2 Stress-Strain Relations

The diagram used (Figure 22, page 49) for the study illustrated here was
furnished in terms of a T/μ versus ϵ relationship. If a T versus ϵ
curve is used then T/μ must be determined. If σ versus ϵ is used, then
the parameter σ/ρ must be determined. Since the units of T/μ as shown
in Figure 22 are given in metric units $\left(\dfrac{meters}{sec.}\right)^2$ and it is desired to
furnish the end results (u and v_t) in ft/sec, it is of course necessary under
these conditions to convert units and therefore several of the steps given
in these sample calculations are merely conversion procedures.

B.3 Impact Velocity Calculations

(a) The T/μ versus ϵ relationship is converted to a tabular form
(Table III, page 137) with T/μ and all subsequent calculated values placed
beneath the corresponding related values of ϵ . The magnitude of $\Delta\epsilon$ is

determined by the curvature of the stress-strain diagram and the need to
preserve accuracy.

In the present case, it varies from 0.1% to 1.0% in size.

(b) T/μ $(\frac{m}{sec})^2$ is converted to units of $(ft/sec)^2$

(c) The slope of the T/μ vs ϵ curve is determined at each one of
the tabulated values of ϵ . The method used to determine this slope depends
on the stress-strain relationship which produces the diagram of the material
under study. In the present illustrated example, the stress-strain curve is
concave-up in part and thus requires the use of the secant method for reasons
given in Section 3.1.1, page 35. The slope of the T/μ vs. ϵ curve from
the origin to ϵ = 2.0% is determined at points along the curve using the
tangent method (Figure 23, page 50). From ϵ = 2.0% to ϵ = 14% the slope is
determined for a secant line joining the point in question with a point of
tangency to the curve, which point varies from ϵ = 2.0% to ϵ = 0.5%.
This procedure (the secant-line method) eliminates concave-up portions of
the curve in the direction of loading. When returning along the curve during
an unloading cycle, the slope is determined by secants which instead eliminate
convex-up portions of the curve. For points ϵ = 14% to ϵ = 23% the tangent
method is applicable for the loading phase only. The units of the slope for
the particular example being presented are $(\frac{meters}{sec.})^2$, and the value of this
term represents c^2.

(d) The square root of each of the items calculated in step (c) is
determined and represents the value of c, the velocity of strain propagation,

in m/sec. at each corresponding value of strain (ϵ). The units of this velocity (m/sec) are then converted to ft/sec. Results are plotted in Figure 24, page 51.

(e) The impact velocity u required to produce any given strain ϵ , was calculated next. According to Equation (3.2), this velocity can be evaluated by finding the area under the c curve (Figure 24). If an equation of the curve is available, then the mathematical integration procedure can be used. In the case being illustrated here, such is not the case and a graphical numerical method is employed. The approximate area under the curve is obtained by the trapezoidal method, i.e. calculating the area of the trapezoid formed between two small intervals and summing the individual areas thus found. The stress-strain curve is convex-up until a strain of 2% is reached so that the secant method of evaluating c does not come into use until ϵ exceeds 2%. Therefore, the area under the c curve proper can be found from $\epsilon = 0$ to $\epsilon = 0.02$.

The area under the c curve which determines u as a function of ϵ is illustrated in Figure B.1. Note that there are three cases:

(a) The entire area representing u lies under the c curve obtained from tangents to the T-ϵ curve.

(b) The area representing u includes a portion under the horizontal line obtained from the appropriate secant* to the T-ϵ curve. The horizontal line involved is different for every ϵ .

---

*In cases where the T-ϵ curve is entirely concave-up, the secant line intersects the T-ϵ curve at the origin and at the value of ϵ for which u is to be found. In the present example of Nylon 300, however, the initial portion of the T-ϵ curve is convex-up; in this case only the upper end of the secant line is truly a secant, the lower end being tangent to the convex-up portion of the T-ϵ curve.

(c) The final portion of the area representing u is again bounded by
the c curve obtained from tangents to the T-ϵ curve. The central

These lines obtained from secants to T-ϵ curve

This curve obtained from tangents to T-ϵ curve

Case (a)

$u = u_1$

Case (b)

$u = u_1 + u_2$

Case (c)

$u = u_1 + u_2 + u_3$
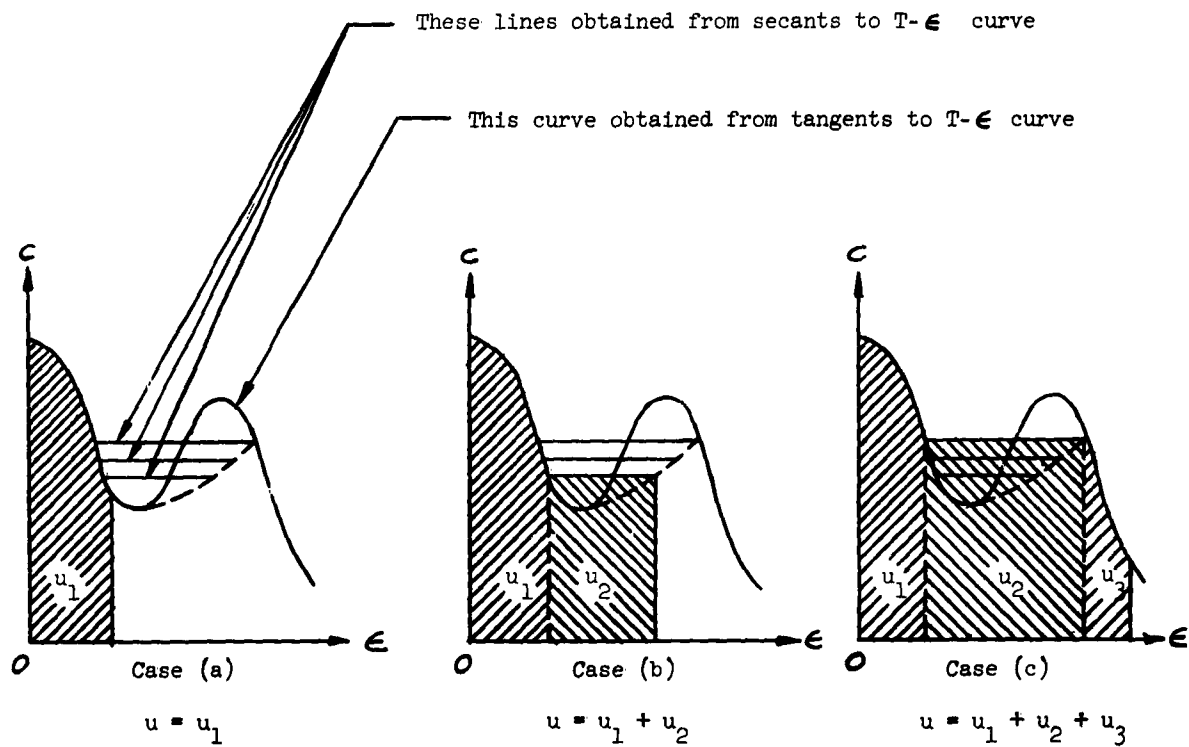
Figure B.1.   Area Representing u

portion of the area is bounded by a horizontal line which exhibits
no further dependence on ϵ.

For convenience in computation, u is decomposed into the sum of three
parts, denoted by u_1, u_2, and u_3. That part of u which is represented in

133

Figure B.1 by the area directly under the bounding horizontal segment is denoted by u_2, the part to the left by u_1, and the part to the right by u_3.

For Case (a), u_1 increases with ϵ, while $u_2 = u_3 = 0$. For Case (b), u_1 decreases as u_2 increases with ϵ, while $u_3 = 0$. For Case (c), u_1 and u_2 are constant, while u_3 increases with ϵ.

For any interval $\Delta\epsilon$, the corresponding Δu_1 is calculated by finding the arithmetic average (dividing the sum by 2) of the two end values of c for the interval and multiplying this result by $\Delta\epsilon$. These values for Δu_1 are not progressively added but are merely recorded for each interval of $\Delta\epsilon$. In going from $\epsilon = 0.02$ to $\epsilon = 0.03$ the value of Δu_1 is negative (-38 ft/sec) because u_1 represents the now decreasing incremental area under the c curve to the left of the secant line. It is necessary in the condition being illustrated to return to the point $\epsilon = 0.011$ where the secant line to the point $\epsilon = 0.03$ initiates. A similar procedure is used to calculate Δu_1 in the intervals up to $\epsilon = 0.14$. The units of Δu_1 are in ft/sec.

The value of u_1 is a summation of the incremental areas represented by Δu. The values of u_1 recorded from $\epsilon = 0.04$ to $\epsilon = 0.12$ are treated as constants, which approximates the actual conditions, and at all other points their actual values are used. The approximation applies because the secant lines drawn on the stress-strain curve are tangent to the curve over a small arc on the curve and it is difficult to distinguish the points of tangency; the lines can be considered as tangent to the curve at the same point. Beyond

$\epsilon = 0.12$ the difference is of discernible magnitude and is tabulated for $\epsilon = 0.13$ and $\epsilon = 0.14$.

The value of u_2 is a summation of the area under the secant line portion of the curve and is merely the product of c and the value of the corresponding $\Delta\epsilon$.

The values Δu_3 represent the increments of areas under the curve from $\epsilon = 0.14$ to the end of the curve. These areas are evaluated similarly to the method used from $\epsilon = 0.0$ to $\epsilon = 0.02$ (see Figure 24, page 51).

The final step is a summation of u_1, u_2, and the accumulated sum of Δu_3. This sum at each incremental value of ϵ represents u, the longitudinal velocity of the cable at the moment of impact. The longitudinal impact tolerance is the maximum value of u. Results are plotted in Figure 25, page 52.

(f) The transverse impact tolerance will now be found. The velocity c* of the kink is first evaluated. The sums, $1 + \epsilon$, are first tabulated for each value of ϵ. The values of $(c*)^2$ are then found from Equation (3.3), $(c*)^2 = (T/\mu)(1 + \epsilon)$, and tabulated. The value of c* is then determined for each value of ϵ. Values of c* are plotted in Figure 24, page 51, on the same graph with c.

(g) The next series of tabulated values is a convenient method for evaluating v_t, the transverse impact velocity at strain ϵ_i. In one case, where $c \geq c*$ (at impact), the relationship $v_t^2 = c* - (c* - u)^2$ holds and this is tabulated as separate steps of $c* - u$, $(c* - u)^2$, and v_t^2. The transverse impact velocity, v_t, is then found for each value of ϵ_i. (See page 36 for simplified form of Equation (3.5) when $\beta = \frac{\pi}{2}$).

135

For the case where $c < c^*$, the relationship becomes, $v_t^2 = (c^● + u - u^●)^2 - (c^● - u^●)^2$, and it is necessary first to calculate the value of u at the point $c = c^*$, and this u is by definition $u^●$. If algebraic expressions for the c and c^* curves are available, the procedure involves a mathematical integration between the limits of zero and the point of strain, $\epsilon^●$, at which $c = c^*$. In the present case, the equations for c and c^* are not available. Therefore, the value of $\epsilon^●$ is found by inspection of Figure 24, page 51 at the point of intersection of the c and c^* curves. This point is then used as outlined under step (e) to determine $u^●$, the magnitude of which is represented by the area under the curve from the origin to the point at which $c = c^*$. The value of v_t^2 is then calculated for this point and all points following it along the curve of c as a function of ϵ. The transverse impact velocity, v_t, for these points is then calculated.

Results for v_t are plotted in Figure 26, page 53. The maximum value of v_t is the transverse impact tolerance of the material.

(h) As a matter of completeness, and while not applicable to the present analysis, the following additional information is presented:

Figure 27, page 54, is essentially a plot of the stress caused by any velocity of transverse impact. Figure 28, page 55, shows the actual slopes along the concave-up portion of the tenacity-strain curve, which are replaced in Figure 23, page 50, by the secant slopes to evaluate the impact tolerance.

The kink angle, $\emptyset$, is the arccos of $\frac{c^* - u}{c^*}$ when $c \geq c^*$ and the arccos of $\frac{c^● - u^●}{c^● + u - u^●}$ when $c < c^*$. The values of the kink angle are not listed in Table III but are plotted in Figure 29, page 56.

136

Table III - IMPACT TOLERANCE DATA FOR NYLON 300 AT 21°C (70°F) & 65% R.H.

ϵ	0.000	0.005	0.008	0.010	0.011	0.020	0.030	0.040	0.050	0.060	0.070	0.080	0.090	0.100	0.110
$\frac{T}{U}(\frac{Mtrs}{sec})^2$	00,000	27,000	35,000	40,000	42,000	60,000	78,000	99,000	121,000	145,000	172,000	202,000	236,000	273,000	315,000
$\frac{T}{U}(\frac{ft}{sec})^2$	000,000	290,000	376,600	430,000	452,0~	646,000	840,000	1,065,000	1,302,000	1,560,000	1,851,000	2,177,000	2,540,000	2,940,000	3,390,000
$\frac{dT}{dU}(\frac{Mtrs}{sec})^2$	26,000,000	3,280,000	3,100,000	2,100,000	1,900,000	1,600,000	1,900,000	1,950,000	2,000,000	2,100,000	2,220,000	2,300,000	2,460,000	2,600,000	2,750,000
$c_s (\frac{Mtrs}{sec})$	5099	1811	1761	1449	1378	1264	1378	1396	1414	1449	1483	1517	1568	1612	1658
c_s (fps)	16,700	5940	5780	4750	4520	4150	4520	4570	4640	4750	4860	4970	5140	5290	5430
$\Delta u_1 (\frac{ft}{sec})$	00	57	18	15	5	38	-38	-5	0	0	0	0	0	0	0
u_1 (fps)	00	57	75	90	95	133	95	90	90	90	90	90	90	90	90
u_2 (fps)	00	00	00	00	00	000	96	137	186	288	292	348	411	476	543
u_1+u_2	00	57	75	90	95	133	181	227	276	328	382	438	501	566	633
Δu_3	00	00	00	00	00	000	000	000	000	000	000	000	000	000	000
$u = \Sigma u$	00	57	75	90	95	133	181	227	276	328	382	438	501	566	633
$1+\epsilon$	1.000	1.005	1.008	1.010	1.011	1.020	1.030	1.040	1.050	1.060	1.070	1.080	1.090	1.100	1.110
$(c*)^2$	000,000	291,700	379,500	434,000	457,000	659,000	865,000	1,108,000	1,367,000	1,654,000	1,981,000	2,348,000	2,770,000	3,230,000	3,760,000
$c*$ (fps)	000	540	616	659	676	812	930	1053	1169	1286	1407	1532	1664	1797	1939
$c*-u$	000	483	541	569	581	679	749	826	893	958	1025	1094	1163	1233	1306
$(c*-u)^2$	000,000	237,200	292,700	324,000	338,000	461,000	561,000	682,000	797,000	918,000	1,051,000	1,197,000	1,350,000	1,520,000	1,710,000
$c*-u°$	-	-	-	-	-	-	-	-	-	-	-	-	-	-	-
$(c*-u°)^2$	-	-	-	-	-	-	-	-	-	-	-	-	-	-	-
$u-u°$	-	-	-	-	-	-	-	-	-	-	-	-	-	-	-
$c*+u-u°$	-	-	-	-	-	-	-	-	-	-	-	-	-	-	-
$(c*+u-u°)^2$	-	-	-	-	-	-	-	-	-	-	-	-	-	-	-
$(v_t)^2$	000,000	54,500	84,800	110,000	119,000	198,000	304,000	426,000	570,000	736,000	930,000	1,151,000	1,420,000	1,710,000	2,050,000
v_t (fps)	000	233	291	332	345	445	551	653	755	858	964	1073	1192	1308	1432
$\frac{dT}{dU}(\frac{Mtrs}{sec})^2$	26,000,000	3,280,000	3,100,000	2,100,000	1,900,000	1,600,000	2,050,000	2,100,000	2,260,000	2,550,000	2,890,000	3,020,000	3,300,000	3,760,000	4,400,000
$c(\frac{Mtrs}{sec})$	5099	1811	1761	1449	1378	1264	1438	1449	1503	1597	1700	1738	1817	1939	2098
$c(\frac{ft}{sec})$	16,700	5940	5780	4750	4520	4150	4700	4756	4930	5240	5578	5702	5963	6361	6882

0.080	0.090	0.100	0.110	0.120	0.130	0.140	0.150	0.160	0.170	0.173 (ε)	0.180	0.190	0.200	0.210	0.220	0.230
202,000	236,000	273,000	315,000	362,000	413,000	468,000	500,000	515,000	525,000	528,000	531,000	535,000	538,000	540,000	540,000	540,000
2,177,000	2,540,000	2,940,000	3,390,000	3,900,000	4,440,000	5,040,000	5,380,000	5,540,000	5,650,000	5,680,000	5,720,000	5,760,000	5,790,000	5,810,000	5,810,000	5,810,000
2,300,000	2,460,000	2,600,000	2,750,000	2,910,000	3,100,000	3,280,000	2,160,000	1,180,000	800,000	620,000	400,000	330,000	180,000	120,000	000,000	000,000
1517	1568	1612	1658	1706	1761	1811	1470	1086	894	787	632	574	424	346	000	000
4970	5140	5290	5430	5600	5780	5940	4820	3560	2930	2580	2070	1880	1390	1134	0000	0000
0	0	0	0	0	-16	-17	00	00	00	00	00	00	00	00	00	00
90	90	90	90	90	74	57	57	57	57	57	57	57	57	57	57	57
348	411	476	543	616	705	802	802	802	802	802	802	802	802	802	802	802
438	501	566	633	706	779	859	859	859	859	859	859	859	859	859	859	859
000	000	000	000	000	000	000	54	42	32	8	16	20	16	13	6	0
438	501	566	633	706	779	859	913	955	987	995 (U*)	1011	1031	1047	1060	1066	1066
1.080	1.090	1.100	1.110	1.120	1.130	1.140	1.150	1.160	1.170	1.173	1.180	1.190	1.200	1.210	1.220	1.230
2,348,000	2,770,000	3,230,000	3,760,000	4,370,000	5,020,000	5,750,000	6,130,000	6,430,000	6,610,000	6,660,000	6,750,000	6,850,000	6,950,000	7,030,000	7,090,000	7,150,000
1532	1664	1797	1939	2090	2241	2398	2476	2536	2571	2580 (σ*)	2598	2617	2636	2651	2663	2674
1094	1163	1233	1306	1384	1468	1539	1563	1581	1584	1585	-	-	-	-	-	-
1,197,000	1,350,000	1,520,000	1,710,000	1,920,000	2,160,000	2,370,000	2,440,000	2,500,000	2,510,000	2,510,000	-	-	-	-	-	-
-	-	-	-	-	-	-	-	-	-	1585	1585	1585	1585	1585	1585	1585
-	-	-	-	-	-	-	-	-	-	2,510,000	2,510,000	2,510,000	2,510,000	2,510,000	2,510,000	2,510,000
-	-	-	-	-	-	-	-	-	-	00	16	36	52	65	71	71
-	-	-	-	-	-	-	-	-	-	2580	2596	2616	2632	2645	2651	2651
-	-	-	-	-	-	-	-	-	-	6,660,000	6,730,000	6,840,000	6,920,000	7,000,000	7,030,000	7,030,000
1,151,000	1,420,000	1,710,000	2,050,000	2,450,000	2,860,000	3,380,000	3,690,000	3,930,000	4,100,000	4,150,000	4,220,000	4,330,000	4,410,000	4,490,000	4,520,000	4,520,000
1073	1192	1308	1432	1565	1691	1838	1921	1982	2025	2037	2054	2081	2100	2119	2126	2126
3,020,000	3,300,000	3,760,000	4,400,000	4,950,000	5,250,000	3,280,000	2,160,000	1,180,000	800,000	620,000	400,000	330,000	180,000	120,000	000,000	000,000
1738	1817	1939	2098	2225	2291	1811	1470	1086	894	787	632	574	424	346	000	000
5702	5963	6361	6882	7300	7520	5940	4820	3560	2930	2580	2070	1880	1390	1134	0000	0000

137

APPENDIX C

STATIC AND DYNAMIC TEST DATA

APPENDIX C1

STATIC TEST DATA
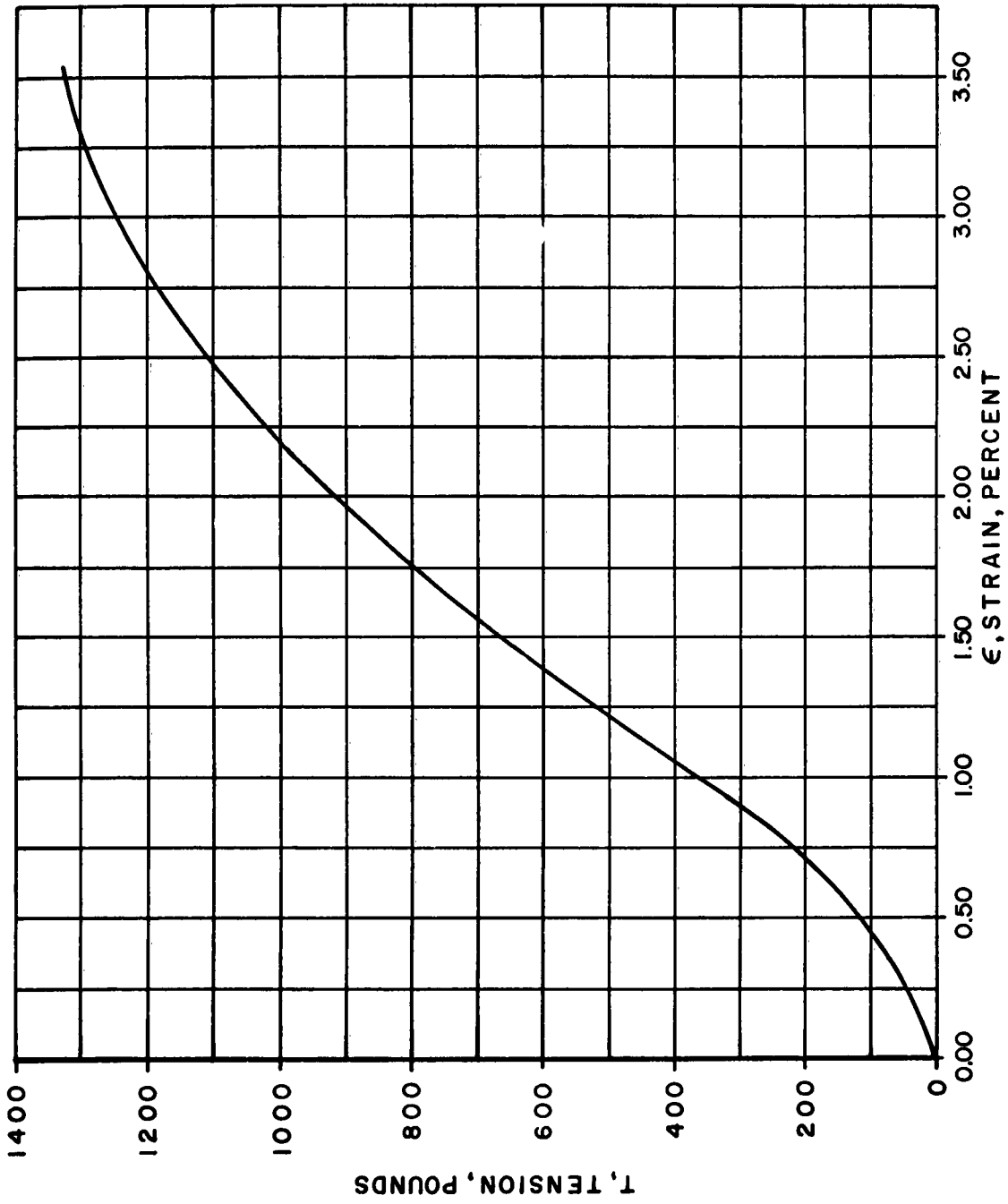
Figure C1-1 - 1/8"-6x19 IMPROVED PLOW STEEL
WIRE ROPE
TENSION-STRAIN DIAGRAM
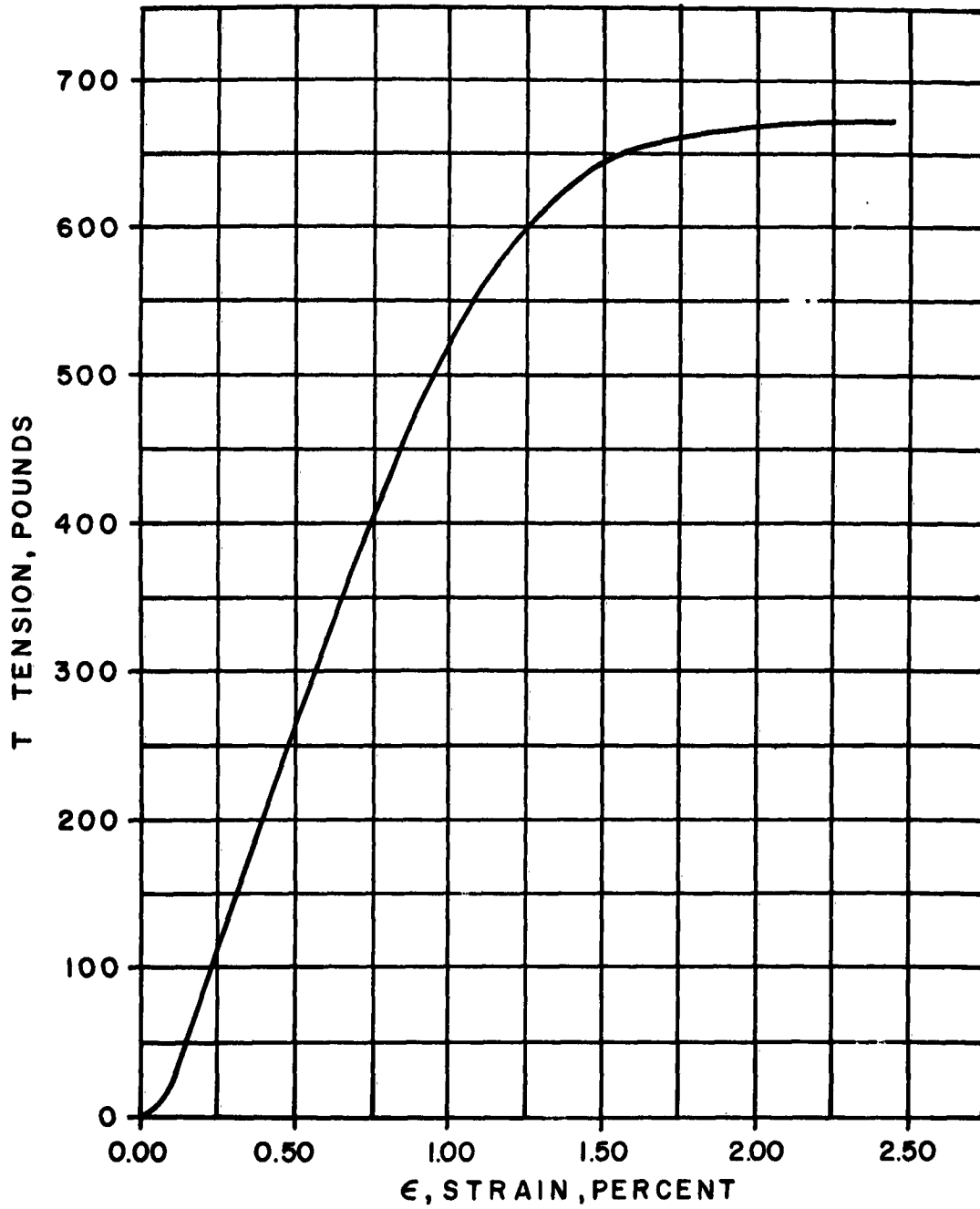
Figure C1-2 - 0.056" DIAM. IMPROVED PLOW STEEL WIRE
TENSION vs. STRAIN
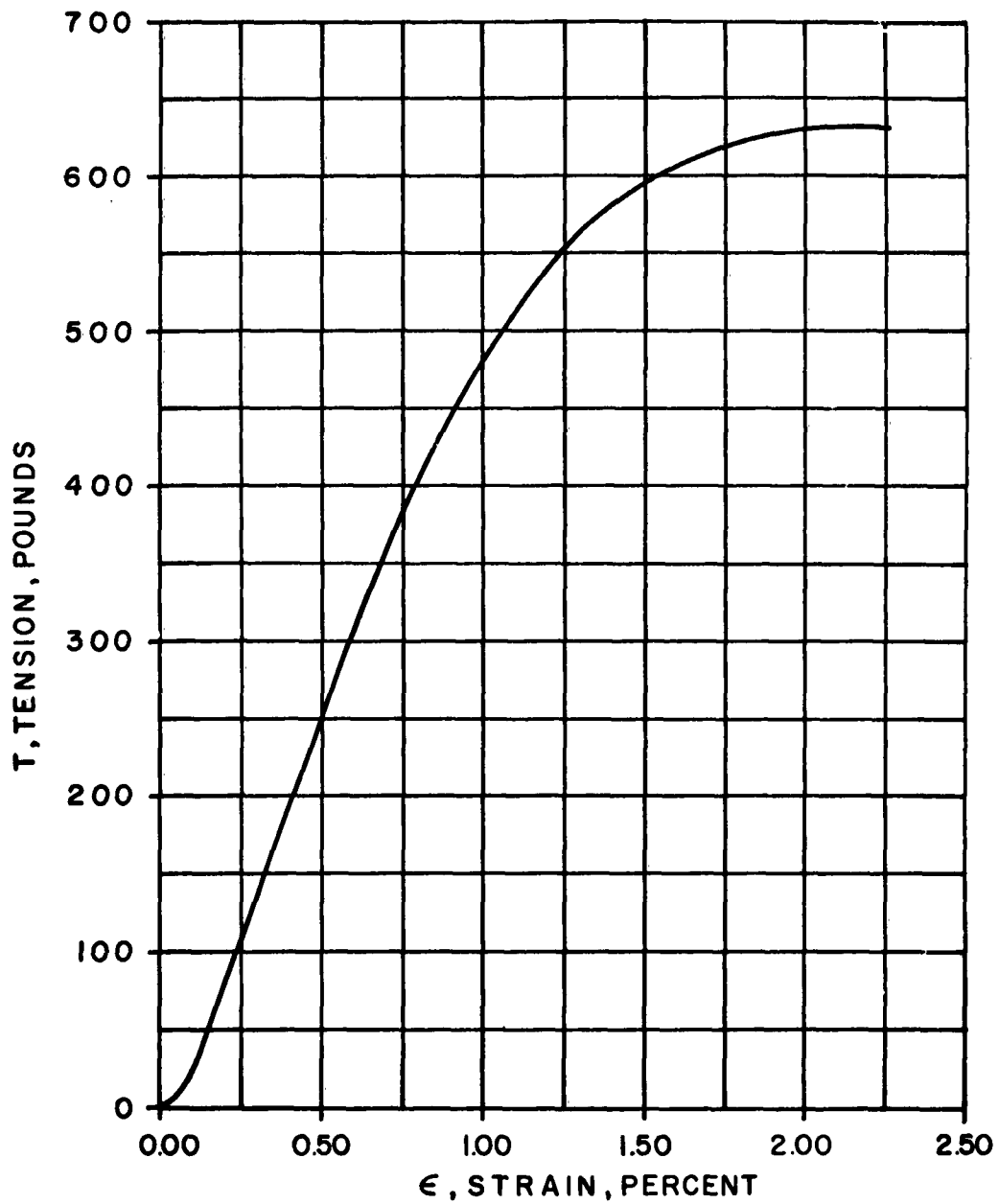
Figure C1-3 — 0.056" PLOW STEEL WIRE
TENSION vs. STRAIN DIAGRAM
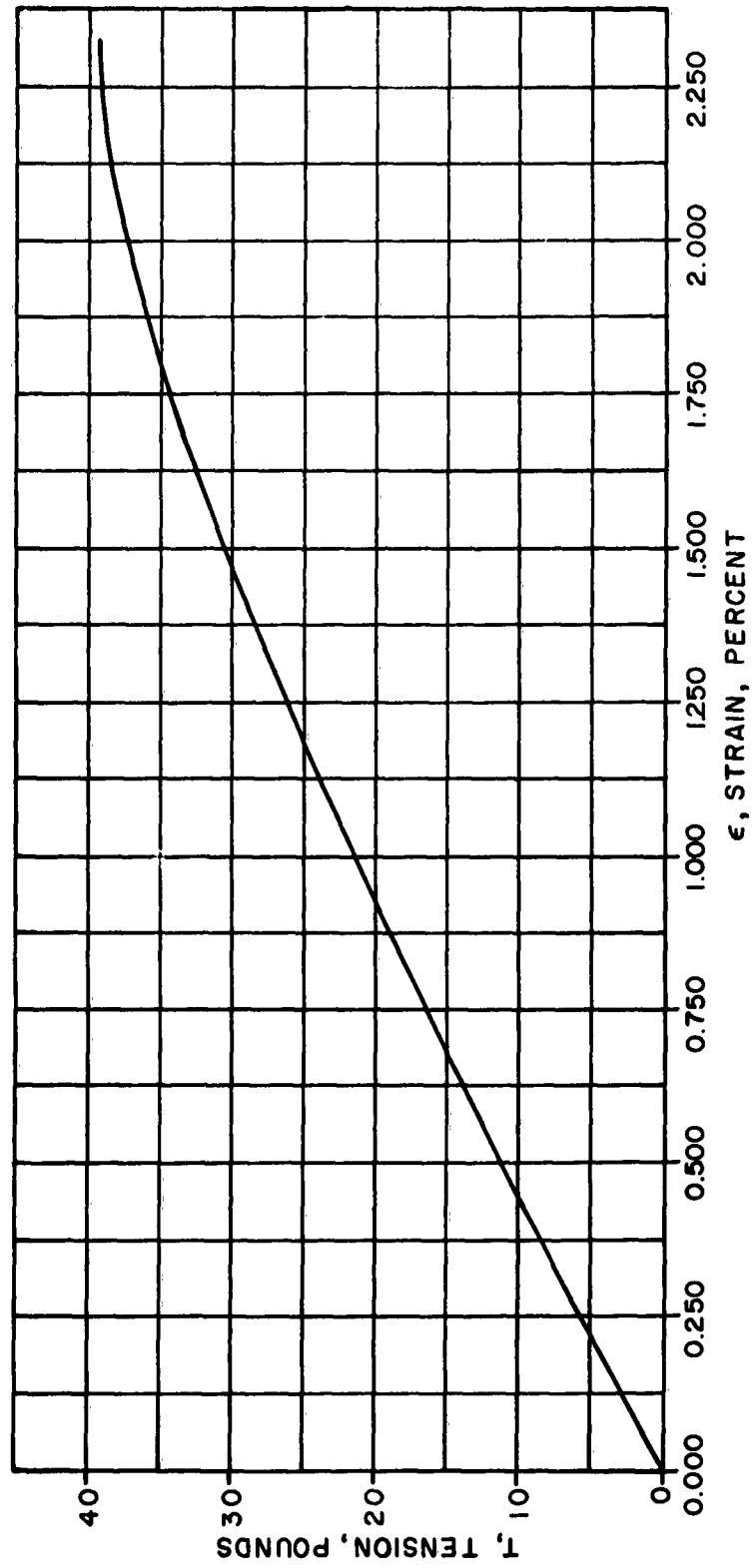
Figure C1-4 - 0.010" HIGH TENSILE WIRE
TENSION-STRAIN DIAGRAM

ε, STRAIN, PERCENT

T, TENSION, POUNDS

143
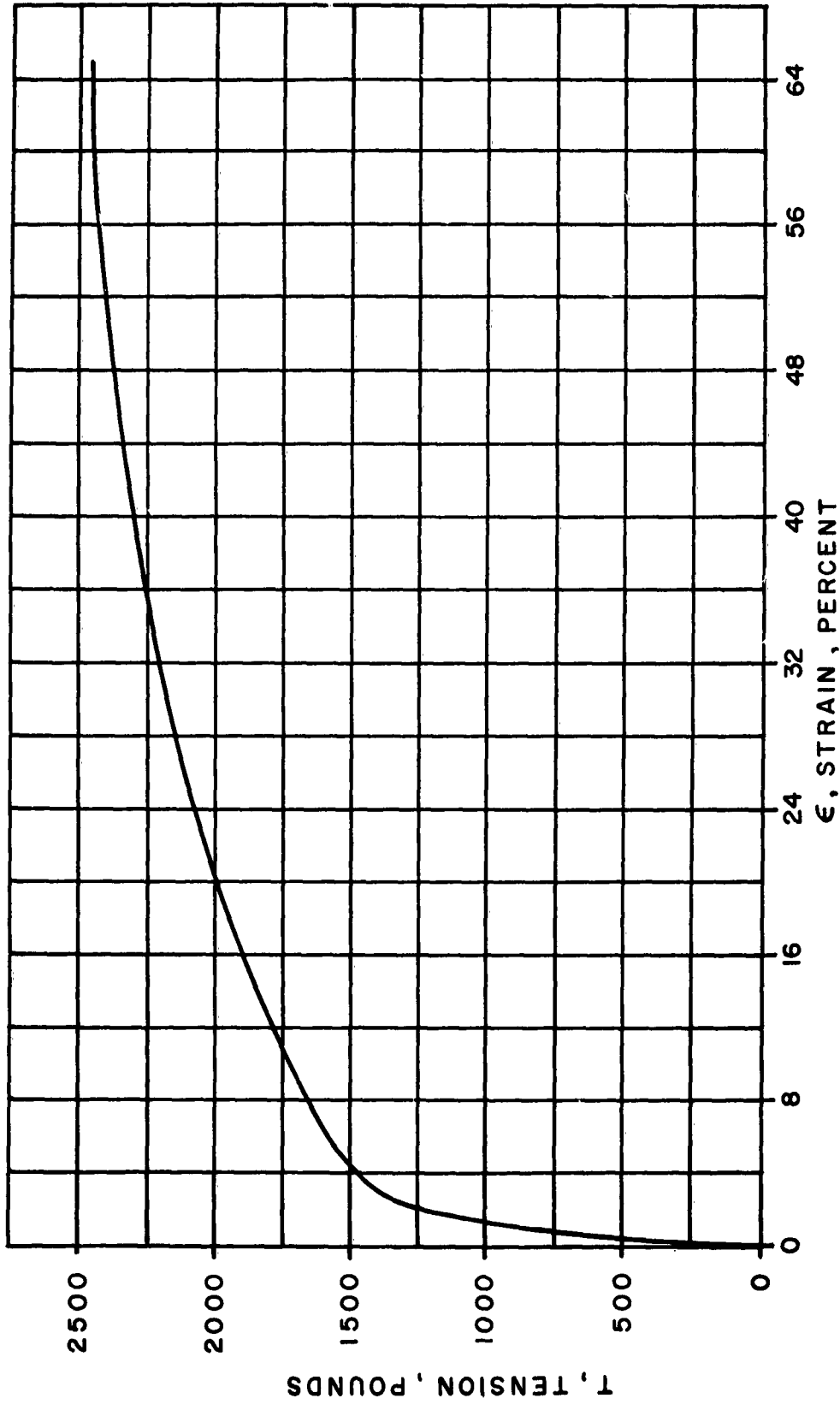
Figure CL-5 - 7/32" - 7x19 E.A. STAINLESS STEEL WIRE ROPE
TENSION-STRAIN DIAGRAM
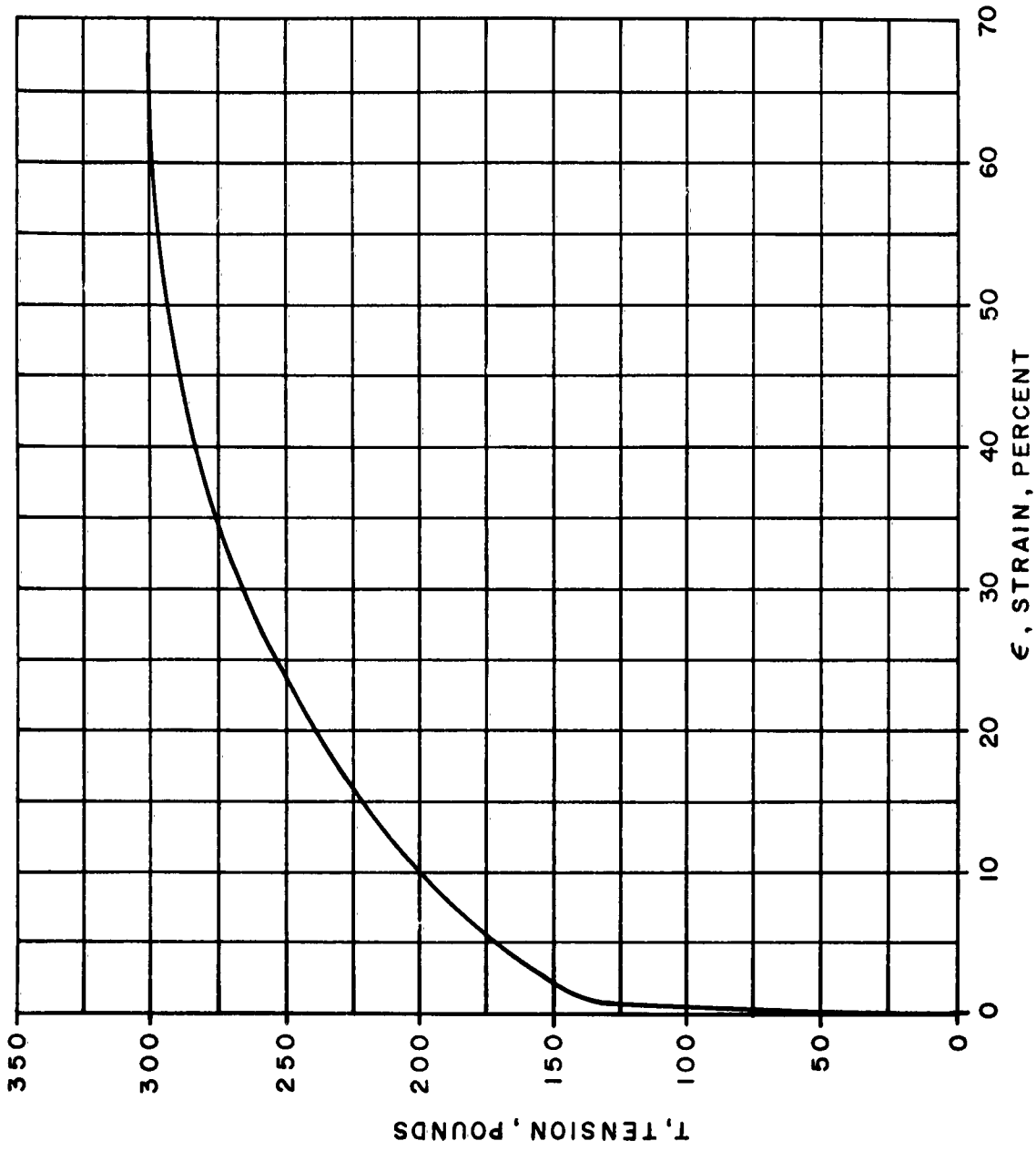
Figure C1-6 - 1/16" (0.062") STAINLESS STEEL WIRE
TENSION-STRAIN DIAGRAM
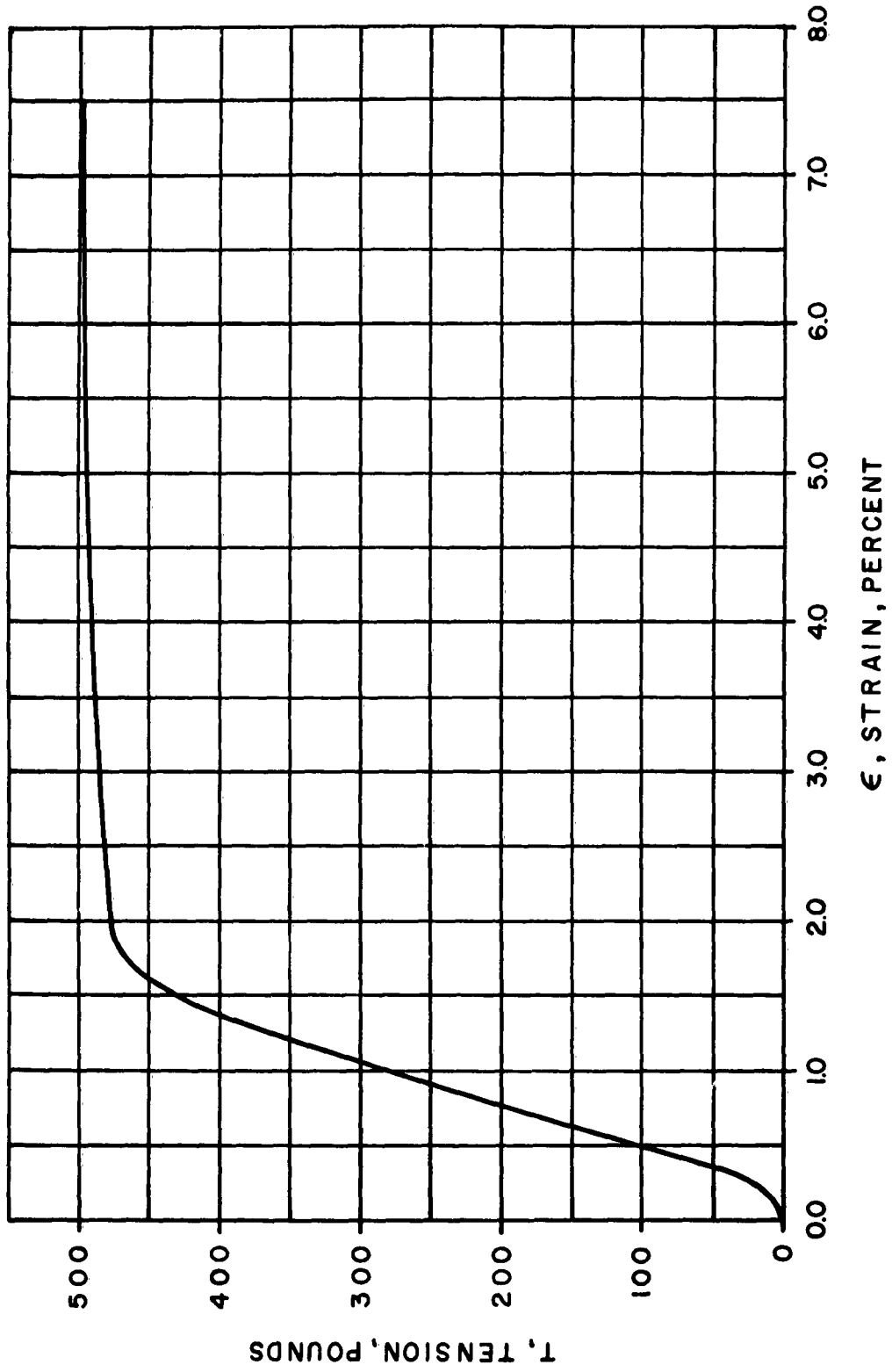
Figure CL-7 - 0.061" DIAMETER (0.00292 SQ.IN.) TITANIUM WIRE
TENSION-STRAIN DIAGRAM

ε, STRAIN, PERCENT

T, TENSION, POUNDS
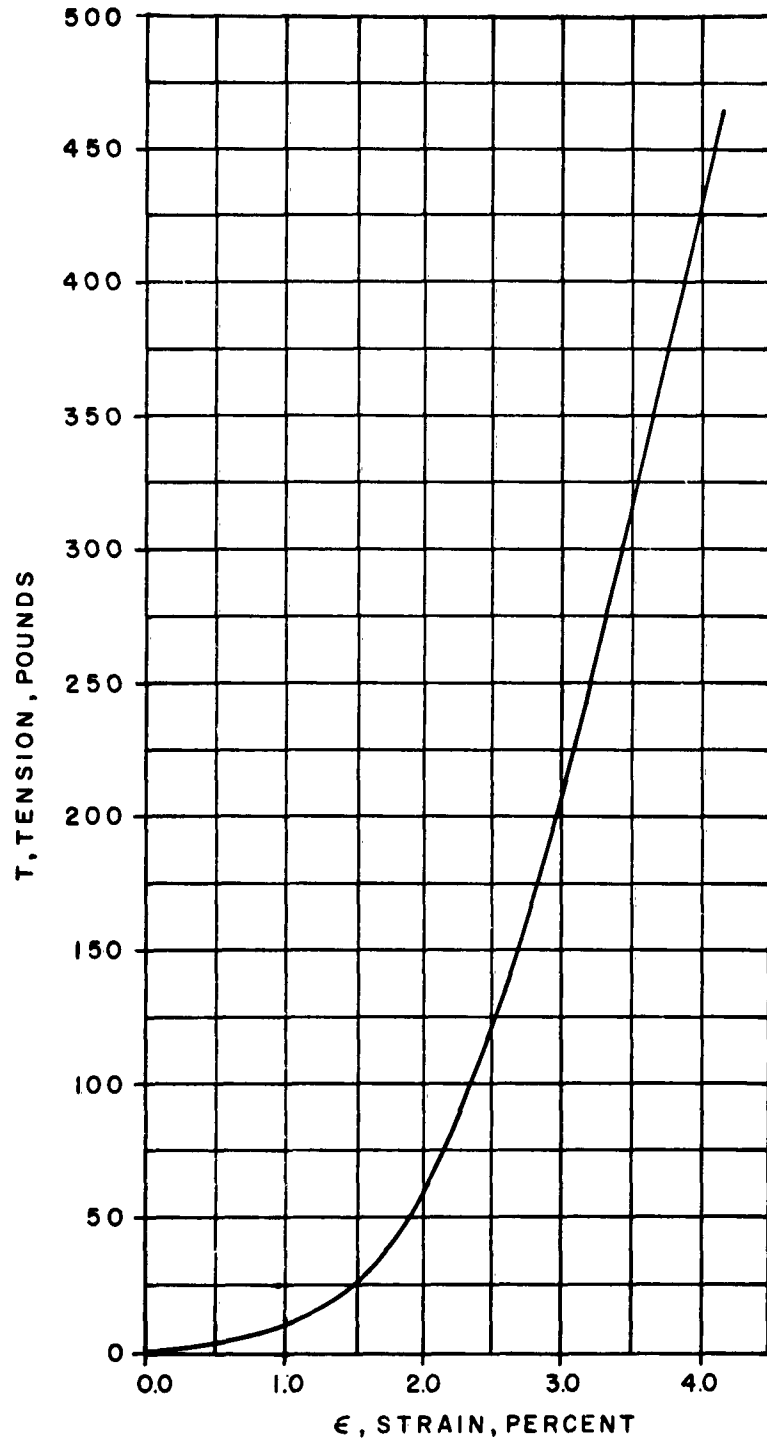
Figure C1-8 - 1/8" UNTREATED FIBERGLASS CORD
TENSION-STRAIN DIAGRAM
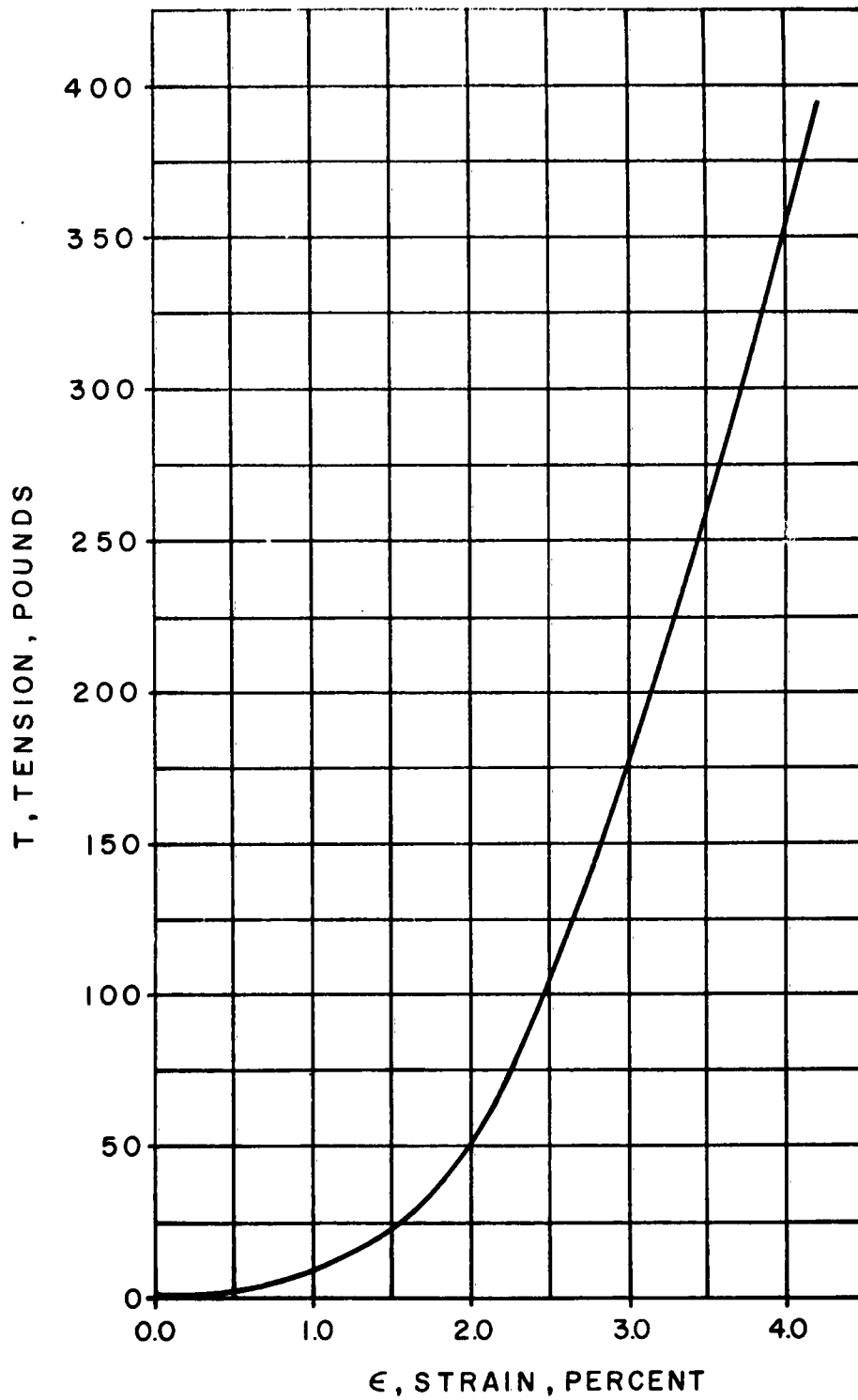
Figure C1-9 - 1/8" TREATED FIBERGLASS CORD
TENSION-STRAIN DIAGRAM

148
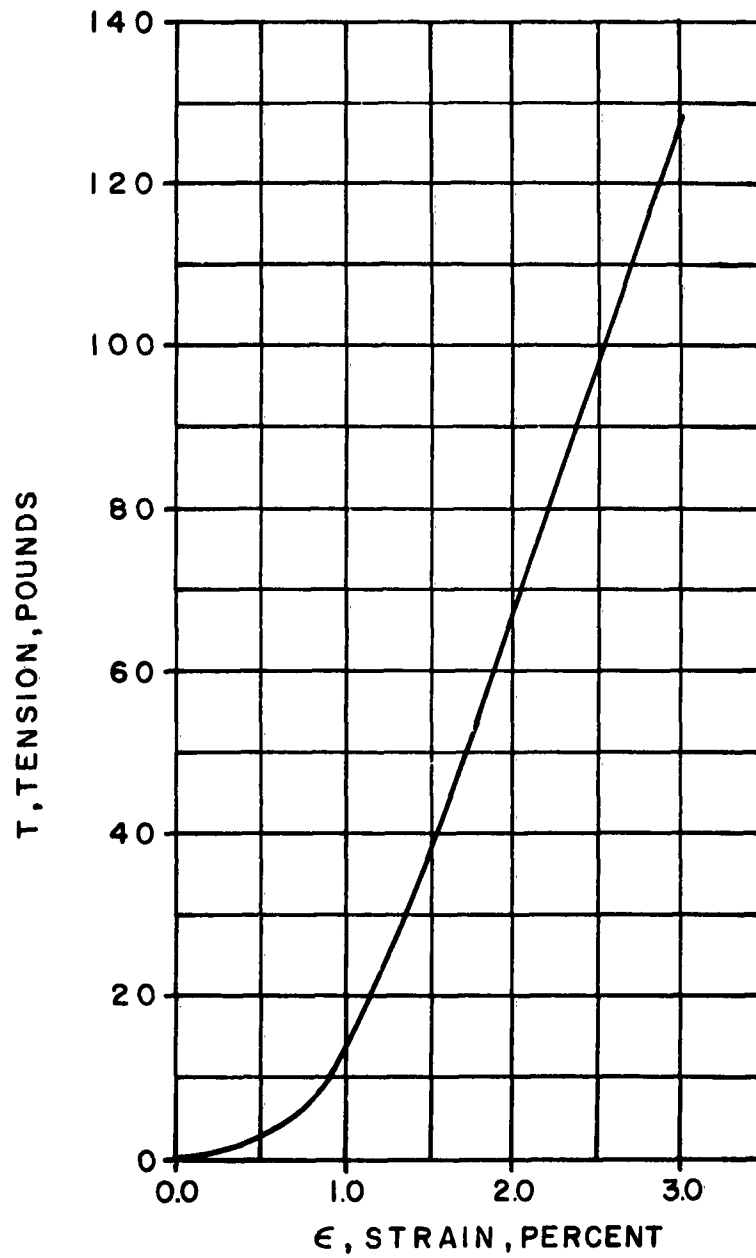
Figure C1-10   0.052" UNTREATED FIBERGLASS CORD
TENSION-STRAIN DIAGRAM
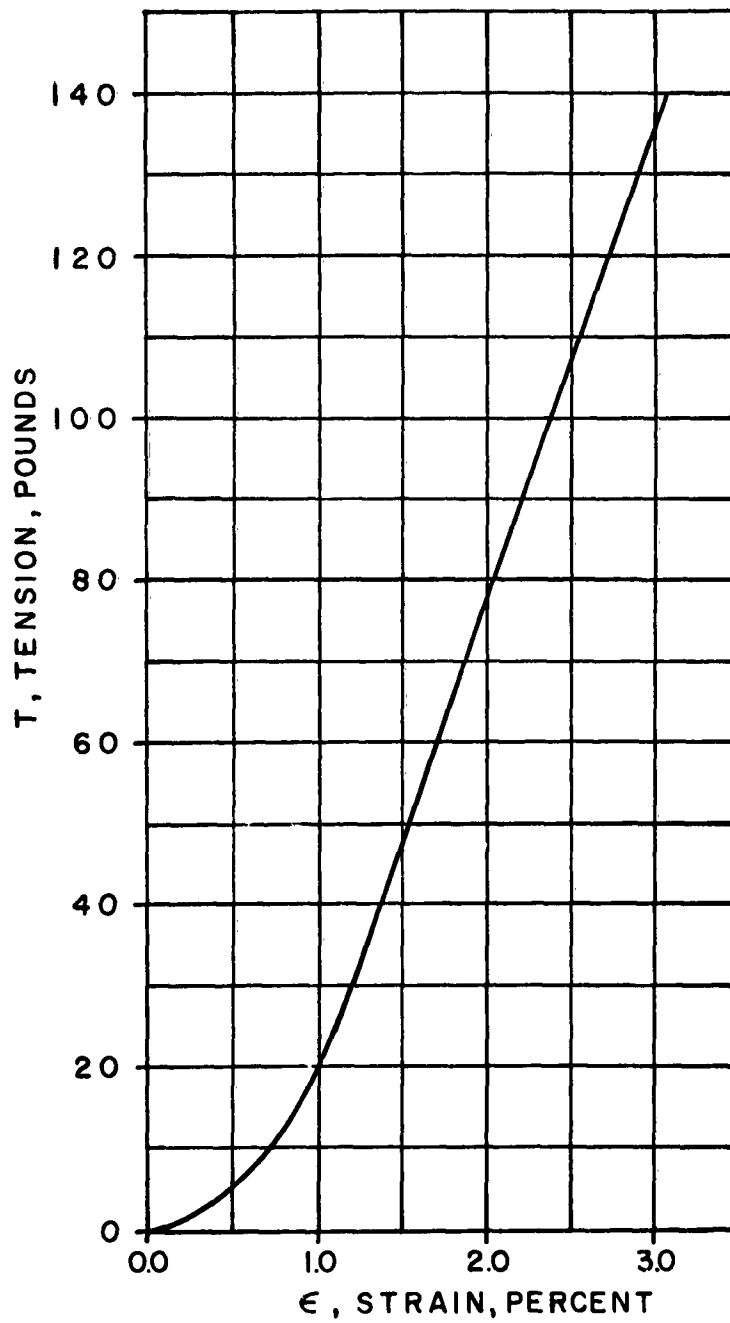
Figure C1-11 0.062" TREATED FIBERGLASS CORD
TENSION vs. STRAIN
DIAGRAM
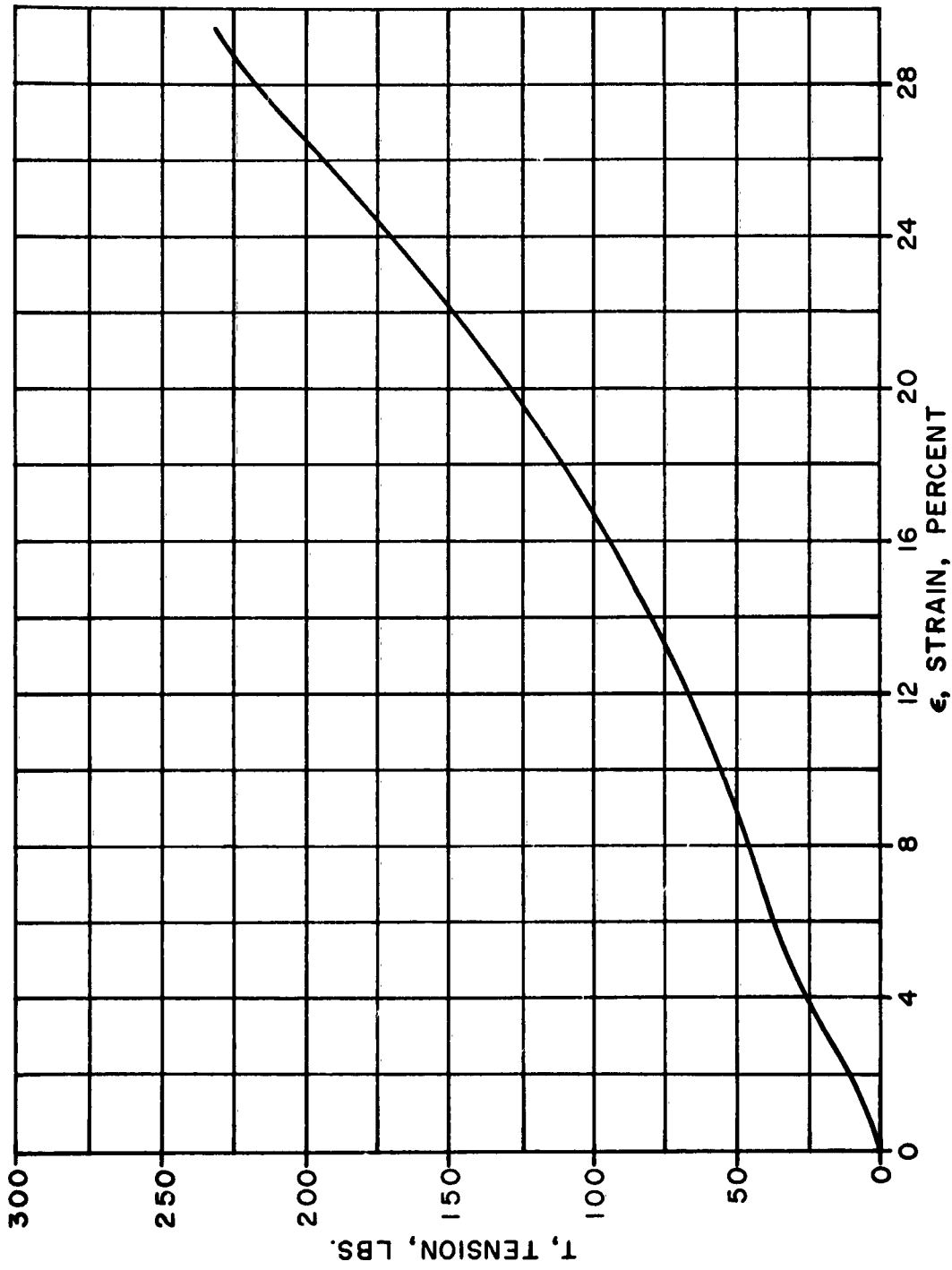
Figure 01-12 – 1/8" NYLON CORD
TENSION-STRAIN DIAGRAM
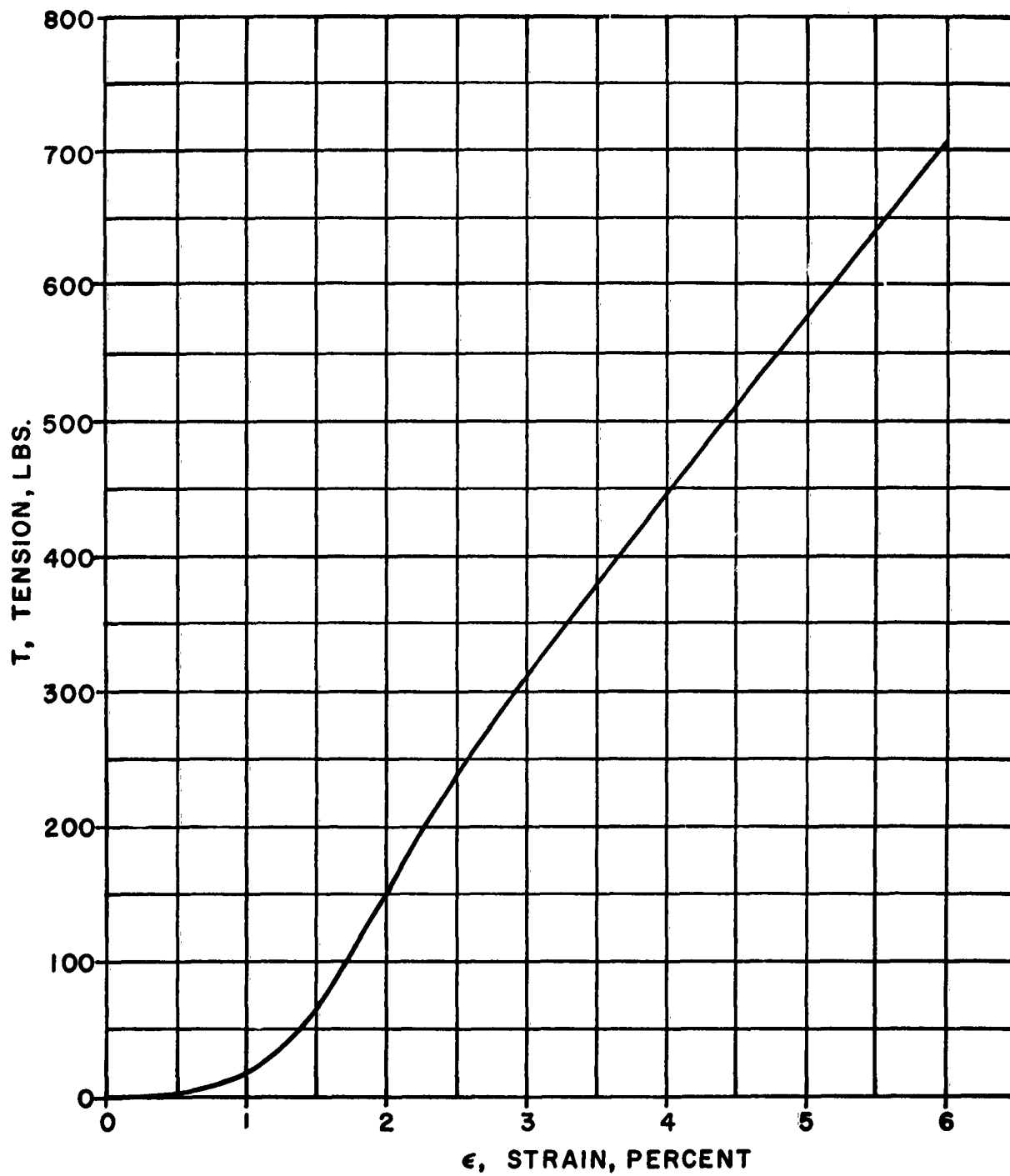
Figure C1-13 - **FORTISAN 36 CORD**
TENSION-STRAIN DIAGRAM
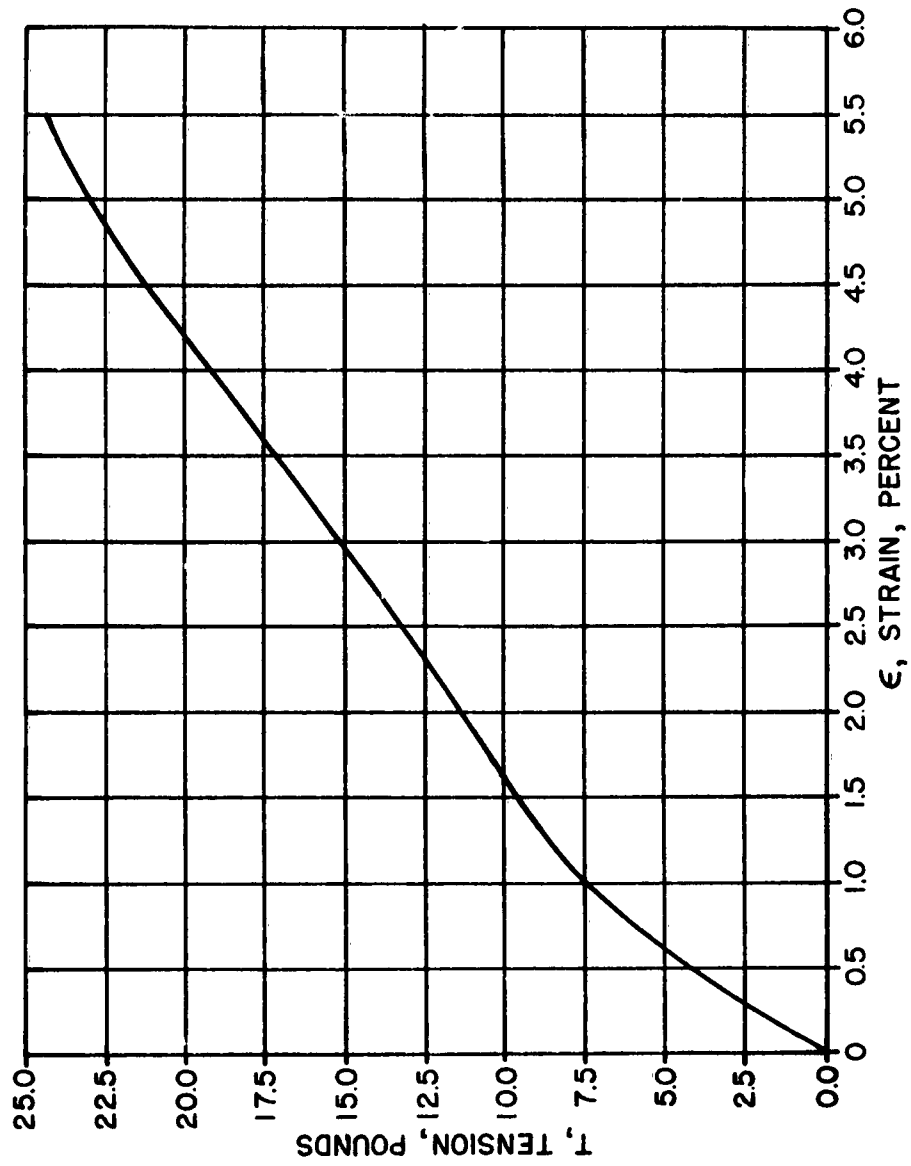
Figure C1-14 — FORTISAN 36 STRAND
(CELANESE CORP. OF AMERICA)
TENSION-STRAIN DIAGRAM

APPENDIX   C2

DYNAMIC TEST DATA

APPENDIX   C2.1

LONGITUDINAL IMPACT TEST DATA

APPENDIX C 2.1

LONGITUDINAL IMPACT TEST DATA

Phase I: To verify the method used to calculate impact velocities.

The sled velocity was determined by means of two breakwires placed
36" apart and at a distance sufficiently away from the gun so that the sled
body had completely left the gun barrel before impacting the first breakwire,
thus insuring that it had attained its maximum velocity. The two breakwires
were severed upon impact with the sled framework during each firing and the
time interval between wire breaks was recorded by means of electric chrono-
graphs connected to the wires. See Fig. D 2.1, page 190. The resulting
velocity data was then compared with the velocity calculated as outlined in
Section 6.0 of this writing. The following data covers this preliminary
phase of the longitudinal impact tests.

Test	Chronometer Measured Impact Velocity (ft/sec)	Calculated Impact Velocity (ft/sec)
a.	265	270
b.	282	286
c.	332	373
d.	370	398
e.	387	401
f.	482	493

The correlation indicated above was considered close enough to justify
the use of the method outlined in Section 6.0 for determining the longitudinal
impact velocity.

156

Phase II: Longitudinal impact velocity tests of tension members.

The tests were started at very low velocities and the first five tests produced too small a pressure-time curve to evaluate the velocity accurately using the method of Section 6.0. However, the velocities produced in these first five tests were not critical to the testing program and the tests are listed below without velocity data merely to furnish a complete report of the testing program as conducted.

Test No.	Longitudinal Impact Velocity (ft/sec)	Specimen	Specimen Failure	Remarks
1	--	1/8" - 6 x 19 Improved Plow Steel Wire Rope	No	Velocity could not be calculated
2	--	1/8" - 6 x 19 Improved Plow Steel Wire Rope	No	Velocity could not be calculated
3	--	1/8" - 6 x 19 Improved Plow Steel Wire Rope	No	Velocity could not be calculated
4	--	1/8" - 6 x 19 Improved Plow Steel Wire Rope	No	Velocity could not be calculated
5	--	1/8" - 6 x 19 Improved Plow Steel Wire Rope	No	Velocity could not be calculated accurately
6	229	1/8" - 6 x 19 Improved Plow Steel Wire Rope	No	
7	154	1/8" - 6 x 19 Improved Plow Steel Wire Rope	No	
8	229	1/8" - 6 x 19 Improved Plow Steel Wire Rope	Yes	

Test No.	Longitudinal Impact Velocity (ft/sec)	Specimen	Specimen Failure	Remarks
9	234	1/16" - Titanium Wire	No	
10	308	1/16" - Titanium Wire	No	
11	187	1/16" - Titanium Wire	No	
12	240	1/16" - Titanium Wire	No	
13	284	1/16" - Titanium Wire	Yes	
14	368	No Specimen	--	Test Shot
15	411	0.010" High Tensile Steel Wire	Yes	
16	429	1/8" Treated Fiberglas Cord	Yes	
17	445	1/16" Stainless Steel Wire	No	
18	414	1/8" Treated Fiberglas Cord	Yes	
19	520	1/16" Stainless Steel Wire	Yes	
20	457	1/16" Stainless Steel Wire	No	
21	548	1/16" Stainless Steel Wire	Yes	
22	474	1/16" Stainless Steel Wire	Yes	Sled damaged by over-filled water bag
23	414	1/8" Treated Fiberglas Cord	Yes	First of 10 tests using damaged sled

Test No.	Longitudinal Impact Velocity (ft/sec)	Specimen	Specimen Failure	Remarks
24	368	1/8" Treated Fiberglas Cord	Yes	
25	276	1/8" Treated Fiberglas Cord	No	
26	308	1/8" Treated Fiberglas Cord	No	
27	352	1/8" Fortisan 36 Cord	No	
28	396	1/8" Fortisan 36 Cord	No	
29	516	1/8" Fortisan 36 Cord	Yes	
30	475	1/8" Fortisan 36 Cord	Yes	
31	392	0.010" High Tensile Steel Wire	Yes	
32	359	1/8" Untreated Fiberglas Cord	No	

APPENDIX C 2.2

<u>TRANSVERSE VELOCITY IMPACT TEST DATA</u>

APPENDIX C 2.2

TRANSVERSE VELOCITY IMPACT TEST DATA

Phase I: Preliminary Calibration Tests Using 1/8"-6 x 19 Imp. Plow Stl. Rope

A. Velocity checks using fully charged shells.

Test No.	Slug Velocity (ft/sec)	Specimen Failure	Remarks
1	1554	Yes	
2	1554	Yes	
3	1554	Yes	
4	1554	Yes	

B. Reduced Velocity Tests.

Test No.	Slug Velocity (ft/sec)	Specimen Failure	Remarks
5	1017	No	Near miss of cable
6	946	No	Near miss of cable
7	1260	Yes	
8	1024	No	Missed cable
9	997	No	Missed cable
10 *	833	Yes	

* A slug recovery unit was added just prior to this test. See Fig. D 2.2-1, page 195, for typical deformation of slug due to impact.

C. To fire one round at 2 ft. length of cable using fully charged shell (Test No. 11). Velocity was recorded as 1550 ft/sec and cable failed.

D. Continuation of reduced velocity test using 1/8" thick .050" diameter aluminum disk cemented to the nose of the slug which was fired at 21' $\pm$ 1/2" length of cable.

Test No.	Slug Velocity (ft/sec)	Specimen Failure	Remarks
12	412	No	
13	---	No	Missed cable
14	615	No	Missed cable
15	---	No	Missed cable
16	---	No	Missed cable
17	---	No	Missed cable
18	632	Yes	Partial cut (3 of 6 strands)

Note to test section D: Misses believed due to instability from low powder charge and use of high tensile strength steel break wire.

E.   Reduced velocity tests with Alcan #5 gun powder.

Test No.	Slug Velocity (ft/sec)	Specimen Failure	Remarks
19	777	Yes	Partial cut (2 of 6 strands)
20	743	Yes	
21	469	No	Missed cable
22	313	. No	Missed cable
23	339	No	
24	---	---	Round not considered valid
25	638	Yes	
26	621	Yes	
27	958	No	Missed cable
28	674	Yes	
29	439	No	
30	1622 *	---	Velocity check
31	1630 *	---	Velocity check
32	1622 *	---	Velocity check

* Used Western Super-X full loads at this point.

F. Continuation of reduced velocity tests.

Test No.	Slug Velocity (ft/sec)	Specimen Failure	Remarks
33	1613	---	Velocity check
34	1613	---	Velocity check
35	620	No	
36	651	Yes	
37	656	Yes	
38	537	Yes	
39	492	Yes	
40	542	Yes	
41	1613	---	Velocity check
42	1596	---	Velocity check
43	1545	---	Velocity check
44	1545	---	Velocity check
45	558	No	Using aluminum disk
46	292	No	Using aluminum disk
47	528	No	Using aluminum disk
48	326	No	Regular slug
49	628	No	Regular slug
50	622	No	Regular slug
51	499	No	Regular slug
52	565	No	Regular slug
53	416	No	Using aluminum disk
54	587	Yes	Using aluminum disk
55	491	No	Using aluminum disk

Test No.	Slug Velocity (ft/sec)	Specimen Failure	Remarks
56	1596	---	Velocity check
57	673	No	Square hit (Reg. slug)
58	632	No	Square hit (Reg. slug)
59	566	No	Square hit (Reg. slug)
60	703	Yes	Square hit (Alum. disk)
61	658	No	Missed cable (Alum. disk)
62	708	No	Slug tumbled (Alum. disk)

NOTE: Tests 1 to 62 were essentially an exploratory series of tests conducted to determine the feasibility of using the velocity impact of a shotgun slug on a test specimen as a method for evaluating the impact tolerance of the specimen. The results justified confidence in the procedure and it was decided to test the specimens listed in Section 5.1.1, page 106, by the use of the slug impact method. The following data covers the results of these latter tests. The set-ups used in all tests are illustrated in Figures D 2.2-2, D 2.2-3, D 2.2-4 and D 2.2-5, page 196.

Phase II: <u>Transverse Impact Tests</u>

A: Reduced velocity tests of tension member specimens.

Test No.	Slug Velocity (ft/sec)	Specimen	Specimen Failure	Remarks
63	1604	1/8" Untreated Fiberglas cord	Yes	
64	1596	1/8" Untreated Fiberglas cord	Yes	
65	1604	1/8" Treated Fiberglas cord	Yes	
66	1587	1/8" Treated Fiberglas cord	Yes	
67	993	1/8" Untreated Fiberglas cord	Yes	
68	1034	1/8" Untreated Fiberglas cord	Yes	
69	1006	1/8" Untreated Fiberglas cord	Yes	
70	1041	1/8" Treated Fiberglas cord	Yes	
71	1041	1/8" Treated Fiberglas cord	Yes	
72	1020	1/8" Treated Fiberglas cord	Yes	
73	759	1/8" Untreated Fiberglas cord	Yes	35% Failure (1 strand broken)
74	769	1/8" Untreated Fiberglas cord	Yes	50% Failure (1 strand broken) (2 strands frayed)
75	755	1/8" Untreated Fiberglas cord	No	5% frayed
76	806	1/8" Treated Fiberglas cord	No	

Test No.	Slug Velocity (ft/sec)	Specimen	Specimen Failure	Remarks
77	813	1/8" Treated Fiberglas cord	No	
78	831	1/8" Treated Fiberglas cord	No	
79	928	1/8" Untreated Fiberglas cord	Yes	
80	906	1/8" Treated Fiberglas cord	Yes	
81	874	1/8" Untreated Fiberglas cord	Yes	
82	869	1/8" Untreated Fiberglas cord	No	Not a direct hit
83	862	1/8" Untreated Fiberglas cord	Yes	
84	849	1/8" Treated Fiberglas cord	Yes	
85	819	1/8" Treated Fiberglas cord	Yes	
86	641	1/8" - 6 x 19 Steel wire rope	Yes	
87	625	1/8" - 6 x 19 Steel wire rope	Yes	
88	---	1/8" - 6 x 19 Steel wire rope	---	Not a direct hit
89	---	1/8" - 6 x 19 Steel wire rope	---	Not a direct hit
90	---	1/8" - 6 x 19 Steel wire rope	---	Not a direct hit
91	---	1/8" - 6 x 19 Steel wire rope	Yes	No chrono reading
92	657	1/8" - 6 x 19 Steel wire rope	Yes	All but one strand

Test No.	Slug Velocity(ft/sec)	Specimen	Specimen Failure	Remarks
93	700	1/8" - 6 x 19 Steel wire rope	Yes	
94	641	1/8" - 6 x 19 Steel wire rope	Yes	
95	665	1/8" - 6 x 19 Steel wire rope	Yes	
96	638	1/8" - 6 x 19 Steel wire rope	Yes	
97	543	1/8" - 6 x 19 Steel wire rope	No	
98	612	1/8" - 6 x 19 Steel wire rope	No	Not a direct hit
99	544	1/8" - 6 x 19 Steel wire rope	Yes	All but 2 strands
100	515	1/8" - 6 x 19 Steel wire rope	No	
101	428	1/8" - 6 x 19 Steel wire rope	No	
102	516	1/8" - 6 x 19 Steel wire rope	No	
103	787	1/8" - Untreated Fiberglas cord	No	
104	802	1/8" - Untreated Fiberglas cord	No	
105	779	1/8" - Untreated Fiberglas cord	No	
106	815	1/8" - Treated Fiberglas cord	No	
107	793	1/8" - Treated Fiberglas cord	No	
108	1657		---	Velocity check

Test No.	Slug Velocity (ft/sec)	Specimen	Specimen Failure	Remarks
109	1657		---	Velocity check
110	819	1/8" Untreated Fiberglas cord	No	
111	879	1/8" Untreated Fiberglas cord	No	Not a direct hit
112	779	1/8" Untreated Fiberglas cord	---	Missed Specimen
113	864	1/8" Untreated Fiberglas cord	No.	
114	877	1/8" Untreated Fiberglas cord	Yes	
115	819	1/8" Untreated Fiberglas cord	No	Not a direct hit
116	857	1/8" Untreated Fiberglas cord	---	Missed specimen
117	882	1/8" Untreated Fiberglas cord	Yes	
118	815	1/8" Untreated Fiberglas cord	---	Missed specimen
119	877	1/8" Untreated Fiberglas cord	Yes	
120	879	1/8" Treated Fiberglas cord	Yes	
121	852	1/8" Treated Fiberglas cord	---	Missed specimen
122	879	1/8" Treated Fiberglas cord	Yes	
123	872	1/8" Treated Fiberglas cord	Yes	80% of cord broken
124	862	1/8" Treated Fiberglas cord	Yes	80% of cord broken

169

Test No.	Slug Velocity (ft/sec)	Specimen	Specimen Failure	Remarks
125	890	1/8" Treated Fiberglas Cord	---	Missed specimen
126	884	1/8" Treated Fiberglas cord	Yes	
127	1578	.015" Fortisan Strand	Yes	
128	1158	.015" Fortisan Strand	---	Missed specimen
129	1271	.015" Fortisan Strand	Yes	
130	1003	.015" Fortisan Strand	Yes	
131	872	.015" Fortisan Strand	---	Missed specimen
132	837	.015" Fortisan Strand	---	Missed specimen
133	849	.015" Fortisan Strand	---	Missed specimen
134	831	.015" Fortisan Strand	No	
135	831	.015" Fortisan Strand	---	Missed specimen
136	847	.015" Fortisan Strand	---	Missed specimen
137	852	.015" Fortisan Strand	No	
138	874	.015" Fortisan Strand	No	
139	864	.015" Fortisan Strand	No	
140	943	.015" Fortisan Strand	---	Missed specimen

Test No.	Slug Velocity (ft/sec)	Specimen	Specimen Failure	Remarks
141	887	.015" Fortisan Strand	No	
142	1621		---	Velocity check
143	735	1/16" Plow Steel Wire	No	
144	650	1/16" Plow Steel Wire	No	
145	699	1/16" Plow Steel Wire	No	
146	877	1/16" Plow Steel Wire	Yes	
147	869	1/16" Plow Steel Wire	Yes	
148	781	1/16" Plow Steel Wire	Yes	
149	821	1/16" Improved Plow Steel Wire	No	Not a direct hit
150	709	1/16" Improved Plow Steel Wire	No	
151	751	1/16" Improved Plow Steel Wire	Yes	
152	744	1/16" Improved Plow Steel Wire	No	Not a direct hit
153	767	1/16" Improved Plow Steel Wire	No	
154	779	1/16" Improved Plow Steel Wire	No	
155	789	1/16" Improved Plow Steel Wire	Yes	
156	783	1/16" Improved Plow Steel Wire	Yes	

Test No.	Slug Velocity (ft/sec)	Specimen	Specimen Failure	Remarks
157	775	1/16" Improved Plow Steel Wire	Yes	
158	815	1/8" Nylon Cord	No	Missed specimen
159	---	1/8" Nylon cord	No	No chronograph reading
160	915	1/8" Nylon cord	No	
161	1612	1/8" Nylon cord	No	Missed specimen
162	1604	1/8" Nylon cord	Yes	
163	1327	1/8" Nylon cord	No	
164	1351	1/8" Nylon cord	No	
165	1500	1/8" Nylon cord	Yes	
166	1485	1/8" Nylon cord	Yes	
167	1463	1/8" Nylon cord	No	
168	1554		---	Velocity check
169	1421	1/8" Nylon cord	Yes	
170	---	1/8" Nylon cord	No	Complete miss
171	1449	1/8" Nylon cord	Yes	
172	1428	1/8" Nylon cord	Yes	
173	1376	1/8" Nylon cord	No	
174	1442	1/8" Nylon cord	Yes	
175	1477	1/8" Nylon cord	Yes	
176	1000	.052" Untreated Fiberglas cord	No	Missed specimen
177	831	.052" Untreated Fiberglas cord	No	Missed specimen

Test No.	Slug Velocity (ft/sec)	Specimen	Specimen Failure	Remarks
178	833	.052" Untreated Fiberglas cord	Yes	
179	733	.052" Untreated Fiberglas cord	No	Missed specimen
180	735	.052" Untreated Fiberglas cord	Yes	
181	597	.052" Untreated Fiberglas cord	No	Missed specimen
182	642	.052" Untreated Fiberglas cord	No	Missed specimen
183	634	.052" Untreated Fiberglas cord	No	Missed specimen
184	622	.052" Untreated Fiberglas cord	No	
185	700	.052" Untreated Fiberglas cord	No	
186	---	.052" Untreated Fiberglas cord	Yes	No chrono reading
187	686	.052" Untreated Fiberglas cord	No	
188	681	.052" Untreated Fiberglas cord	No	
189	---	.062" Treated Fiberglas cord	No	No chrono reading
190	680	.062" Treated Fiberglas cord	No	Missed specimen
191	696	.062" Treated Fiberglas cord	No	Slug Tumbled
192	722	.062" Treated Fiberglas cord	No	
193	645	.052" Untreated Fiberglas cord	Yes	

173

Test No.	Slug Velocity (ft/sec)	Specimen	Specimen Failure	Remarks
194	630	.052" Untreated Fiberglas cord	Yes	
195	837	.062" Treated Fiberglas cord	No	
196	824	.062" Treated Fiberglas cord	No	
197	887	.062" Treated Fiberglas cord	Yes	
198	882	.062" Treated Fiberglas cord	Yes	
199	831	.062" Treated Fiberglas cord	No	Not a direct hit
200	849	.062" Treated Fiberglas cord	Yes	
201	837	.062" Treated Fiberglas cord	Yes	
202	842	.062" Treated Fiberglas cord	Yes	
203	1595		---	Velocity check
204	1060	.010" Carbon Steel Wire (500,000 psi ult)	Yes	
205	826	.010" Carbon Steel Wire (500,000 psi ult)	Yes	
206	751	.010" Carbon Steel Wire (500,000 psi ult)	No	
207	808	.010" Carbon Steel Wire (500,000 psi ult)	No	Not a direct hit
208	824	.010" Carbon Steel Wire (500,000 psi ult)	No	

Test No.	Slug Velocity (ft/sec)	Specimen	Specimen Failure	Remarks
194	630	.052" Untreated Fiberglas cord	Yes	
195	837	.062" Treated Fiberglas cord	No	
196	824	.062" Treated Fiberglas cord	No	
197	887	.062" Treated Fiberglas cord	Yes	
198	882	.062" Treated Fiberglas cord	Yes	
199	831	.062" Treated Fiberglas cord	No	Not a direct hit
200	849	.062" Treated Fiberglas cord	Yes	
201	837	.062" Treated Fiberglas cord	Yes	
202	842	.062" Treated Fiberglas cord	Yes	
203	1595		---	Velocity check
204	1060	.010" Carbon Steel Wire (500,000 psi ult)	Yes	
205	826	.010" Carbon Steel Wire (500,000 psi ult)	Yes	
206	751	.010" Carbon Steel Wire (500,000 psi ult)	No	
207	808	.010" Carbon Steel Wire (500,000 psi ult)	No	Not a direct hit
208	824	.010" Carbon Steel Wire (500,000 psi ult)	No	

174

Test No.	Slug Velocity (ft/sec)	Specimen	Specimen Failure	Remarks
209	815	.010" Carbon Steel Wire (500,000 psi ult)	No	
210	810	.010" Carbon Steel Wire (500,000 psi ult)	No	
211	852	.010" Carbon Steel Wire (500,000 psi ult)	No	
212	824	.010" Carbon Steel Wire (500,000 psi ult)	No	
213	817	.010" Carbon Steel Wire (500,000 psi ult)	No	
214	---	.010" Carbon Steel Wire (500,000 psi ult)	No	No chrono reading
215	857	.010" Carbon Steel Wire (500,000 psi ult)	No	
216	882	.010" Carbon Steel Wire (500,000 psi ult)	No	
217	872	.010" Carbon Steel Wire (500,000 psi ult)	No	
218	882	.010" Carbon Steel Wire (500,000 psi ult)	No	
219	887	.010" Carbon Steel Wire (500,000 psi ult)	No	
220	869	.010" Carbon Steel Wire (500,000 psi ult)	No	Missed specimen

175

Test No.	Slug Velocity (ft/sec)	Specimen	Specimen Failure	Remarks
221	890	.010" Carbon Steel Wire (500,000 psi ult)	No	Missed specimen
222	900	.010" Carbon Steel ire (500,000 psi ult)	Yes	
223	1562	7/32" - 7 x 19 Stainless Steel Rope	Yes	
224	1562	1/8" Fortisan 36 Cord	Yes	
225	925	1/8" Fortisan 36 Cord	---	Missed specimen
226	879	7/32" - 7 x 19 Stainless Steel Rope	Yes	All but 2 strands broke
227	931	1/8" Fortisan 36 Cord	---	Missed specimen
228	867	1/8" Fortisan 36 Cord	---	Missed specimen
229	920	1/8" Fortisan 36 Cord	No	
230	869	7/32" - 7 x 19 Stainless Steel Rope	---	Missed specimen
231	946	7/32" - 7 x 19 Stainless Steel Rope	Yes	14 Wires Cut
232	---	--------	---	No Chrono Reading
233	---	1/8" Fortisan 36 Cord	No	No chrono Reading
234	---	1/8" Fortisan 36 Cord	No	No Chrono Reading

176

Test No.	Slug Velocity (ft/sec)	Specimen	Specimen Failure	Remarks
235	----	1/8" Fortisan 36 Cord	No	No Chrono reading
236	----	1/8" Fortisan 36 Cord	No	No Chrono reading
237	1562		---	Velocity check
238	686	7/32" - 7 x 19 Stainless Steel Rope	No	
239	----	7/32" - 7 x 19 Stainless Steel Rope	Yes	No Chrono reading
240	833	7/32" - 7 x 19 Stainless Steel Rope	---	Missed specimen
241	882	7/32" - 7 x 19 Stainless Steel Rope	No	
242	835	0.052" Untreated Fiberglas Cord	No	Powder trouble causing erratic results
243	----	0.052" Untreated Fiberglas Cord	---	Powder trouble causing erratic results; missed specimen
244	500	0.052" Untreated Fiberglas Cord	No	Powder trouble causing erratic results
245	369	0.052" Untreated Fiberglas Cord	No	Powder trouble causing erratic results
246	475	1/16" Plow Steel Wire	No	
247	----	1/16" Plow Steel Wire	Yes	No Chrono reading

177

Test No.	Slug Velocity (ft/sec)	Specimen	Specimen Failure	Remarks
248	733	1/16" Plow Steel Wire	Yes	
249	587	1/16" Plow Steel Wire	No	
250	---	1/16" Plow Steel Wire	No	No Chrono reading
251	721	1/16" Plow Steel Wire	No	
252	721	1/16" Plow Steel Wire	No	
253	729	1/16" Plow Steel Wire	No	
254	643	1/16" Improved Plow Steel Wire	No	
255	545	1/16" Improved Plow Steel Wire	No	
256	1595		---	Velocity check
257	621	.010" High Tensile Steel Wire	---	Missed specimen
258	826	.010" High Tensile Steel Wire	No	
259	828	.010" High Tensile Steel Wire	No	
260	898	.010" High Tensile Steel Wire	No	
261	420	.010" High Tensile Steel Wire	No	
262	890	.010" High Tensile Steel Wire	No	
263	892	.010" High Tensile Steel Wire	Yes	

Test No.	Slug Velocity (ft/sec)	Specimen	Specimen Failure	Remarks
264	---	.010" High Tensile Steel Wire	Yes	No Chrono reading
265	961	.010" High Tensile Steel Wire	Yes	
266	1522		---	Velocity check
267	917	.010" High Tensile Steel Wire	Yes	
268	937	.010" High Tensile Steel Wire	Yes	
269	821	.010" High Tensile Steel Wire	No	
270	777	.010" High Tensile Steel Wire	Yes	
271	813	.010" High Tensile Steel Wire	---	Missed specimen
272	806	.010" High Tensile Steel Wire	No	Very Near Breaking Point
273	847	.010" High Tensile Steel Wire	Yes	
274	946	.010" High Tensile Steel Wire	Yes	
275	1530		---	Velocity check
276	831	1/16" Improved Plow Steel Wire	No	
277	751	1/16" Improved Plow Steel Wire	Yes	
278	582	1/16" Improved Plow Steel Wire	No	
279	606	1/16" Improved Plow Steel Wire	No	
280	779	1/16" Improved Plow Steel Wire	Yes	

Test No.	Slug Velocity (ft/sec)	Specimen	Specimen Failure	Remarks
281	738	1/16" Improved Plow Steel Wire	No	
282	719	1/16" Improved Plow Steel Wire	Yes	
283	561	1/16" Plow Steel Wire	No	
284	700	1/16" Plow Steel Wire	Yes	
285	717	1/16" Plow Steel Wire	Yes	
286	735	1/16" Plow Steel Wire	No	
287	737	1/16" Plow Steel Wire	No	
288	742	1/16" Plow Steel Wire	Yes	
289	707	1/16" Plow Steel Wire	No	
290	937	.015" Fortisan Strand	No	
291	898	.015" Fortisan Strand	No	
292	890	.015" Fortisan Strand	No	
293	955	.015" Fortisan Strand	No	
294	934	.015" Fortisan Strand	Yes	75% Failure
295	1530		---	Velocity check

Test No.	Slug Velocity (ft/sec)	Specimen	Specimen Failure	Remarks
296	845	7/32" - 7 x 19 Stainless Steel Rope	Yes	45% Failure
297	842	7/32" - 7 x 19 Stainless Steel Rope	Yes	65% Failure
298	874	7/32" - 7 x 19 Stainless Steel Rope	Yes	65% Failure
299	854	7/32" - 7 x 19 Stainless Steel Rope	Yes	65% Failure
300	---	7/32" - 7 x 19 Stainless Steel Rope	Yes	No Chrono Reading 14% Failure
301	757	7/32" - 7 x 19 Stainless Steel Rope	Yes	One Wire Cut
302	777	7/32" - 7 x 19 Stainless Steel Rope	Yes	28% Failure
303	937	1/8" Fortisan 36 Cord	No	
304	1304	1/8" Fortisan 36 Cord	Yes	50% Failure
305	1276	1/8" Fortisan 36 Cord	Yes	Complete Break
306	1260	1/8" Fortisan 36 Cord	Yes	50% Failure
307	1176	1/8" Fortisan 36 Cord	Yes	33% Failure
308	1204	1/8" Fortisan 36 Cord	Yes	10% Failure

Test No.	Slug Velocity (ft/sec)	Specimen	Specimen Failure	Remarks
309	721	1/16" Stainless Steel Wire	No	
310	717	1/16" Stainless Steel Wire	No	
311	781	1/16" Stainless Steel Wire	No	
312	779	1/16" Stainless Steel Wire	No	
313	828	1/16" Stainless Steel Wire	No	
314	824	1/16" Stainless Steel Wire	---	Missed Specimen
315	862	1/16" Stainless Steel Wire	---	Missed Specimen
316	810	1/16" Stainless Steel Wire	No	
317	797	1/16" Stainless Steel Wire	No	
318	852	1/16" Stainless Steel Wire	No	
319	847	1/16" Stainless Steel Wire	No	
320	---	1/16" Stainless Steel Wire	Yes	No Chrono reading
321	898	1/16" Stainless Steel Wire	No	
322	934	1/16" Stainless Steel Wire	No	
323	900	1/16" Stainless Steel Wire	Yes	

Test No.	Slug Velocity (ft/sec)	Specimen	Specimen Failure	Remarks
324	917	1/16" Stainless Steel Wire	No	
325	911	1/16" Stainless Steel Wire	Yes	
326	869	1/16" Titanium Wire	Yes	
327	840	1/16" Titanium Wire	Yes	
328	882	1/16" Titanium Wire	Yes	
329	882	1/16" Titanium Wire	---	Not a direct hit
330	817	1/16" Titanium Wire	Yes	
331	813	1/16" Titanium Wire	No	
332	842	1/16" Titanium Wire	Yes	
333	835	1/16" Titanium Wire	Yes	
334	795	1/16" Titanium Wire	Yes	
335	831	1/16" Titanium Wire	Yes	
336	802	1/16" Titanium Wire	Yes	
337	761	1/16" Titanium Wire	No	

APPENDIX D

PHOTOGRAPHS OF TEST EQUIPMENT AND TEST EFFECTS

184

APPENDIX D1

<u>STATIC TEST PHOTOGRAPHS</u>
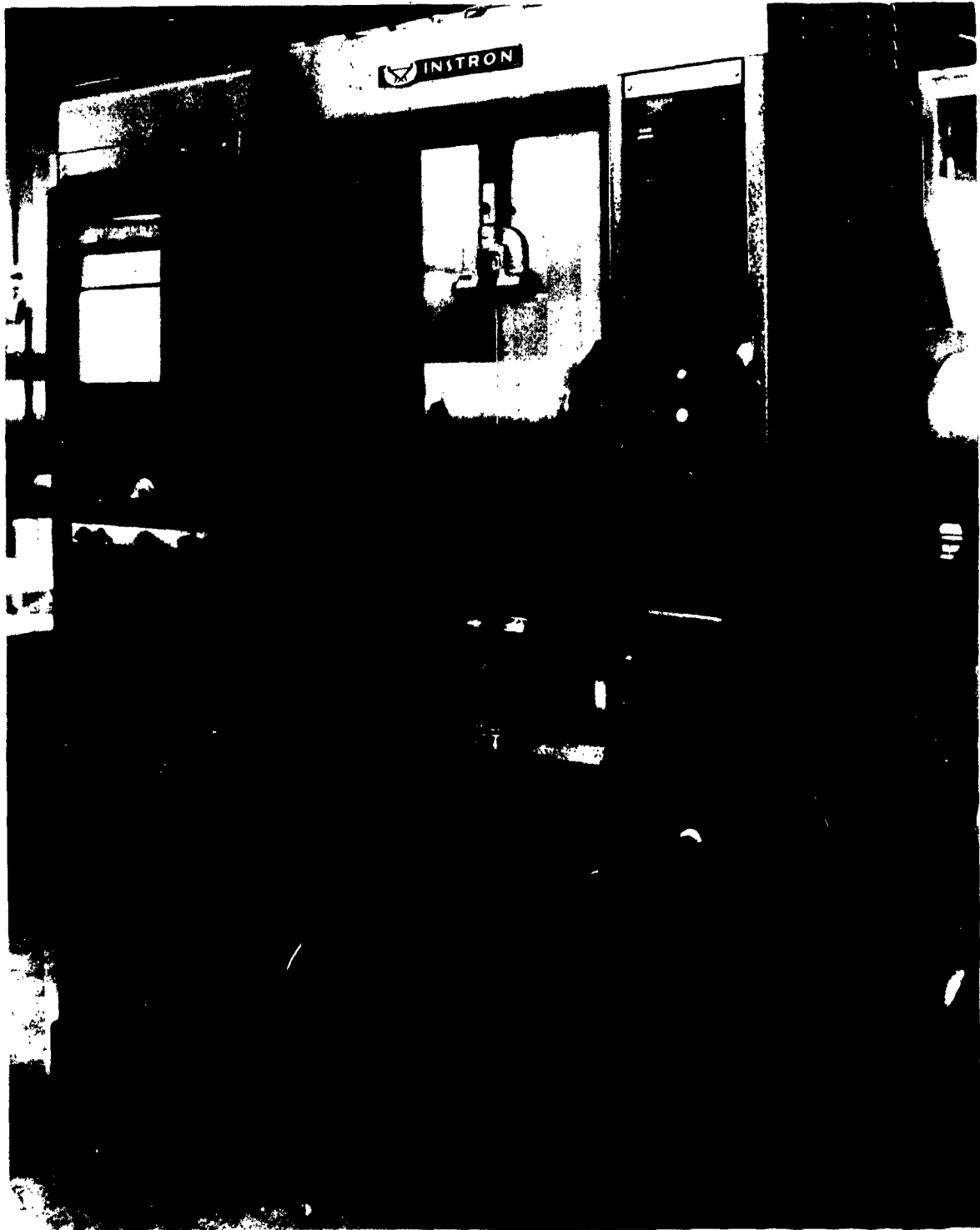
Figure D1-1.   Equipment Used for Static (Tensile) Test.

Figure D1-2. Method of Fastening Specimen for Tensile Test in Instron Tensile Tester, Model TTC-M1.

APPENDIX D2

<u>DYNAMIC TEST PHOTOGRAPHS</u>

APPENDIX D2.1

<u>LONGITUDINAL IMPACT TEST PHOTOGRAPHS</u>

Figure D2.1-2. Close-up View of Impacting Sled and Gun Used to Fire Sled.

Figure D2.1-4. Chronometer Set-up Used for Calibration of Method Used in Determining Velocity of Sled at Impact.

Figure D2.1-1. Test Set-up for Longitudinal Impact Tolerance Tests of Tension Members.

Figure D2.1-3. View of Track Used for Testing With Water Filled Trough Employed to Stop Sled after Firing.

190

Figure D2.1-6. Another View of Longitudinal Impact Test in Action at End of Braking Run After Impact.

Figure D2.1-8. (Test 8) Longitudinal Impact Test of 1/8"-6x19 Improved Plow Steel Wire Rope (Complete Break).

Figure D2.1-5. View (Rear) of Longitudinal Impact Test in Action. Note Spray from Water Braking Procedure Used to Stop Sled After Impact.

Figure D2.1-7. Close-up View of Damaged Front Wing of Impacting Sled. Sled Was Still Suitable for Use in Testing Program after Damage.
(See Test 22)

Figure D2.1-10. (Test 15) Longitudinal Impact Test of 0.010" High Tensile Wire (Complete Break).

Figure D2.1-12. (Test 20) Longitudinal Impact Test of 1/16" Stainless Steel Wire (Complete Break).

Figure D2.1-9. (Test 13) Longitudinal Impact Test of 1/16" Titanium Wire (Complete Break).

Figure D2.1-11. (Test 16) Longitudinal Impact Test of 1/8" Neoprene Treated Fiberglas Cord (Complete Break).

192
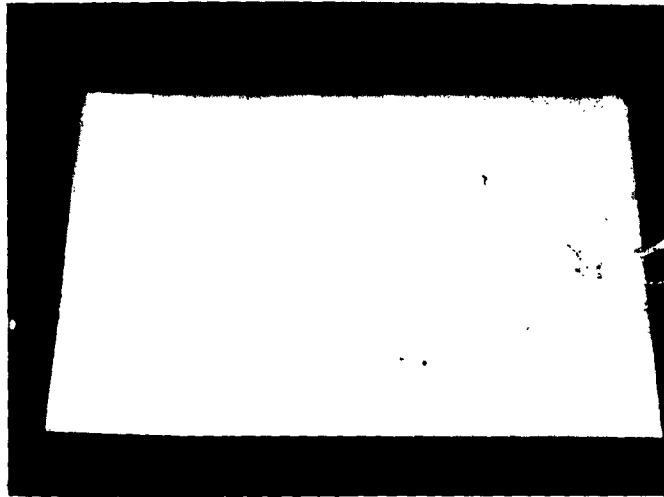
Figure D2.1-13. (Test 29) Longitudinal
                 Impact Test of 1/8" Fortisan
                 36 Cord.

APPENDIX D2.2

TRANSVERSE IMPACT TEST PHOTOGRAPHS

194

Figure D2.2-1.   Effects of Transverse Velocity
Impact on 12-Gauge Rifle Slug.

Figure D2.2-3. Test Set-up for Reduced Velocity Tests to Determine Transverse Impact Tolerance Capacity of Tension Members (Side View).

Figure D2.2-5. Method of Tying Specimen Ends Using Low Tensile Strength String to Simulate Free Ended Condition for Transverse Impact Tests.

Figure D2.2-2. Test Set-up During Preliminary Firing Tests.

Figure D2.2-4. Test Set-up for Reduced Velocity Tests to Determine Transverse Impact Tolerance Capacity of Tension Members (Rear View).

196
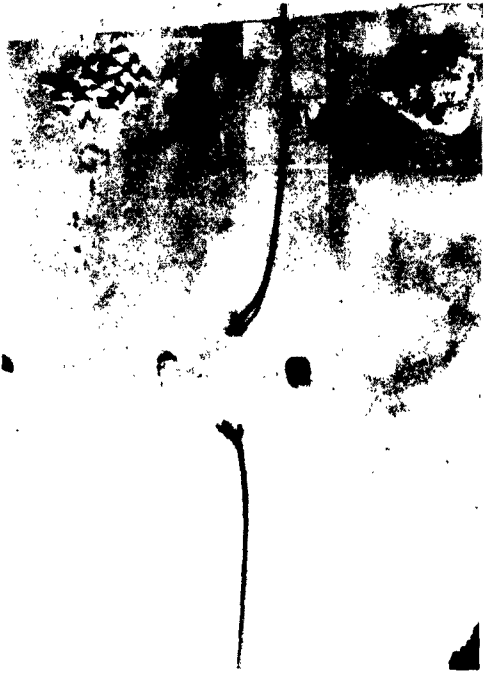
Figure D2.2-7. (Test 2) Transverse Impact
Test of 1/8"-6x19 Improved
Plow Steel Wire Rope
(Complete Break).
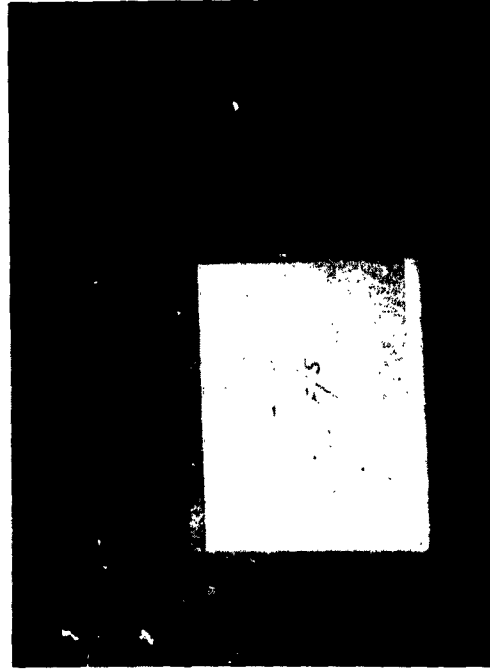
Figure D2.2-9. (Test 18) Transverse Impact
Test of 1/8"-6x19 Improved
Plow Steel Wire Rope
(Failure).
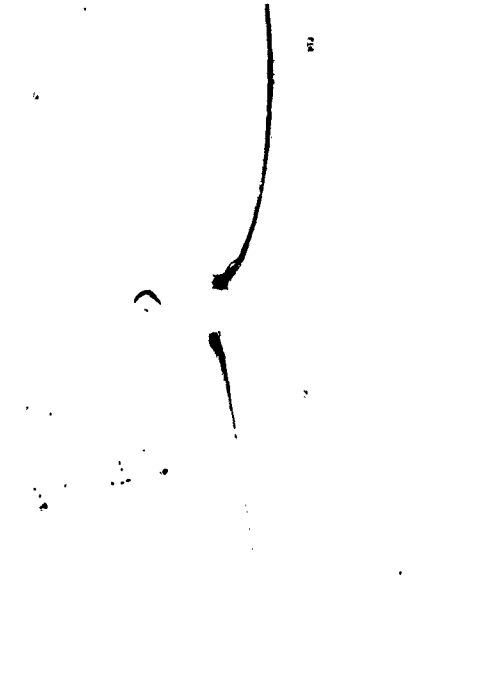
Figure D2.2-6. (Test 1) Transverse Impact
Test of 1/8"-6x19 Improved
Plow Steel Wire Rope
(Complete Break).
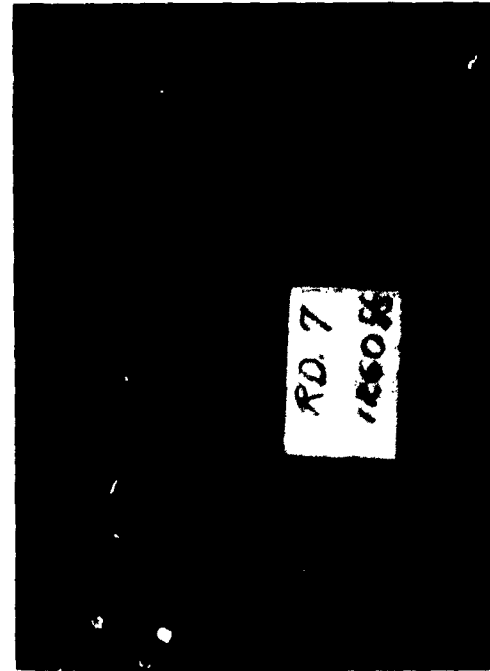
Figure D2.2-8. (Test 7) Transverse Impact
Test of 1/8"-6x19 Improved
Plow Steel Wire Rope
(Complete Break).

197

Figure D2.2-11. (Test 156) Transverse Impact Test of 1/16" Improved Plow Steel Wire (Complete Break).

Figure D2.2-13. (Test 172) Transverse Impact Test of 1/8" Nylon Cord (Complete Break).
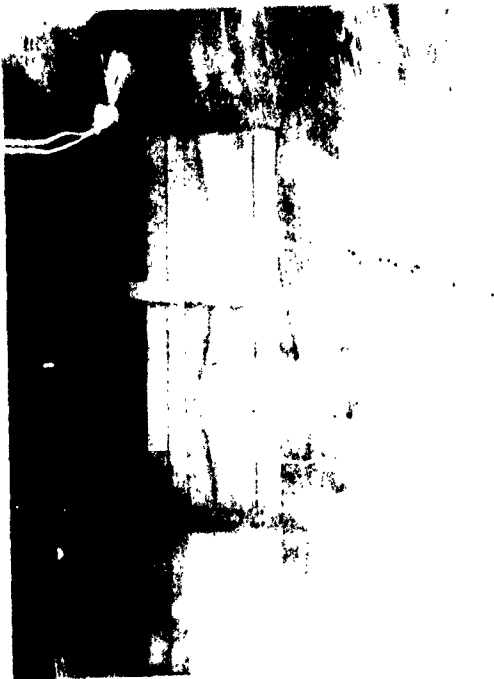
Figure D2.2-10. (Test 100) Transverse Impact Test of 1/8"-6x19 Improved Plow Steel Wire Rope (No Failure).

Figure D2.2-12. (Test 148) Tranverse Impact Test of 1/16" Plow Steel Wire (Complete Break).

198

Figure D2.2-15. (Test 198) Transverse Impact Test of 0.962" Treated Fiberglas Cord (Complete Break).

Figure D2.2-17. (Test 114) Transverse Impact Test of 1/8" Untreated Fiberglas Cord (Complete Break).

Figure D2.2-14. (Test 178) Transverse Impact Test of 0.052" Untreated Fiberglas Cord (Complete Break).

Figure D2.2-16. (Test 73) Transverse Impact Test of 1/8" Untreated Fiberglas Cord (Failure).

199

Figure D2.2-19. (Test 75) Transverse Impact Test of 1/8" Treated Fiberglas Cord (No Failure).

Figure D2.2-21. (Test 224) Transverse Impact Test of 1/8" Fortisan-36 Cord (Complete Break).

Figure D2.2-18. (Test 79) Transverse Impact Test of 1/8" Treated Fiberglas Cord (Complete Break).

Figure D2.2-20. (Test 127) Transverse Impact Test of 0.0152" Fortisan-36 Strand (Complete Break).

Figure D2.2-23. (Test 270) Transverse Impact Test of 0.056" Plow Steel Wire (Complete Break).


Figure D2.2-25. (Test 330) Transverse Impact Test of 1/16" Titanium Wire (Complete Break).

Figure D2.2-22. (Test 223) Transverse Impact Test of 7/32"-7x19 Stainless Steel Rope (Complete Break).

Figure D2.2-24. (Test 320) Transverse Impact Test of 1/16" Stainless Steel Wire (Complete Break).